

**BIOCHEMICAL STUDIES OF RETROVIRAL REPLICATION
AND TRIM5 α RESTRICTION**

by

Charles R. Langelier

A dissertation submitted to the faculty of
The University of Utah
in partial fulfillment of the requirements for the degree of

Doctor of Philosophy

Department of Biochemistry

The University of Utah

May 2010

UMI Number: 3411436

All rights reserved

INFORMATION TO ALL USERS

The quality of this reproduction is dependent upon the quality of the copy submitted.

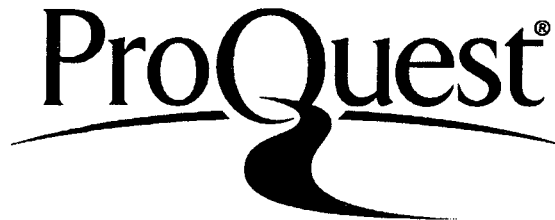
In the unlikely event that the author did not send a complete manuscript and there are missing pages, these will be noted. Also, if material had to be removed, a note will indicate the deletion.



UMI 3411436

Copyright 2010 by ProQuest LLC.

All rights reserved. This edition of the work is protected against unauthorized copying under Title 17, United States Code.



ProQuest LLC
789 East Eisenhower Parkway
P.O. Box 1346
Ann Arbor, MI 48106-1346

Copyright © Charles R. Langelier 2010

All Rights Reserved

THE UNIVERSITY OF UTAH GRADUATE SCHOOL

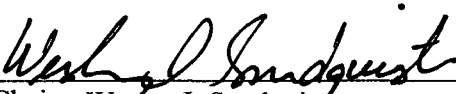
SUPERVISORY COMMITTEE APPROVAL

of a dissertation submitted by

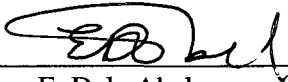
Charles Langelier

This dissertation has been read by each member of the following supervisory committee and by majority vote has been found to be satisfactory.

17 August, 2009


Chair: Wesley I. Sundquist


28 August, 2009


E. Dale Abel

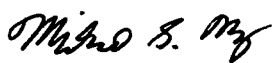
31 July 2009


Dana Carroll

13 August 2009


Christopher P. Hill

11 Aug. 2009


Michael S. Kay

THE UNIVERSITY OF UTAH GRADUATE SCHOOL

FINAL READING APPROVAL

To the Graduate Council of the University of Utah:

I have read the dissertation of Charles Langelier in its final form and have found that (1) its format, citations, and bibliographic style are consistent and acceptable; (2) its illustrative materials including figures, tables, and charts are in place; and (3) the final manuscript is satisfactory to the supervisory committee and is ready for submission to The Graduate School.

August 17, 2009
Date

Wesley I. Sundquist
Wesley I. Sundquist
Chair: Supervisory Committee

Approved for the Major Department

Wesley I. Sundquist
Wesley I. Sundquist and Christopher P. Hill
Chair/Dean

Approved for the Graduate Council

Charles A. Wight
Charles A. Wight
Dean of The Graduate School

ABSTRACT

During early stages of infection, HIV-1 and other lentiviruses progress through a series of cytoplasmic events that include capsid uncoating, reverse transcription and formation of the preintegration complex (PIC). In certain primates, the intrinsic immune factor TRIM5 α can bind to lentiviral capsids and disrupt this program. Neither TRIM5 α restriction nor early retroviral replication is understood in mechanistic detail and both were therefore the targets of investigation for research described in this dissertation.

Chapter 2 describes a system for producing multimilligram quantities of an active TRIM5 α variant, termed TRIM5-21R. TRIM5-21R is a chimeric protein composed primarily of the TRIM5 α from rhesus (rh) monkeys, except for the N-terminal RING domain, which comes from the human TRIM21 protein. Recombinant TRIM5-21R was functional, as judged by its ability to autoubiquitylate in reconstituted ubiquitin transfer reactions and to bind specifically to HIV and EIAV capsid assemblies. Gel filtration and analytical ultracentrifugation experiments demonstrated that TRIM5-21R formed stable dimers, and chemical crosslinking experiments showed that TRIM5 α proteins expressed in mammalian cells are also predominantly dimeric. We anticipate that this system for producing pure recombinant TRIM5-21R will facilitate future

studies of the biochemistry, mechanism, and structural biology of this important class of antiretroviral proteins.

Research described in the remaining chapters of this thesis characterized the requirement for the ESCRT-II complex in HIV budding and endosomal protein sorting (Chapter 4), structural and biochemical properties of the ubiquitin-binding EAP45 GLUE domain (Chapter 5), the molecular mechanism of (ESCRT-II involvement in) Hepcidin-mediated Ferroportin down-regulation (Chapter 6) and self-assembly of pure recombinant ESCRT-III proteins into helical tubes (Chapter 7).

TABLE OF CONTENTS

ABSTRACT.....	iv
ACKNOWLEDGMENTS.....	viii
Chapter	
1. INTRODUCTION.....	1
HIV-1 Organization.....	2
General Lifecycle Overview.....	4
Core Uncoating.....	7
Reverse Transcription and Preintegration Complex (PIC) Formation.....	8
PIC Transport, Nuclear Import and Additional Early Lifecycle Events.....	9
Summary of Early Events.....	9
Host Cell Factors That Restrict Early Stages of HIV-1 Replication.....	10
TRIM5 α	11
Assays to Examine Early Retroviral Replication and TRIM5 α Restriction.....	15
Research Overview: Retroviral Replication and TRIM5 α Restriction.....	17
References.....	19
2. BIOCHEMICAL CHARACTERIZATION OF A RECOMBINANT TRIM5 α PROTEIN THAT RESTRICTS HUMAN IMMUNODEFICIENCY VIRUS TYPE 1 REPLICATION.....	29
Abstract.....	30
Introduction.....	30
Materials and Methods.....	31
Results.....	33
Discussion.....	40
Acknowledgments.....	41
References.....	41

3.	HUMAN ESCRT-II COMPLEX AND ITS ROLE IN HUMAN IMMUNODEFICIENCY VIRUS TYPE 1 RELEASE.....	43
	Abstract.....	44
	Introduction.....	44
	Materials and Methods.....	46
	Results.....	47
	Discussion.....	56
	Acknowledgments.....	57
	References.....	57
4.	STRUCTURAL BASIS FOR UBIQUITIN RECOGNITION BY THE HUMAN ESCRT-II EAP45 GLUE DOMAIN.....	60
	Abstract.....	61
	Introduction.....	61
	Acknowledgments.....	62
	References.....	62
5.	THE MOLECULAR MECHANISM OF HEPCIDIN-MEDIATED FERROPORTIN DOWN REGULATION.....	63
	Abstract.....	64
	Introduction.....	64
	Materials and Methods.....	64
	Results.....	65
	Discussion.....	70
	Acknowledgments.....	73
	References.....	73
6.	STRUCTURAL BASIS FOR ESCRT-III PROTEIN AUTOINHIBITION.....	74
	Abstract.....	75
	Introduction.....	75
	Results.....	76
	Discussion.....	82
	Methods.....	83
	Acknowledgments.....	83
7.	CONCLUSIONS AND FUTURE DIRECTIONS.....	85
	TRIM5 α Restriction.....	85
	Early Events in Lentiviral Replication and the Development of Cell-Free Uncoating and Restriction Assays.....	89
	References.....	92

ACKNOWLEDGMENTS

I would like to thank several people who helped greatly during this process. First, I want to thank my parents and grandparents for their support. I would like to thank Wes Sundquist, my advisor, for providing a model of excellence both as a scientist and as a human being. I would like to thank Terri for her support, love, and adventurous spirit. Finally, I would like to thank the members of the Sundquist, Hill, Kay, and Kaplan labs for their collegiality, contributions, and discussions that made this work possible.

CHAPTER 1

INTRODUCTION

Retroviruses have played a decisive role in the survival and demise of vertebrates throughout their natural history. Human Immunodeficiency Virus-1 (HIV-1) has been the most destructive of the known human retroviruses and has caused more than 25 million deaths and a profound degree of suffering during the past 25 years (86). In the most heavily affected countries, HIV-1 has reduced life expectancy by more than 20 years, slowed economic growth, and deepened household poverty (96). In sub-Saharan Africa alone, the epidemic has orphaned nearly 12 million children. According to the United Nations Development Programme (UNDP), HIV-1 has inflicted the “single greatest reversal in human development” in modern history.

The magnitude of the global AIDS pandemic provides strong impetus for scientific investigation of retroviral pathogenesis and has driven worldwide research efforts aimed at understanding the molecular and structural biology of HIV-1. The dissertation research described here was undertaken as part of these efforts. Specifically, we have examined host/pathogen interactions in both early and late stages of HIV-1 replication, with a principal focus on the early events in replication and the antiviral intrinsic immunity protein, TRIM5 α .

HIV-1 Organization

HIV-1, like all retroviruses, uses the enzyme reverse transcriptase (RT) to convert a single stranded RNA genome into double stranded DNA that integrates into a host cell chromosome (19). HIV-1 is subclassified in the genus *lentiviridae* due to its: 1) characteristic latent replication profile, 2) complex genome that encodes additional accessory proteins not found in all retroviruses, 3) ability to infect both dividing and nondividing cells, and 4) distinct conical capsid (18). Retroviral genomes contain three basic genes: *gag*, which encodes structural proteins; *pol*, which encodes viral enzymes necessary for replication; and *env*, which encodes the viral envelope protein (19).

The mature HIV-1 virion is surrounded by a lipid membrane studded with hetero-trimeric glycoprotein spikes of the envelope (ENV) protein. Each Env protein is composed of three copies of the gp120/SU and three copies of gp41/TM (Figure 1.1). A layer of MA protein (the “matrix”) is located beneath the lipid bilayer. Inside the matrix is a conical ribonucleoprotein complex called the core. The outer shell of the core is called the capsid, and is comprised of CA protein subunits. The capsid encloses two copies of the RNA genome, annealed tRNA^{Lys,3} primers, reverse transcriptase/RNaseH (RT), integrase (IN), nucleocapsid (NC), protease (PR), and other accessory proteins (Figure 1.1). All retroviral capsids are composed of hexameric arrays of the CA protein, as well as 12 CA pentamers, which introduce the declination necessary to close the hexameric lattice (35). Capsid morphologies vary owing to different distributions of the CA pentamers, and this results in a diversity of capsid shapes, including

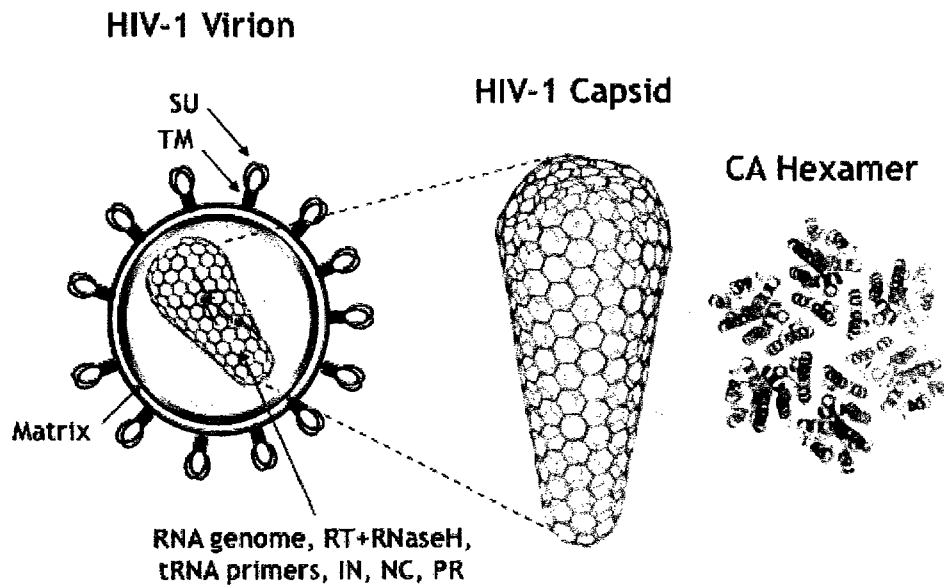


Figure 1.1. Structural features and protein components of the mature HIV-1 virion. An outer lipid envelope contains ENV glycoprotein spikes composed of SU and TM subunits. The envelope surrounds a matrix shell comprised of MA proteins, which in turn encloses the viral core particle. The outer capsid shell of the core particle is comprised of hexameric CA protein building blocks (yellow, with expanded view showing CA monomers in different colors) and is closed by the introduction of 12 pentameric defects. The capsid encloses two copies of the RNA genome, annealed tRNA primers, reverse transcriptase/RNaseH (RT), integrase (IN), nucleocapsid (NC), protease (PR) and other accessory proteins. Figure adapted from: (36, 37).

cones, rods and rounded particles. The capsids of lentiviruses, like HIV-1 and equine infectious anemia virus (EIAV), predominantly form geometric objects called fullerene cones, with five CA pentamers at the narrow end of the cone and seven CA pentamers at the wide end (Figure 1.1) (12, 35-37, 45, 50).

General Lifecycle Overview

Retroviral replication can be categorized into early and late events (Figure 1.2). Early events encompass the lifecycle stages that occur prior to transcription of viral genes (Figure 1.2). Replication begins when ENV interacts with the CD4 receptor and either the CXCR4 or the CCR5 co-receptors at the host cell membrane (1, 21, 53, 76). Receptor binding induces dramatic conformational changes in ENV that lead to fusion of viral and host cell membranes, releasing the viral core particle into the cytoplasm (27, 28, 81). Within the cytoplasm, uncoating of the viral core takes place in a manner that allows for reverse transcription of the viral RNA genome to produce a dsDNA product that integrates into the host cell genome. The early cytoplasmic replication steps are described in greater detail below.

Late replication events begin with RNA polymerase II-mediated transcription of the integrated provirus. This process is greatly enhanced by the HIV-1 transcriptional activating protein, Tat, which interacts with cellular transcription factors in a manner that enhances RNA Pol II processivity and

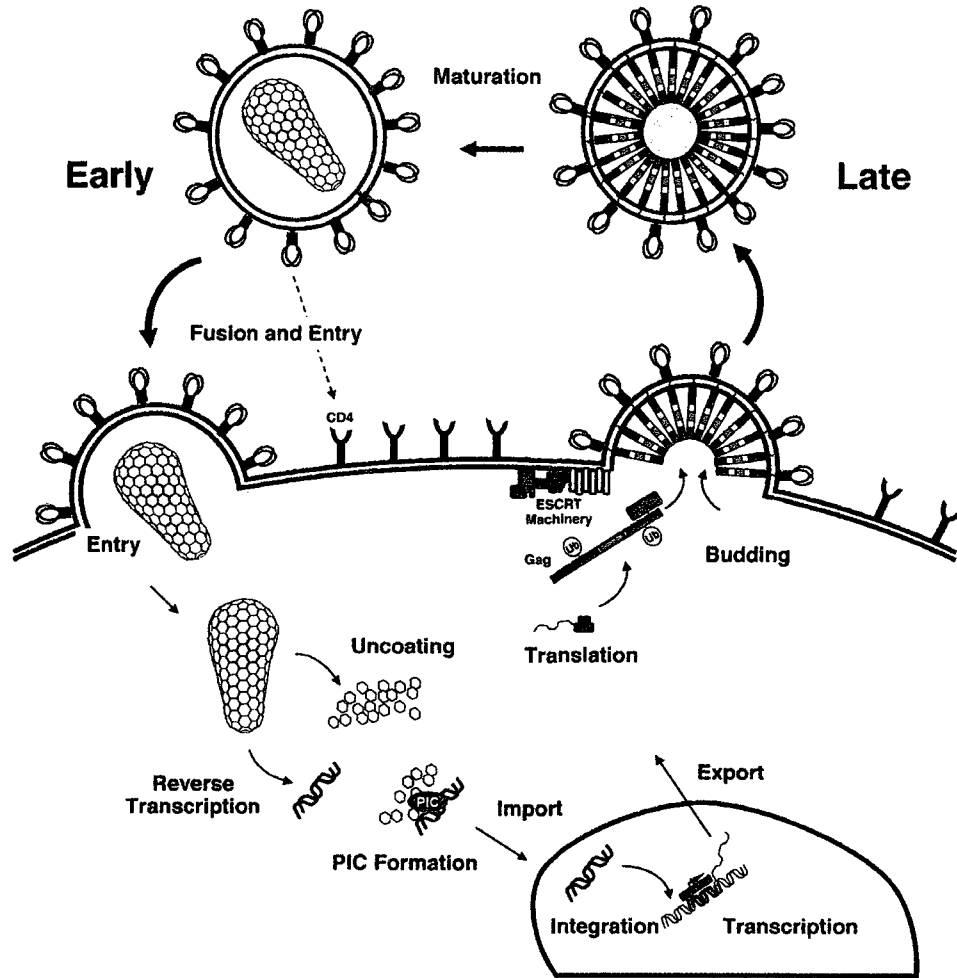


Figure 1.2. The HIV-1 lifecycle. Early stages of retroviral replication (left half of diagram) include fusion, entry, uncoating, reverse transcription, pre integration complex (PIC) formation, nuclear entry and integration. The late stages of replication (right side of diagram) include transcription, nuclear export, translation, assembly, budding and maturation.

increases transcript production by several orders of magnitude (41). The viral protein Rev mediates export of partially spliced and unspliced viral mRNAs out of the nucleus to the cytoplasm where translation of viral proteins takes place (19). The Gag polyprotein is translated on free ribosomes and acquires an N-terminal myristyl group co-translationally. Transcripts containing the *Env* gene, in contrast, are targeted to Endoplasmic Reticulum (ER)-associated ribosomes for translation, glycosylation, and subsequent trafficking to the plasma membrane (19, 30).

Following translation, Gag is targeted to the plasma membrane through a bipartite signal composed of the myristyl group together with PI(4,5)P₂ binding sites in the MA domain (33). Gag multimerization and assembly are coupled with NC-mediated genome encapsidation, and prior to cellular egress immature particles bud through limiting membranes of the host cell (11, 32). This process depends upon Gag recruitment of the ESCRT-I complex through direct interactions with its TSG101 subunit. The ESCRT complexes comprise an endogenous cellular pathway that normally functions in both vesicle formation at the multivesicular body and in cytokinesis (64, 100, 104). HIV-1 usurps much of the ESCRT machinery, with the exception of ESCRT-II and some ESCRT-III subunits, to catalyze final abscission of the vesicle/budding virion and possibly also to deform the host cell's limiting membrane and sort cargo/Gag into forming vesicles (87, 97, 102).

Before the infectious lifecycle is complete, a final maturation step takes place during which Gag is cleaved by the viral protease into three structural

proteins, MA, CA, and NC, resulting in a dramatic rearrangement of the virion (30, 104). In the mature virion, MA forms a matrix shell that is associated with the viral envelope, CA condenses to form the conical capsid shell of the core particle, and NC along with the genome and accessory proteins is encapsided within the core (30). Following maturation, the virion is competent to recognize a new host cell and begin subsequent rounds of infection.

Core Uncoating

In the cytoplasm, the outer capsid shell of the core particle is disassembled in a process termed “uncoating” (49, 69). Uncoating appears to be an essential process, as CA mutations that either destabilize or hyper-stabilize the viral capsid impair reverse transcription, nuclear import and ultimately viral replication (25, 31, 108). Lentiviruses are unique amongst retroviruses in their ability to infect nondividing cells, and proper uncoating is required to support this unique pathogenic characteristic. For example, HIV-1 capsids with core-stability altering mutations (that disrupt uncoating) lose their cell-cycle independence. Furthermore, HIV-1 particles with chimeric, non lentiviral capsids lose their ability to infect nondividing cells (107, 108). The exact location at which uncoating takes place within the cytoplasm is controversial, although several reports suggest that uncoating occurs en route to the nucleus in concert with reverse transcription and preintegration complex (PIC) formation (60, 65). In summary, uncoating is a critical, but poorly understood stage in the retroviral lifecycle.

Reverse Transcription and Preintegration

Complex (PIC) Formation

Like uncoating, reverse transcription takes place in the cytoplasm and ultimately produces a dsDNA copy of the positive sense RNA genome through the action of the reverse transcriptase (RT) enzyme (5, 19). RT is located within a ribonucleoprotein complex termed the Reverse Transcription Complex (RTC) whose major components are genomic RNA and the nucleic acid binding protein, NC (29, 112). Reverse transcription requires a specific host cell derived tRNA^{Lys,3} primer that is annealed to the genome at the primer binding site (PBS) to initiate production of a negative sense DNA strand complementary to the 5' end of the RNA genome (65). The intrinsic RNase H activity of RT then degrades the RNA component of this early transcript, allowing the newly synthesized strand to translocate onto the complementary long terminal repeat (LTR) at the 3' end of the genome and serve as a template for synthesis of full length minus strand DNA (19, 63). As the minus strand DNA is produced, the RNase H activity of RT degrades most of the template RNA, except for a purine rich sequence termed the polypurine tract (PPT), which serves as a primer for synthesis of the positive strand DNA genome. Positive strand DNA synthesis also requires a second strand transfer event. The fully synthesized DNA genome then assembles into the pre integration complex (PIC) (69, 82).

PIC Transport, Nuclear Import and Additional

Early Lifecycle Events

PICs are large nucleoprotein complexes composed of reverse transcribed dsDNA, integrase (IN) and additional viral and host cell proteins including NC and Vpr (3, 16, 25). To access the nucleus, mature PICs navigate the cytoplasm via interactions with both microtubules and the actin cytoskeleton (3, 66). Karyophilic signals within the PIC, in addition to the IN-binding host protein LEDGF/p75, help target the PIC to the nucleus (56, 57). PIC nuclear import is thought to take place via an ATP-dependent process that involves interactions with the nuclear pore complex (15, 34). Following import, IN catalyzes integration of the viral genome into host chromosomal DNA to form the provirus (10, 13, 14). The late stages of replication can then take place, which include transcription, translation, assembly of viral proteins, and budding through the host cell lipid membrane (69).

Summary of Early Events

The temporal relationship between uncoating, reverse transcription, PIC formation and nuclear transport are currently unclear. There are conflicting reports as to whether these events occur simultaneously or sequentially, and whether capsid structure is retained until nuclear import. Limited evidence suggests that reverse transcription may initiate within intact virions (80, 95, 99),

although it is more widely accepted that reverse transcription and uncoating are interdependent processes, and that expansion of the viral nucleic acid trapped within the core during reverse transcription may contribute to uncoating (3, 65, 69, 83, 112). The events and factors that dictate uncoating and the temporally related processes of reverse transcription, PIC formation and nuclear trafficking are of considerable interest and also form the focus of some of the research described here.

Host Cell Factors That Restrict Early

Stages of HIV-1 Replication

Successful completion of early retroviral replication depends upon host cell resources and adherence to the normal program of uncoating, replication, translocation, and integration. Thus, these early replication events represent exploitable targets for inhibiting viral infections. Indeed, it is now clear that host intrinsic immune systems employ a cadre of antiviral proteins, many of which specifically target and inhibit early stages of retroviral replication (9, 101). These proteins, termed restriction factors, presumably evolved owing to the strong evolutionary advantage conferred by an enhanced ability to resist retroviral invasion (9).

Pioneering work on retroviral restriction utilized mouse genetics to identify the *Fv1* gene as a locus that conferred resistance to the Friend Murine Leukemia Virus (MLV) (8, 54, 78, 79, 101). Two major *Fv1* alleles were identified in laboratory mouse strains: *Fv1^b* in Balb/c mice and *Fv1ⁿ* in NIH Swiss mice.

These two alleles were found to confer resistance to N-tropic and B-tropic MLVs, respectively. *Fv1* restriction occurs early in retroviral infection, prior to nuclear entry (46, 110). The viral capsid is the major determinant of *Fv1* antiviral activity, and a single point mutation at CA residue 110 can switch allelic restriction susceptibility (46, 110). Furthermore, viruses deficient in replication, but with *Fv1*-sensitive capsids, can saturate *Fv1* activity (a phenomenon termed abrogation), suggesting that *Fv1* binds incoming capsids (6, 26).

Cell lines from several primate species were subsequently found to possess retroviral restriction activities similar to those of *Fv1*. For example, human cell lines can restrict N-MLV infection and cells from other primates can restrict HIV-1 replication (39, 40, 88, 93). As with *Fv1*, restriction activity in primate cell lines is saturable, occurs prior to nuclear entry, and is dependent on the viral capsid (20, 38, 72). However, unlike *Fv1* restriction, primate cell restriction typically blocks the accumulation of reverse transcripts (rather than blocking nuclear import).

TRIM5 α

In 2004, Stremlau and colleagues identified TRIM5 α as the key cellular factor responsible for HIV-1 restriction in rhesus macaque cells (90, 91).

Subsequent work revealed that the orthologous human TRIM5 α protein restricted N-tropic MLV replication and that a unique TRIM5-cyclophilin-A chimera was responsible for resistance to HIV-1 infection in owl monkeys (7, 75). It has since become apparent that TRIM5 α is a principal determinant of retroviral species

tropism and that TRIM5 α specificity can be attributed to sequence variations that result in differential abilities of TRIM5 α homologs to recognize retroviral capsids (9, 68, 90, 94). Under normal restrictive conditions, TRIM5 α blocks the accumulation of retroviral reverse transcripts, and accelerates the rate at which viral capsids dissociate from high molecular weight complexes into lower molecular weight subunits (Figure 1.3) (74, 90, 91).

Like other tripartite motif (TRIM) family members, TRIM5 α contains RING, B-box, coiled-coil, and B30.2/SPRY domains, each of which contributes to restriction activity (70). The RING domain of TRIM5 α has intrinsic E3 ubiquitin ligase activity, which is important both for autoubiquitylation and for TRIM5 α turnover *in vivo* (24, 43, 106, 109). The E3 ubiquitin ligase activity partially contributes to restriction (43, 73, 90), but the precise function of ubiquitylation is not yet fully understood.

Proteasome activity is not strictly required for TRIM5 α antiviral activity *per se* (24, 73), but proteasome inhibitors can alter the normal progression of TRIM5 α restriction by allowing reverse transcripts to accumulate and by impairing accelerated dissociation of intact viral capsids (2, 22, 105). Furthermore, proteasome-dependent degradation of TRIM5 α accompanies restriction of incoming capsids, which again supports the idea that the proteasome contributes to the mechanism of restriction.

B-Box-2 domains are zinc coordinating motifs that are structurally related to RING domains and are unique to tripartite motif family proteins (51, 59, 61).

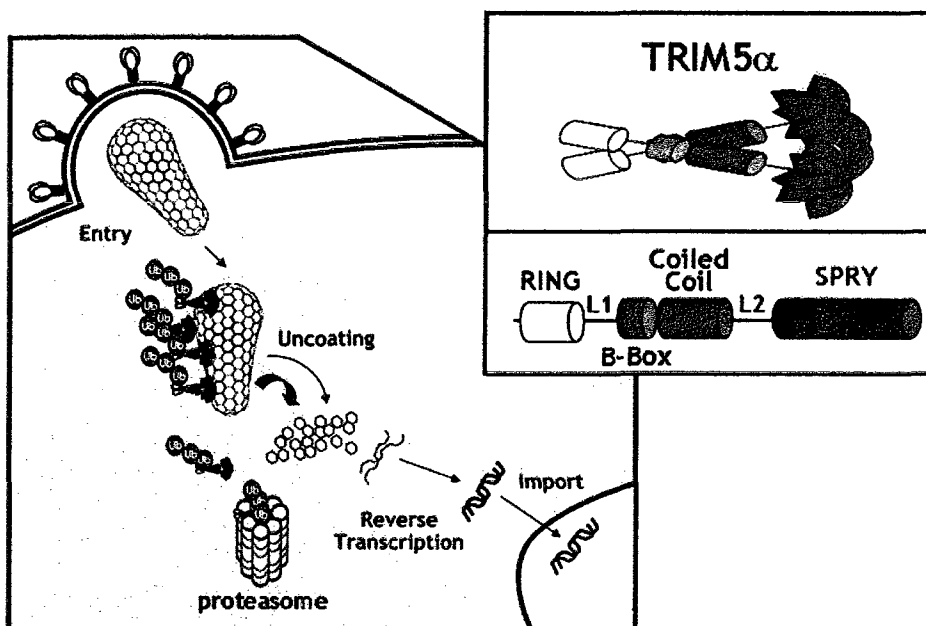


Figure 1.3. Possible mechanisms of TRIM5 α restriction. Current models hold that TRIM5 α restriction probably involves an initial capsid binding event that results in TRIM5 α autoubiquitylation and subsequent proteasomal degradation, accelerated dissociation of the capsid into smaller subunits, and a block in reverse transcript production. In the presence of proteasome inhibitors, however, reverse transcripts are produced, the capsid does not prematurely dissociate, and restriction takes place at a later stage, prior to nuclear entry.

TRIM proteins may be equipped with B-box-1, B-box-2 (two distinct B-box variants) or tandem B-box domains. Assigned B-box functions include protein oligomerization, higher-order assembly, intracellular localization and protein-protein interactions (61). The B-box-2 domain of TRIM5 α plays an essential but still not well understood role in restriction activity, as mutations in this domain can abolish restriction, influence protein turnover, and affect subcellular localization (23). A recent report suggests that the B-box-2 domain contributes to the higher-

order assembly of TRIM5 proteins, presumably on retroviral capsid templates, and that TRIM5 α assembly is important for inducing premature capsid dissociation and inhibiting reverse transcript accumulation (51).

The coiled-coil (CC) and adjacent linker 2 (L2) regions of TRIM5 α contribute to protein oligomerization and are important for efficient capsid binding and restriction (44, 62). Early studies that examined the SDS-PAGE mobilities of crosslinked TRIM5 α proteins suggested a trimeric oligomeric state (62). However, my subsequent studies of pure recombinant TRIM5 proteins using more rigorous biophysical techniques demonstrated that TRIM5 α (and likely other TRIM proteins) are actually dimeric, but exhibit aberrant SDS-PAGE mobilities when crosslinked (Chapter 2) (47, 48).

The C-terminal B30.2/SPRY domain of TRIM5 α is essential for viral capsid recognition. This domain is predicted to share structural homology with immunoglobulin domains, and is the key determinant of antiviral specificity (42, 70, 71, 73, 89-91, 103, 111). Several studies indicate that TRIM5 α proteins recognize the hexameric lattice of the viral capsid rather than individual CA subunits (12, 35-37, 45, 50, 51). Several motifs within the SPRY domain exhibit evidence of strong positive selection and display pronounced variability between species, suggesting that they are key determinants of retroviral capsid recognition (55, 71, 84, 85, 89, 92). In particular, variable region 1 (V1: residues 323-350 in rhesus TRIM5 α) is critical both for efficient restriction and for capsid binding, and a single amino acid alteration at position 332 of the V1 loop allows human TRIM5 α to bind HIV-1 capsids and inhibit HIV-1 replication (52, 89, 111).

Assays to Examine Early Retroviral Replication and TRIM5 α Restriction

The observations that TRIM5 α binds the viral capsid and accelerates capsid dissociation suggest that uncoating is the stage of the viral lifecycle that is most likely disrupted during restriction. However, despite extensive work conducted since the discovery of TRIM5 α , the mechanism by which initial capsid binding events ultimately inhibit reverse transcription is still not fully understood.

The technical challenges involved in studying early stages of retroviral replication and TRIM5 α restriction present a significant barrier to obtaining a comprehensive mechanistic understanding of these processes. One such challenge arises because, even at high multiplicities of infection (MOI), very few cores enter the host cell cytoplasm, and even fewer go on to complete successful replication (58). Moreover, most of the retroviral particles in a typical inoculum are noninfectious, and these particles can contribute substantial background in any bulk measurement of viral replication. Indeed, it has been estimated that only between 1 in 10 and 1 in 60,000 HIV-1 particles are capable of infection (69, 77). Finally, there are limitations in the available assays for probing the different stages early retroviral replication. For example, recently developed fluorescence live-cell microscopy assays represent a significant step forward, but are still in early stages of development and are limited by the availability of relevant fluorescent probes (17, 108).

Cell-free assays represent an alternative approach for dissecting the early events of retroviral replication and TRIM5 α restriction, and have the potential to overcome some of the limitations of cell-based assays. The first such *in vitro* system was developed for the avian sarcoma and leukocytosis virus subgroup-A (ASLV-A) and was based on arresting pH-dependent virion fusion intermediates within endosomes, purifying the endosomes, adding them to cell-free extracts, and then restarting virion fusion by lowering the pH (67). This work demonstrated a requirement for cellular factors and ATP hydrolysis in retroviral DNA synthesis (67). A subsequent study utilized an alternative approach to demonstrate that soluble cell extracts from activated, but not quiescent CD4+ lymphocytes could induce the dissociation of membrane-stripped HIV-1 capsids and stimulate the formation of reverse-transcription products (4). More recently, an *in vitro* system used detergent-permeabilized HIV-1 virions to demonstrate that soluble factors present in extracts from a variety of human cell types modestly enhance the production of complete double-stranded DNA transcripts (98). Together, the above reports indicate that cell extracts can influence reverse transcript production and demonstrate the potential utility of *in vitro* assays for studying early lifecycle events and TRIM5 α retroviral restriction. However, all of these assays utilized crude viral inputs and none has gained widespread usage.

In Chapter 3, I describe the development of a novel *in vitro* assay designed to examine the early events of lentiviral replication and TRIM5 α restriction. In this system, purified EIAV core particles are incubated with cell extracts, dNTPs, and an ATP regeneration system. Reverse transcript

production is then quantified by real-time PCR, while capsid uncoating/dissociation is monitored using ultracentrifugation to separate dissociated CA monomers from intact capsids. We have used this system to show that purified EIAV cores undergo ATP and extract-dependent reverse transcription and uncoating. In addition, we have extended our assay to examine TRIM5 α restriction and demonstrate that in extracts, both cell-expressed and recombinant TRIM5 α molecules are necessary and sufficient to recapitulate restriction *in vitro*.

Research Overview: Retroviral Replication and TRIM5 α Restriction

TRIM5 α restriction and early retroviral replication are essential components of HIV-1 pathogenesis and innate immune retroviral defense. Characterization of these processes offers the potential to both elucidate the mechanistic details of these fundamental events and benefit human health.

The research described in this dissertation addresses both early and late stages of retroviral replication, but with a principal focus on TRIM5 α restriction and other early events in HIV-1 replication. Chapter 2 reports the development of systems to express, purify and characterize recombinant TRIM5 proteins. Chapter 3 describes my work examining the role of the ESCRT-II complex in viral release and MVB vesicle formation. Chapter 4 describes a study in which I collaborated to examine the structure and function of a novel ubiquitin binding domain present in the ESCRT-II protein, EAP45. Chapter 5 describes a study in

which I collaborated to examine the role of the ESCRT machinery in the down regulation of the iron export protein, Ferroportin. Chapter 6 reports the structural basis for ESCRT-III protein autoinhibition, a study for which I performed electron microscopy-based analyses. Finally, Chapter 7 summarizes my research, discusses its relevance to the understanding retroviral replication, and reflects on future directions in the field.

References

1. **Alkhatib, G., C. Combadiere, C. C. Broder, Y. Feng, P. E. Kennedy, P. M. Murphy, and E. A. Berger.** 1996. CC CKR5: a RANTES, MIP-1alpha, MIP-1beta receptor as a fusion cofactor for macrophage-tropic HIV-1. *Science* **272**:1955-8.
2. **Anderson, J. L., E. M. Campbell, X. Wu, N. Vandegraaff, A. Engelman, and T. J. Hope.** 2006. Proteasome inhibition reveals that a functional preintegration complex intermediate can be generated during restriction by diverse TRIM5 proteins. *J Virol* **80**:9754-60.
3. **Anderson, J. L., and T. J. Hope.** 2005. Intracellular trafficking of retroviral vectors: obstacles and advances. *Gene Ther* **12**:1667-78.
4. **Auewarakul, P., P. Wacharapornin, S. Srichatrapimuk, S. Chutipongtanate, and P. Puthavathana.** 2005. Uncoating of HIV-1 requires cellular activation. *Virology* **337**:93-101.
5. **Baltimore, D.** 1970. RNA-dependent DNA polymerase in virions of RNA tumour viruses. *Nature* **226**:1209-11.
6. **Bassin, R. H., G. Duran-Troise, B. I. Gerwin, and A. Rein.** 1978. Abrogation of Fv-1b restriction with murine leukemia viruses inactivated by heat or by gamma irradiation. *J Virol* **26**:306-15.
7. **Berthoux, L., S. Sebastian, E. Sokolskaja, and J. Luban.** 2005. Cyclophilin A is required for TRIM5{alpha}-mediated resistance to HIV-1 in Old World monkey cells. *Proc Natl Acad Sci U S A* **102**:14849-53.
8. **Best, S., P. Le Tissier, G. Towers, and J. P. Stoye.** 1996. Positional cloning of the mouse retrovirus restriction gene Fv1. *Nature* **382**:826-9.
9. **Bieniasz, P. D.** 2004. Intrinsic immunity: a front-line defense against viral attack. *Nat Immunol* **5**:1109-15.
10. **Bowerman, B., P. O. Brown, J. M. Bishop, and H. E. Varmus.** 1989. A nucleoprotein complex mediates the integration of retroviral DNA. *Genes Dev* **3**:469-78.
11. **Briggs, J. A., M. N. Simon, I. Gross, H. G. Krausslich, S. D. Fuller, V. M. Vogt, and M. C. Johnson.** 2004. The stoichiometry of Gag protein in HIV-1. *Nat Struct Mol Biol* **11**:672-5.

12. **Briggs, J. A., T. Wilk, R. Welker, H. G. Krausslich, and S. D. Fuller.** 2003. Structural organization of authentic, mature HIV-1 virions and cores. *Embo J* **22**:1707-15.
13. **Brown, P. O., B. Bowerman, H. E. Varmus, and J. M. Bishop.** 1987. Correct integration of retroviral DNA in vitro. *Cell* **49**:347-56.
14. **Brown, P. O., B. Bowerman, H. E. Varmus, and J. M. Bishop.** 1989. Retroviral integration: structure of the initial covalent product and its precursor, and a role for the viral IN protein. *Proc Natl Acad Sci U S A* **86**:2525-9.
15. **Bukrinsky, M. I., N. Sharova, M. P. Dempsey, T. L. Stanwick, A. G. Bukrinskaya, S. Haggerty, and M. Stevenson.** 1992. Active nuclear import of human immunodeficiency virus type 1 preintegration complexes. *Proc Natl Acad Sci U S A* **89**:6580-4.
16. **Bukrinsky, M. I., N. Sharova, T. L. McDonald, T. Pushkarskaya, W. G. Tarpley, and M. Stevenson.** 1993. Association of integrase, matrix, and reverse transcriptase antigens of human immunodeficiency virus type 1 with viral nucleic acids following acute infection. *Proc Natl Acad Sci U S A* **90**:6125-9.
17. **Campbell, E. M., O. Perez, M. Melar, and T. J. Hope.** 2007. Labeling HIV-1 virions with two fluorescent proteins allows identification of virions that have productively entered the target cell. *Virology* **360**:286-93.
18. **Coffin, J. M., S. H. Hughes, and H. Varmus.** 1997. *Retroviruses*. Cold Spring Harbor Laboratory Press, Plainview, N.Y.
19. **Coffin, J. M., S. H. Hughes, and H. E. Varmus.** 1997. *Retroviruses*. Cold Spring Harbor Press, Plainview, New York.
20. **Cowan, S., T. Hatzioannou, T. Cunningham, M. A. Muesing, H. G. Gottlinger, and P. D. Bieniasz.** 2002. Cellular inhibitors with Fv1-like activity restrict human and simian immunodeficiency virus tropism. *Proc Natl Acad Sci U S A* **99**:11914-9.
21. **Deng, H., R. Liu, W. Ellmeier, S. Choe, D. Unutmaz, M. Burkhart, P. Di Marzio, S. Marmon, R. E. Sutton, C. M. Hill, C. B. Davis, S. C. Peiper, T. J. Schall, D. R. Littman, and N. R. Landau.** 1996. Identification of a major co-receptor for primary isolates of HIV-1. *Nature* **381**:661-6.
22. **Diaz-Griffero, F., A. Kar, M. Lee, M. Stremlau, E. Poeschla, and J. Sodroski.** 2007. Comparative requirements for the restriction of retrovirus infection by TRIM5alpha and TRIMCyp. *Virology* **369**:400-10.

23. **Diaz-Griffero, F., A. Kar, M. Perron, S. H. Xiang, H. Javanbakht, X. Li, and J. Sodroski.** 2007. Modulation of retroviral restriction and proteasome inhibitor-resistant turnover by changes in the TRIM5alpha B-box 2 domain. *J Virol* **81**:10362-78.
24. **Diaz-Griffero, F., X. Li, H. Javanbakht, B. Song, S. Welikala, M. Stremlau, and J. Sodroski.** 2006. Rapid turnover and polyubiquitylation of the retroviral restriction factor TRIM5. *Virology* **349**:300-15.
25. **Dismuke, D. J., and C. Aiken.** 2006. Evidence for a functional link between uncoating of the human immunodeficiency virus type 1 core and nuclear import of the viral preintegration complex. *J Virol* **80**:3712-20.
26. **Duran-Troise, G., R. H. Bassin, A. Rein, and B. I. Gerwin.** 1977. Loss of Fv-1 restriction in Balb/3T3 cells following infection with a single N tropic murine leukemia virus particle. *Cell* **10**:479-88.
27. **Eckert, D. M., and P. S. Kim.** 2001. Mechanisms of viral membrane fusion and its inhibition. *Annu Rev Biochem* **70**:777-810.
28. **Eckert, D. M., V. N. Malashkevich, L. H. Hong, P. A. Carr, and P. S. Kim.** 1999. Inhibiting HIV-1 entry: discovery of D-peptide inhibitors that target the gp41 coiled-coil pocket. *Cell* **99**:103-15.
29. **Fassati, A., and S. P. Goff.** 2001. Characterization of intracellular reverse transcription complexes of human immunodeficiency virus type 1. *J Virol* **75**:3626-35.
30. **Fields, B. N., D. M. Knipe, and P. M. Howley.** 1996. *Fields Virology*, 3rd Edition. Lippincott Williams and Wilkins, Philadelphia.
31. **Forshey, B. M., U. von Schwedler, W. I. Sundquist, and C. Aiken.** 2002. Formation of a human immunodeficiency virus type 1 core of optimal stability is crucial for viral replication. *J Virol* **76**:5667-77.
32. **Freed, E. O.** 1998. HIV-1 gag proteins: diverse functions in the virus life cycle. *Virology* **251**:1-15.
33. **Freed, E. O.** 2006. HIV-1 Gag: flipped out for PI(4,5)P(2). *Proc Natl Acad Sci U S A* **103**:11101-2.
34. **Fried, H., and U. Kutay.** 2003. Nucleocytoplasmic transport: taking an inventory. *Cell Mol Life Sci* **60**:1659-88.

35. **Ganser, B. K., S. Li, V. Y. Klishko, J. T. Finch, and W. I. Sundquist.** 1999. Assembly and analysis of conical models for the HIV-1 core. *Science* **283**:80-3.
36. **Ganser-Pornillos, B. K., A. Cheng, and M. Yeager.** 2007. Structure of full-length HIV-1 CA: a model for the mature capsid lattice. *Cell* **131**:70-9.
37. **Ganser-Pornillos, B. K., M. Yeager, and W. I. Sundquist.** 2008. The structural biology of HIV assembly. *Curr Opin Struct Biol* **18**:203-17.
38. **Hatzioannou, T., S. Cowan, S. P. Goff, P. D. Bieniasz, and G. J. Towers.** 2003. Restriction of multiple divergent retroviruses by Lv1 and Ref1. *EMBO J* **22**:385-94.
39. **Himathongkham, S., and P. A. Luciw.** 1996. Restriction of HIV-1 (subtype B) replication at the entry step in rhesus macaque cells. *Virology* **219**:485-8.
40. **Hofmann, W., D. Schubert, J. LaBonte, L. Munson, S. Gibson, J. Scammell, P. Ferrigno, and J. Sodroski.** 1999. Species-specific, postentry barriers to primate immunodeficiency virus infection. *J Virol* **73**:10020-8.
41. **Isel, C., and J. Karn.** 1999. Direct evidence that HIV-1 Tat stimulates RNA polymerase II carboxyl-terminal domain hyperphosphorylation during transcriptional elongation. *J Mol Biol* **290**:929-41.
42. **James, L. C., A. H. Keeble, Z. Khan, D. A. Rhodes, and J. Trowsdale.** 2007. Structural basis for PRYSPRY-mediated tripartite motif (TRIM) protein function. *Proc Natl Acad Sci U S A* **104**:6200-5.
43. **Javanbakht, H., F. Diaz-Griffero, M. Stremlau, Z. Si, and J. Sodroski.** 2005. The contribution of RING and B-box 2 domains to retroviral restriction mediated by monkey TRIM5alpha. *J Biol Chem* **280**:26933-40.
44. **Javanbakht, H., W. Yuan, D. F. Yeung, B. Song, F. Diaz-Griffero, Y. Li, X. Li, M. Stremlau, and J. Sodroski.** 2006. Characterization of TRIM5alpha trimerization and its contribution to human immunodeficiency virus capsid binding. *Virology* **353**:234-46.
45. **Jin, Z., L. Jin, D. L. Peterson, and C. L. Lawson.** 1999. Model for lentivirus capsid core assembly based on crystal dimers of EIAV p26. *J Mol Biol* **286**:83-93.
46. **Jolicoeur, P., and D. Baltimore.** 1976. Effect of Fv-1 gene product on synthesis of N-tropic and B-tropic murine leukemia viral RNA. *Cell* **7**:33-9.

47. **Kar, A. K., F. Diaz-Griffero, Y. Li, X. Li, and J. Sodroski.** 2008. Biochemical and biophysical characterization of a chimeric TRIM21-TRIM5alpha protein. *J Virol* **82**:11669-81.
48. **Langelier, C. R., V. Sandrin, D. M. Eckert, D. E. Christensen, V. Chandrasekaran, S. L. Alam, C. Aiken, J. C. Olsen, A. K. Kar, J. G. Sodroski, and W. I. Sundquist.** 2008. Biochemical characterization of a recombinant TRIM5alpha protein that restricts human immunodeficiency virus type 1 replication. *J Virol* **82**:11682-94.
49. **Lehmann-Che, J., and A. Saib.** 2004. Early stages of HIV replication: how to hijack cellular functions for a successful infection. *AIDS Rev* **6**:199-207.
50. **Li, S., C. P. Hill, W. I. Sundquist, and J. T. Finch.** 2000. Image reconstructions of helical assemblies of the HIV-1 CA protein. *Nature* **407**:409-13.
51. **Li, X., and J. Sodroski.** 2008. The TRIM5alpha B-box 2 domain promotes cooperative binding to the retroviral capsid by mediating higher-order self-association. *J Virol* **82**:11495-502.
52. **Li, Y., X. Li, M. Stremlau, M. Lee, and J. Sodroski.** 2006. Removal of arginine 332 allows human TRIM5alpha to bind human immunodeficiency virus capsids and to restrict infection. *J Virol* **80**:6738-44.
53. **Lifson, J. D., M. B. Feinberg, G. R. Reyes, L. Rabin, B. Banapour, S. Chakrabarti, B. Moss, F. Wong-Staal, K. S. Steimer, and E. G. Engleman.** 1986. Induction of CD4-dependent cell fusion by the HTLV-III/LAV envelope glycoprotein. *Nature* **323**:725-8.
54. **Lilly, F.** 1967. Susceptibility to two strains of Friend leukemia virus in mice. *Science* **155**:461-2.
55. **Liu, H. L., Y. Q. Wang, C. H. Liao, Y. Q. Kuang, Y. T. Zheng, and B. Su.** 2005. Adaptive evolution of primate TRIM5alpha, a gene restricting HIV-1 infection. *Gene* **362**:109-16.
56. **Llano, M., M. Vanegas, O. Fregoso, D. Saenz, S. Chung, M. Peretz, and E. M. Poeschla.** 2004. LEDGF/p75 determines cellular trafficking of diverse lentiviral but not murine oncoretroviral integrase proteins and is a component of functional lentiviral preintegration complexes. *J Virol* **78**:9524-37.

57. **Maertens, G., P. Cherepanov, W. Pluymers, K. Busschots, E. De Clercq, Z. Debyser, and Y. Engelborghs.** 2003. LEDGF/p75 is essential for nuclear and chromosomal targeting of HIV-1 integrase in human cells. *J Biol Chem* **278**:33528-39.
58. **Marechal, V., F. Clavel, J. M. Heard, and O. Schwartz.** 1998. Cytosolic Gag p24 as an index of productive entry of human immunodeficiency virus type 1. *J Virol* **72**:2208-12.
59. **Massiah, M. A., J. A. Matts, K. M. Short, B. N. Simmons, S. Singireddy, Z. Yi, and T. C. Cox.** 2007. Solution structure of the MID1 B-box2 CHC(D/C)C(2)H(2) zinc-binding domain: insights into an evolutionarily conserved RING fold. *J Mol Biol* **369**:1-10.
60. **McDonald, D., M. A. Vodicka, G. Lucero, T. M. Svitkina, G. G. Borisy, M. Emerman, and T. J. Hope.** 2002. Visualization of the intracellular behavior of HIV in living cells. *J Cell Biol* **159**:441-52.
61. **Meroni, G., and G. Diez-Roux.** 2005. TRIM/RBCC, a novel class of 'single protein RING finger' E3 ubiquitin ligases. *Bioessays* **27**:1147-57.
62. **Mische, C. C., H. Javanbakht, B. Song, F. Diaz-Griffero, M. Stremlau, B. Strack, Z. Si, and J. Sodroski.** 2005. Retroviral restriction factor TRIM5alpha is a trimer. *J Virol* **79**:14446-50.
63. **Mitra, S. W., S. Goff, E. Gilboa, and D. Baltimore.** 1979. Synthesis of a 600-nucleotide-long plus-strand DNA by virions of Moloney murine leukemia virus. *Proc Natl Acad Sci U S A* **76**:4355-9.
64. **Morita, E., and W. I. Sundquist.** 2004. Retrovirus budding. *Annu Rev Cell Dev Biol* **20**:395-425.
65. **Mougel, M., L. Houzet, and J. L. Darlix.** 2009. When is it time for reverse transcription to start and go? *Retrovirology* **6**:24.
66. **Naghavi, M. H., and S. P. Goff.** 2007. Retroviral proteins that interact with the host cell cytoskeleton. *Curr Opin Immunol* **19**:402-7.
67. **Narayan, S., and J. A. Young.** 2004. Reconstitution of retroviral fusion and uncoating in a cell-free system. *Proc Natl Acad Sci U S A* **101**:7721-6.
68. **Nisole, S., and A. Saib.** 2004. Early steps of retrovirus replicative cycle. *Retrovirology* **1**:9.
69. **Nisole, S., and A. Saib.** 2004. Early steps of retrovirus replicative cycle. *Retrovirology* **1**:9.

70. **Nisole, S., J. P. Stoye, and A. Saib.** 2005. TRIM family proteins: retroviral restriction and antiviral defence. *Nat Rev Microbiol* **3**:799-808.
71. **Ohkura, S., M. W. Yap, T. Sheldon, and J. P. Stoye.** 2006. All three variable regions of the TRIM5alpha B30.2 domain can contribute to the specificity of retrovirus restriction. *J Virol* **80**:8554-65.
72. **Owens, C. M., P. C. Yang, H. Gottlinger, and J. Sodroski.** 2003. Human and simian immunodeficiency virus capsid proteins are major viral determinants of early, postentry replication blocks in simian cells. *J Virol* **77**:726-31.
73. **Perez-Caballero, D., T. Hatzioannou, A. Yang, S. Cowan, and P. D. Bieniasz.** 2005. Human tripartite motif 5alpha domains responsible for retrovirus restriction activity and specificity. *J Virol* **79**:8969-78.
74. **Perron, M. J., M. Stremlau, M. Lee, H. Javanbakht, B. Song, and J. Sodroski.** 2007. The human TRIM5alpha restriction factor mediates accelerated uncoating of the N-tropic murine leukemia virus capsid. *J Virol* **81**:2138-48.
75. **Perron, M. J., M. Stremlau, B. Song, W. Ulm, R. C. Mulligan, and J. Sodroski.** 2004. TRIM5alpha mediates the postentry block to N-tropic murine leukemia viruses in human cells. *Proc Natl Acad Sci U S A* **101**:11827-32.
76. **Philpott, S. M.** 2003. HIV-1 coreceptor usage, transmission, and disease progression. *Curr HIV Res* **1**:217-27.
77. **Piatak, M., Jr., M. S. Saag, L. C. Yang, S. J. Clark, J. C. Kappes, K. C. Luk, B. H. Hahn, G. M. Shaw, and J. D. Lifson.** 1993. High levels of HIV-1 in plasma during all stages of infection determined by competitive PCR. *Science* **259**:1749-54.
78. **Pincus, T., J. W. Hartley, and W. P. Rowe.** 1971. A major genetic locus affecting resistance to infection with murine leukemia viruses. I. Tissue culture studies of naturally occurring viruses. *J Exp Med* **133**:1219-33.
79. **Pincus, T., J. W. Hartley, and W. P. Rowe.** 1975. A major genetic locus affecting resistance to infection with murine leukemia viruses. IV. Dose-response relationships in Fv-1-sensitive and resistant cell cultures. *Virology* **65**:333-42.
80. **Raffa, S., B. Albiani, A. Allegritti, M. Fontana, C. Loria, P. Manzi, S. Sottili, and M. Grassi.** 1997. [The treatment of chronic viral hepatitis with

- recombinant alpha-2 interferon: meta analysis and clinical contribution]. *Clin Ter* **148**:421-35.
81. **Root, M. J., M. S. Kay, and P. S. Kim.** 2001. Protein design of an HIV-1 entry inhibitor. *Science* **291**:884-8.
 82. **Roth, M. J., P. L. Schwartzberg, and S. P. Goff.** 1989. Structure of the termini of DNA intermediates in the integration of retroviral DNA: dependence on IN function and terminal DNA sequence. *Cell* **58**:47-54.
 83. **Saib, A.** 2004. [Viral hijacking of cell functions]. *Pathol Biol (Paris)* **52**:58-9.
 84. **Sawyer, S. L., M. Emerman, and H. S. Malik.** 2007. Discordant evolution of the adjacent antiretroviral genes TRIM22 and TRIM5 in mammals. *PLoS Pathog* **3**:e197.
 85. **Sawyer, S. L., L. I. Wu, M. Emerman, and H. S. Malik.** 2005. Positive selection of primate TRIM5alpha identifies a critical species-specific retroviral restriction domain. *Proc Natl Acad Sci U S A* **102**:2832-7.
 86. **Scherer, E., D. Douek, and A. McMichael.** 2008. 25 years of HIV research on virology, virus restriction, immunopathogenesis, genes and vaccines. *Clin Exp Immunol* **154**:6-14.
 87. **Scott, A., H. Y. Chung, M. Gonciarz-Swiatek, G. C. Hill, F. G. Whitby, J. Gaspar, J. M. Holton, R. Viswanathan, S. Ghaffarian, C. P. Hill, and W. I. Sundquist.** 2005. Structural and mechanistic studies of VPS4 proteins. *EMBO J* **24**:3658-69.
 88. **Shibata, R., H. Sakai, M. Kawamura, K. Tokunaga, and A. Adachi.** 1995. Early replication block of human immunodeficiency virus type 1 in monkey cells. *J Gen Virol* **76 (Pt 11)**:2723-30.
 89. **Song, B., B. Gold, C. O'Huigin, H. Javanbakht, X. Li, M. Stremlau, C. Winkler, M. Dean, and J. Sodroski.** 2005. The B30.2(SPRY) domain of the retroviral restriction factor TRIM5alpha exhibits lineage-specific length and sequence variation in primates. *J Virol* **79**:6111-21.
 90. **Stremlau, M., C. M. Owens, M. J. Perron, M. Kiessling, P. Autissier, and J. Sodroski.** 2004. The cytoplasmic body component TRIM5alpha restricts HIV-1 infection in Old World monkeys. *Nature* **427**:848-53.
 91. **Stremlau, M., M. Perron, M. Lee, Y. Li, B. Song, H. Javanbakht, F. Diaz-Griffero, D. J. Anderson, W. I. Sundquist, and J. Sodroski.** 2006.

- Specific recognition and accelerated uncoating of retroviral capsids by the TRIM5alpha restriction factor. *Proc Natl Acad Sci U S A* **103**:5514-9.
92. **Stremlau, M., M. Perron, S. Welikala, and J. Sodroski.** 2005. Species-specific variation in the B30.2(SPRY) domain of TRIM5alpha determines the potency of human immunodeficiency virus restriction. *J Virol* **79**:3139-45.
 93. **Towers, G., M. Bock, S. Martin, Y. Takeuchi, J. P. Stoye, and O. Danos.** 2000. A conserved mechanism of retrovirus restriction in mammals. *Proc Natl Acad Sci U S A* **97**:12295-9.
 94. **Towers, G. J.** 2007. The control of viral infection by tripartite motif proteins and cyclophilin A. *Retrovirology* **4**:40.
 95. **Trono, D.** 1992. Partial reverse transcripts in virions from human immunodeficiency and murine leukemia viruses. *J Virol* **66**:4893-900.
 96. **UNAIDS/WHO.** 2007. UNAIDS/WHO global AIDS statistics.
 97. **von Schwedler, U. K., M. Stuchell, B. Muller, D. M. Ward, H. Y. Chung, E. Morita, H. E. Wang, T. Davis, G. P. He, D. M. Cimbora, A. Scott, H. G. Krausslich, J. Kaplan, S. G. Morham, and W. I. Sundquist.** 2003. The protein network of HIV budding. *Cell* **114**:701-13.
 98. **Warrilow, D., L. Meredith, A. Davis, C. Burrell, P. Li, and D. Harrich.** 2008. Cell factors stimulate human immunodeficiency virus type 1 reverse transcription in vitro. *J Virol* **82**:1425-37.
 99. **Warrilow, D., D. Stenzel, and D. Harrich.** 2007. Isolated HIV-1 core is active for reverse transcription. *Retrovirology* **4**:77.
 100. **Williams, R. L., and S. Urbe.** 2007. The emerging shape of the ESCRT machinery. *Nat Rev Mol Cell Biol* **8**:355-68.
 101. **Wolf, D., and S. P. Goff.** 2008. Host restriction factors blocking retroviral replication. *Annu Rev Genet* **42**:143-63.
 102. **Wollert, T., C. Wunder, J. Lippincott-Schwartz, and J. H. Hurley.** 2009. Membrane scission by the ESCRT-III complex. *Nature* **458**:172-7.
 103. **Woo, J. S., H. Y. Suh, S. Y. Park, and B. H. Oh.** 2006. Structural basis for protein recognition by B30.2/SPRY domains. *Mol Cell* **24**:967-76.
 104. **Wright, E. R., J. B. Schooler, H. J. Ding, C. Kieffer, C. Fillmore, W. I. Sundquist, and G. J. Jensen.** 2007. Electron cryotomography of

immature HIV-1 virions reveals the structure of the CA and SP1 Gag shells. *EMBO J* **26**:2218-26.

105. **Wu, X., J. L. Anderson, E. M. Campbell, A. M. Joseph, and T. J. Hope.** 2006. Proteasome inhibitors uncouple rhesus TRIM5alpha restriction of HIV-1 reverse transcription and infection. *Proc Natl Acad Sci U S A* **103**:7465-70.
106. **Xu, L., L. Yang, P. K. Moitra, K. Hashimoto, P. Rallabhandi, S. Kaul, G. Meroni, J. P. Jensen, A. M. Weissman, and P. D'Arpa.** 2003. BTBD1 and BTBD2 colocalize to cytoplasmic bodies with the RBCC/tripartite motif protein, TRIM5delta. *Exp Cell Res* **288**:84-93.
107. **Yamashita, M., and M. Emerman.** 2004. Capsid is a dominant determinant of retrovirus infectivity in nondividing cells. *J Virol* **78**:5670-8.
108. **Yamashita, M., O. Perez, T. J. Hope, and M. Emerman.** 2007. Evidence for direct involvement of the capsid protein in HIV infection of nondividing cells. *PLoS Pathog* **3**:1502-10.
109. **Yamauchi, K., K. Wada, K. Tanji, M. Tanaka, and T. Kamitani.** 2008. Ubiquitination of E3 ubiquitin ligase TRIM5 alpha and its potential role. *Febs J* **275**:1540-55.
110. **Yang, W. K., J. O. Kiggans, D. M. Yang, C. Y. Ou, R. W. Tennant, A. Brown, and R. H. Bassin.** 1980. Synthesis and circularization of N- and B-tropic retroviral DNA Fv-1 permissive and restrictive mouse cells. *Proc Natl Acad Sci U S A* **77**:2994-8.
111. **Yap, M. W., S. Nisole, and J. P. Stoye.** 2005. A single amino acid change in the SPRY domain of human Trim5alpha leads to HIV-1 restriction. *Curr Biol* **15**:73-8.
112. **Zhang, H., G. Dornadula, J. Orenstein, and R. J. Pomerantz.** 2000. Morphologic changes in human immunodeficiency virus type 1 virions secondary to intravirion reverse transcription: evidence indicating that reverse transcription may not take place within the intact viral core. *J Hum Virol* **3**:165-72.

CHAPTER 2

BIOCHEMICAL CHARACTERIZATION OF A RECOMBINANT TRIM5 α

PROTEIN THAT RESTRICTS HUMAN IMMUNODEFICIENCY

VIRUS TYPE 1 REPLICATION

Biochemical Characterization of a Recombinant TRIM5 α Protein That Restricts Human Immunodeficiency Virus Type 1 Replication[†]

Charles R. Langelier,¹ Virginie Sandrin,¹ Debra M. Eckert,¹ Devin E. Christensen,¹
 Viswanathan Chandrasekaran,¹ Steven L. Alam,¹ Christopher Aiken,² John C. Olsen,³
 Alak Kanti Kar,⁴ Joseph G. Sodroski,⁴ and Wesley I. Sundquist^{1*}

Department of Biochemistry, University of Utah, Salt Lake City, Utah 84112-5650¹; Department of Microbiology and Immunology, Vanderbilt University School of Medicine, A-5301 Medical Center North, Nashville, Tennessee 37232-2363²; Department of Medicine, Cystic Fibrosis/Pulmonary Research and Treatment Center, University of North Carolina at Chapel Hill, Chapel Hill, North Carolina 27599³; and Department of Cancer Immunology and AIDS, Dana-Farber Cancer Institute, Division of AIDS, Harvard Medical School, Boston, Massachusetts 02115⁴

Received 23 July 2008/Accepted 5 September 2008

The rhesus monkey intrinsic immunity factor TRIM5 α_{rh} recognizes incoming capsids from a variety of retroviruses, including human immunodeficiency virus type 1 (HIV-1) and equine infectious anemia virus (EIAV), and inhibits the accumulation of viral reverse transcripts. However, direct interactions between restricting TRIM5 α proteins and retroviral capsids have not previously been demonstrated using pure recombinant proteins. To facilitate structural and mechanistic studies of retroviral restriction, we have developed methods for expressing and purifying an active chimeric TRIM5 α_{rh} protein containing the RING domain from the related human TRIM21 protein. This recombinant TRIM5-21R protein was expressed in SF-21 insect cells and purified through three chromatographic steps. Two distinct TRIM5-21R species were purified and shown to correspond to monomers and dimers, as analyzed by analytical ultracentrifugation. Chemically cross-linked recombinant TRIM5-21R dimers and mammalian-expressed TRIM5-21R and TRIM5 α proteins exhibited similar sodium dodecyl sulfate-polyacrylamide gel electrophoresis mobilities, indicating that mammalian TRIM5 α proteins are predominantly dimeric. Purified TRIM5-21R had ubiquitin ligase activity and could autoubiquitylate with different E2 ubiquitin conjugating enzymes *in vitro*. TRIM5-21R bound directly to synthetic capsids composed of recombinant HIV-1 CA-NC proteins and to authentic EIAV core particles. HIV-1 CA-NC assemblies bound dimeric TRIM5-21R better than either monomeric TRIM5-21R or TRIM5-21R constructs that lacked the SPRY domain or its V1 loop. Thus, our studies indicate that TRIM5 α proteins are dimeric ubiquitin E3 ligases that recognize retroviral capsids through direct interactions mediated by the SPRY domain and demonstrate that these activities can be recapitulated *in vitro* using pure recombinant proteins.

Susceptibility to retroviral infections influences species survival and has driven the evolution of cellular restriction factors that inhibit retroviral replication. One important antiretroviral intrinsic immune response is mediated by TRIM5 α , which can block early postentry steps in the replication of certain retroviruses in specific primate lineages (3, 37, 55, 58). Under normal restrictive conditions, TRIM5 α proteins block accumulation of retroviral reverse transcripts (55) and accelerate the rate at which viral capsids dissociate from high-molecular-weight complexes into lower-molecular-weight subunits (42, 56). The allelic specificity of TRIM5 α restriction is illustrated by the fact that rhesus macaque TRIM5 α potently inhibits human immunodeficiency virus type 1 (HIV-1) replication, whereas human TRIM5 α instead exhibits restriction activity against N-tropic murine leukemia virus but not HIV-1 (23, 29, 43, 55, 67). These differences can be attributed to the differ-

ential abilities of TRIM5 α proteins to interact with retroviral capsids after viral entry (34, 42, 56).

Like other tripartite (TRIM) family members, TRIM5 α contains RING, B-box, coiled-coil, and B30.2/SPRY domains, and each of these domains contributes to restriction activity. The RING domain of TRIM5 α has intrinsic E3 ubiquitin ligase activity (63, 64), which is important both for autoubiquitylation and for protein turnover *in vivo* (12, 26). The E3 ubiquitin ligase activity also contributes to restriction but is not absolutely required (26, 41, 55), and the precise functions of ubiquitylation and the role of the ubiquitin/proteasome system in retroviral restriction are not yet fully understood. Specifically, proteasome activity is not required for TRIM5 α antiviral activity *per se* (12, 41), but proteasome inhibitors do alter the normal progression of TRIM5 α restriction, allowing reverse transcripts to accumulate and impairing the ability of TRIM5 α to accelerate the dissociation of intact viral capsids (2, 10, 62). Moreover, the restriction of incoming capsids results in proteasome-dependent degradation of TRIM5 α (47), again suggesting possible involvement of the proteasome in the normal stepwise progression of restriction.

The B-box domain of TRIM5 α plays an essential, but still

* Corresponding author. Mailing address: Department of Biochemistry, University of Utah, Salt Lake City, UT 84112-5650. Phone: (801) 585-5402. Fax: (801) 581-7959. E-mail: wes@biochem.utah.edu.

[†] Supplemental material for this article may be found at <http://jvi.asm.org/>.

[‡] Published ahead of print on 17 September 2008.

undefined role in restriction activity, and mutations in this domain can influence protein turnover, intracellular localization, and restriction activity (11). The coiled-coil and ensuing linker 2 (L2) regions of TRIM5 α also contribute to efficient capsid binding and restriction, and these elements appear to function primarily in protein oligomerization (27, 36). Cross-linking studies have suggested that TRIM5 α may function as a trimer, but trimerization has not been rigorously demonstrated by biophysical studies of pure TRIM5 proteins (36). Finally, the C-terminal B30.2/SPRY domain of TRIM5 α is essential for viral capsid recognition and is the key determinant of antiviral specificity (38, 41, 54–56, 68). Several motifs within the SPRY domain have been subject to significant positive selection and exhibit pronounced variability between species (35, 38, 49, 50, 54, 57). In particular, variable region 1 (V1, residues 323 to 350 in rhesus TRIM5 α) is critical both for efficient restriction and for capsid binding, and a single amino acid alteration at position 332 of the V1 loop allows human TRIM5 α to bind HIV-1 capsids and inhibit HIV-1 replication (34, 54, 68). These and other observations show that the SPRY domain dictates retroviral capsid recognition, although direct binding interactions have not yet been demonstrated and characterized using pure TRIM5 α proteins.

TRIM5 α proteins appear to recognize the outer shell of the retroviral core particle, which is called the capsid. Lentiviruses such as HIV-1 and equine infectious anemia virus (EIAV) have conical capsids composed of CA protein hexamers that form hexagonal assemblies called fullerene cones (4, 19–21, 28, 32). Intact retroviral core particles can be isolated from membrane-stripped retroviruses and purified by using sucrose-gradient centrifugation, but these assemblies are rather unstable and typically disassemble spontaneously in buffer (1, 17, 30, 46, 60). Structural and biochemical studies of the HIV-1 capsid have therefore frequently used synthetic assemblies created from pure recombinant CA proteins (20). The assemblies formed by pure HIV-1 CA-NC proteins on DNA templates are particularly stable and can be formed under near physiological conditions (7, 21). These CA-NC/DNA assemblies are a mixture of cylindrical and conical structures that recapitulate the hexagonal lattice of CA hexamers found in authentic viral capsids (4, 21, 32). Synthetic HIV-1 CA-NC/DNA assemblies, like membrane-stripped viral capsids, also bind exogenously expressed TRIM5 α proteins present in crude cell lysates (51, 56), indicating that the CA-NC/DNA assemblies recapitulate the key elements required for TRIM5 α recognition.

In summary, it is now well established that capsid recognition dictates the allelic specificity of TRIM5 α restriction. However, direct interactions between pure TRIM5 proteins and retroviral capsids have not yet been demonstrated in vitro, largely owing to the technical challenges of creating suitable capsid targets and of expressing and purifying recombinant TRIM5 α proteins. To date, soluble full-length TRIM5 α proteins have not been expressed successfully in *Escherichia coli*, and TRIM5 α proteins tend to turnover rapidly and aggregate into cytoplasmic bodies when overexpressed in mammalian systems (6, 12, 53). However, replacing the TRIM5 α RING domain with the RING domain from the homologous TRIM21 protein reduces protein turnover without compromising HIV-1 restriction substantially (12, 33). We have taken advantage of this observation to develop systems for expressing and purify-

ing chimeric TRIM5-21R proteins in quantities suitable for biochemical and biophysical characterization.

MATERIALS AND METHODS

Cell cultures. Human 293T and HeLa cells were maintained in Dulbecco modified Eagle medium supplemented with 10% fetal calf serum. HeLa cells stably expressing rhesus TRIM5 α (TRIM5 α_{rh}) (55) were maintained with an additional supplement of 1 μ g of puromycin/ml.

Expression vectors. The pLPCX TRIM5-21R expression vector, encoding a hemagglutinin (HA)-tagged TRIM5-21R (12), was used as a PCR template to create a DNA fragment containing the TRIM5-21R gene with KpnI and XhoI restriction sites. This fragment was ligated into the pCAG.OSFT (WISP-08-189) backbone, which itself was modified from the pCAG vector backbone (Addgene) to encode an N-terminal OneStrep and Flag (OSF) epitope tag followed by a TEV protease cleavage site. The resulting vector, pCAG.OSFT-TRIM5-21R (WISP-08-176), was used as a PCR template to amplify a DNA fragment with terminal attB sites to allow for recombination into the pDONR221 Gateway Entry Vector (Invitrogen) to create the pDONR221.OSFT-TRIM5-21R Entry Vector (WISP-08-177). This vector was used as a template for QuikChange site-directed mutagenesis (Stratagene) to create pDONR221.OSFT-TRIM5-21RAV1 (WISP-08-178) (deletion in the V1 variable loop of the SPRY domain corresponding to TRIM5 α_{rh} residues 332 to 344) and pDONR221.OSFT-TRIM5-21RASPRY (WISP-08-179) (deletion of the entire SPRY domain and L2 element, TRIM5 α_{rh} residues 233 to 497). The pCAG.OSFT-TRIM5 α_{rh} and pDONR221.OSFT-TRIM5 α_{rh} vectors (WISP-08-197 and -08-198) were constructed in an analogous fashion. Recombinant baculoviruses expressing TRIM5-21R, TRIM5-21RAV1, and TRIM5-21RASPRY were prepared in situ by using the BaculoDirect system (Invitrogen). Equivalent mammalian cell expression constructs were generated in the Gateway pDNA-DEST40 vector (WISP-08-180, -181, -182, and -199, respectively). pET28-based plasmids for bacterial expression of UbcH5 (WISP-08-190), UbcH6 (WISP-08-191), UbcH7 (WISP-08-192), and Uba1 (WISP-08-192) were generous gifts from Rachel Klevit (University of Washington) (5, 8), and the Uba1 gene was originally a gift from Richard Vierstra (University of Wisconsin) (22).

Expression and purification of recombinant proteins. (i) **TRIM5-21R.** Two liters of SF-21 insect cells were grown to a density of 2×10^6 cells/ml in SF-900 II media (Invitrogen), infected at a multiplicity of infection of 1.0 with recombinant baculoviruses encoding TRIM5-21R and variants, and the expressed proteins were allowed to accumulate for 36 to 44 h (100 rpm shaking, 27°C). All subsequent steps were carried out at 4°C, except where noted. Cells were collected by centrifugation at $500 \times g$ for 8 min, resuspended in 1.25 (vol/vol) of lysis buffer (50 mM NaCl, 50 mM Tris [pH 8.0], 1.5% Triton X-100, 1 mM TCEP, and mammalian protease inhibitor cocktail [Sigma] at 1:150 [vol/vol]), and lysed in a 100-ml Dounce homogenizer (15 strokes). The lysate was clarified by ultracentrifugation (Beckman Ti 50.2 rotor; 45,000 rpm, 184,000 $\times g$, 40 min), filtered (0.45 μ m), and loaded at 2 ml/min onto a 10-ml StrepTactin Superflow affinity column (IBA). The bound protein was washed with 50 ml of buffer (50 mM NaCl, 50 mM Tris [pH 8.0], 1 mM TCEP) and eluted with wash buffer supplemented with 2.5 mM D-desthiobiotin. The eluate was loaded directly onto two 5-ml HiTrap Q-Sepharose anion-exchange columns connected in series (GE Healthcare) and eluted with a NaCl gradient from 50 mM to 1 M over 200 ml of buffer (50 mM Tris [pH 8.0], 1 mM TCEP). Purified TRIM5-21R eluted in two peaks (see Fig. 1B). Fractions containing the early eluting peak were pooled, concentrated to 2 ml (Vivaspin concentrator; Sartorius), and loaded onto a 120-ml Superose-6 gel filtration column. The later eluting protein fraction peak tended to aggregate under high-ionic-strength conditions and was therefore loaded directly onto a Superose-6 column without concentration (4-ml fractions). Gel filtration chromatography was performed at 1 ml/min in 25 mM NaCl, 50 mM Tris (pH 8.0), 1 mM TCEP. The gel filtration column was calibrated by using the HMW standard gel filtration calibration kit (GE Healthcare), and the two TRIM5-21R species eluted with apparent molecular masses of 232 kDa (dimer, second anion exchange peak) and 70 kDa (monomer, first anion exchange peak). The purified monomer could be concentrated to 10 mg/ml, whereas the dimer tended to precipitate at concentrations above 3 mg/ml. Concentrated proteins were stored at 4°C for short-term use but tended to precipitate when stored for multiple days. Alternatively, proteins were flash frozen in liquid nitrogen and retained CA-NC binding and autoubiquitylation activities when thawed.

(ii) **Ubiquitin-related proteins.** Recombinant E1 and E2 proteins were expressed in BL21-Codon Plus (DE3)-RIPL bacteria (Stratagene) grown in LB media and purified as described previously (8). Briefly, human Ubc15c, UbcH6, and UbcH7 were purified by cation-exchange chromatography (SP Sepharose) and eluted with a 0 to 0.5 M NaCl gradient in 30 mM MES (morpholinethane-

TABLE 1. Posttranslational modifications of TRIM5-21R and TRIM5 α_{nb} proteins

Cell type	Protein	No. of peptides identified ^a	% Coverage	MASCOT score (total protein score)
SF-21	TRIM5-21R	77*	54	7365
	Ubiquitin	7†	79	138
293T	TRIM5 α_{nb} -HA	42*	47	2162
	Ubiquitin	2	23	63

^a * Two nested TRIM5-21R phosphopeptides were identified: ⁸¹LREVKLSPEEGQK⁹³ and ⁸³EVKLSPEEGQK⁹³. † One ubiquitylated ubiquitin peptide was identified: ⁴⁹LIFAGKQLEEDGR⁵⁴.

sulfonic acid)-1 mM EDTA (pH 6.0). E2-rich fractions were pooled and purified further by size exclusion chromatography in 25 mM sodium phosphate (pH 7.0)-150 mM NaCl. Wheat His₆-Uba1 (E1) was purified by Ni²⁺-affinity chromatography, followed by size exclusion chromatography. Ubiquitin was purified as described previously (44).

Mass spectrometry. Monomeric and dimeric TRIM5-21R proteins were desalted for electrospray ionization mass spectrometry using a C18 ZipTip (Millipore) and analyzed on a Quattro-II mass spectrometer (Micromass, Inc.). The data were acquired with a cone voltage of 50 eV, a spray voltage of 2.8 kV, and scanning from 800 to 1,400 *m/z* in 4 s. Spectra were combined, and the multiply charged molecular ions were deconvoluted into a molecular-mass spectrum by using MaxEnt software (Micromass, Inc.).

Liquid chromatography tandem mass spectrometry experiments were used to examine posttranslational modifications of both TRIM5 α_{nb} expressed in 293T cells and TRIM5-21R expressed in SF-21 cells. TRIM5 α_{nb} contained a C-terminal HA tag (55) and was affinity purified from 293T cells by using α -HA-conjugated Sepharose matrices as described below for cross-linking experiments. Dimeric TRIM5-21R was purified by anion-exchange chromatography, concentrated, and mixed with an equal volume of 2 \times sodium dodecyl sulfate (SDS) loading buffer. In both cases, samples were boiled, separated by SDS-4 to 20% polyacrylamide gel electrophoresis (PAGE), and visualized using Coomassie blue staining. Major bands corresponding to each TRIM5 protein, as well as minor bands corresponding to higher-molecular-mass (modified) TRIM5 proteins were excised, digested with TPCK (tolylsulfonil phenylalanyl chloromethyl ketone)-modified trypsin (Promega) and introduced by nanoLC (Eksigent, Inc.) with nano-electrospray ionization (ThermoElectron Corp) into a LTQ-FT hybrid mass spectrometer (ThermoElectron Corp). Peptide molecular masses were measured by Fourier transform ion cyclotron resonance, and peptide sequencing was performed by collision-induced dissociation in the linear ion trap of the instrument. Protein identification and posttranslational modifications (phosphorylation and ubiquitylation) of peptides in tryptic digests were determined by using the MASCOT search engine (Matrix Science) and the NCBI_{nr} mammalian taxonomy database using a significance threshold of $P < 0.05$ and an ion score cutoff value of 20 (Table 1).

Equilibrium sedimentation analyses. Equilibrium sedimentation of purified TRIM5-21R proteins was performed using Optima XL-I and XL-A centrifuges (Beckman) at protein subunit concentrations of 6.09, 3.05, and 1.53 μ M (monomer) or 6.0, 3.0, and 1.5 μ M (dimer) in 50 mM Tris-HCl (pH 8.0)-50 mM NaCl-1 mM β -mercaptoethanol (monomer) or in 25 mM NaCl-50 mM Tris-HCl (pH 8.0)-1 mM TCEP (dimer). Centrifugation (4°C) was performed at two speeds: 14,000 and 18,000 rpm (monomer) and 14,000 and 16,000 rpm (dimer). The resulting six data sets for each oligomeric species were globally fit to single ideal species models with fixed or floating molecular masses using the nonlinear least-squares algorithms in the Heteroanalysis software (9). Solvent density and the partial specific volume of TRIM5-21R were calculated by using the program SEDNTERP (version 1.09) (31).

Autoubiquitylation activity assays. TRIM5-21R-directed ubiquitylation assays were carried out in 50- μ l reaction mixtures containing 1.0 μ M TRIM5-21R, 1.0 μ M concentrations of the specified E2 enzyme, 20 μ M ubiquitin, and 0.5 μ M wheat Uba1. Reactions were incubated for 60 min with or without addition of 5 mM ATP-10 mM MgCl₂, and reaction products were analyzed by SDS-7.5% PAGE and Western blotting as described below.

Cross-linking reactions. (i) **Cross-linking of recombinant TRIM5-21R proteins.** Pure recombinant TRIM5-21R proteins were dialyzed overnight into phosphate-buffered saline (PBS; 1 mM KH₂PO₄, 5.6 mM Na₂HPO₄, 154 mM NaCl) plus 1 mM TCEP. Cross-linking reactions were then performed for 10 min at

25°C in 30- μ l reaction volumes at final protein concentrations of 0.5 μ M, along with 0, 0.1, 0.5, or 1 mM fresh EGS [ethylene glycol-bis(succinimidyl succinate)] cross-linker. Reactions were quenched by addition of 30 μ l of 0.1 M Tris-HCl (pH 7.5), and samples were mixed with SDS loading buffer plus 1.2% β -mercaptoethanol, and analyzed by SDS-7.5% PAGE and Western blotting. For reactions performed in the presence of mammalian cell lysate, recombinant TRIM5-21R proteins in PBS plus 1 mM TCEP buffer were incubated in 30- μ l reactions containing final concentrations of 50% clarified lysate prepared from 293T cells (see below), 0.25 μ M TRIM5-21R, and EGS at 0, 0.1, 0.5, or 1 mM (20 min, 25°C). Reactions were quenched by the addition of 30 μ l of 0.1 M Tris-HCl (pH 7.5), diluted to 400 μ l with PBS plus 1 mM EDTA, and incubated with 30 μ l of StrepTactin Sepharose (IBA) at 4°C for 2 h. The matrix was washed four times with PBS plus 0.5% NP-40 and resuspended in 30 μ l of SDS loading buffer plus 1.2% β -mercaptoethanol for Western blot analysis.

(ii) **Cross-linking of TRIM proteins expressed in mammalian cells.** For each cross-linking series (four samples), a 10-cm plate of confluent 293T cells expressing OSF-tagged TRIM5-21R or HA-tagged TRIM5 α_{nb} was lysed in 300 μ l of PBS plus 0.5% NP-40 supplemented 1:150 with protease inhibitor cocktail (Sigma) for 15 min on ice. Lysates were clarified by centrifugation at 16,100 \times g for 30 min, and the resulting supernatant was diluted to a final volume of 1.7 ml with PBS plus 1 mM EDTA. Then, 400- μ l aliquots of diluted lysate were incubated with 0, 0.1, 0.5, or 1.0 mM EGS (20 min at 25°C). Reactions were quenched by the addition of 400 μ l of 0.1 M Tris-HCl (pH 7.5), mixed with 30 μ l of pre-equilibrated StrepTactin Sepharose (TRIM21-5R; IBA) or α -HA-conjugated Sepharose (TRIM5 α_{nb} ; Sigma), and incubated for 2 h at 4°C. Matrices were washed four times with PBS plus 0.5% NP-40 and resuspended in 30 μ l of SDS loading buffer plus 1.2% β -mercaptoethanol for Western blot analysis using SDS-7.5% PAGE.

Western blotting. Proteins were separated by SDS-PAGE, transferred to PVDF-FL membranes (Millipore) in Tris-glycine-10% methanol buffer, blocked in 5% milk-Tris-buffered saline (20 min), and incubated with primary antibodies diluted in 5% nonfat milk-Tris-buffered saline plus 0.1% Tween 20 (16 h, 4°C). Blots were visualized by using an Odyssey infrared imaging system (Li-Cor, Inc.) to detect Alexa 680-nm (Molecular Probes; 1:10,000) or IRDye 800-nm (Rockland; 1:10,000) secondary antibodies. The primary antibodies and dilutions used were as follows: mouse anti-FLAG (Sigma) at 1:3,000 for OSF-TRIM5-21R (Fig. 1, 3 to 5, and 7), mouse anti-HA.11 (Sigma) at 1:1,000 for TRIM5 α -HA (Fig. 3), rabbit anti-HIV-1 CA (UT415 made against purified NL4-3 CA protein and affinity purified) at 1:15,000 (Fig. 5), and rabbit anti-EIAV CA (UT418 made against purified EIAV CA protein and affinity-purified) at 1:5,000 (Fig. 7).

Restriction assays. (i) **HIV-1 restriction assays.** The HIV-1 vector pCMV Δ 8.2, which expresses a lacZ reporter, was packaged into vesicular stomatitis virus G-pseudotyped HIV-1 as described previously (48a, 59a). For restriction assays, 3×10^6 HeLa-M cells were seeded in 24-well plates and transfected (Lipofectamine 2000) 24 h later with 1 μ g of the control pcDNA-DEST40 vector or with vectors expressing OSFT-TRIM5 α_{nb} , OSFT-TRIM5-21R, OSFT-TRIM5-21R Δ V1, or OSFT-TRIM5-21R Δ SPRY. Cells were incubated for 24 h, washed with media, transduced for 24 h with various quantities of the HIV-1 vector, washed again, and the percentage of infected cells was determined by assaying for lacZ expression at 48 h post infection. Equivalent expression levels of the different TRIM5 constructs were verified by Western blotting.

(ii) **EIAV restriction assay.** To assay for restriction, 293T cells were transfected in a 10-cm plate with the CeGFPW EIAV vector system as described below, and infectivity was subsequently assayed as previously described (48). Briefly, dilutions of vector preparations were added to target cells (HeLa or HeLa-TRIM5 α_{nb} , 2.0×10^6 cells/well, six-well plate) and incubated for 72 h at 37°C. Transduction efficiencies were determined from the percentage of GFP-positive cells measured by fluorescence-activated cell sorting.

EIAV core isolation. EIAV cores were prepared by using an adaptation of a method described previously (30). Briefly, EIAV virions were produced by co-transfection of 293T cells (16 \times 10-cm plates) with an EIAV vector system. Each 10-cm plate of cells was transfected (CalPhos mammalian transfection kit, Clontech) with 8.1 μ g of pEV53 (EIAV structural proteins), 7.5 μ g of pSIN6.1CeGFPW (packaged GFP expression vector), and 2.7 μ g of pCMV-VSV-G (VSV-G envelope) (39, 69). After 36 h, the supernatants were removed, pooled (four plates/pool), filtered (0.45- μ m pore size), and pelleted through a 4-ml 20% sucrose cushion in a Beckman SW-32Ti rotor (134,000 \times g, 2 h, 4°C). Each set of pelleted virions was resuspended by gentle pipetting (4 h at 4°C) in 400 μ l of ST buffer (10 mM Tris-HCl [pH 7.4], 50 mM NaCl). Four 11.5-ml sucrose gradients (30 and 70% [w/vol] sucrose in ST buffer) were prepared in 14-by-89-mm tubes using a gradient mixer (Biocomp). The gradients were overlaid with a 0.3-ml cushion of 15% sucrose containing 1% Triton X-100 and then with a 0.3-ml barrier layer of 7.5% sucrose in ST buffer. Each tube of concen-

trated EIAV particles was carefully layered on top of a gradient and centrifuged in a Beckman SW-41 rotor (210,000 × g, 16 h, 4°C). Twelve 1-ml fractions were collected from the bottom of each tube, and fraction densities were measured by using a digital refractometer (Leica), and EIAV CA was assayed by Western blotting. Three 1-ml fractions of the correct density (1.22 to 1.26 g/ml) contained intact EIAV core particles and were pooled, repelleted by centrifugation in a Beckman SW-41 rotor (2,000 × g, 2 h, 4°C), and resuspended in 40 μl of ST buffer for binding assays.

Capsid binding assays. Recombinant HIV-1 CA-NC was expressed and purified as described previously (21). Cylindrical and conical assemblies were created by incubating 10 μM CA-NC and 2 μM d(TG)₅₀ oligonucleotide (15) in 1 ml of assembly buffer (50 mM Tris-HCl [pH 8.0], 500 mM NaCl) for 16 h at 4°C. Assembled complexes were enriched by centrifugation at 10,000 rpm in a microcentrifuge (~9,000 × g) for 5 min, and pelleted assemblies were resuspended in 200 μl of supernatant. TRIM5-21R proteins were added at final concentrations of 5.0 μM (for the experiments described in Fig. 5B and 6B comparing different TRIM5-21R constructs), 0.5 or 0.15 μM (0.3×) (for the more stringent binding assays described in Fig. 5C), or 0.36 μM (for the EIAV core binding assays described in Fig. 7B). TRIM5-21R proteins were mixed with 20 μl of concentrated CA-NC particles (see the figure legends for quantities) or with purified EIAV cores (~100 ng, ~20 nM CA) in reaction volumes of 200 μl, with a final buffer composition of 10 mM Tris, 2 mM KH₂PO₄, 11 mM Na₂HPO₄, and 280 mM NaCl (Fig. 5B), 308 mM NaCl (Fig. 5C, 1×), 316 mM NaCl (Fig. 5C, 0.3×), or 250 mM NaCl (Fig. 7B). Reactions were incubated for 45 min at 25°C (CA-NC binding assays) or 4°C (EIAV core assays) with gentle mixing at 10-min intervals. Prior to centrifugation, a 10-μl sample was removed and mixed with SDS loading buffer (input). Binding reactions were layered onto a 4.2-ml cushion of 70% (CA-NC) or 57% (EIAV cores) sucrose (wt/vol; sucrose-PBS plus 1 mM TCEP) in 13-by-51-mm tubes and centrifuged in a Beckman SW-50.1 rotor (110,000 × g, 1 h, 4°C). Samples of the supernatant remaining above the sucrose cushion were saved (supernatant), the sucrose cushions were removed by aspiration, and the pellet was resuspended in 40 μl of 1× SDS loading buffer. Input, supernatant, and pellet samples were analyzed by Western blotting at concentrations in which the supernatant samples corresponded to 1.25% (CA-NC) and 2% (EIAV cores) of the total supernatant, and pellet samples corresponded to 80% of the total pellet. Under these conditions, ~2.5% of the input EIAV cores pelleted, and ~1.6% (5.0 μM input TRIM5-21R), 1.6% (0.5 μM input TRIM5-21R), and 2.4% (0.15 μM input TRIM5-21R) of the CA-NC assemblies pelleted.

Transmission electron microscopy analyses of TRIM-bound CA-NC tubes. For transmission electron microscopy analyses, binding reactions containing 5-μl suspensions of CA-NC particles (prepared as described above) were incubated with final TRIM5-21R concentrations of 20 to 50 μM (15-μl total volumes, 25°C, 45 min, with gentle mixing every 10 min). Carbon-coated grids were placed on aliquots of each reaction mixture (7 μl, 90 s), washed with 3 to 4 drops of 0.1 M KCl, stained with 3 or 4 drops of 4% uranyl acetate, and air dried. Samples were imaged on Hitachi 7100 and Philips Tecnai 12 transmission electron microscopes at magnifications between ×25,000 and ×100,000. Each electron microscopic analysis was repeated at least three times with proteins from at least three separate purifications.

RESULTS

TRIM5-21R expression and purification. Wild-type rhesus TRIM5 α accumulates at low levels and tends to aggregate when overexpressed in mammalian and insect cells (12; data not shown). These properties have made it difficult to obtain sufficient quantities of pure recombinant TRIM5 α proteins for biophysical and structural studies. Substitution of the TRIM5 α_{th} RING domain with the RING domain of the homologous human TRIM21 protein (58% identity), however, generates a fusion protein (designated TRIM5-21R) that has a longer half-life and accumulates to higher levels in mammalian cells than does wild-type TRIM5 α (12). Importantly, TRIM5-21R restricts HIV-1 replication, although its activity is slightly reduced relative to wild-type TRIM5 α (12; see also Fig. S1A in the supplemental material). TRIM5-21R was therefore an attractive candidate for large-scale expression in insect cells.

TRIM5-21R constructs with N-terminal OSF epitope tags were expressed in SF-21 cells using baculoviral expression sys-

tems. TRIM5-21R expression was detectable in Western blots of soluble lysates of infected SF-21 cells but not in control lysates (Fig. 1A, upper panel, compare lanes 1 and 2). The soluble TRIM5-21R protein was affinity purified on a Strep-Tactin matrix, and elution with D-desthiobiotin yielded TRIM5-21R as essentially the only protein detectable by either Western blotting (upper panel, lane 3) or Coomassie blue staining (lower panel). The protein was further purified by anion-exchange chromatography, where it separated into two distinct species, both of which corresponded to TRIM5-21R (Fig. 1B, upper panel, and Fig. 1A, lanes 4 and 5). The ratios of the two species varied between preparations, but it was common for the late-eluting species to predominate, as shown in Fig. 1B.

Gel filtration chromatography was used as a final step to purify the two distinct TRIM5-21R species. The two species again exhibited different chromatographic behavior, eluting with apparent molecular weights of 232 kDa (late-eluting anion-exchange peak) and 77 kDa (early-eluting anion-exchange peak). The apparent size of the smaller protein suggested that it was likely to be a TRIM5-21R monomer, whereas the apparent size of the larger protein suggested that it was probably either a trimer or a dimer with an extended Stokes radius. Typical yields were 150 μg (larger species) and 200 μg (smaller species) per liter of infected SF-21 cells.

The identities of the two purified recombinant TRIM5-21R proteins were confirmed by electrospray mass spectrometric (ESI/MS) analyses of the intact proteins, and by liquid chromatography tandem mass spectrometric analyses of tryptic digests. The mass of the intact smaller species corresponded to a TRIM5-21R protein that was missing the N-terminal methionine and was acetylated at the N terminus ($MW_{\text{actual}} = 62,518$ g/mol, $MW_{\text{calculated}} = 62,520$ g/mol), and the mass spectra revealed no evidence for posttranslational modifications. In contrast, the oligomeric species showed a protein of the same mass ($MW_{\text{actual}} = 62,517$ g/mol), as well as a second protein with a mass that corresponded to a singly phosphorylated protein ($MW_{\text{actual}} = 62,596$ g/mol, $MW_{\text{calc}} = 62,595$; ~30% of protein). Peptide mapping experiments were therefore performed on TRIM5-21R proteins produced in both SF-21 (insect) and 293T (mammalian) cells. These studies identified a single phosphoserine residue at position 87 within the L1 linker between the RING and B-box domains in TRIM5-21R proteins isolated from both insect and human cells (Table 1, TRIM5 α_{th} numbering). Given its location, this phosphorylation site could, in principle, modulate a postulated interaction between the RING and adjacent L1 elements (24). Ubiquitin-derived peptides were also detected in trypsin digests of purified TRIM5-21R expressed in both insect and mammalian cells, indicating that the protein was also ubiquitinated at low levels. Interestingly, ubiquitin peptides with Lys-48 isopeptide linkages were also detected, indicating that TRIM5-21R could be polyubiquitinated with Lys-48 chains.

In summary, we have developed methods that can be used to express and purify up to milligram quantities of two different TRIM5-21R oligomers, and the larger species can be phosphorylated and ubiquitinated in human and in insect cells.

Recombinant TRIM5-21R proteins are monomers and dimers. Equilibrium sedimentation centrifugation experiments can provide shape-independent measures of protein solution mass,

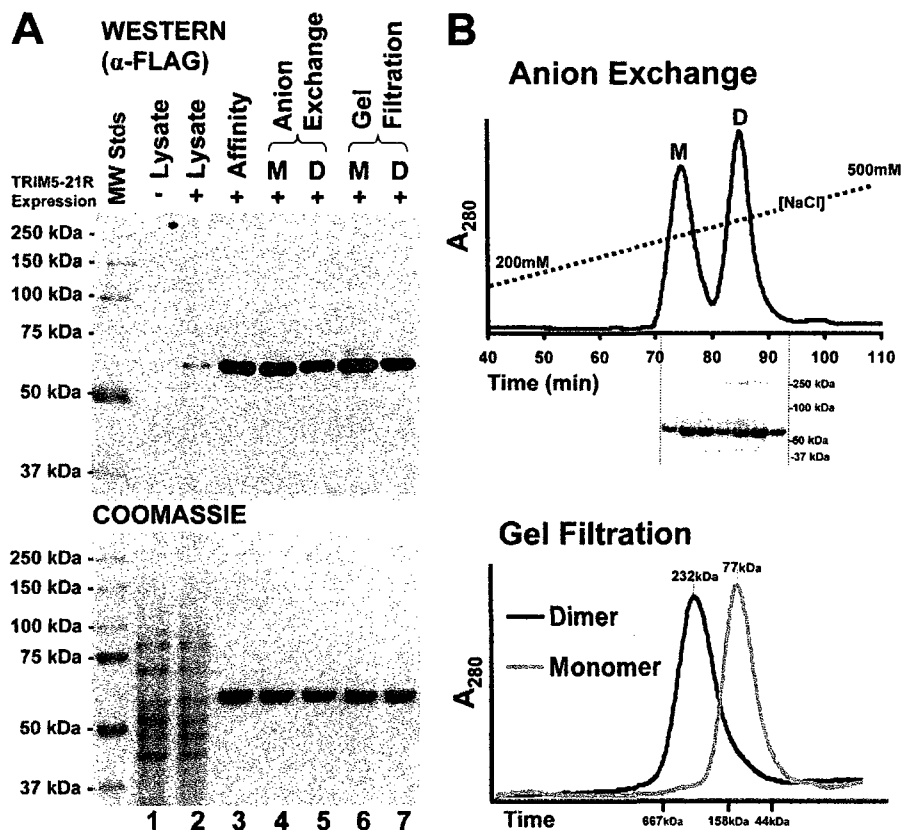


FIG. 1. TRIM5-21R expression and purification. (A) Western blot (upper, anti-FLAG) and Coomassie blue-stained SDS-PAGE gel (lower) showing the stepwise purification of recombinant TRIM5-21R proteins. Lane 1, soluble lysate from control SF-21 cells; lane 2, lysate from SF-21 cells infected with baculovirus expressing TRIM5-21R; lane 3, StrepTactin affinity-purified TRIM5-21R; lanes 4 and 5, monomeric (M, early eluting peak) and dimeric (D, late eluting peak) TRIM5-21R proteins purified by anion-exchange chromatography; lanes 6 and 7, monomeric (M, late eluting peak) and dimeric (D, early eluting peak) TRIM5-21R proteins purified by gel filtration chromatography. (B) Anion-exchange (upper) and gel filtration (lower) chromatographs showing the elution profiles of monomeric (M) and dimeric (D) TRIM5-21R proteins. Inset (upper panel) shows a Coomassie blue-stained SDS-PAGE analysis of the designated fractions. Elution positions of control molecular mass standards are shown below the gel filtration chromatograph for reference, and estimated molecular masses are given above the peaks of monomeric and dimeric TRIM5-21R.

and this approach was therefore used to determine the oligomeric state of each TRIM5-21R species. Sedimentation data were collected at three different protein concentrations and two rotor speeds, yielding a total of six data sets for each TRIM5-21R species. These six data sets were globally fit to single species models in which the molecular weight was allowed to float and also to monomer, dimer, and trimer models with fixed molecular weights. As illustrated in Fig. 2A, the distribution of the smaller TRIM5-21R species fit a protein with a predicted mass of 59,305 g/mol, which matched the mass expected for a TRIM5-21R monomer ($M_{\text{obs}}/M_{\text{calc}} = 0.95$). The data for three initial concentrations of

TRIM5-21R centrifuged at 14,000 rpm are shown together with the global fits (Fig. 2A, upper panel), and the small, random residuals indicate that the data were satisfactorily fit by a simple single species model (lower panels). Global fits to the three data sets collected at 18,000 rpm were also satisfactory (data not shown). Similarly, when fixed monomer, dimer, or trimer molecular weights were used during the global fitting procedure, the monomer model was clearly the best fit to the data (see Fig. S2A in the supplemental material).

In contrast, equilibrium distributions of the larger TRIM5-21R species indicated that this TRIM5-21R protein was a dimer. As shown in Fig. 2B, data fit with a floating molecular

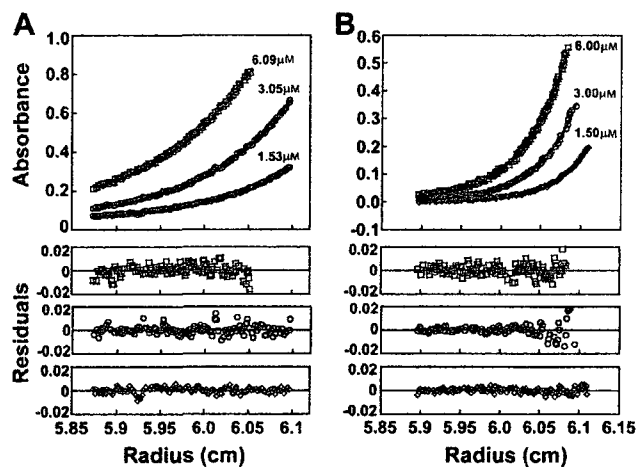


FIG. 2. Recombinant TRIM5-21R proteins are monomers and dimers. Equilibrium sedimentation distributions of purified monomeric (A) and dimeric (B) TRIM5-21R proteins (upper panels), and residual differences between the data and the single species models (lower panels). The data are shown for initial subunit protein concentrations of 6.09, 3.05, and 1.53 μM (monomer), and 6.0, 3.0, and 1.5 μM (dimer) at rotor speeds of 14,000 rpm. The data sets were also collected at 18,000 rpm (monomer) and 16,000 (dimer), and all of the data were globally fit to a single species model in which the molecular weight was allowed to float during the refinement. The data points are shown in open symbols, and the best-fit curves are shown as solid lines. Estimated molecular weights were as follows: TRIM5-21R monomer, 59,305 g/mol ($M_{\text{W}_{\text{monomer}}} = 62,520$ g/mol, $M_{\text{obs}}/M_{\text{calc}} = 0.95$); and TRIM5-21R dimer, 123,825 g/mol ($M_{\text{W}_{\text{dimer}}} = 125,040$ g/mol, $M_{\text{obs}}/M_{\text{monomer}} = 1.98$).

weight gave an estimated mass of 123,825 g/mol, which matched the molecular weight expected for a TRIM5-21R dimer (125,040 g/mol, $M_{\text{obs}}/M_{\text{monomer}} = 1.98$), and the global fits again exhibited small, random residuals (Fig. 2B and data not shown). The dimer model was also clearly best when the data were globally fit to fixed TRIM5-21R monomer, dimer, or trimer models (see Fig. S2B in the supplemental material). We therefore conclude that the smaller TRIM5-21R species is a monomer and that the larger species is a dimer.

Recombinant TRIM5-21R dimers and mammalian TRIM5-21R and TRIM5 α proteins exhibit similar cross-linking patterns. The observation that recombinant TRIM5-21R formed monomers and dimers was somewhat surprising because previous studies had suggested that TRIM5 α proteins might be trimers (36). This conclusion was based upon the SDS-PAGE electrophoretic mobilities of chemically cross-linked, mammalian-expressed TRIM5 α proteins, whose mobilities appeared to correspond to trimers (~ 150 kDa). To reconcile these observations, we tested whether chemically cross-linked TRIM5 dimers exhibited anomalously slow SDS-PAGE electrophoretic mobilities. Our first set of experiments examined the mobilities of pure recombinant monomeric and dimeric TRIM5-21R proteins cross-linked with EGS. The monomeric protein was used as a control to ensure that protein and cross-linker concentrations were sufficiently low to prevent nonspecific intermolecular cross-linking of nonassociated proteins. As shown in Fig. 3A, TRIM5-21R dimers formed intermolecular cross-links efficiently, whereas TRIM5-21R monomers did not. The major cross-linked species for the TRIM5-21R dimer migrated at an apparent molecular mass of ~ 160 kDa on a

SDS-7.5% PAGE gel, and a species migrating at ~ 125 kDa was also observed at trace levels. Thus, the major cross-linked form of the TRIM5-21R dimer exhibits anomalously slow SDS-PAGE mobility.

In a second set of experiments, we tested whether the oligomeric state or cross-linking properties of TRIM5 α proteins could be altered by cross-linking in crude lysates, by expression in human versus insect cells, or by the non-native N-terminal OSF tag or RING domain of the TRIM5-21R construct. As shown in the first panel of Fig. 3B, the cross-linking pattern did not change significantly when the pure recombinant TRIM5-21R dimers were cross-linked either in a buffer solution or in a soluble mammalian cell extract, indicating that TRIM5-21R dimer does not appreciably cross-link with extract proteins under these conditions (compare the first panel of Fig. 3B to Fig. 3A). A very similar cross-linking pattern was also seen when TRIM5-21R proteins were expressed in human 293T cells and cross-linked directly in their soluble extracts (compare Fig. 3B, second and third panels), although in this case the minor, faster-migrating cross-linked species was more evident. This experiment indicates that TRIM5-21R forms similar dimers when expressed in human or insect cells. Finally, we examined the cross-linking of an authentic TRIM5 α protein expressed in 293T cells. Although the C-terminally HA-tagged TRIM5 α had a slightly lower molecular weight than TRIM5-21R, the cross-linking pattern of the authentic TRIM5 α -HA protein expressed in human 293T cells was again very similar to those seen for the various TRIM5-21R proteins. Thus, TRIM5-21R and TRIM5 α proteins are predominantly dimeric when ex-

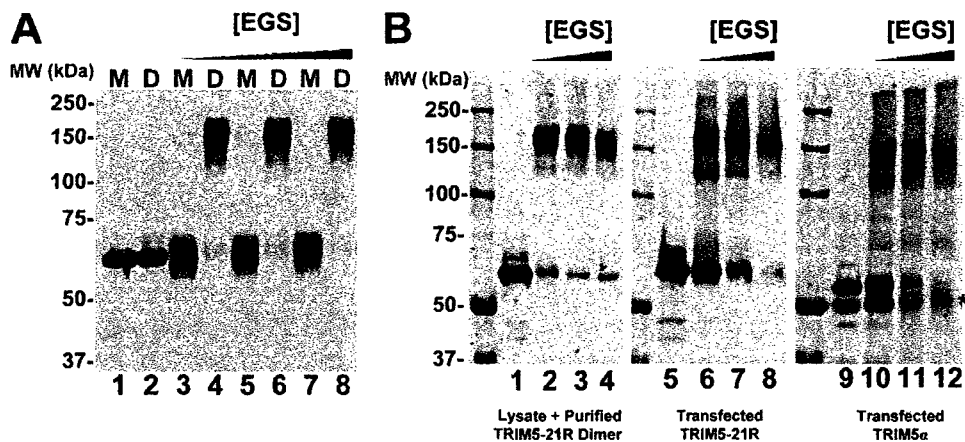


FIG. 3. Recombinant TRIM5-21R dimers and mammalian-expressed TRIM5-21R and TRIM5 α proteins exhibit similar cross-linking patterns. (A) Western blot (anti-FLAG) showing purified monomeric (M) and dimeric (D) proteins cross-linked with increasing concentrations of EGS (lanes 3 to 8) or controls without EGS (lanes 1 and 2). (B) Western blots (anti-FLAG) showing purified recombinant TRIM5-21R dimer added to 293T cell lysate and cross-linked in the presence of increasing concentrations of EGS (first panel); TRIM5-21R expressed in 293T cells, cross-linked directly in the lysate, and concentrated by StrepTactin affinity purification (second panel); and TRIM5 α expressed in 293T cells, cross-linked directly in the lysate, and concentrated by α -HA affinity purification (third panel). Lanes 1, 5, and 9 show controls in the absence of EGS, and the asterisk denotes contaminating immunoglobulin G heavy chain eluted from the HA-Sepharose beads. Note that all of the samples were run on the same gel, and migration positions can therefore be compared directly.

pressed in human or insect cells, but the cross-linked dimers exhibit anomalously slow electrophoretic mobilities.

Autoubiquitylation of recombinant TRIM5-21R proteins. TRIM5 α exhibits ubiquitin E3 ligase activity (63, 64), and a recent study showed that a partially purified, recombinant MBP-TRIM5 α fusion protein could pair with the UbcH5b E2 enzyme and exhibit ubiquitin E3 ligase activity in vitro (64). We also tested whether our purified TRIM5-21R proteins were active for autoubiquitylation in vitro, using three different pure E2 enzymes. As shown in Fig. 4, both monomeric and dimeric TRIM5-21R proteins paired successfully with UbcH5c and UbcH6, but not with UbcH7 in our in vitro autoubiquitylation assays. Ubiquitylation was particularly efficient in the

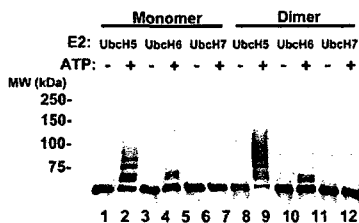


FIG. 4. TRIM5-21R proteins can be autoubiquitylated in vitro. Purified monomeric (lanes 1 to 6) and dimeric (lanes 7 to 12) TRIM5-21R proteins were incubated with the wheat Uba1 E1 enzyme, ubiquitin, and one of three ubiquitin E2-conjugating enzymes—UbcH5c, UbcH6, or UbcH7—in the presence or absence of ATP. Reactions were terminated after 60 min, and TRIM5-21R reaction products were analyzed by Western blotting (α -FLAG).

UbcH5 reactions, where most of the TRIM5-21R dimer was modified with ubiquitin (compare lanes 8 and 9). Control reactions behaved as expected in that ubiquitylated products were not observed in the absence of ATP (compare even and odd lanes).

Interestingly, UbcH5 and UbcH6 produced dramatically different product distributions, with UbcH5 catalyzing polyubiquitylation (or possibly multimonomubiquitylation) and UbcH6 catalyzing only monoubiquitylation of TRIM5-21R. These results demonstrate that the purified TRIM5-21R protein is an active ubiquitin E3 ligase and are in good agreement with the report of Yamauchi et al. (64), who found that MBP-TRIM5 α was active with UbcH5b but not with UbcH7 (UbcH6 was not tested). Our results are also consistent with the observations that TRIM5 α , TRIM21, and TRIM5-21R can self-ubiquitylate to form polyubiquitin chains in vivo, which can contain Lys-48 linkages (64; the present study). Finally, our experiments raise the possibility that TRIM5 α and TRIM21 may exhibit different product distributions when paired with different E2 ubiquitin-conjugating enzymes in vivo. Such behavior has been seen previously for other RING and U-box E3 ligases (e.g., BRCA1 and CHIP, respectively) (8, 72) but remains to be confirmed with in vivo studies of nonchimeric TRIM5 α and TRIM21 proteins.

Recombinant TRIM5-21R proteins bind HIV-1 CA-NC assemblies. Although numerous studies have established that the B30.2/SPRY domains of TRIM5 α proteins dictate the specificity of retroviral capsid recognition (34, 38, 41, 54–56, 68), direct binding of TRIM5 α proteins to retroviral CA protein assemblies has not yet been demonstrated. We therefore tested whether pure recombinant TRIM5-21R proteins could bind

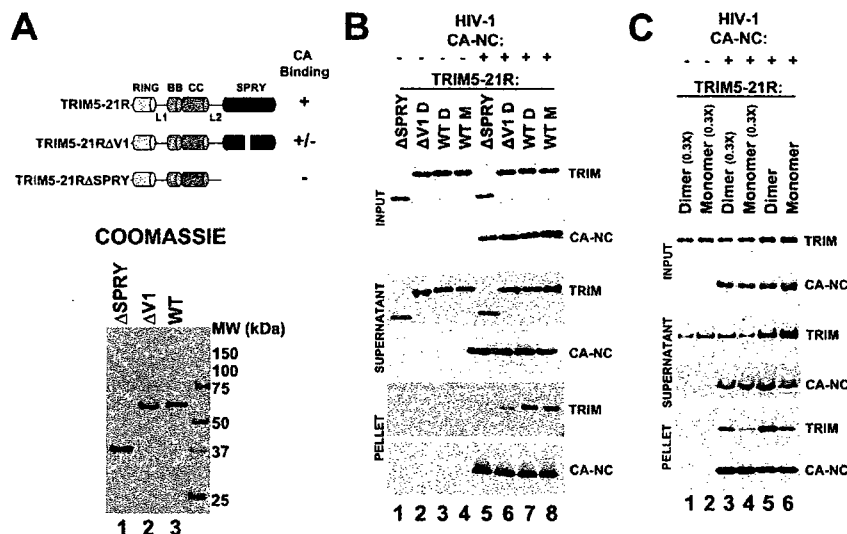


FIG. 5. TRIM5-21R binds CA-NC assemblies. (A) Schematic summary (above) and SDS-PAGE/Coomassie blue analyses (below) of purified full-length dimeric TRIM5-21R (lane 3, denoted WT), a dimeric TRIM5-21R construct missing part of the V1 loop (lane 2, denoted Δ V1), and a monomeric TRIM5-21R construct missing the entire SPRY domain (lane 1, denoted Δ SPRY). (B) TRIM5-21R protein binding to CA-NC/DNA assemblies. Monomeric (M) or dimeric (D) TRIM5-21R (WT, lanes 3 and 4 and lanes 7 and 8), TRIM5-21R Δ V1 (Δ V1, lanes 2 and 6), or TRIM5-21R Δ SPRY (Δ SPRY, lanes 1 and 5) proteins were incubated alone (lanes 1 to 4) or with CA-NC/DNA assemblies (lanes 5 to 8) and then centrifuged through a 70% sucrose cushion to separate CA-NC assemblies and bound proteins (pellet) from unbound and lower-molecular-weight proteins (supernatant). Western blots show the distribution of TRIM (α -FLAG, first, third, and fifth panels) and CA-NC (α -CA, second, fourth, and sixth panels). Note that CA-NC assemblies bound full-length TRIM5-21R constructs better than either TRIM5-21R Δ V1 or TRIM5-21R Δ SPRY. Ratios of bound CA-NC and TRIM5-21R proteins were obtained by combining known input protein concentrations, and quantification of bound CA-NC levels using a standard curve of known CA-NC protein concentrations, and quantification of Western blot band intensities. Estimated bound ratios were as follows: CA-NC/TRIM5-21R dimer = 1.1, CA-NC/TRIM5-21R monomer = 0.8, and CA-NC/TRIM5-21R Δ V = 0.18. (C) CA-NC/DNA assemblies bind better to dimeric TRIM5-21R proteins than to monomeric proteins under stringent conditions. Monomeric (lanes 2, 4, and 6) or dimeric (lanes 1, 3, and 5) proteins were incubated alone (lanes 1 and 2) or with CA-NC/DNA assemblies (lanes 3 to 6) and then centrifuged through a 70% sucrose cushion to separate CA-NC assemblies and bound proteins (pellet) from unbound and lower molecular weight proteins (supernatant). Western blots show the distribution of TRIM5-21R (α -FLAG, TRIM panels) and CA-NC (α -CA, CA-NC panels). The concentrations of TRIM5-21R proteins in lanes 5 and 6 were 3.33-fold higher than in lanes 3 and 4, and all binding assays were performed at lower protein concentrations than those shown in part (B) (see Materials and Methods). Note that under these conditions, CA-NC assemblies bound dimeric TRIM5-21R better than monomeric TRIM5-21R. The estimated ratios of bound proteins were as follows: CA-NC/TRIM5-21R dimer (0.15 μ M input) = 0.025; CA-NC/TRIM5-21R monomer (0.15 μ M input) = 0.01, CA-NC/TRIM5-21R dimer (0.5 μ M input) = 0.068; and CA-NC/TRIM5-21R monomer (0.5 μ M input) = 0.028.

the tubular and conical assemblies formed *in vitro* by pure recombinant HIV-1 CA-NC proteins on DNA templates. Previous studies have shown that these CA-NC/DNA assemblies form the same hexagonal surface lattices as authentic HIV-1 capsids and should therefore present native-like capsid surfaces for TRIM5-21R recognition. Our binding studies took advantage of the observation that CA-NC/DNA assemblies can be separated from free proteins by centrifugation through sucrose cushions (56). TRIM5-21R proteins therefore remained in the supernatants above the cushion, unless they bound and copelleted with the CA-NC/DNA assemblies.

Our studies used both monomeric and dimeric wild-type TRIM5-21R proteins, as well as two mutant TRIM5-21R proteins used as specificity controls (Fig. 5A). The first specificity control (denoted TRIM5-21R Δ V1) lacked 13 residues from the middle of the V1 recognition loop of the SPRY domain (10). This loop is required for efficient HIV-1 capsid binding

and restriction, although the TRIM5-21R Δ V1 protein does retain modest residual HIV-1 restriction activity (10; see Fig. S1A in the supplemental material). The recombinant TRIM5-21R Δ V1 protein behaved like wild-type TRIM5-21R in that it formed both monomers and dimers, and the purified TRIM5-21R Δ V1 dimer was used in our studies. The second specificity control (denoted TRIM5-21R Δ SPRY) lacked the entire SPRY domain and the preceding L2 linker. This control was used because TRIM5 constructs lacking SPRY domains cannot bind HIV-1 capsid in extracts or restrict HIV-1 replication *in vivo* (56). This construct differed from wild-type TRIM5-21R in that it was exclusively monomeric (data not shown), and the purified monomer was therefore used in our studies.

As shown in Fig. 5B, CA-NC/DNA proteins formed a mixture of assembled tubes and cones, which pelleted to the bottom of the sucrose cushion, and disassembled proteins, which remained in the supernatant (lanes 5 to 8). As expected, all

TRIM5-21R proteins remained exclusively in the supernatant in the absence of CA-NC/DNA assemblies (lanes 1 to 4, compare panels 3 and 5). In the presence of CA-NC/DNA assemblies, however, both monomeric and dimeric wild-type TRIM5-21R proteins partitioned between the supernatant and pellet fractions, indicating that both TRIM5-21R proteins could bind CA-NC/DNA assemblies (compare lanes 7 and 8 to lanes 3 and 4 in the sixth panel). The TRIM5-21R Δ V1 protein also bound detectably to CA-NC/DNA assemblies (compare lane 6 to lane 3), but at much lower levels than either of the two wild-type TRIM5-21R proteins (compare lane 6 to lanes 7 and 8). A deletion in the SPRY domain V1 loop therefore reduced, but did not entirely eliminate, CA-NC/DNA binding. The TRIM5-21R Δ SPRY protein did not bind CA-NC/DNA assemblies detectably in this assay, indicating that the SPRY domain was required for CA-NC/DNA binding (compare lane 5 to lanes 7 and 8). These experiments demonstrate that pure recombinant TRIM5-21R proteins bind directly to CA-NC/DNA assemblies and show that efficient binding requires the SPRY domain and its V1 loop.

Although our binding experiments were not performed under equilibrium conditions, we have nevertheless estimated the concentrations and stoichiometries of the binding reaction components in an initial effort to define the parameters that govern the TRIM5-CA interaction. CA-NC tubes and cones can assemble and disassemble reversibly, and we therefore estimated the concentration of CA-NC protein in the pelletable assemblies by quantifying Western blot band intensities and comparing them to a standard curve of known CA-NC concentrations. Analyzed in this fashion, the pelletable CA-NC protein in each experiment shown in Fig. 5B corresponded to 11 pmol (corresponding to an initial concentration of 55 nM). The initial concentration of TRIM5-21R subunits in each reaction mixture was 5 μ M, and the quantity of pelleted TRIM5-21R dimer corresponded to 12 pmol of protein. Thus, in this experiment, the binding reaction was performed with substantial excess of TRIM5-21R dimer over assembled CA-NC protein (~100-fold), and under these conditions the ratio of bound TRIM5-21 to CA-NC was approximately 1:1. The TRIM5-21R Δ V1 protein bound less well in this experiment, at a TRIM5-21R Δ V1/CA-NC ratio of 0.18:1. Although these estimated values neglect several potential complications, including possible incomplete CA-NC tube pelleting efficiency and dissociation of CA-NC assemblies during the assay, the data nevertheless imply that TRIM5-21R can bind assembled CA-NC lattices at nearly stoichiometric levels.

CA-NC/DNA assemblies bind TRIM5-21R dimers more efficiently than monomers. TRIM5 α protein oligomerization has been shown to enhance retroviral capsid binding owing to avidity effects (27), and it was therefore surprising that CA-NC/DNA assemblies bound equivalent levels of TRIM5-21R monomers and dimers in the previous assay. We therefore tested whether more stringent binding conditions might reveal differential CA-NC binding of TRIM5-21R monomers and dimers. The stringency was increased by reducing the TRIM5-21R concentration, and under these conditions CA-NC/DNA assemblies bound TRIM5-21R dimers better than monomers. This effect is illustrated in Fig. 5C, which shows that TRIM5-21R dimers bound better at two different initial TRIM5-21R concentrations (0.5 and 0.15 μ M, compare lanes 3 and 4 to

lanes 5 and 6 in the bottom panel). Under these more stringent conditions, the quantity of pelletable CA-NC protein did not change, but the ratios of pelletable CA-NC to bound TRIM5-21R proteins were substantially lower, demonstrating that the binding conditions were indeed more stringent (see the caption to Fig. 5C). These data suggest that although TRIM5-21R monomers and dimers can both bind CA-NC/DNA assemblies, TRIM5-21R dimerization enhances the efficiency of binding under more stringent conditions, in agreement with the observation that disruption of the coiled-coil oligomerization motif of TRIM5 α inhibits restriction (27).

Electron microscopic analyses of TRIM5-21R-decorated CA-NC tubes. The effects of TRIM5-21R binding to CA-NC tubes were visualized by using transmission electron microscopy of negatively stained CA-NC/DNA assemblies incubated with a 10- to 50-fold excess of TRIM5-21R prior to imaging. As shown in Fig. 6, TRIM5-21R binding did not dramatically alter the appearance of CA-NC/DNA tubes, but two effects were evident. First, CA-NC/DNA tubes incubated with excess TRIM5-21R consistently exhibited increased exterior stain deposition compared to tubes incubated with control TRIM5-21R Δ V1 or TRIM5-21R Δ SPRY proteins. The simplest explanation for this effect is that it reflects formation of TRIM5-21R coats on the CA-NC/DNA tube exteriors. This effect was sometimes subtle and difficult to discern, but in extreme cases resulted in a thick, dark irregular coat on tube exteriors, as though the TRIM5-21R were aggregating about the tube (Fig. 6, panel 8). Second, CA-NC/DNA tubes decorated with TRIM5-21R frequently appeared more broken and irregular than their counterparts incubated with control TRIM5-21R Δ V1 or TRIM5-21R Δ SPRY proteins (tube breaks are highlighted by arrows in Fig. 6, panels 5 to 8). This observation suggests that high levels of TRIM5-21R destabilized the tubes and increased their fragmentation, although the effect was modest, and most tubes remained intact. Overall, our electron microscopic data indicate that TRIM5-21R can coat and destabilize CA-NC/DNA assemblies, but both effects were subtle. Higher-resolution cryo-electron microscopic analyses will be required to determine the density and location of TRIM5-21 binding sites on the CA-NC/DNA assemblies.

EIAV core binding assays. Retroviral cores are the actual targets of TRIM5 α restriction, and we therefore tested whether TRIM5-21R could bind authentic, purified core particles. Cores isolated from EIAV vectors were used in these experiments because TRIM5 α_{rh} restricts EIAV (10, 23, 71; see Fig. S1B in the supplemental material) and because we are able to purify cores from membrane-stripped EIAV virions more reproducibly and in higher yields than HIV-1 cores. EIAV cores were membrane stripped with a brief Triton X-100 detergent treatment (30) and then purified on a sucrose gradient where they concentrated at the expected density of ~1.24 g/ml (Fig. 7A).

Purified EIAV cores were incubated with a ~16-fold excess of pure recombinant TRIM5-21R or control Δ V1 or Δ SPRY variants. As in the CA-NC/DNA binding assay, high-molecular-weight EIAV cores were pelleted by centrifugation through a sucrose cushion (Fig. 7B, lanes 4 to 6 in the sixth panel). Wild-type dimeric TRIM5-21R protein bound and copelleted with the EIAV cores but did not pellet in the absence of cores (compare lanes 3 and 6, fifth panel). In contrast, much lower

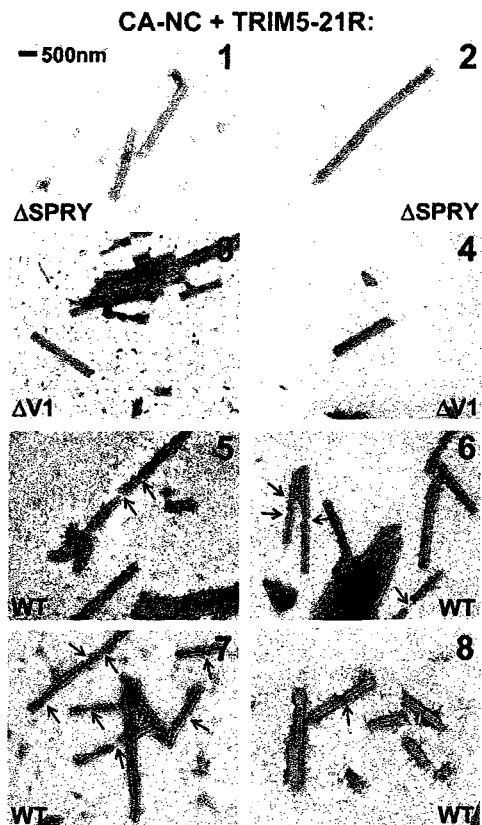


FIG. 6. Electron microscopic images of CA-NC assemblies incubated with full-length TRIM5-21R or deletion mutants. Negatively stained, transmission electron microscopic images of CA-NC assemblies incubated with monomeric TRIM5-21R Δ SPRY (panels 1 and 2), dimeric TRIM5-21R Δ V1 (panels 3 and 4), or full-length dimeric TRIM5-21R (panels 5 to 8). Note that CA-NC/DNA assemblies incubated with TRIM5-21R show enhanced exterior staining and more frequent breaks (arrows) compared to the TRIM5-21R Δ V1 or TRIM5-21R Δ SPRY controls. TRIM5-21R-induced breaks were quantified by scoring randomly selected electron microscopic images of CA-NC/DNA tubes for the presence of discontinuities (see arrows), with the following results: TRIM5-21R Δ SPRY-treated tubes (0% broken, 0 total breaks, $n = 26$ tubes), TRIM5-21R Δ V1-treated tubes (4% broken, 2 total breaks, $n = 50$), and TRIM5-21R-treated tubes (42% broken, 55 total breaks, $n = 50$).

levels of the control TRIM5-21R Δ V1 protein copelleted with the EIAV cores (compare lanes 5 and 6), and no detectable TRIM5-21R Δ SPRY protein copelleted with the cores (compare lanes 4 and 6). We therefore conclude that TRIM5-21R binds and copellets with authentic EIAV core particles and that this interaction is specific because the wild-type TRIM5-21R protein binds much better than control proteins lacking part of the V1 loop or the entire SPRY domain.

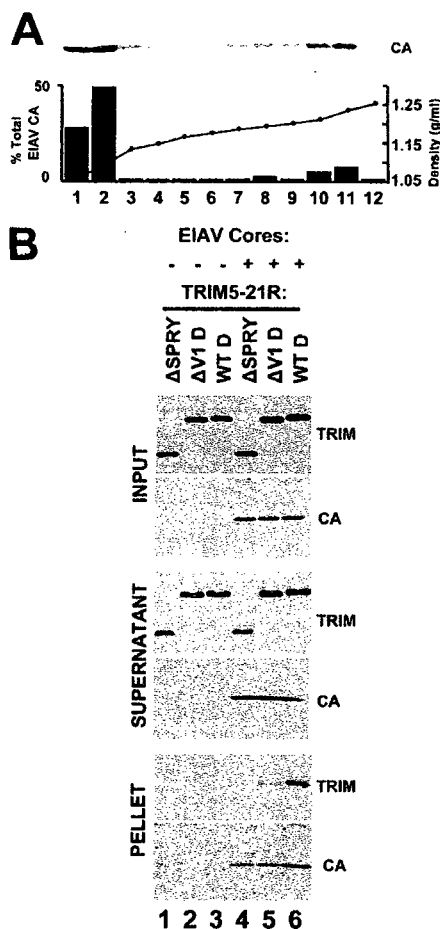


FIG. 7. TRIM5-21R binds EIAV cores. (A) Sucrose gradient purification of membrane-stripped cores produced by an EIAV vector. The Western blot (α -CA) shows the distribution of EIAV CA protein across a sucrose density gradient (with fraction densities shown). The CA distribution is quantified below, and the CA protein in fractions 10 to 12 corresponds to core particles. (B) TRIM5-21R protein binding to purified EIAV cores. Dimeric TRIM5-21R (WT, lanes 3 and 6), dimeric TRIM5-21R Δ V1 (Δ V1, lanes 2 and 5), or monomeric TRIM5-21R Δ SPRY (Δ SPRY, lanes 1 and 4) proteins were incubated alone (lanes 1 to 3) or with purified EIAV cores (lanes 4 to 6) and then centrifuged through a 57% sucrose cushion to separate EIAV cores and bound proteins (pellet) from unbound and lower-molecular-weight proteins (supernatant). Western blots show the distribution of TRIM (α -FLAG, TRIM panels) and EIAV CA (α -CA, CA panels). Note that the pelleted EIAV cores bound full-length TRIM5-21R better than either TRIM5-21R Δ V1 or TRIM5-21R Δ SPRY.

DISCUSSION

We have described the expression, purification, and characterization of TRIM5-21R, which represents the first study of a pure recombinant TRIM5 α protein capable of restricting HIV-1 replication. Our experiments provide direct experimental support for the importance of both TRIM5 α protein oligomerization and the B30.2/SPRY domain in retroviral capsid recognition. Specifically, we found that deletion of the SPRY domain eliminates binding to both HIV-1 CA-NC assemblies and EIAV cores, that a deletion in the V1 loop reduces binding significantly, and that TRIM5-21R dimerization enhances binding to HIV-1 CA-NC assemblies under stringent binding conditions. These *in vitro* binding activities correlate well with restriction activities *in vivo*, indicating that our *in vitro* experiments accurately recapitulate interactions between capsids and TRIM5 proteins during retroviral restriction.

Our experiments indicate that restricting TRIM5 α proteins, including TRIM5 α itself, are dimers. Previous studies had established that TRIM5 α proteins oligomerize and that the oligomeric state might be trimeric (27, 36). We now show, however, that TRIM5-21R forms dimers but that chemically cross-linked TRIM5-21R dimers exhibit anomalously slow electrophoretic mobility, causing them to appear trimeric. Cross-linked TRIM5 α proteins expressed in mammalian cells exhibit very similar mobilities, implying that authentic TRIM5 α proteins are also dimeric. It will be of interest to determine whether other members of the TRIM protein family are also dimers. In this regard, we note that others have reported that the related TRIM21 protein forms trimers (45). This conclusion was again based upon the electrophoretic mobility of chemically cross-linked TRIM21 proteins, however, which may be subject to the same uncertainties as cross-linked TRIM5 α proteins. Moreover, another group has reported that the TRIM21/SS-A/Ro52 protein may instead be dimeric, based on its gel filtration mobility (59), and two groups have reported that the isolated coiled-coil region of TRIM21 forms dimers rather than trimers (27, 40). We therefore speculate that dimerization may be a common property of many members of the tripartite motif protein family. If so, there are several intriguing similarities between TRIM proteins and immunoglobulin G proteins, since both types of protein can dimerize to display a pair of terminal immunoglobulin-like domains that can recognize antigens, including repeating motifs on viral capsid surfaces.

Once formed, TRIM5-21R dimers are stable and can be purified without appreciable dissociation. Similarly, we saw no evidence of monomer accumulation in equilibrium distributions of TRIM5-21R dimers across a range of micromolar concentrations, again indicating that assembled TRIM5-21R dimers are highly stable (or kinetically inert). Nevertheless, monomeric TRIM5-21R proteins were produced in our baculoviral expression system. These TRIM5-21R monomers did not exhibit a propensity to dimerize, suggesting that they may be kinetically "trapped," perhaps owing to misfolding of the coiled-coil motif. Not surprisingly, a TRIM5-21R construct missing the SPRY domain and preceding L2 linker was exclusively monomeric, a finding consistent with previous experiments showing that the TRIM5 α L2 region is required for oligomerization (40).

SPRY domains of TRIM proteins, presumably including TRIM5 α , adopt immunoglobulin-like folds consisting of two antiparallel β -sheets. The ligand binding surface is located at one end of the β -sandwich and is composed of six extended loops and two pockets (25, 61). The loops, which are hyper-variable in both amino acid composition and length, share homology with the complementarity-determining region loops of immunoglobulins and account for the species specificity of restriction. In particular, the variable region 1 loop of TRIM5 α_{rh} is a critical determinant of capsid binding and antiviral activity, and a deletion within the V1 loop also reduced capsid recognition by TRIM5-21R in our *in vitro* binding assays. Our results are therefore in good agreement with the prevailing model that retroviral capsid recognition is mediated by the variable loops of the SPRY domain of TRIM5 α (34, 54, 68). Furthermore, our experiments demonstrate that this interaction is direct and can be highly efficient. Indeed, under some conditions we observed essentially stoichiometric binding of TRIM5-21R to CA-NC assemblies. Electron microscopic images of CA-NC tubes decorated with TRIM5-21R proteins also suggest that TRIM5-21R can "coat" the CA-NC surface, although higher-resolution studies will be necessary to confirm and extend this finding.

TRIM5 α restriction represents a very intriguing problem in molecular recognition because specific TRIM5 α alleles are able to recognize a remarkable variety of different retroviral capsids, despite their substantial variation in amino acid sequence and surface topology. This attribute is exemplified by TRIM5 α_{rh} , which is able to recognize both EIAV and HIV-1 capsids even though the HIV-1 and EIAV CA proteins share only ~25% sequence identity. Retroviral capsids do share a common organization, however, since all capsids are assembled on a hexagonal surface lattice composed of CA hexamers. It is therefore likely that both reading heads of the dimeric TRIM5 α protein engage similar sites on the capsid surface, and this is most easily accomplished by binding across a local twofold symmetry axis on the capsid lattice (although asymmetric binding is also a formal possibility). Hexagonal HIV-1 CA arrays exhibit two distinct types of local twofold symmetry, one of which is colinear with the local sixfold axes and the other of which connects adjacent hexamers. These two sites have different subunit orientations and spacing, and it is therefore likely that only one of these sites is the preferred TRIM5 α binding site.

In solution, HIV-1 CA forms dimers that correspond to the twofold symmetric interactions between adjacent hexamers in the assembled hexagonal lattice. Expression of HIV-1 CA alone does not abrogate restriction, however, indicating that the CA dimer alone probably does not create a high-affinity TRIM5 α binding site (14, 16, 51, 52). It is possible that CA alone cannot abrogate restriction because the CA solution dimer is not the preferred TRIM5 α binding site or because this CA dimer is weak and/or inherently flexible. However, an interesting alternative is that isolated SPRY domains, and even isolated TRIM5 α dimers, may have weak intrinsic capsid binding energies and that high-affinity binding is achieved through the cooperative formation of even higher-order TRIM5 α assemblies. This model would be consistent with the observation that TRIM5 α proteins are highly susceptible to aggregation or assembly *in vitro* and *in vivo*. Indeed, fluorescence images

indicate that at least in some cases, large numbers of TRIM5 α proteins can assemble on HIV-1 capsids *in vivo* (6). This model could also help explain how individual TRIM5 alleles can bind such a variety of different retroviral capsid surfaces because direct TRIM5 α -CA interfaces would not need to form a large number of favorable interactions but rather could utilize just a few specific interactions and then be stabilized by the cooperative formation of multiple TRIM5 α -CA and TRIM5 α -TRIM5 α interfaces. In contrast, isolated TRIM-Cyp proteins, in which a cyclophilin A domain replaces the SPRY domain, may bind specific retroviral capsids with higher affinities because the cyclophilin A domain can make specific interactions with individual HIV-1 CA subunits (18, 70). This "high-affinity" recognition mechanism could explain why the upstream RING and B-box domains play less important roles in TRIM-Cyp restriction activity (10, 13, 65, 66) but may come at the cost of reducing the ability of TRIM-Cyp restriction factors to recognize as broad a variety of different retroviral capsids as canonical TRIM5 α alleles.

Our electron microscopic analyses also indicated that high-level TRIM5-21R binding destabilizes the CA-NC lattice to some degree because TRIM5-21R induced many more breaks in CA-NC/DNA tubes than did nonbinding control TRIM5-21R constructs. Destabilization of the CA-NC lattice could reflect steric hindrance upon saturation binding of TRIM5-21R and/or mismatches in the symmetry or spacing between the CA-NC lattice and putative higher-order TRIM5-21R assemblies. We emphasize, however, that the capsid destabilization induced by TRIM5-21R binding was a relatively minor effect because most CA-NC assemblies remained largely intact, even in the presence of a large excess of TRIM5-21R. Similarly, EIAV cores remained pelletable in the presence of excess TRIM5-21R. Thus, the dramatic destabilization of retroviral capsids observed under restrictive conditions *in vivo* does not appear to be a direct consequence of TRIM5 α binding. Rather, it appears that capsid recognition by TRIM5 α and subsequent destabilization/restriction are largely separable events. This idea is consistent with a series of other observations, including the fact that mutations in the B-box region of TRIM5 α can abrogate restriction without apparently affecting capsid recognition (11), and that capsid destabilization is abrogated upon inhibition of the proteasome (6, 10).

In summary, our biochemical and biophysical studies have established that purified recombinant TRIM5-21R forms stable dimers that can bind specifically to higher-order HIV-1 CA-NC assemblies and to authentic EIAV core particles. It will be important to ascertain precisely how TRIM5 α binds the capsid lattice and to determine the minimal CA assembly required for high-affinity binding, and we anticipate that the availability of recombinant TRIM5-21R protein will facilitate such studies.

ACKNOWLEDGMENTS

We are grateful to Chad Nelson and the University of Utah Mass Spectrometry facility for ESI and LC mass spectral analyses, Rachel Kleit for the gift of expression vectors for E1 and E2 enzymes, and Chris Hill for critical review of the manuscript.

This research was supported by National Institutes of Health grants AI076121 (to C.A.), AI063978 and AI076094 (to J.G.S.), and AI045405 and GM082545 (to W.L.S.).

REFERENCES

1. Accola, M. A., A. Ohagen, and H. G. Gottlinger. 2000. Isolation of human immunodeficiency virus type 1 cores: retention of Vpr in the absence of p6(gag). *J. Virol.* 74:6198–6202.
2. Anderson, J. L., E. M. Campbell, X. Wu, N. Vandegraaff, A. Engelman, and T. J. Hope. 2006. Proteasome inhibition reveals that a functional preintegration complex intermediate can be generated during restriction by diverse TRIM5 proteins. *J. Virol.* 80:9754–9760.
3. Bieniasz, P. D. 2004. Intrinsic immunity: a front-line defense against viral attack. *Nat. Immunol.* 5:1109–1115.
4. Briggs, J. A., T. Wilk, R. Welker, H. G. Krausslich, and S. D. Fuller. 2003. Structural organization of authentic, mature HIV-1 virions and cores. *EMBO J.* 22:1707–1715.
5. Brzovic, P. S., A. Lissounov, D. E. Christensen, D. W. Hoyt, and R. E. Kleit. 2006. A UbcH5/ubiquitin noncovalent complex is required for processive BRCA1-directed ubiquitination. *Mol. Cell* 21:873–880.
6. Campbell, E. M., O. Perez, J. L. Anderson, and T. J. Hope. 2008. Visualization of a proteasome-independent intermediate during restriction of HIV-1 by rhesus TRIM5 α . *J. Cell Biol.* 180:549–561.
7. Campbell, S., and V. M. Vogt. 1995. Self-assembly *in vitro* of purified CA-NC proteins from Rous sarcoma virus and human immunodeficiency virus type 1. *J. Virol.* 69:6487–6497.
8. Christensen, D. E., P. S. Brzovic, and R. E. Kleit. 2007. E2-BRCA1 RING interactions dictate synthesis of mono- or specific polyubiquitin chain linkages. *Nat. Struct. Mol. Biol.* 14:941–948.
9. Cole, J. L. 2004. Analysis of heterogeneous interactions. *Methods Enzymol.* 384:212–232.
10. Diaz-Griffero, F., A. Kar, M. Lee, M. Stremiau, E. Poeschla, and J. Sodroski. 2007. Comparative requirements for the restriction of retrovirus infection by TRIM5 α and TRIMCyp. *Virology* 369:400–410.
11. Diaz-Griffero, F., A. Kar, M. Perron, S. H. Xiang, H. Javanbakht, X. Li, and J. Sodroski. 2007. Modulation of retroviral restriction and proteasome inhibitor-resistant turnover by changes in the TRIM5 α B-box 2 domain. *J. Virol.* 81:10362–10378.
12. Diaz-Griffero, F., X. Li, H. Javanbakht, B. Song, S. Wellkala, M. Stremiau, and J. Sodroski. 2006. Rapid turnover and polyubiquitylation of the retroviral restriction factor TRIM5. *Virology* 349:300–315.
13. Diaz-Griffero, F., N. Vandegraaff, Y. Li, K. McGee-Estrada, M. Stremiau, S. Wellkala, Z. Si, A. Engelman, and J. Sodroski. 2006. Requirements for capsid-binding and an effector function in TRIMCyp-mediated restriction of HIV-1. *Virology* 351:404–419.
14. Dodding, M. F., M. Bock, M. W. Yap, and J. P. Stoye. 2005. Capsid processing requirements for abrogation of fvl and ref1 restriction. *J. Virol.* 79:10571–10577.
15. Fisher, R. J., A. Rein, M. Fivash, M. A. Urbaneja, J. R. Casas-Finet, M. Medaglia, and L. E. Henderson. 1998. Sequence-specific binding of human immunodeficiency virus type 1 nucleocapsid protein to short oligonucleotides. *J. Virol.* 72:1902–1909.
16. Forshey, B. M., J. Shi, and C. Alken. 2005. Structural requirements for recognition of the human immunodeficiency virus type 1 core during host restriction in owl monkey cells. *J. Virol.* 79:869–875.
17. Forshey, B. M., U. von Schwedler, W. I. Sundquist, and C. Alken. 2002. Formation of a human immunodeficiency virus type 1 core of optimal stability is crucial for viral replication. *J. Virol.* 76:5667–5677.
18. Gamble, T. R., F. V. Vajdos, S. Yoo, D. K. Worthylnke, M. Houseweart, W. I. Sundquist, and C. P. Hill. 1996. Crystal structure of human cyclophilin A bound to the amino-terminal domain of HIV-1 capsid. *Cell* 87:1285–1294.
19. Ganser-Pornillos, B. K., A. Cheng, and M. Yeager. 2007. Structure of full-length HIV-1 CA: a model for the mature capsid lattice. *Cell* 131:70–79.
20. Ganser-Pornillos, B. K., M. Yeager, and W. I. Sundquist. 2008. The structural biology of HIV assembly. *Curr. Opin. Struct. Biol.* 18:203–217.
21. Ganser, B. K., S. Li, V. Y. Klishko, J. T. Finch, and W. I. Sundquist. 1999. Assembly and analysis of conical models for the HIV-1 core. *Science* 283:80–83.
22. Hatfield, P. M., J. Callis, and R. D. Vierstra. 1990. Cloning of ubiquitin activating enzyme from wheat and expression of a functional protein in *Escherichia coli*. *J. Biol. Chem.* 265:15813–15817.
23. Hatziloannou, T., S. Cowan, S. P. Goff, P. D. Bieniasz, and G. J. Towers. 2003. Restriction of multiple divergent retroviruses by Lv1 and Ref1. *EMBO J.* 22:385–394.
24. Hennig, J., A. Bresell, M. Sandberg, K. D. Hennig, M. Wahren-Herlenius, B. Persson, and M. Sunnerhagen. 2008. The fellowship of the RING: the RING-B-box linker region interacts with the RING in TRIM21/Ro52, contains a native autoantigenic epitope in Sjogren syndrome, and is an integral and conserved region in TRIM proteins. *J. Mol. Biol.* 377:431–449.
25. James, L. C., A. H. Keeble, Z. Khan, D. A. Rhodes, and J. Trowsdale. 2007. Structural basis for PRYSPRY-mediated tripartite motif (TRIM) protein function. *Proc. Natl. Acad. Sci. USA* 104:6200–6205.
26. Javanbakht, H., F. Diaz-Griffero, M. Stremiau, Z. Si, and J. Sodroski. 2005. The contribution of RING and B-box 2 domains to retroviral restriction mediated by monkey TRIM5 α . *J. Biol. Chem.* 280:26933–26940.

27. Javanbakht, H., W. Yuan, D. F. Yeung, B. Song, F. Diaz-Griffero, Y. Li, X. Li, M. Stremlau, and J. Sodroski. 2006. Characterization of TRIM5 α trimerization and its contribution to human immunodeficiency virus capsid binding. *Virology* 353:234–246.
28. Jin, Z., L. Jin, D. L. Peterson, and C. L. Lawson. 1999. Model for lentivirus capsid core assembly based on crystal dimers of EIAV p26. *J. Mol. Biol.* 286:83–93.
29. Kekesova, Z., L. M. Ylenn, and G. J. Towers. 2004. The human and African green monkey TRIM5 α genes encode Rfl1 and Lvl retroviral restriction factor activities. *Proc. Natl. Acad. Sci. USA* 101:10780–10785.
30. Kotov, A., J. Zhou, P. Flicker, and C. Alken. 1999. Association of Nef with the human immunodeficiency virus type 1 core. *J. Virol.* 73:8824–8830.
31. Laue, T., B. Shah, T. Ridgeway, and S. Pelletier. 1992. Computer-aided interpretation of analytical sedimentation data for proteins, p. 90–125. In A. Rowe and J. Horton (ed.), *Ultracentrifugation in biochemistry and polymer science*. Royal Society of Chemistry, Cambridge, England.
32. Li, S., C. P. Hill, W. I. Sundquist, and J. T. Finch. 2000. Image reconstructions of helical assemblies of the HIV-1 CA protein. *Nature* 407:409–413.
33. Li, X., B. Gold, C. O'Huigin, F. Diaz-Griffero, B. Song, Z. Si, Y. Li, W. Yuan, M. Stremlau, C. Mische, H. Javanbakht, M. Scally, C. Winkler, M. Dean, and J. Sodroski. 2006. Unique features of TRIM5 α among closely related human TRIM family members. *Virology* 360:419–433.
34. Li, Y., X. Li, M. Stremlau, M. Lee, and J. Sodroski. 2006. Removal of arginine 332 allows human TRIM5 α to bind human immunodeficiency virus capsids and to restrict infection. *J. Virol.* 80:6738–6744.
35. Liu, H. L., Y. Q. Wang, C. H. Liao, Y. Q. Kuang, Y. T. Zheng, and B. Su. 2005. Adaptive evolution of primate TRIM5 α , a gene restricting HIV-1 infection. *Gene* 362:109–116.
36. Mische, C. C., H. Javanbakht, B. Song, F. Diaz-Griffero, M. Stremlau, B. Strack, Z. Si, and J. Sodroski. 2005. Retroviral restriction factor TRIM5 α is a trimer. *J. Virol.* 79:14446–14450.
37. Nisole, S., and A. Saib. 2004. Early steps of retrovirus replicative cycle. *Retrovirology* 1:9.
38. Ohkura, S., M. W. Yap, T. Sheldon, and J. P. Stoye. 2006. All three variable regions of the TRIM5 α B30.2 domain can contribute to the specificity of retrovirus restriction. *J. Virol.* 80:8554–8565.
39. O'Rourke, J. P., J. C. Olson, and B. A. Bunnell. 2005. Optimization of equine infectious anemia derived vectors for hematopoietic cell lineage gene transfer. *Gene Ther.* 12:22–29.
40. Ottosson, L., J. Hennig, A. Espinosa, S. Brauner, M. Wahren-Herlenius, and M. Sommerbom. 2006. Structural, functional, and immunologic characterization of folded subdomains in the Ro52 protein targeted in Sjogren's syndrome. *Mol. Immunol.* 43:588–598.
41. Perez-Caballero, D., T. Hatziloannou, A. Yang, S. Cowan, and P. D. Bieniasz. 2005. Human tripartite motif 5 α domains responsible for retrovirus restriction activity and specificity. *J. Virol.* 79:8969–8978.
42. Perron, M. J., M. Stremlau, M. Lee, H. Javanbakht, B. Song, and J. Sodroski. 2007. The human TRIM5 α restriction factor mediates accelerated uncoating of the N-tropic murine leukemia virus capsid. *J. Virol.* 81:2138–2148.
43. Perron, M. J., M. Stremlau, B. Song, W. Ulm, R. C. Mulligan, and J. Sodroski. 2004. TRIM5 α mediates the postentry block to N-tropic murine leukemia viruses in human cells. *Proc. Natl. Acad. Sci. USA* 101:11827–11832.
44. Pickart, C. M., and S. Ransil. 2005. Controlled synthesis of polyubiquitin chains. *Methods Enzymol.* 399:21–36.
45. Rhodes, D. A., and J. Trowsdale. 2007. TRIM21 is a trimeric protein that binds IgG Fc via the B30.2 domain. *Mol. Immunol.* 44:2406–2414.
46. Roberts, M. M., and S. Oroszlan. 1989. The preparation and biochemical characterization of intact capsids of equine infectious anemia virus. *Biochem. Biophys. Res. Commun.* 160:486–494.
47. Rold, C. J., and C. Alken. 2008. Proteasomal degradation of TRIM5 α during retrovirus restriction. *PLoS Pathog.* 4:e1000074.
48. Sandrin, V., and F. L. Cosset. 2006. Intracellular versus cell surface assembly of retroviral pseudotypes is determined by the cellular localization of the viral glycoprotein, its capacity to interact with Gag, and the expression of the Nef protein. *J. Biol. Chem.* 281:528–542.
- 48a. Sanes, J. R., J. L. Rubenstein, and J. F. Nicolas. 1986. Use of recombinant retrovirus to study post-implantation cell lineage in mouse embryos. *Embo J.* 5:3133–3142.
49. Sawyer, S. L., M. Emerman, and H. S. Malik. 2007. Discordant evolution of the adjacent antiretroviral genes TRIM22 and TRIM5 in mammals. *PLoS Pathog.* 3:e197.
50. Sawyer, S. L., L. I. Wu, M. Emerman, and H. S. Malik. 2005. Positive selection of primate TRIM5 α identifies a critical species-specific retroviral restriction domain. *Proc. Natl. Acad. Sci. USA* 102:2832–2837.
51. Sebastlan, S., and J. Luban. 2005. TRIM5 α selectively binds a restriction-sensitive retroviral capsid. *Retrovirology* 2:40.
52. Shi, J., and C. Alken. 2006. Saturation of TRIM5 α -mediated restriction of HIV-1 infection depends on the stability of the incoming viral capsid. *Virology* 350:493–500.
53. Song, B., F. Diaz-Griffero, D. H. Park, T. Rogers, M. Stremlau, and J. Sodroski. 2005. TRIM5 α association with cytoplasmic bodies is not required for antiretroviral activity. *Virology* 343:201–211.
54. Song, B., B. Gold, C. O'Huigin, H. Javanbakht, X. Li, M. Stremlau, C. Winkler, M. Dean, and J. Sodroski. 2005. The B30.2(SPRY) domain of the retroviral restriction factor TRIM5 α exhibits lineage-specific length and sequence variation in primates. *J. Virol.* 79:6111–6121.
55. Stremlau, M., C. M. Owens, M. J. Perron, M. Klessling, P. Autstler, and J. Sodroski. 2004. The cytoplasmic body component TRIM5 α restricts HIV-1 infection in Old World monkeys. *Nature* 427:848–853.
56. Stremlau, M., M. Perron, M. Lee, Y. Li, B. Song, H. Javanbakht, F. Diaz-Griffero, D. J. Anderson, W. I. Sundquist, and J. Sodroski. 2006. Specific recognition and accelerated uncoating of retroviral capsids by the TRIM5 α restriction factor. *Proc. Natl. Acad. Sci. USA* 103:5514–5519.
57. Stremlau, M., M. Perron, S. Wellkula, and J. Sodroski. 2005. Species-specific variation in the B30.2(SPRY) domain of TRIM5 α determines the potency of human immunodeficiency virus restriction. *J. Virol.* 79:3139–3145.
58. Towers, G. J. 2007. The control of viral infection by tripartite motif proteins and cyclophilin A. *Retrovirology* 4:40.
59. Wang, D., J. P. Buyon, Z. Yang, F. Di Donato, M. E. Miranda-Carus, and E. K. Chan. 2001. Leucine zipper domain of 52 kDa SS-A/Ro promotes protein dimer formation and inhibits in vitro transcription activity. *Biochim. Biophys. Acta* 1568:155–161.
- 59a. Ward, D. M., M. B. Vaughn, S. L. Shifflett, P. L. White, A. L. Pollock, J. Hill, R. Schnegelsberger, W. I. Sundquist, and J. Kaplan. 2005. The role of LIP5 and CHMP5 in multivesicular body formation and HIV-1 budding in mammalian cells. *J. Biol. Chem.* 280:10548–10555.
60. Welker, R., H. Hohenberg, U. Tessmer, C. Huckhagel, and H. G. Krausslich. 2000. Biochemical and structural analysis of isolated mature cores of human immunodeficiency virus type 1. *J. Virol.* 74:1168–1177.
61. Woo, J. S., H. Y. Suh, S. Y. Park, and B. H. Oh. 2006. Structural basis for protein recognition by B30.2(SPRY) domains. *Mol. Cell* 24:967–976.
62. Wu, X., J. L. Anderson, E. M. Campbell, A. M. Joseph, and T. J. Hope. 2006. Proteasome inhibitors uncouple rhesus TRIM5 α restriction of HIV-1 reverse transcription and infection. *Proc. Natl. Acad. Sci. USA* 103:7465–7470.
63. Xu, L., L. Yang, P. K. Moltra, K. Hashimoto, P. Rallabhandi, S. Kaul, G. Meroni, J. P. Jensen, A. M. Welsman, and P. D'Arpa. 2003. BTBD1 and BTBD2 colocalize to cytoplasmic bodies with the RBCC/tripartite motif protein, TRIM5 α . *Exp. Cell Res.* 288:84–93.
64. Yamauchi, K., K. Wada, K. Tanji, M. Tanaka, and T. Kamitani. 2008. Ubiquitination of E3 ubiquitin ligase TRIM5 α and its potential role. *FEBS J.* 275:1540–1555.
65. Yap, M. W., M. P. Dodding, and J. P. Stoye. 2006. Trim-cyclophilin A fusion proteins can restrict human immunodeficiency virus type 1 infection at two distinct phases in the viral life cycle. *J. Virol.* 80:4061–4067.
66. Yap, M. W., G. B. Mortuza, I. A. Taylor, and J. P. Stoye. 2007. The design of artificial retroviral restriction factors. *Virology* 365:302–314.
67. Yap, M. W., S. Nisole, C. Lynch, and J. P. Stoye. 2004. Trim5 α protein restricts both HIV-1 and murine leukemia virus. *Proc. Natl. Acad. Sci. USA* 101:10786–10791.
68. Yap, M. W., S. Nisole, and J. P. Stoye. 2005. A single amino acid change in the SPRY domain of human Trim5 α leads to HIV-1 restriction. *Curr. Biol.* 15:73–78.
69. Yee, J. K., A. Mlyanohara, P. LaPorte, K. Bouc, J. C. Burns, and T. Friedmann. 1994. A general method for the generation of high-titer, pantropic retroviral vectors: highly efficient infection of primary hepatocytes. *Proc. Natl. Acad. Sci. USA* 91:9564–9568.
70. Yoo, S., D. G. Myska, C. Yeh, M. McMurray, C. P. Hill, and W. I. Sundquist. 1997. Molecular recognition in the HIV-1 capsid/cyclophilin A complex. *J. Mol. Biol.* 269:780–795.
71. Zhang, F., T. Hatziloannou, D. Perez-Caballero, D. Derse, and P. D. Bieniasz. 2006. Antiretroviral potential of human tripartite motif-5 and related proteins. *Virology* 353:396–409.
72. Zhang, M., M. Windheim, S. M. Roe, M. Peggie, P. Cohen, C. Prodromou, and L. H. Pearl. 2005. Chaperoned ubiquitination: crystal structures of the CHIP U box E3 ubiquitin ligase and a CHIP-Ubc13-Uev1a complex. *Mol. Cell* 20:525–538.

CHAPTER 3

HUMAN ESCRT-II COMPLEX AND ITS ROLE IN HUMAN IMMUNODEFICIENCY VIRUS TYPE 1 RELEASE

Human ESCRT-II Complex and Its Role in Human Immunodeficiency Virus Type 1 Release†

Charles Langelier,¹ Uta K. von Schwedler,¹ Robert D. Fisher,¹ Ivana De Domenico,² Paul L. White,¹ Christopher P. Hill,¹ Jerry Kaplan,² Diane Ward,² and Wesley I. Sundquist^{1*}

Departments of Biochemistry¹ and Pathology,² University of Utah, Salt Lake City, Utah 84112

Received 22 May 2006/Accepted 8 July 2006

The budding of many enveloped RNA viruses, including human immunodeficiency virus type 1 (HIV-1), requires some of the same cellular machinery as vesicle formation at the multivesicular body (MVB). In *Saccharomyces cerevisiae*, the ESCRT-II complex performs a central role in MVB protein sorting and vesicle formation, as it is recruited by the upstream ESCRT-I complex and nucleates assembly of the downstream ESCRT-III complex. Here, we report that the three subunits of human ESCRT-II, EAP20, EAP30, and EAP45, have a number of properties in common with their yeast orthologs. Specifically, EAP45 bound ubiquitin via its N-terminal GRAM-like ubiquitin-binding in EAP45 (GLUE) domain, both EAP45 and EAP30 bound the C-terminal domain of TSG101/ESCRT-I, and EAP20 bound the N-terminal half of CHMP6/ESCRT-III. Consistent with its expected role in MVB vesicle formation, (i) human ESCRT-II localized to endosomal membranes in a VPS4-dependent fashion and (ii) depletion of EAP20/ESCRT-II and CHMP6/ESCRT-III inhibited lysosomal targeting and downregulation of the epidermal growth factor receptor, albeit to a lesser extent than depletion of TSG101/ESCRT-I. Nevertheless, HIV-1 release and infectivity were not reduced by efficient small interfering RNA depletion of EAP20/ESCRT-II or CHMP6/ESCRT-III. These observations indicate that there are probably multiple pathways for protein sorting/MVB vesicle formation in human cells and that HIV-1 does not utilize an ESCRT-II-dependent pathway to leave the cell.

Enveloped RNA viruses like human immunodeficiency virus (HIV) acquire lipid bilayers and exit infected cells by budding through limiting membranes. The process of HIV budding shares a number of similarities with the cellular process of vesicle formation at the multivesicular body (MVB) (reviewed in references 2, 14, 25, 26, 33, 40, and 51). MVB vesicles and HIV virions both bud away from the cytoplasm (58) and share the following mechanistic similarities: (i) a requirement for ubiquitin (Ub) in formation and cargo incorporation (reviewed in references 40 and 81), (ii) recruitment and utilization of the cellular ESCRT-I complex (6, 15, 19, 22, 47, 48, 52, 70, 79), and (iii) a requirement for ESCRT-III, LIP5, and VPS4 ATPase activities (22, 46, 69, 83, 85). In spite of these similarities, however, MVB biogenesis and viral budding ultimately create different vesicles, and it is therefore of interest to determine the precise relationship between the two processes.

Genetic screens in *Saccharomyces cerevisiae* defined the basic machinery of MVB vesicle formation and identified 17 soluble yeast proteins that are essential for MVB biogenesis (the “class E” proteins) (40, 59). Complementary biochemical analyses revealed that MVB vesicle formation proceeds through an ordered pathway in which a series of soluble class E complexes, termed ESCRT-I (39), ESCRT-II (4), and ESCRT-III (3), are sequentially recruited to endosomal membranes, where they function in vesicle formation (Fig. 1A). Although the processes of vesicle formation and cargo incorporation are not yet understood

in mechanistic detail, ESCRT-I and -II appear to function primarily as adaptors that recognize protein cargoes and help recruit ESCRT-III, which in turn appears to function more directly in protein sorting and vesicle formation.

As the central complex in the yeast ESCRT pathway, ESCRT-II bridges ESCRT-I and ESCRT-III and also interacts with ubiquitylated cargoes. As shown in Fig. 1B, crystal structures of the yeast ESCRT-II core (30, 74) have revealed that the yeast ESCRT-II complex contains two copies of Vps25p (EAP20) that bind asymmetrically to single copies of Vps22p (EAP30) and Vps36p (EAP45) (human protein names are provided in parentheses for reference). The two Vps25p (EAP20) proteins project away from the Vps22p-Vps36p dimer, so that the overall complex assumes a trilobed “Y” shape. The three ESCRT-II subunits are related structurally, as each contains two copies of the winged-helix (WH) protein motif. Two of the proteins also contain N-terminal extensions: Vps22p (EAP30) has an extended helix (Fig. 1B), and Vps36p (EAP45) contains a linker and an N-terminal GRAM-like ubiquitin-binding in EAP45 (GLUE) domain (not present in the core structure). Structural and biochemical analyses of the Vps36p GLUE domain have shown that it is a split PH domain that binds phosphatidylinositol phosphates, particularly PI(3)P (67, 73). An extended insert within the GLUE domain contains two Npl4 zinc fingers (NZF), which are small globular zinc binding modules that mediate protein-protein interactions (49). The first, NZF-N, binds Vps28p (ESCRT-I) and helps recruit ESCRT-II to the endosomal membrane (73), whereas the second, NZF-C, binds ubiquitin and is required for efficient sorting of ubiquitylated cargoes (1).

The human and yeast ESCRT-II complexes are likely to be related structurally, because mammalian ESCRT-II can be iso-

* Corresponding author. Mailing address: Department of Biochemistry, 15 N. Medical Drive East, Room 4100, University of Utah School of Medicine, Salt Lake City, UT 84112-5650. Phone: (801) 585-5402. Fax: (801) 581-7959. E-mail: wes@biochem.utah.edu.

† Supplemental material for this article may be found at <http://jvi.asm.org>.

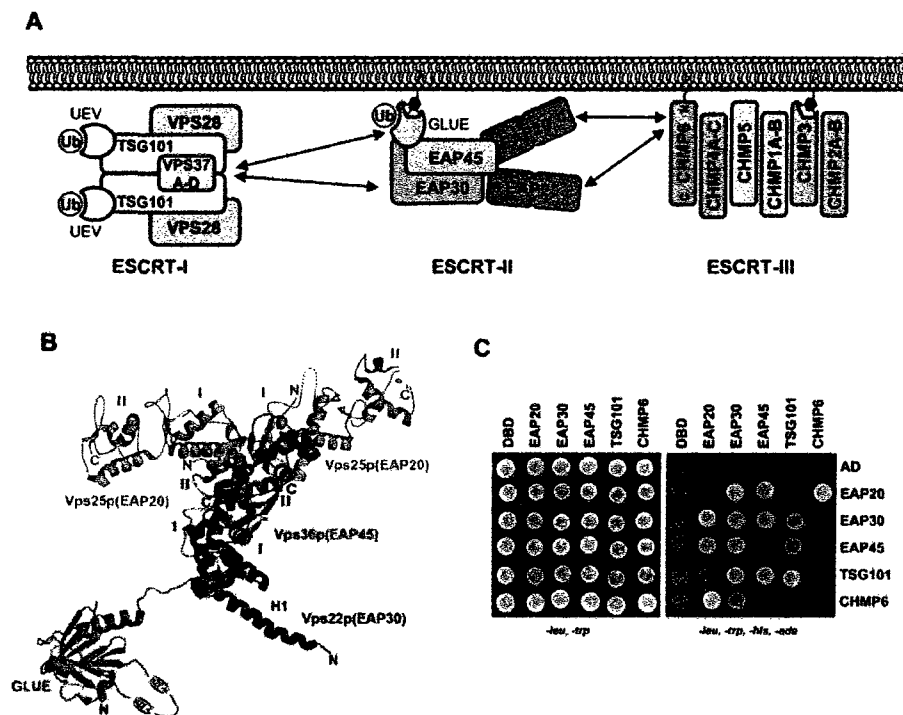


FIG. 1. ESCRT-II structure and interactions. (A) Schematic model summarizing the protein interactions of the human ESCRT-II complex (see the text for details). Note that the stoichiometries and compositions of the ESCRT-I and ESCRT-III complexes have not yet been defined unambiguously. The complexes are therefore simply shown with all possible subunits. (B) Three-dimensional structure of the yeast ESCRT-II complex. The structure of the ESCRT-II core was determined by X-ray crystallography (30, 74). The N-terminal region of Vps36 (EAP45) (shown schematically) has not yet been determined but contains two NZF domains (1) embedded within a GLUE domain (67). The structural elements/domains correspond approximately to the following residues (human homologs are in parentheses): for Vps36p (EAP45), GLUE domain, 1 to 285 (1 to 135); NZF-1, 177 to 205; NZF-2, 242 to 259 (neither NZF motif is present in EAP45); linker domain, 286 to 404 (136 to 238); WH-1, 405 to 491 (239 to 316); and WH-2, 492 to 566 (317 to 386); for Vps22p (EAP30), helix I (H1), 1 to 51 (1 to 55); WH-1, 90 to 165 (95 to 176); and WH-2, 166 to 233 (177 to 258); for Vps25p (EAP20), WH-1, 19 to 127 (22 to 103), and WH-2, 128 to 200 (104 to 176). (C) Summary of the positive yeast two-hybrid interactions between ESCRT-II proteins and all known human class E proteins. The right array shows doubly transformed yeast replica plated on minus Leu, minus Trp, minus His, minus Ade selection media, where successful growth represents a positive protein interaction. The left array shows replica-plated yeast on minus Leu, minus Trp media (a control for equivalent transformation and yeast growth). The indicated constructs were fused to DBDs (rows) or ADs (columns). Unfused DBD and AD constructs are shown as negative controls. Note that the interaction between DBD-EAP30 and AD-CHMP6 was judged to be negative because it was very weak and was not detected in the reciprocal direction. Analogous data were summarized previously in reference 83.

lated as a stable, soluble complex composed of three proteins that share 19 to 36% pairwise identity with their *S. cerevisiae* homologs (excluding the N-terminal region of Vps36p/EAP45) (37, 61). We have therefore used the crystal structure of the *S. cerevisiae* ESCRT-II core as a working model for the human ESCRT-II complex (Fig. 1B) (see Materials and Methods). Mammalian ESCRT-II functions are less well studied than those of the yeast complex, but the mammalian EAP20 and EAP45 proteins do colocalize with ESCRT-III components and with ubiquitylated proteins on endosomal membranes (67, 88). Like their yeast counterparts, EAP20 can bind the ESCRT-III protein, CHMP6 (46, 83, 88), and the N-terminal

GLUE domain of murine EAP45 was recently shown to bind ubiquitin (67). These observations all support the idea that the mammalian and *S. cerevisiae* ESCRT-II complexes are functional homologs. Nevertheless, there must also be important differences between human and yeast ESCRT-II proteins. For example, the mammalian complex lacks both NZF domains and therefore must interact differently with both ESCRT-I and ubiquitin. Moreover, ESCRT-II and CHMP6 overexpression does not inhibit HIV type 1 (HIV-1) budding (46), and it was recently reported that ESCRT-II is not required for lysosomal degradation of major histocompatibility complex I (MHC-I) or epidermal growth factor receptor (EGFR), indicating that the

complex is not absolutely required for membrane protein sorting or MVB vesicle formation (11). Indeed, several groups have proposed that ESCRT-II complexes in other species may perform functions that appear to be unrelated to MVB protein sorting. These include a role for mammalian ESCRT-II in transcriptional elongation (37, 61, 65) and a role for the *Schizosaccharomyces pombe* ESCRT-II protein EAP30 in meiotic spindle pole body amplification (35). The relationship between MVB protein sorting and these other putative ESCRT-II activities, if any, is not yet clear.

During HIV-1 assembly, human class E proteins are recruited by two short sequence motifs (termed "late domains") within the C-terminal p6 region of the Gag polyprotein (reviewed in references 15, 19, 22, 47, 48, 52, 70, and 79). The first p6^{late} late domain is a PTAP tetrapeptide motif that binds and recruits TSG101 (tumor susceptibility gene 101; yeast Vps23p). TSG101 is the central protein of the human ESCRT-I complex, and there is good evidence that the entire ESCRT-I complex functions directly in HIV-1 release (15, 19, 22, 24, 48). The second late domain within p6^{late} is a YPX_nL motif (where X_n can vary in identity and length) that binds and recruits ALIX/AIP1 (yeast Bro1p) (69, 80). ALIX functions late in MVB biogenesis (56) and binds both ESCRT-I (83) and ESCRT-III (41) proteins but is not a permanent subunit of any of the three discrete ESCRT complexes. Like TSG101, ALIX functions directly in virus release, although disruptions of the PTAP-TSG101 interaction generally inhibit HIV-1 budding to a greater degree than do disruptions of the ALIX-YPX_nL interaction (16, 46). As noted above, there are also indications that HIV-1 budding requires the activities of the late-acting ESCRT-III, LIP5, and VPS4 class E proteins (22, 46, 69, 83, 85). Specifically, HIV-1 release is dominantly inhibited by overexpression of VPS4 ATPase mutants and ESCRT-III proteins with large N- or C-terminal extensions (22, 46, 69, 83). HIV-1 release is also impaired by small interfering RNA (siRNA) depletion of the VPS4 binding protein LIP5 (85). It is important to note, however, that these experiments do not definitively establish a direct role for these proteins in HIV-1 budding, because the inhibitory effects could also arise from sequestration of the entire ESCRT machinery at aberrant endosomal compartments (called "class E" compartments).

In summary, HIV-1 uses the ESCRT-I complex to bud from cells and also requires the activities of downstream ESCRT-III and VPS4-LIP5 complexes. In *S. cerevisiae*, ESCRT-II physically bridges the ESCRT-I and ESCRT-III complexes and is essential for MVB protein sorting and vesicle formation (4). The mammalian ESCRT-II function appears to be more complex, however, and we therefore undertook this study with the goals of characterizing the biochemical properties of human ESCRT-II and testing its role in HIV release.

MATERIALS AND METHODS

ESCRT-II homology modeling. A working model for the human ESCRT-II core was created as follows. Protein Data Bank (PDB) coordinates from a yeast ESCRT-II crystal structure (PDB accession no. 1U5T) were utilized to create a consensus template using Swiss-PdbViewer (<http://www.expasy.org/spdbv/>). The human and yeast ESCRT-II sequences were then aligned within Swiss-PdbViewer, the alignment was used to thread the human sequence onto the yeast ESCRT-II template, and the model was energy minimized within Swiss-PdbViewer.

Plasmids. Genes for human EAP20, EAP30, EAP45, and CHMP6 used in yeast two-hybrid and biochemical experiments were amplified from expressed sequence tag clones as described previously (83). A complete list of all constructs used in this study is provided in Table S1 in the supplemental material. Genes and fragments for yeast two-hybrid experiments were cloned into pGADT7 (activation domain) and pGBKT7 (binding domain) vectors (Clontech) using 5' NdeI and 3' BamHI or BglII cloning sites. Recombinant proteins used in biochemical experiments were expressed as glutathione S-transferase (GST) C-terminal fusions from a modified pGEX vector (GE Biosciences). This vector (pGEX2T-TEV) contained a tobacco etch virus (TEV) protease cleavage site and 5' NdeI and 3' BamHI or BglII cloning sites following the GST gene. Expression constructs for deletion mutants were created by amplifying and subcloning the desired fragments or by introducing a stop codon using Quickchange mutagenesis (Stratagene). For mammalian expression, ESCRT genes were cloned as EcoRI-BamHI fragments into pcDNA3.1(-)-MycHis in frame with the C-terminal Myc tag, and with a Kozak sequence, ACC, inserted between the EcoRI site and the ATG start codon.

Preparation of recombinant EAP20. GST-EAP20 was expressed in *Escherichia coli* BL21(DE3) transformed with WISP05-68 (see Table S1 in the supplemental material) by induction in mid-log phase (0.4 mM IPTG [isopropyl- β -D-thiogalactopyranoside]) and allowing the protein to accumulate for 4 hours at 23°C. The cells were lysed by lysozyme treatment (2.5 mg/ml) in 50 mM Tris, pH 8.0, 300 mM NaCl, 10% glycerol, 1 mM dithiothreitol (DTT), followed by sonication and centrifugation (at 27,000 \times g for 45 min) to remove cell debris. Soluble GST-EAP20 was bound to a glutathione-Sepharose affinity matrix (GSTPrep FF; GE Healthcare), washed, and eluted with a step gradient of 20 mM glutathione. Protein fractions were dialyzed into 25 mM Tris (pH 8.0), 150 mM NaCl, and 1 mM DTT, and the fusion protein was cleaved during dialysis with 1 mg TEV protease per 100 mg protein (24 h; 23°C). The TEV cleavage reaction mixture was adjusted to 25 mM Tris (pH 8.0), 300 mM NaCl, 10% glycerol, 1 mM DTT, and free EAP20 was separated from GST and GST-EAP20 by size exclusion chromatography (Superdex 200; GE Healthcare). This purification method typically yielded ~1.5 mg of pure protein per liter of starting culture.

Preparation of recombinant CHMP6 proteins. GST-CHMP6 expression, affinity purification, and TEV cleavage were carried out as described for GST-EAP20. Following TEV cleavage, free GST was removed by glutathione-Sepharose affinity chromatography. The solution was then diluted six-fold to reduce the salt in the buffer to 50 mM NaCl, and the CHMP6 protein was purified to homogeneity by anion-exchange chromatography on immobilized Q-Sepharose (GE Biosciences). CHMP6 eluted at ~400 mM NaCl from a linear gradient of 50 mM to 1 M NaCl in 25 mM Tris (pH 8.0), 10% glycerol, 1 mM DTT.

GST pull-down assays. GST and GST-CHMP6 fusion proteins were expressed in *E. coli* BL21(DE3) and induced at mid-log phase with 0.4 mM IPTG. Ten-milliliter cultures of cells expressing GST-CHMP6 were pelleted, resuspended in 2 ml of 300 mM NaCl, 0.1% NP-40, 10% glycerol, 1 mM DTT, 50 mM Tris (pH 8.0); and lysed by lysozyme treatment and sonication. Soluble GST-CHMP6 was incubated with 100 μ l glutathione-Sepharose resin. Approximately 30 μ l purified recombinant EAP20 was added to 2 μ M (equivalent) of immobilized GST-CHMP6 and incubated for 30 min at 4°C in resuspension buffer. Unbound EAP20 was removed by washing with lysis buffer, and bound proteins were released from the resin by boiling in sodium dodecyl sulfate-polyacrylamide gel electrophoresis (SDS-PAGE) loading buffer and were analyzed on Coomassie-stained 4 to 20% SDS-PAGE gradient gels.

Yeast two-hybrid binding assays. Directed yeast two-hybrid assays were performed using the Matchmaker GAL4 Yeast Two Hybrid 3 system (Clontech). Briefly, *Saccharomyces cerevisiae* AH-109 was cotransformed with pGADT7 or pGBKT7 cloning vector (Clontech) containing the inserts of interest. The transformed yeast colonies were grown for 3 days at 30°C on yeast extract-peptone-dextrose plates with minus Leu, minus Trp selection. Ten to 100 colonies were pooled, resuspended in a liquid culture of Sabouraud dextrose broth (minus Leu, minus Trp), selected on Sabouraud dextrose broth (minus Leu, minus Trp, minus Ade, minus His) plates, and allowed to grow for 3 days.

Antibody production. Antibodies against the purified recombinant proteins EAP20 (UT461 and -462) and CHMP6 (UT463 and -464) were raised in rabbits by Covance Inc., following their 87-day protocol (http://abservices.crpinc.com/ab_sampleprotocols.aspx). UT461 and UT463 were affinity purified with the respective proteins, as described previously (83).

Biosensor binding experiments. EAP45-ubiquitin biosensor binding experiments were performed at 20°C using a BIACORE 2000 (Biacore AB, Uppsala, Sweden) equipped with a research grade CM4 sensor chip. Approximately 5,000 response units (RU) anti-GST antibody was immobilized on all four flow cells using amine-coupling chemistry (36). GST-EAP45₁₋₂₂₉, GST-EAP45₁₋₁₃₉, or recombinant GST alone from soluble *E. coli* lysates was diluted in running buffer

(20 mM Tris, pH 8.0, 100 mM NaCl, 1 mM DTT, 0.2 mg/ml bovine serum albumin [BSA], and 0.005% P20) and captured on the antibody surfaces at densities of ~0.5 KRU. Pure GST alone was also captured as a blank reference. Ubiquitin was purified (84), diluted in running buffer, and injected in duplicate or triplicate over the four flow cells at concentrations of 0 to 1,250 μ M. Responses were collected at a rate of 2 Hz during the 30-s association and dissociation phases. Binding isotherms from the equilibrium phases were fitted to simple 1:1 binding models to determine the dissociation constant and statistical fitting errors (see Fig. 4) (53). To obtain more accurate estimates for the dissociation constant and standard errors, the interaction between GST-EAP45₁₋₁₃₉ and ubiquitin was measured in six independent experiments, yielding values of 410 \pm 90 μ M. Biosensor binding experiments for EAP20 and GST-CHMP6 were performed as described for the EAP45-ubiquitin interaction, except that a BLA-CORE 3000 instrument was used and binding was examined in a buffer containing 50 mM Tris, pH 8.0, 300 mM NaCl, 10% glycerol, 1 mM DTT, 0.2 mg/ml BSA, and 0.005% P20. Anti-GST antibody was immobilized over all four flow cells (~13,000 RU/cell), and CHMP6, CHMP6₁₋₁₀₀, and CHMP6₁₀₁₋₂₀₀ were captured to densities of ~2,700 RU. Purified EAP20 was diluted in running buffer and injected in triplicate at 0.03 to 560 μ M concentrations.

Immunofluorescence. COS-7 cells grown on collagen-coated glass coverslips in 12-well plates were transfected with 0.5 μ g of pEGFP-VPS4A-KQ DNA and, in some experiments, 0.5 μ g pcDNA3.1-EAP20-myc DNA or pcDNA3.1-EAP30-myc DNA, using 2 μ l Lipofectamine 2000 (Invitrogen) following the manufacturer's instructions. The cells were fixed 24 h posttransfection in 4% paraformaldehyde-phosphate-buffered saline (PBS), blocked in 10% fetal calf serum (FCS) in PBS containing 0.1% Triton X-100, and incubated at room temperature with murine monoclonal anti-Myc (9E10; Covance Inc.) to detect transfected Myc-tagged ESCRT-II proteins or with anti-EAP20 UT461 (1:1,000) or anti-CHMP6 UT463 (1:1,000) antibody to detect endogenous ESCRT proteins. Secondary antibodies were anti-mouse Alexa 594- or anti-rabbit Alexa 594-conjugated antibodies (Molecular Probes; 1:1,000). Images of 0.5- μ m-thick Z sections were collected as single wavelengths on an Olympus FV300 confocal fluorescence microscope, using Fluoview 2.0.39 software.

Viral infectivity assays. EAP20 and CHMP6 were silenced by transfecting 5 μ l of 20 μ M annealed siRNAs, together with 1 μ g of pSL1180 (carrier DNA) and 9 μ l Lipofectamine 2000, into 293T cells in six-well plates (22). The sense strands of the siRNAs were as follows (lowercase letters denote RNA, and uppercase letters denote DNA nucleotides [nt]): EAP20 (start site, nt 218), cgaucagauug uuuuagATT; CHMP6-1 (start site, nt 257), ccaugguuacagauuugaATT; and CHMP6-2 (start site, nt 284), agaucaaaugaagauuATT. TSG101 and INV (TSG101) siRNA constructs have been described previously (22). The levels of protein depletion were estimated by quantifying the intensities of bands in Western blots using NIH ImageJ software.

Viral-particle production was initiated during a second siRNA transfection ($t = 24$ h) by replacing the 1- μ g carrier DNA either with an HIV-1 vector system or with an infectious R9 HIV-1 NL4-3 plasmid. Virus was harvested 24 h after the second transfection, and the titers were measured using single-cycle MAGIC assays (70). The HIV-1 vector system contained 0.38 μ g pCMV Δ R8.2 (54), 0.12 μ g pRSV-Rev (18), 0.12 μ g pMD.G (57), and 0.38 μ g pWPTS-nlsLacZ (all generous gifts from D. Trono, Swiss Federal Institute of Technology). HIV-packaged LacZ vectors were harvested 48 h later and titered on HeLaM cells as described previously (85).

Western blotting. Viral supernatants and cellular proteins from transfected 293T cells were prepared using standard procedures (82). For Western blots, virions or cytoplasmic proteins were separated by 12% SDS-PAGE, transferred to nitrocellulose (TSG101) or polyvinylidene difluoride (all others) membranes in Tris-glycine-10% MeOH buffer, blocked in 1% (TSG101) or 5% milk, and incubated with antibodies diluted in Tris-buffered saline-0.1% Tween 20 buffer (anti-TSG101), or in 1% BSA or 5% nonfat milk in Tris-buffered saline-0.1% Tween 20. Proteins were detected by enhanced chemiluminescence (Pierce) or by imaging Alexa 680-nm (Molecular Probes; 1:10,000) or IRDye 800-nm (Rockland; 1:20,000) secondary antibody on an Odyssey scanner (Li-Cor Inc.). The primary antibodies used were rabbit anti-HIV CA (UT415 made against purified NL4-3 CA protein and affinity-purified; 1:15,000); rabbit anti-HIV MA from Didier Trono, Swiss Institute of Technology (1:25,000); rabbit anti-EAP20 UT461 (1:1,000); rabbit anti-CHMP6 UT463 or UT464 (1:1,000); and mouse anti-TSG101 (GeneTex; 1:1,000).

EGFR degradation assays. 293T or HeLa cells were plated on duplicate six-well plates in Dulbecco's modified Eagle's medium-10% fetal bovine serum, and transfected with either oligofectamine or Lipofectamine 2000 and specific siRNAs (see above). During the second siRNA transfection ($t = 24$ h), 1 μ g R9 HIV plasmid was added to one set of cells (to control for knockdown efficiency and viral production), together with the second aliquot of 5 μ l siRNA. In this

case, virus and cells were harvested 48 h later ($t = 72$ h) and analyzed by Western blotting and MAGIC infectivity assays. The other set of cells, used in EGFR assays, was transfected a second time with siRNA-oligofectamine alone. Twenty-four hours after the second transfection ($t = 48$ h), the cells were reseeded on polylysine (Sigma)-coated coverslips and the next day were incubated in serum-free medium for 18 h. The cells were then incubated in the presence of 1 μ g/ml human EGF (Molecular Probes/Invitrogen) for 1 h (HeLa) or 2 h (293T cells); fixed in 3.7% formaldehyde-PBS, pH 7.2, at room temperature for 20 min; and incubated with mouse anti-human EGFR (1:100; Neomarkers) in 0.1% saponin-1% bovine serum albumin-PBS, pH 7.2, at room temperature for 60 min. The cells were washed extensively and incubated in Alexa 488-conjugated goat anti-mouse immunoglobulin G (1:750) (Molecular Probes/Invitrogen). The cells were imaged using an epifluorescence microscope with MagnaFire software or an Olympus FV300 confocal fluorescence microscope with Fluoview 2.0.3.9 software using 0.5- μ m sections. The fluorescence intensities were quantified using NIH ImageJ software.

EGF-lysosome colocalization assays. HeLa cells were plated on duplicate six-well plates in Dulbecco's modified Eagle's medium-10% fetal bovine serum and transfected twice with either oligofectamine or Lipofectamine 2000 ($t = 0$ and $t = 24$ h) with the siRNA oligonucleotides listed above and with EAP20-2 (start site, nt 477; gcacaagccagagaucauCTT). At $t = 48$ h, the cells were reseeded on polylysine (Sigma)-coated coverslips, and at $t = 72$ h, the cells were switched to serum-free media for 18 more hours while being incubated with 0.1 mg/ml Alexa 488-conjugated dextran (molecular weight, 10,000). The cells were then washed extensively in growth medium followed by a 4-h chase in dextran-free/serum-free medium, placed at 0°C, incubated with 1 μ g/ml EGF-Alexa Fluor 555-streptavidin complex (Molecular Probes/Invitrogen) for 60 min, and washed extensively in growth medium. Finally, the cells were incubated for 30 min at 37°C to allow time for EGF internalization and trafficking. Fluorescent images were captured with an Olympus FV300 confocal fluorescence microscope with Fluoview 2.0.3.9 software using 0.5- μ m sections and analyzed using NIH ImageJ software. Three to seven fields of cells were analyzed for each sample, and the EGF-lysosome localization was scored manually, with a positive score given to any cell showing significant colocalization of the EGF and dextran markers.

KK3-mediated MHC-1 downregulation. EAP20 and CHMP6 were silenced as described above with the addition of either 2 μ g of pTRACER-K3 or pTRACER empty control plasmid transfected at 24 and 48 h. Thirty-six hours after the second transfection, 5×10^5 cells were incubated in suspension with anti-human HLA-ABC antibody (1 μ g/ μ l; eBioscience) for 1 h at 4°C in a solution of 10% FCS in PBS. The cells were washed once with 1 ml of PBS and then incubated with phycoerythrin-labeled goat anti-mouse immunoglobulin (1 μ g/ μ l; BD Biosciences) in 10% FCS-PBS, followed by an additional wash with PBS. The cells were pelleted by centrifugation and resuspended in 1 ml PBS, and surface HLA-ABC levels were analyzed using the FACScan system (BD Biosciences).

RESULTS

Protein interactions within the ESCRT-II complex. To survey the protein interactions of human ESCRT-II, we tested for yeast two-hybrid interactions between each of the three human ESCRT-II proteins and all known human class E proteins (83). As shown in Fig. 1C, the following positive interactions were observed: EAP20-EAP30, EAP20-EAP45, EAP20-CHMP6, EAP30-EAP30, EAP30-EAP45, EAP30-TSG101, and EAP45-TSG101 (and TSG101-TSG101). All of these interactions were positive in both directions, and none of the ESCRT-II proteins interacted with control DNA binding domain (DBD) or activation domain (AD) constructs (Fig. 1C) or with any other class E proteins (data not shown). As noted above, ESCRT-II contains two copies of EAP20 and single copies of EAP30 and EAP45. Hence, all of the expected heteromeric interactions within the human ESCRT-II complex were observed, because EAP20, EAP30, and EAP45 all interacted with one another. The absence of EAP20 and EAP45 homomeric interactions can also be rationalized, because there is only a single copy of EAP45 in the complex and the two copies of EAP20 within ESCRT-II do not contact one another directly (30, 74). The observed homomeric EAP30-EAP30 interaction was unex-

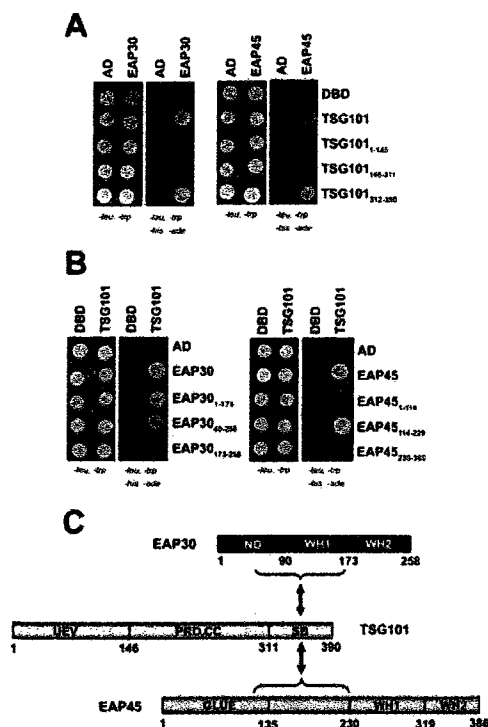


FIG. 2. Yeast two-hybrid mapping of the interaction sites between TSG101 and the EAP30 and EAP45 proteins. (A) Fragments of TSG101 binding to full-length EAP30 (left) and EAP45 (right). Selection media in the right and left arrays of each pair are the same as in Fig. 1C. (B) Full-length TSG101 binding to fragments of EAP45 (left) and EAP30 (right). (C) Schematic summary of fragment maps and interaction sites of TSG101, EAP30, and EAP45.

pected, however, and may have arisen because EAP30 was overexpressed in the absence of its other ESCRT-II binding partners. Alternatively, the interaction may reflect a natural tendency for ESCRT-II oligomerization (either directly or via bridging yeast proteins). In summary, all observed heteromeric intra-ESCRT-II interactions were consistent with structural models for the yeast and human ESCRT-II complexes, but the homomeric EAP30 interaction was not readily explained by the structure of isolated ESCRT-II.

ESCRT-I-ESCRT-II interactions. Two ESCRT-II proteins, EAP30 and EAP45, also interacted with TSG101, the central component of the ESCRT-I complex. Further mapping studies revealed that a fragment corresponding to the C-terminal region of TSG101 (termed the steadiness box [20, 42, 73]), was necessary and sufficient for both ESCRT-II protein interactions (Fig. 2A). Conversely, full-length TSG101 interacted with EAP30₁₋₁₇₃ and EAP45₁₁₄₋₂₂₉, but not with fragments outside of these regions (Fig. 2B). Thus, the TSG101 interaction site

on EAP45 maps to the linker region between the GLUE domain and the first WH repeat. The TSG101 interaction site on EAP30 spans both the long N-terminal helical extension and the WH repeat. TSG101 also interacted, albeit less robustly, with an EAP30 fragment that extends beyond the segment of the N-terminal helix that extends beyond the globular body of EAP30. Hence, the full EAP30 N-terminal helical extension is not strictly required for TSG101 binding, although this helix may contribute to the interaction, particularly as the full helix is predicted to extend to EAP30 residue 55.

As noted above, interactions between ESCRT-I and ESCRT-II must differ in the human and yeast systems, because the GLUE domain of human EAP45/ESCRT-II lacks the N-terminal NZF motif that forms the ESCRT-II interface in the yeast Vps28p/ESCRT-I-Vps36p/ESCRT-II complex (73). Nevertheless, we observed two-hybrid interactions for both EAP45/ESCRT-II and EAP30/ESCRT-II with human TSG101/ESCRT-I, indicating that the human ESCRT-I and ESCRT-II complexes can still interact, albeit via different ESCRT-I binding partners. Furthermore, the overall orientation of the ESCRT-I-ESCRT-II interaction may also be conserved, because the C-terminal region of TSG101 forms an extended interface with VPS28 (9, 42, 48, 73) and the TSG101 binding site on EAP45 lies immediately downstream (or at the very C-terminal end) of the GLUE domain. Thus, interactions between ESCRT-I and ESCRT-II appear to be retained in higher eukaryotes, although more detailed analyses of binding sites and energetics must await the production of pure recombinant human ESCRT complexes.

ESCRT-II-ESCRT-III interactions. In yeast, ESCRT-II recruits the downstream ESCRT-III complex through direct interactions between the ESCRT-II protein Vps25p (EAP20) and the ESCRT-III component Vps20p (CHMP6) (human homologs are in parentheses) (3, 74). Similarly, the human EAP20 and CHMP6 proteins also interacted in our two-hybrid survey of human class E proteins (Fig. 1C and 3A). Yeast two-hybrid mapping studies revealed that this interaction was mediated by the N-terminal half of CHMP6 binding to the C-terminal half of EAP20 (Fig. 3A), consistent with earlier reports (74, 88). The two C-terminal domains of EAP20 are exposed at the ends of the Y-shaped ESCRT-II complex, where they would be ideally positioned to nucleate ESCRT-III deposition through bivalent binding interactions (Fig. 1B).

GST pull-down and biosensor binding experiments with purified recombinant EAP20 and CHMP6 proteins demonstrated that the EAP20-CHMP6 interaction was direct, and these experiments again confirmed that EAP20 bound to the N-terminal half of CHMP6 (Fig. 3B and 4). As shown in Fig. 4A and B, the equilibrium binding isotherm for EAP20 binding to the full-length CHMP6 proteins fitted a simple 1:1 binding model with a dissociation constant of $5.3 \pm 0.2 \mu\text{M}$. Interestingly, EAP20 bound even more tightly to the N-terminal half of CHMP6 alone (residues 1 to 100) (equilibrium dissociation constant [K_D] = $601 \pm 9 \text{ nM}$), and the increased affinity primarily reflected a significantly lower rate of EAP20 dissociation from the truncated CHMP6 fragment. This observation demonstrates that C-terminal sequences in CHMP6 reduce the EAP20 binding affinity, providing direct physical evidence for the proposal that isolated full-length ESCRT-III proteins can

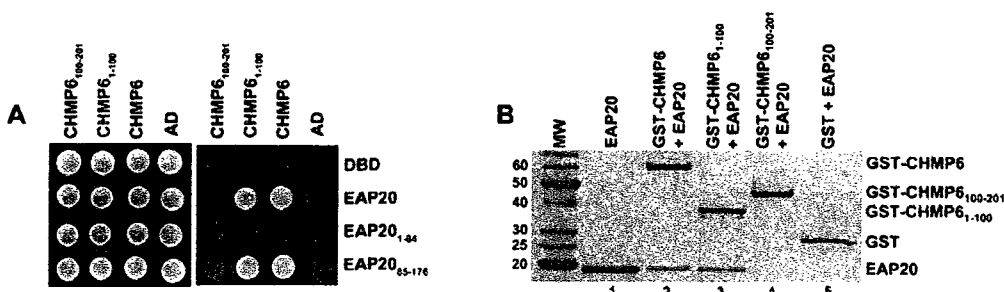


FIG. 3. Interactions between EAP20 and CHMP6. (A) Yeast two-hybrid mapping of the interaction sites between EAP20 and CHMP6. (B) GST pull-down experiment showing a direct interaction between EAP20 and the N-terminal half of CHMP6. The proteins present in each incubation mixture are given above lanes 2 to 5. Pure recombinant EAP20 is shown in lane 1 for reference. MW, molecular weight.

adopt autoinhibited "foldback" conformations (45). In this regard, it is interesting that several different CHMP proteins can be posttranslationally modified and that the unmodified CHMP proteins preferentially localize to the cytoplasm (68, 83). The posttranslational modifications might therefore destabilize autoinhibitory conformations, thereby enhancing the

protein-protein interactions that help dictate ESCRT-III protein localization.

EAP45-ubiquitin interactions. The yeast ESCRT-II complex helps sort ubiquitylated protein cargoes and binds ubiquitin through the second NZF motif (NZF-C) within the N-terminal GLUE domain of Vps36p (1). Mammalian EAP45 proteins

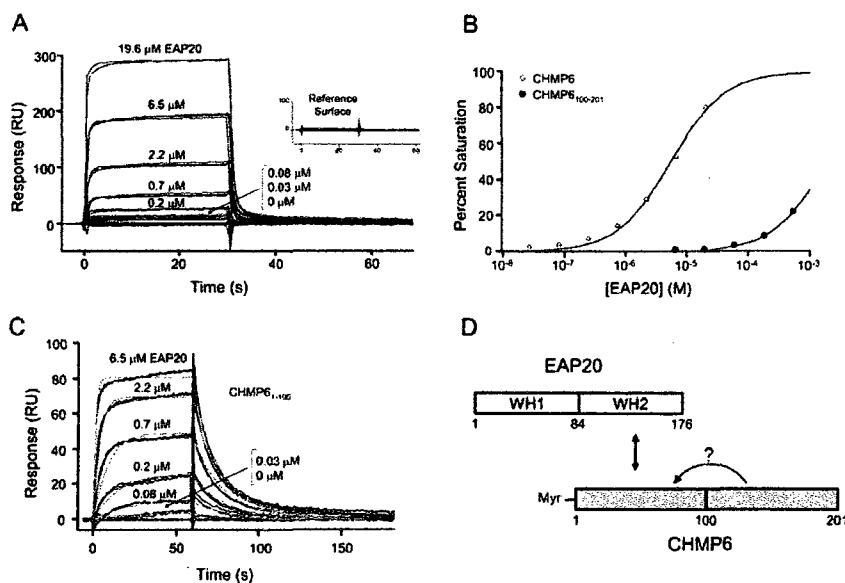


FIG. 4. Biosensor quantification of EAP20 binding to full-length and truncated CHMP6 proteins. (A) Sensorgrams showing different concentrations of EAP20 binding to full-length, immobilized GST-CHMP6. The inset shows EAP20 binding to a control GST surface. (B) Binding isotherms for EAP20 binding to full-length GST-CHMP6 ($K_D = 5.3 \pm 0.2 \mu$ M) and GST-CHMP¹⁰⁰⁻²⁰¹ ($K_D > 1$ mM). Dissociation constants and errors were derived by fitting simple 1:1 models to the equilibrium binding data (panel A and data not shown). (C) Sensorgrams showing different concentrations of EAP20 binding to GST-CHMP¹⁻¹⁰⁰. The association and dissociation phases were globally fitted to simple 1:1 interaction models. The light-gray lines show global fits with the following parameters: association rate constant $k_a = (1.46 \pm 0.04) \times 10^7 \text{ M}^{-1} \text{ s}^{-1}$, dissociation rate constant $k_d = 0.088 \pm 0.003 \text{ s}^{-1}$, and $K_D = 601 \pm 9 \text{ nM}$. (D) Schematic summary of the interaction sites between EAP20 and CHMP6. The arrow with the question mark illustrates a possible "autoinhibitory" interaction between the N- and C-terminal regions of CHMP6.

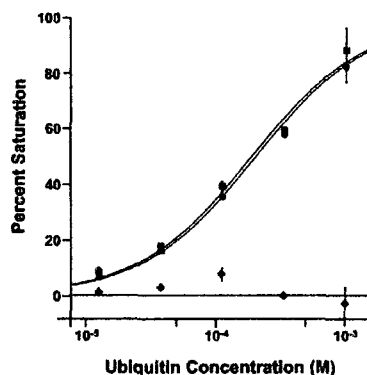


FIG. 5. Biosensor binding analyses of EAP45₁₋₂₂₉-ubiquitin interactions. Binding isotherms for wild-type Ub (circles) ($K_D = 210 \pm 10 \mu\text{M}$), F4A Ub (squares) ($K_D = 170 \pm 10 \mu\text{M}$), and 144A Ub (diamonds) ($K_D > 1 \text{ mM}$) binding to immobilized GST-EAP45₁₋₂₂₉. The error bars represent standard deviations.

lack NZF motifs, however, and it has therefore been unclear whether they could still interact with ubiquitylated protein cargoes. This puzzle has recently been resolved by Slagsvold and colleagues, who showed that a minimal N-terminal fragment of murine EAP45 spanning residues 1 to 139 binds directly to ubiquitin ($K_D = 460 \mu\text{M}$) and also binds phosphoinositides (67).

We independently tested for ubiquitin binding activity in the human EAP45 protein using the entire region of human EAP45 that is missing from the crystal structure of yeast Vps36p (EAP45₁₋₂₂₉). Biosensor binding analyses revealed that ubiquitin bound specifically to GST-EAP45₁₋₂₂₉, with an estimated dissociation constant of $210 \pm 10 \mu\text{M}$ in the experiment shown in Fig. 5. EAP45₁₋₂₂₉ binding was strongly inhibited by the Ub 144A mutation, but not by a F4A mutation, demonstrating that the exposed hydrophobic Ub 144 surface forms at least part of the EAP45 binding site. This same binding surface is also recognized by nearly all of the other ubiquitin binding proteins characterized to date (29). Ubiquitin also bound with a similar affinity to a minimal EAP45₁₋₁₃₉ construct ($K_D = 410 \pm 90 \mu\text{M}$; $n = 6$), indicating that the ubiquitin binding site is located within the N-terminal GLUE domain. These data are all in excellent agreement with recent analyses of ubiquitin binding to the murine EAP45 GLUE domain (67).

EAP20 and CHMP6 accumulate on aberrant endosomal class E compartments in the absence of VPS4 ATPase activity. Under steady-state conditions, all three ESCRT complexes are predominantly cytoplasmic but assemble transiently on the endosomal membrane to participate in vesicle formation. The assembled ESCRT complexes are then recycled off the endosomal membrane by the action of the VPS4 AAA ATPases (5). Inhibition of human and yeast VPS4 ATPase activity therefore traps class E proteins, including the VPS4 proteins themselves, on aberrant endosomal class E compartments (3–5, 8, 21, 83, 89).

To test whether human ESCRT-II associated with endosomal membranes in a VPS4-dependent fashion, we examined the localization of two different ESCRT-II components, EAP20 and EAP30, in the presence of a mutant VPS4A protein (green fluorescent protein [GFP]-VPS4A_{K173Q}) previously shown to block ATP binding and to dominantly inhibit VPS4 activity in cells (8). As shown in Fig. 6A and B, antibodies against EAP20 detected endogenous EAP20 in COS-7 cells, albeit weakly. These antibodies also cross-reacted with a second protein of ~36 kDa (data not shown). We therefore also examined the localization of exogenous, Myc-tagged EAP20 to take advantage of the enhanced immunofluorescence signal of the tagged, overexpressed protein (Fig. 6C). In both cases, EAP20 localized to the enlarged endosomes induced by GFP-VPS4A_{K173Q} overexpression. In the absence of GFP-VPS4A_{K173Q}, both endogenous and overexpressed EAP20 were distributed throughout the cytoplasm, as has been seen for other ESCRT complexes (Fig. 6B and D). To confirm that these results accurately represented the distribution of the entire ESCRT-II complex, the localization of a second ESCRT-II component, EAP30, was also examined. Once again, the overexpressed, Myc-tagged EAP30 protein was seen throughout the cell, but it became trapped on the class E compartments induced by dominant-negative GFP-VPS4A_{K173Q} (compare Fig. 6E and F). Hence, ESCRT-II was recruited to class E compartments, where it became trapped in the absence of VPS4 ATPase activity. Localization of the endogenous ESCRT-III protein, CHMP6, was also examined, and this protein was also strongly recruited to aberrant class E compartments (Fig. 6G and H and data not shown). Similar results were obtained using the other dominant-negative ATPase constructs, GFP-VPS4A_{E228Q}, DsRed-VPS4B_{K180Q}, and DsRed-VPS4B_{E235Q} (22, 83), and with human osteosarcoma cells (data not shown). These data are all consistent with the idea that human EAP20/ESCRT-II, EAP30/ESCRT-II, and CHMP6/ESCRT-III function in vesicle formation and cargo sorting at the MVB.

HIV-1 particles are released efficiently from cells depleted of EAP20. To test whether ESCRT-II is required for efficient HIV-1 budding, we measured the levels of HIV-1 vector and virus production following siRNA depletion of EAP20 or TSG101 (positive control). As shown in Fig. 7A and C, both EAP20 and TSG101 were successfully depleted to nearly undetectable levels, as determined by quantification of Western blots of cellular extracts (Fig. 7A and C, “Cells,” top two rows). Importantly, intracellular Gag expression levels were not significantly altered by depletion of either protein (“Cells,” bottom rows). As expected, the release of virions was dramatically reduced upon TSG101 depletion (Fig. 7A and C, “Virions,” lanes “TSG101”), and the infectious titers were reduced ~20-fold (Fig. 7B and D). Surprisingly, however, depletion of EAP20 did not significantly affect viral release as measured in Western blot assays (Fig. 7A and C, “Virions,” lanes “EAP20”), and actually increased vector titers slightly at the 24-h time point (Fig. 7B and D, bars 4), although at a later time point (48 h), HIV-1 titers were reduced twofold (data not shown). We therefore conclude that efficient depletion of EAP20 does not significantly inhibit the release or infectivity of HIV-1.

HIV-1 particles are also efficiently released from cells depleted of CHMP6. The efficient release of HIV-1 from EAP20-

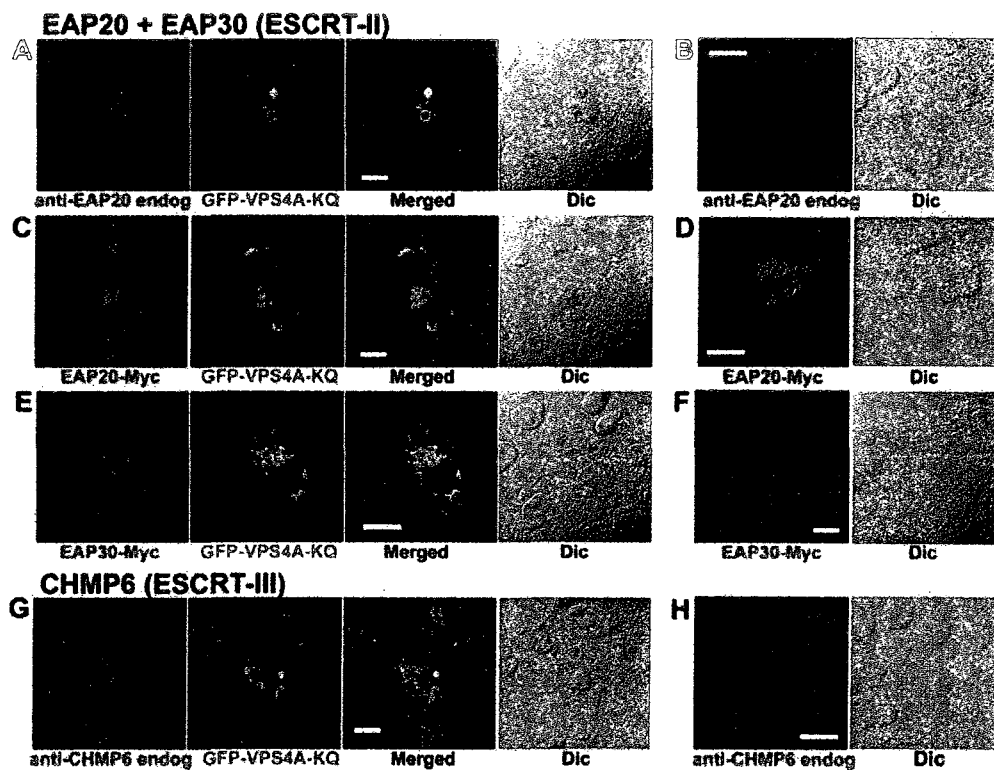


FIG. 6. Localization of ESCRT-II and ESCRT-III proteins by immunofluorescence. COS7 cells expressing fluorescent, exogenous, dominant-negative GFP-VPS4A_{K173Q} (denoted GFP-VPS4A-KQ) were cotransfected and/or costained to detect the following proteins: (A) endogenous (endog) EAP20 protein (antibody UT461), (C) exogenous EAP20-Myc (anti-Myc antibody), (E) exogenous EAP30-myc (anti-Myc), and (G) endogenous CHMP6 (UT463). Column 1 (from left), ESCRT proteins alone (red); column 2, GFP-VPS4A-KQ proteins alone (green); column 3, overlaid (merged) images (colocalization on class E compartments is in yellow); column 4, differential interference contrast (Dic) images. Panels B, D, F, and H show the protein distributions in the absence of dominant-negative VPS4. Scale bars, 20 μ m. Note that our two EAP20 antibodies also stained COS7 and human osteosarcoma cell centrosomes and spindles (Fig. 6B), and one of our two CHMP6 antibodies, UT 464, exhibited a punctate nuclear staining pattern in addition to staining class E membranes (not shown).

depleted cells was unexpected, and the implications of this observation were examined further by testing the requirement for CHMP6/ESCRT-III in virus release. CHMP6 was selected for study because it binds EAP20, forms the only known connection between ESCRT-II and ESCRT-III, is the only myristoylated CHMP protein (3, 88), and appears to initiate ESCRT-III assembly in yeast (3).

The effects of CHMP6 depletion on the release and infectivity of HIV-1 vectors and virus are shown in Fig. 8. As expected, virus release and infectivity were again substantially reduced upon siRNA depletion of TSG101 (Fig. 8A to D, lanes "TSG101" and bars 2), whereas treatment with an inverted control siRNA had no significant effect on virus release (defined as 100% infectivity; lanes "INV" and bars 3). Two different siRNAs were used to knock down CHMP6 (designated CHMP6-1 and CHMP6-2), and both siRNAs decreased

CHMP6 levels very significantly (Fig. 8A and C, "Cells," second row) without affecting Gag protein expression or processing (third row). As with EAP20 depletion, CHMP6 depletion again failed to reduce HIV-1 release or infectivity substantially (Fig. 8A and 8C, "Virions," and B and D). Although there was some variability in multiple repetitions of this experiment, the average viral titers nevertheless fell within 40% of control levels following treatment with both CHMP6-1 and CHMP6-2 (Fig. 8B and D). At a later time point (48 h), viral infectivities were reduced four- to fivefold, possibly owing to secondary effects on general protein trafficking. We therefore conclude that normal cellular levels of CHMP6 are not required for efficient HIV-1 release or infectivity.

EAP20 and CHMP6 are required for efficient downregulation of the EGF receptor. The EGFR is normally present on the cell surface, where it can bind EGF and transmit growth

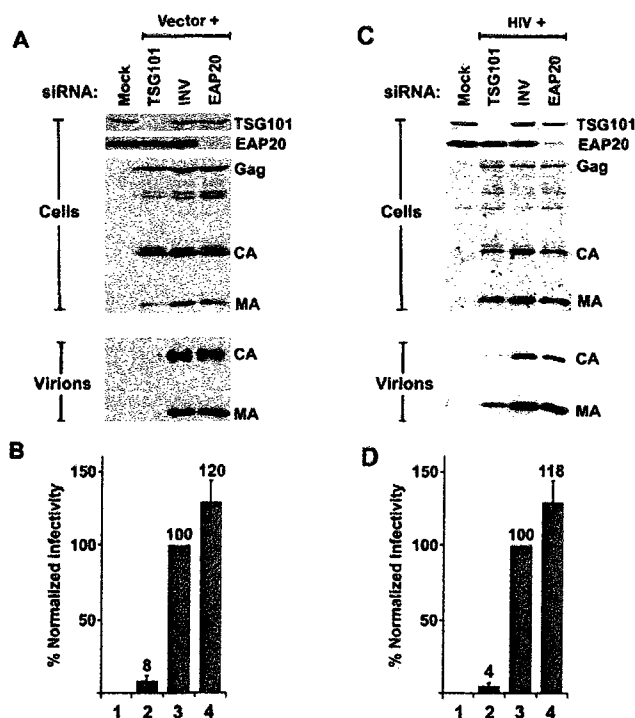


FIG. 7. siRNA depletion of EAP20 does not diminish HIV-1 vector release or transduction efficiency. (A) Western blot analysis of 293T cell extracts showing the efficiency of siRNA depletion of TSG101 (positive control, lane TSG101 in top gel) or EAP20 (lane EAP20 in second gel from top) and the effects on Gag protein expression (third gel from top) and virus-like particle release (virions, bottom gel) from a cotransfected HIV-1 vector system. Lanes Mock and INV are negative controls showing cells that were mock transfected without the HIV-1 vector or cotransfected with an inverted siRNA against TSG101 (INV), respectively. Cellular Gag, CA, and MA levels were monitored to ensure equal transfection and protein expression levels. Extracellular CA and MA levels reflect the relative efficiencies of virus-like particle release. The TSG101 signal intensity for TSG101-depleted cells was 1% of that of the control, and the EAP20 signal intensity for EAP20-depleted cells was 2% of that of the control. Quantification of at least three repetitions of this experiment showed the following levels of MA and CA release: TSG101 siRNA, 9% \pm 2% of the control; inverted siRNA, 100% (defined as the control); EAP20, 108% \pm 12%. The data were collected 48 h after the second siRNA transfection. (B) HIV-1 viral-vector titers produced by cells depleted of EAP20 or TSG101 (positive control). Vector transduction levels were normalized to the negative control (INV) and averaged from six independent experiments. Control vector titers were 2.5×10^5 to 3.2×10^5 /ml. The data were collected 48 h after the second siRNA transfection. (C) Western blot analysis showing the efficiency and effects of siRNA-mediated silencing of EAP20 in analogous experiments with wild-type (wt) HIV-1_{NL4.3} virus. The experiment was similar to that shown in panels A and B, except that wt HIV-1_{NL4.3} virus was utilized. Quantification of at least three repetitions of this experiment showed the following levels of MA and CA release: TSG101 siRNA, 12% \pm 9% of the control; inverted siRNA, 100% (defined as the control); EAP20, 75% \pm 4%. The data were collected 26 h after the second siRNA transfection. (D) HIV-1 titers produced by cells depleted of EAP20 or TSG101 (positive control). Control viral titers were 0.9×10^6 to 4×10^6 /ml of supernatant. The values represent the average and standard error of eight independent experiments. The data were collected 24 to 26 h after the second siRNA transfection.

signals. Following high levels of EGF stimulation, the receptor is internalized, trafficked through the MVB pathway, and degraded in the lysosome, thereby attenuating the growth signal (32, 43). The lack of a requirement for EAP20 and CHMP6 in HIV-1 budding was surprising, and we therefore tested whether depletion of these proteins altered EGFR downregulation, as would be expected for proteins that function in MVB vesicle formation and protein sorting. These experiments also served as controls for our ability to deplete TSG101, EAP20, and CHMP6 to functionally significant levels.

As shown in Fig. 9, depletion of TSG101/ESCRT-I, EAP20/ESCRT-II, and CHMP6/ESCRT-III significantly reduced the efficiency of EGFR degradation in response to EGF stimulation, although the block was not complete and was somewhat greater for TSG101/ESCRT-I than for EAP20/ESCRT-II and CHMP6/ESCRT-III. Total cellular EGFR protein levels and localization were assayed by immunofluorescence, using an anti-EGFR antibody. In the absence of EGF stimulation, EGFR was located almost exclusively on the surfaces of 293T cells (Fig. 9A, column 1 [from left] and inset). Following EGF

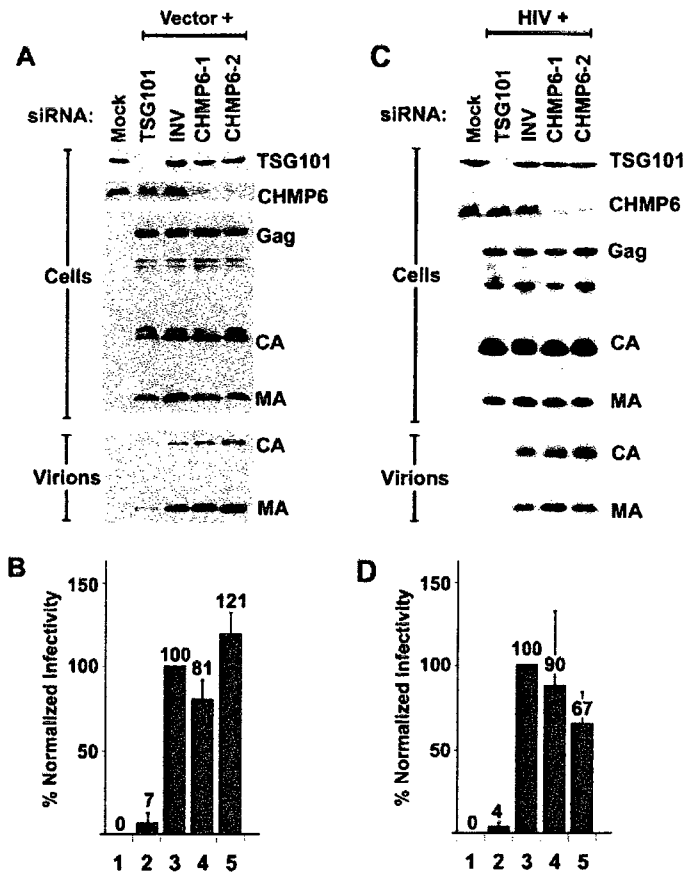


FIG. 8. HIV release and infectivity are minimally affected by CHMP6 depletion. (A) Western blot analysis of 293T cell extracts showing the efficiency of siRNA depletion of TSG101 (positive control; lane TSG101 in the top gel) or CHMP6 (lanes CHMP6-1 and -2 in the second gel from the top) and the effects on Gag protein expression (third gel from the top) and virus-like particle release (virions; bottom gel) from a cotransfected HIV-1 vector system. CHMP6 was depleted using two different siRNAs (denoted CHMP6-1 and CHMP6-2). Lanes Mock and INV are negative controls showing cells that were mock transfected without the HIV-1 vector or cotransfected with an inverted siRNA against TSG101 (INV), respectively. Cellular Gag, CA, and MA levels were monitored to ensure equal transfection and protein expression levels. The extracellular CA and MA levels reflect the relative efficiencies of virus-like particle release. The TSG101 signal intensity for TSG101-depleted cells was 2% of that of the control, and the CHMP6 signal intensities for CHMP6-depleted cells were 12% (CHMP6-1) and 3% (CHMP6-2) relative to the control. Quantification of at least three repetitions of this experiment showed the following levels of MA and CA release: inverted siRNA, 100% (defined as the control); CHMP6-1, 133% \pm 14%; and CHMP6-2, 105% \pm 35%. The data were collected 48 h after the second siRNA transfection. (B) HIV-1 viral-vector titers produced by cells depleted of CHMP6 or TSG101 (positive control). Vector transduction levels were normalized to the negative control (INV) and averaged from four independent experiments. The data were collected 48 h after the second siRNA transfection. (C) Western blot analysis showing the efficiency and effects of siRNA-mediated silencing of the CHMP6 protein. The experiment was similar to that shown in panel A except that wild-type HIV-1_{NLA-3} virus was used. Quantification of at least three repetitions of this experiment showed the following levels of MA and CA release: inverted siRNA, 100% (defined as the control); CHMP6-1, 109% \pm 22%; and CHMP6-2, 94% \pm 38%. The data were collected 26 h after the second siRNA transfection. (D) HIV-1 titers produced by cells depleted of CHMP6 or TSG101 (positive control). Viral transduction levels were normalized to the negative control (INV) and averaged from eight independent experiments. The data were collected 26 h after the second siRNA transfection. The error bars represent standard deviations.

stimulation for 2 h, >90% of the EGFR was internalized and degraded (column 2). Importantly, EGFR degradation was significantly reduced by treatment with siRNAs against TSG101 (column 4), EAP20 (column 5), and CHMP6 (column

6), but not by treatment with a control siRNA (column 3). Depletion of the three ESCRT components did not affect receptor internalization but rather induced intracellular accumulation of internalized receptors, consistent with a defect in

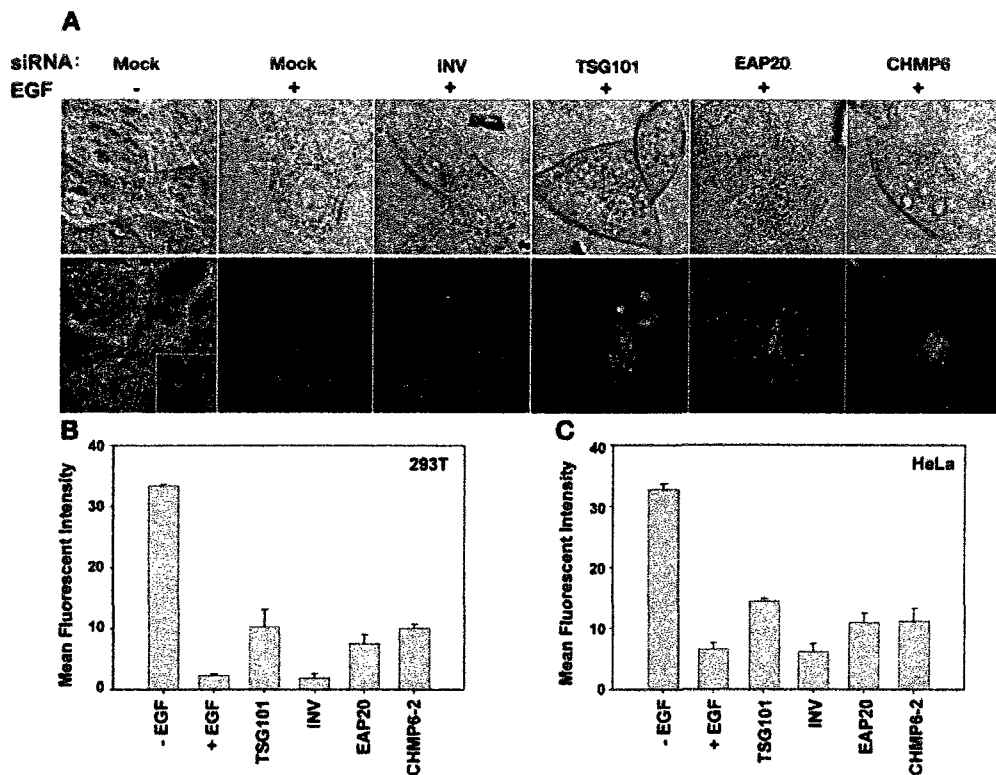


FIG. 9. EGF receptor downregulation is inhibited by depletion of TSG101, EAP20, and CHMP6. (A) 293T cells treated with siRNA were serum starved and then incubated in the presence or absence of EGF. Fixed and permeabilized cells were visualized by differential interference contrast (Nomarski) microscopy (top row) or by immunofluorescence to determine EGFR levels and localization (bottom row). Stacked whole-cell images are shown in all cases, with a central confocal slice (inset) also shown in the first image in the bottom row to demonstrate that the EGFR is located on the cell surface prior to EGF stimulation. (B) Quantification of the total levels of EGFR in 293T cells under the different conditions described for panel A. Each bar in the histogram represents the average fluorescence of individual cells as measured in three different images containing two to five cells per image. The error bars show the standard errors of the mean. The data were collected 91 h after the second siRNA transfection. (C) Quantification of total levels of EGFR in HeLa cells under the conditions described for panel A. The data were collected 92 h after the second siRNA transfection.

MVB trafficking. We note that treatment with siRNAs against TSG101 resulted in the accumulation of EGFR in larger class E compartments (17) than were seen in cells treated with siRNAs against EAP20 or CHMP6. The EGFR trafficking defects seen in the absence of ESCRT activities were similar in 293T and HeLa cells, as shown quantitatively in Fig. 9B and C. The efficiencies of protein depletion and virus release were monitored in parallel experiments that confirmed that the targeted proteins were depleted as expected and that HIV-1 release was significantly reduced by TSG101 depletion, but not by depletion of EAP20 or CHMP6 (data not shown).

Bowers et al. recently reported that siRNA depletion of EAP20 did not measurably inhibit the lysosomal degradation of MHC-I and EGF-EGFR complexes (11). This differs from

our conclusion that EAP20 depletion reduced the efficiency of EGFR degradation, and we therefore investigated the issue further by testing the effects of depleting TSG101/ESCRT-I, EAP20/ESCRT-II, and CHMP6/ESCRT-III on (i) MHC-I degradation and (ii) movement of fluorescent EGF to the lysosome. In the former experiments, we found that depletion of TSG101/ESCRT-I reduced the stimulation of MHC-I receptor degradation by the Kaposi's sarcoma-associated herpesvirus ubiquitin ligase KK3 (13, 28), whereas depletion of EAP20/ESCRT-II and CHMP6/ESCRT-III did not (data not shown). These results are in excellent agreement with those of Bowers et al. (11), and we therefore conclude that efficient MHC-I downregulation requires TSG101/ESCRT-I but not EAP20/ESCRT-II or CHMP6/ESCRT-III. Thus, the ESCRT

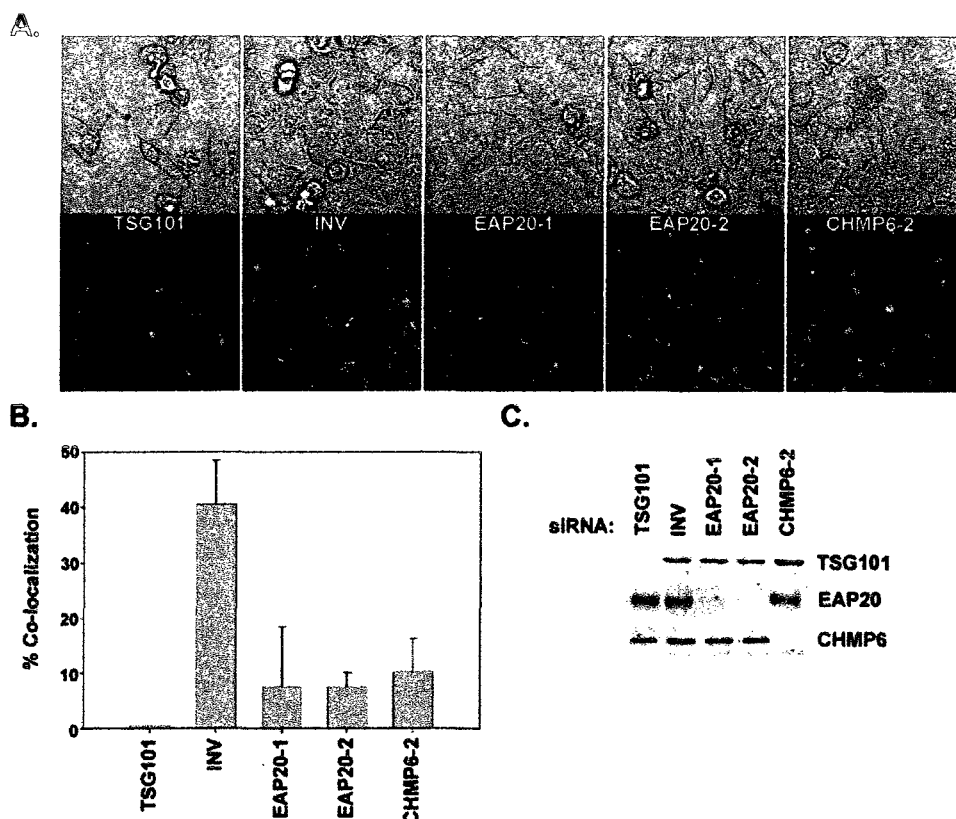


FIG. 10. Colocalization of EGF and lysosomal fluid phase markers upon depletion of TSG101, EAP20, and CHMP6. (A) HeLa cells were treated with the designated siRNA, Alexa 488-dextran (green), and EGF-Alexa Fluor 555 streptavidin (red) as described in Materials and Methods. (B) Quantification of the fractions of cells showing some colocalization of Alexa 488-dextran and EGF-Alexa Fluor 555 streptavidin under the different conditions described for panel A. The quantification of EGF (red) coincident with lysosome dextran (green) was performed in single-plane overlay analyses using the Olympus Fluoview software. Cells were scored as positive if the overlap coefficient (R) was greater than 0.5. The error bars represent standard deviations. (C) Western blot analysis showing the efficiency of siRNA-mediated depletion of TSG101, EAP20, and CHMP6.

requirements for MHC-I downregulation are similar to the requirements for HIV-1 budding.

We examined the trafficking of EGF to the lysosome in cells depleted of TSG101/ESCRT-I, EAP20/ESCRT-II, or CHMP6/ESCRT-III. HeLa cells depleted of TSG101/ESCRT-I, EAP20/ESCRT-II, or CHMP6/ESCRT-III were incubated with the fluid phase marker Alexa 488-dextran for 18 h, followed by a 4-h chase in dextran-free medium, which allows the fluid phase marker to accumulate in lysosomes (12, 78). As shown above, the unstimulated EGFR is predominantly localized to the plasma membrane. Incubation of cells with EGF-Alexa Fluor 555 streptavidin induced the internalization of the EGFR, and after 30 min, fluorescent EGF colocalized with lysosomes in 41% of the cells examined (Fig. 10, "INV,")

(86/208 cells). In contrast, cells depleted of TSG101/ESCRT-I showed no colocalization of EGF with lysosomes ("TSG101") (0/29 cells tested). Cells depleted of either EAP20/ESCRT-II or CHMP6/ESCRT-III showed intermediate phenotypes, with 7 to 10% of the cells showing EGF staining at the lysosome. To control for possible differences between different siRNA oligonucleotides, we also tested one of the siRNA oligonucleotides used to deplete EAP20 in the study by Bowers et al. This oligonucleotide (EAP20-2) also efficiently depleted EAP20 levels (Fig. 10C) and again gave an intermediate EGF localization phenotype (Fig. 10A and B, "EAP20-2") (19/258 cells positive for EAP20-2 versus 10/140 cells for EAP20-1 and 22/213 cells for CHMP6-2).

As will be reported elsewhere, we have also now found that

degradation of ferroportin, a cell surface receptor that is down-regulated by hepcidin binding (55), shows a strong dependence on TSG101, EAP20, and CHMP6 (I. De Domenico, D. M. Ward, C. Langelier, M. B. Vaughn, E. Nemeth, W. I. Sundquist, T. Ganz, G. Musci, and J. Kaplan, unpublished data). We therefore conclude that lysosomal targeting of different cell surface receptors can differ in EAP20 and CHMP6 requirements. Some receptors, such as MHC-I, exhibit little or no requirement for these proteins, while other receptors, such as ferroportin, exhibit strong requirements, and still others, such as EGFR, exhibit intermediate phenotypes. These experiments indicate that there are probably multiple pathways for sorting membrane proteins into the MVB vesicles of mammalian cells.

DISCUSSION

Not surprisingly, our studies have revealed that the human ESCRT-II complex has a number of features in common with its better-characterized yeast counterpart. The similarities include interactions with ESCRT-I, ESCRT-III, and ubiquitin; transient association with endosomal membranes; and functional participation in receptor downregulation. These observations are all consistent with the idea that ESCRT-II can play a central role in the human ESCRT pathway, interacting with the upstream ESCRT-I and downstream ESCRT-III complexes and with ubiquitylated cargos as they are sorted into MVB vesicles. Nevertheless, depletion of EAP20/ESCRT-II and CHMP6/ESCRT-III did not significantly reduce HIV-1 release from cultured 293T or HeLa cells, indicating that only a subset of the mammalian ESCRT machinery is required for efficient virus release from these cell types.

Role of EAP20/ESCRT-II in HIV-1 release. We considered several possible explanations for the observation that EAP20/ESCRT-II depletion does not inhibit HIV-1 release. As with all siRNA depletion experiments, it is possible that even the very low levels of EAP20 remaining after depletion were still sufficient to function in HIV-1 release (and MHC-I downregulation). While we cannot rule out this possible explanation, it seems unlikely because EAP20 was efficiently depleted in our experiments (Fig. 7 and 10), and this depletion measurably inhibited EGFR degradation and lysosomal targeting (Fig. 9 and 10). Furthermore, EAP20 depletion actually produced a slight, but reproducible, increase in HIV-1 infectivity (Fig. 7), which could be explained if the endogenous ESCRT-II complex binds and competes for other factors essential for virus budding (e.g., ESCRT-I). It is also conceivable that ESCRT-II may remain active even without EAP20 subunits. This explanation again seems unlikely, because the two copies of EAP20 comprise half of the ESCRT-II subunits and form the only known link between ESCRT-II and ESCRT-III. Furthermore, ESCRT-II activity is blocked by deletion of EAP20/Vps25p in both *S. cerevisiae* and *Drosophila* (4, 76, 77). We therefore conclude that the most likely explanation for our data is that ESCRT-II is not required for efficient HIV-1 release from human cells, either because the complex does not normally participate in virus budding or because the viral budding machinery still functions efficiently in its absence.

Our results also imply that if HIV-1 utilizes the late-acting ESCRT-III and VPS4 complexes to bud from cells, then there must be other proteins or complexes, in addition to ESCRT-II,

that can bridge ESCRT-I and ESCRT-III. In principle, ALIX/AIP1 could be one such bridging protein, as it can bind directly to both TSG101 (83) and to the CHMP4 proteins (38, 41, 69, 83), although simultaneous depletion of ALIX and EAP20 did not synergistically inhibit EGFR degradation (11). Similarly, interactions between the yeast ESCRT-I components, Vps37p and Vps28p, and the ESCRT-III component, Vps20p (CHMP6), have been reported (10), although we did not observe analogous ESCRT-I-ESCRT-III interactions between the isolated human proteins in two-hybrid experiments. Finally, the deubiquitylating enzyme, AMSH, binds both the upstream HRS-STAM complex (which binds to TSG101) (71) and the ESCRT-III components CHMP3 and CHMP4 (23). In principle, these (and other) bridging interactions could help to recruit ESCRT-III to sites of MVB vesicle formation and virus budding even in the absence of ESCRT-II.

Role of ESCRT-III in HIV-1 release. Models for the roles of ESCRT-III (and VPS4) in virus budding must take into account the observation that HIV-1 release is not significantly inhibited by depletion of endogenous CHMP5 and CHMP6 (reference 85 and this work), yet virus release is very potently inhibited by overexpression of dominant-negative CHMP5 or CHMP6 protein (46, 69, 70). siRNA depletion of these individual CHMP proteins therefore imposes a less severe (or less general) block in the ESCRT pathway than the dominant-negative ESCRT-III and VPS4 constructs. A likely explanation for this difference is that dominant-negative CHMP (and VPS4) constructs function by inducing the formation of aberrant endosomal compartments (class E compartments) that not only inhibit the functions of the modified CHMP proteins themselves, but also sequester other ESCRT complexes and possibly many other MVB proteins required for HIV-1 budding. Thus, we cannot rule out the possibility that wild-type CHMP and VPS4 proteins do not normally function in HIV-1 release but rather affect virus budding only when present in dominant-negative forms. However, we favor a model in which at least a subset of the ESCRT-III and VPS4 proteins do actually participate directly in virus release but where depletion of individual CHMP5 or CHMP6 proteins does not inhibit virus budding owing to (i) functional redundancy within the MVB pathway arising from the presence of 10 different CHMP proteins, (ii) the possibility that CHMP5 (and possibly other CHMP proteins) may function at a step following MVB vesicle formation (7, 66), and/or (iii) the presence of multiple distinct ESCRT pathways in human cells. It therefore continues to be important to determine precisely which subset of different ESCRT proteins is utilized directly by HIV-1 and other viruses.

Complexity of MVB vesicle formation and protein sorting in higher eukaryotes. Genetic studies have identified the basic machinery required for MVB vesicle formation and protein sorting in *S. cerevisiae*. Importantly, deletion of each of the six known yeast ESCRT-I and ESCRT-II subunits ultimately leads to a strong block in protein sorting and MVB vesicle formation (the class E phenotype) (40). While it seems almost certain that the basic mechanism of MVB biogenesis is highly conserved, because human cells have at least one ortholog of every known yeast class E protein (33, 51), our studies add to the growing number of indications that MVB protein-sorting/vesicle formation pathways are more complex in higher eu-

karyotes than in yeast. One level of increased complexity is suggested by the fact that unique yeast class E proteins often have multiple orthologs in mammalian cells. Examples include the 4 different human homologs of the single yeast Vps37p protein (6, 19, 70), the 10 different human homologs of the six yeast ESCRT-III proteins (51), and the 2 (or more) different human homologs of yeast Vps4p (60). Thus, unique proteins or complexes that are essential for MVB formation in yeast may play redundant or overlapping roles in higher eukaryotes. For example, simultaneous depletion of both VPS37B and VPS37C inhibits PTAP-dependent retrovirus budding to a greater extent than depletion of either single VPS37 paralog alone (48).

A second level of complexity is suggested by the fact that even unique ESCRT-I or ESCRT-II subunits do not appear to be required for metazoan MVB vesicle formation in all contexts. For example, a knockout of the *Drosophila* Vps28/ESCRT-I protein has only modest effects on MVB morphology and no measurable effect on the downregulation of several different cell surface receptors *in vivo*, even though there is only a single *vps28* gene in *Drosophila* (63). Similarly, agonist-induced lysosomal degradation of the delta opioid receptor is inhibited by dominant-negative VPS4B mutants and by depletion of HRS, but not by depletion of TSG101/ESCRT-I (31). Hence, an intact ESCRT-I complex is apparently not required for downregulation of all cell surface receptors via the MVB pathway (27, 31). Similarly, EAP20/ESCRT-II is not required for MHC-I receptor downregulation induced by Kaposi's sarcoma-associated herpesvirus KK3 (reference 11 and data not shown).

Retroviruses also differ in their requirements for ESCRT-I. HIV-1, which binds directly to TSG101, requires all of the known ESCRT-I components for efficient release (19, 22, 48), whereas equine infectious anemia virus and Moloney murine leukemia virus, which bud primarily via ALIX and the Nedd4 E3 ligases, respectively, exhibit little or no requirement for TSG101/ESCRT-I (22, 48, 62, 64, 72). Nevertheless, all retroviruses are inhibited by dominant-negative ESCRT-III and VPS4 proteins, suggesting a common use of these downstream factors (22, 46, 69, 83). This model is consistent with the idea that ESCRT-I and ESCRT-II may function primarily as adaptor complexes that help recruit cargoes into the pathway, whereas the ESCRT-III/VPS4 machinery functions more directly in vesicle formation. Indeed, the genomes of *Plasmodium falciparum* and *Toxoplasma gondii* reportedly lack ESCRT-I and ESCRT-II entirely but do encode ESCRT-III and VPS4 proteins and require VPS4 to create multivesicular bodies (87). Finally, we note that even the ESCRT-III/VPS4 machinery appears to be dispensable in some cases, as the melanosomal protein Pmel17 is sorted into MVB vesicles via an ESCRT-independent pathway that is also insensitive to inhibition by dominant-negative forms of VPS4 (75). The apparent diversity of MVB sorting pathways raises the intriguing possibility that viral systems may also have evolved to utilize such "noncanonical" MVB pathways to escape the cell (34).

Roles for mammalian ESCRT-I and ESCRT-II in receptor downregulation. Although ESCRT-I and ESCRT-II are not absolutely required for the efficient downregulation of all receptors or for the release of all retroviruses, both complexes clearly play very important roles in downregulating certain cell surface receptors. Indeed, a number of recent studies indicate

that both ESCRT-I and ESCRT-II exhibit growth/tumor suppressor activities by virtue of their roles in cell surface receptor downregulation. For example, all three known ESCRT-I components (TSG101, VPS28, and VPS37) have now been implicated in cell growth and tumor suppression. TSG101 was initially identified in a genetic screen for genes with tumor suppressor activity, and depletion of TSG101 induces NIH 3T3 cell overproliferation in culture and metastatic tumor formation in nude mice (44). Similarly, deletion of *erupted*, the *Drosophila* TSG101 ortholog, inhibits Notch receptor degradation and activates the JAK-STAT (and possibly other) signaling pathway and thereby induces tissue overproliferation (50). Likewise, depletion of one of the four mammalian VPS37 proteins (6, 19, 70), VPS37A/HCRP-1, enhances the growth of cultured hepatocellular carcinoma BEL-7404 cells and elevates their invasive ability (86). Interestingly, VPS37A/HCRP-1 is also downregulated in some hepatocellular carcinomas. Finally, we have observed that depletion of VPS28 can relieve contact-inhibited growth in cultured 293T cells (J. Garrus, personal communication). ESCRT-II also appears to play an important role in growth receptor downregulation, as deletion of the *Drosophila vps25* gene leads to tissue overproliferation through aberrant stabilization of the Notch and DPP (and possibly other) receptors (76, 77). Similarly, we observed that depletion of EAP20 (human VPS25) reduces the degradation rates of EGFR (Fig. 9 and 10), ferroportin (De Domenico, et al., unpublished), and presumably other cell surface receptors following ligand stimulation. Thus, just as the proteasome functions to degrade soluble proteins, the mammalian ESCRT pathway, including ESCRT-II, can play a critical role in mediating both homeostatic and regulated lysosomal degradation of integral membrane proteins.

ACKNOWLEDGMENTS

This work was supported by NIH funding to C.P.H. (GM066521), J.K. (HL29622 and DK070947), and W.I.S. (AI51174).

We thank Chris Rodesch, David Myszk, and Rebecca Rich for assistance with immunofluorescence and biosensor experiments.

REFERENCES

- Alam, S. L., J. Sun, M. Payne, B. D. Welch, B. K. Blake, D. R. Davis, H. H. Meyer, S. D. Emr, and W. I. Sundquist. 2004. Ubiquitin interactions of NZF zinc fingers. *EMBO J.* 23:1411-1421.
- Babst, M. 2005. A protein's final ESCRT. *Traffic* 6:2-9.
- Babst, M., D. Katzmann, E. Estepa-Sabal, T. Meerloo, and S. Emr. 2002. Escrt-III. An endosome-associated heterooligomeric protein complex required for mvb sorting. *Dev. Cell* 3:271-282.
- Babst, M., D. Katzmann, W. Snyder, B. Wendland, and S. Emr. 2002. Endosome-associated complex, ESCRT-II, recruits transport machinery for protein sorting at the multivesicular body. *Dev. Cell* 3:283-289.
- Babst, M., B. Wendland, E. J. Estepa, and S. D. Emr. 1998. The Vps4p AAA ATPase regulates membrane association of a Vps protein complex required for normal endosome function. *EMBO J.* 17:2982-2993.
- Bache, K. G., T. Slagsvold, A. Cabezas, K. R. Rosendal, C. Raiborg, and H. Stenmark. 2004. The growth-regulatory protein HCRP1/hVps37A is a subunit of mammalian ESCRT-I and mediates receptor downregulation. *Mol. Biol. Cell* 15:4337-4346.
- Bache, K. G., S. Stuffers, L. Malerød, T. Slagsvold, C. Raiborg, D. Lechardeur, S. Walchli, G. L. Lukacs, A. Brech, and H. Stenmark. 2006. The ESCRT-III subunit hVps24 is required for degradation but not silencing of the epidermal growth factor receptor. *Mol. Biol. Cell* 17:2513-2523.
- Bishop, N., and P. Woodman. 2000. ATPase-defective mammalian VPS4 localizes to aberrant endosomes and impairs cholesterol trafficking. *Mol. Biol. Cell* 11:227-239.
- Bishop, N., and P. Woodman. 2001. TSG101/mammalian VPS23 and mammalian VPS28 interact directly and are recruited to VPS4-induced endosomes. *J. Biol. Chem.* 276:11735-11742.
- Bowers, K., J. Lottridge, S. B. Hellwell, L. M. Goldthwaite, J. P. Luzio, and

- T. H. Stevens. 2004. Protein-protein interactions of ESCRT complexes in the yeast *Saccharomyces cerevisiae*. *Traffic* 5:194-210.
11. Bowers, K., S. C. Piper, M. A. Edelling, S. R. Gray, D. J. Owen, P. J. Lehner, and J. P. Luzio. 2006. Degradation of endocytosed epidermal growth factor and virally ubiquitinated major histocompatibility complex class I is independent of mammalian ESCRTII. *J. Biol. Chem.* 281:5094-5105.
 12. Bright, N. A., B. J. Reaves, B. M. Mullock, and J. P. Luzio. 1997. Dense core lysosomes can fuse with late endosomes and are re-formed from the resultant hybrid organelles. *J. Cell Sci.* 110:2027-2040.
 13. Coscoy, L., D. J. Sanchez, and D. Ganem. 2001. A novel class of herpesvirus-encoded membrane-bound E3 ubiquitin ligases regulates endocytosis of proteins involved in immune recognition. *J. Cell Biol.* 155:1265-1273.
 14. Demirov, D. G., and E. O. Freed. 2004. Retrovirus budding. *Virus Res.* 106:87-102.
 15. Demirov, D. G., A. Ono, J. M. Orenstein, and E. O. Freed. 2002. Overexpression of the N-terminal domain of TSG101 inhibits HIV-1 budding by blocking late domain function. *Proc. Natl. Acad. Sci. USA* 99:955-960.
 16. Demirov, D. G., J. M. Orenstein, and E. O. Freed. 2002. The late domain of human immunodeficiency virus type 1 p6 promotes virus release in a cell type-dependent manner. *J. Virol.* 76:105-117.
 17. Doyotte, A., M. R. Russell, C. R. Hopkins, and P. G. Woodman. 2005. Depletion of TSG101 forms a mammalian "Class E" compartment: a multivesicular early endosome with multiple sorting defects. *J. Cell Sci.* 118:3003-3017.
 18. Dull, T., R. Zufferey, M. Kelly, R. J. Mandel, M. Nguyen, D. Trono, and L. Naldini. 1998. A third-generation lentivirus vector with a conditional packaging system. *J. Virol.* 72:8463-8471.
 19. Eastman, S. W., J. Martin-Serrano, W. Chung, T. Zang, and P. D. Bieniasz. 2005. Identification of human VPS37C, a component of endosomal sorting complex required for transport-I important for viral budding. *J. Biol. Chem.* 280:628-636.
 20. Feng, G. H., C. J. Lih, and S. N. Cohen. 2000. TSG101 protein steady-state level is regulated posttranslationally by an evolutionarily conserved COOH-terminal sequence. *Cancer Res* 60:1736-1741.
 21. Fujita, H., M. Yamanaka, K. Imanura, Y. Tanaka, A. Nara, T. Yoshimori, S. Yokota, and M. Himeoto. 2003. A dominant negative form of the AAA ATPase SKD1/VPS4 impairs membrane trafficking out of endosomal/lysosomal compartments: class E *vps* phenotype in mammalian cells. *J. Cell Sci.* 116:401-414.
 22. Garrus, J. E., U. K. von Schwedler, O. W. Pornillos, S. G. Morham, K. H. Zavitz, H. E. Wang, D. A. Wettstein, K. M. Stray, M. Cote, R. L. Rich, D. G. Myszka, and W. I. Sundquist. 2001. Tsg101 and the vacuolar protein sorting pathway are essential for HIV-1 budding. *Cell* 107:55-65.
 23. Glot, L., J. S. Bader, C. Brouwer, A. Chaudhuri, B. Kuang, Y. Li, Y. L. Hao, C. E. Ooi, B. Godwin, E. Vitols, G. Vijayadamar, P. Pochart, H. Machineni, M. Welsh, Y. Kong, B. Zerhusen, R. Malcolm, Z. Varrone, A. Collis, M. Minto, S. Burgess, L. McDaniel, E. Stimpson, F. Spriggs, J. Williams, K. Neurath, N. Iolme, M. Agee, E. Voss, K. Furtak, R. Renzulli, N. Aanesen, S. Carroll, E. Bickelhaupt, Y. Lazovatsky, A. DaSilva, J. Zhong, C. A. Stanyon, R. L. Finley, Jr., K. P. White, M. Braverman, T. Jarvie, S. Gold, M. Leach, J. Knight, R. A. Shinkets, M. P. McKenna, J. Chant, and J. M. Rothberg. 2003. A protein interaction map of *Drosophila melanogaster*. *Science* 302:1727-1736.
 24. Golla-Gaur, R., D. G. Demirov, J. M. Orenstein, A. Ono, and E. O. Freed. 2003. Defects in human immunodeficiency virus budding and endosomal sorting induced by TSG101 overexpression. *J. Virol.* 77:6507-6519.
 25. Gould, S. J., A. M. Booth, and J. E. Hildreth. 2003. The Trojan exosome hypothesis. *Proc. Natl. Acad. Sci. USA* 100:10592-10597.
 26. Gruenberg, J., and H. Stenmark. 2004. The biogenesis of multivesicular endosomes. *Nat. Rev. Mol. Cell Biol.* 5:317-323.
 27. Gullapalli, A., B. L. Wolfe, C. T. Griffin, T. Magnuson, and J. Trejo. 2006. An essential role for SNX1 in lysosomal sorting of protease-activated receptor-1: evidence for retromer-, Hrs-, and Tsg101-independent functions of sorting nexins. *Mol. Biol. Cell.* 17:1228-1238.
 28. Hewitt, E. W., L. Duncan, D. Muftic, J. Baker, P. G. Stevenson, and P. J. Lehner. 2002. Ubiquitination of MHC class I by the K3 viral protein signals internalization and TSG101-dependent degradation. *EMBO J.* 21:2418-2429.
 29. Hicke, L., H. L. Schubert, and C. P. Hill. 2005. Ubiquitin-binding domains. *Nat. Rev. Mol. Cell Biol.* 6:610-621.
 30. Hierro, A., J. Sun, A. S. Rusnak, J. Kim, G. Prag, S. D. Emr, and J. H. Hurley. 2004. Structure of the ESCRT-II endosomal trafficking complex. *Nature* 431:221-225.
 31. Hislop, J. N., A. Marley, and M. Von Zastrow. 2004. Role of mammalian vacuolar protein-sorting proteins in endocytic trafficking of a non-ubiquitinated G protein-coupled receptor to lysosomes. *J. Biol. Chem.* 279:22522-22531.
 32. Huang, F., D. Kirkpatrick, X. Jiang, S. Gygi, and A. Sorkin. 2006. Differential regulation of EGF receptor internalization and degradation by multibubiquitination within the kinase domain. *Mol. Cell.* 21:737-748.
 33. Hurley, J. H., and S. D. Emr. 2006. The ESCRT complexes: structure and mechanism of a membrane-trafficking network. *Annu. Rev. Biophys. Biomol. Struct.* 35:277-298.
 34. Irie, T., J. M. Licata, J. P. McGettigan, M. J. Schnell, and R. N. Harty. 2004. Budding of PPxY-containing rhabdoviruses is not dependent on host proteins TGS101 and VPS4A. *J. Virol.* 78:2657-2665.
 35. Jin, Y., J. J. Mancuso, S. Uzawa, D. Cronembold, and W. Z. Cande. 2005. The fission yeast homolog of the human transcription factor EAP30 blocks meiotic spindle pole body amplification. *Dev. Cell.* 9:63-73.
 36. Johnson, B., S. Lofas, and G. Lindquist. 1991. Immobilization of proteins to a carboxymethylated dextran-modified gold surface for biospecific interaction analysis in surface plasmon resonance sensors. *Anal. Biochem.* 198:268-277.
 37. Kamura, T., D. Burlan, H. Khalili, S. L. Schmidt, S. Sato, W. J. Liu, M. N. Conrad, R. C. Conaway, J. W. Conaway, and A. Shilatifard. 2001. Cloning and characterization of ELL-associated proteins EAP45 and EAP20. A role for yeast EAP-like proteins in regulation of gene expression by glucose. *J. Biol. Chem.* 276:16528-16533.
 38. Katoh, K., H. Shibata, H. Suzuki, A. Nara, K. Ishidoh, E. Kominami, T. Yoshimori, and M. Makl. 2003. The ALG-2-interacting protein Alix associates with CHMP4b, a human homologue of yeast Snf7 that is involved in multivesicular body sorting. *J. Biol. Chem.* 278:39104-39113.
 39. Katzmann, D. J., M. Babst, and S. D. Emr. 2001. Ubiquitin-dependent sorting into the multivesicular body pathway requires the function of a conserved endosomal protein sorting complex, ESCRT-I. *Cell* 106:145-155.
 40. Katzmann, D. J., G. Odorizzi, and S. D. Emr. 2002. Receptor downregulation and multivesicular-body sorting. *Nat. Rev. Mol. Cell Biol.* 3:893-905.
 41. Kim, J., S. Sitaraman, A. Hierro, B. M. Beach, G. Odorizzi, and J. H. Hurley. 2005. Structural basis for endosomal targeting by the Bro1 domain. *Dev. Cell.* 8:937-947.
 42. Kostelansky, M. S., J. Sun, S. Lee, J. Kim, R. Ghirlando, A. Hierro, S. D. Emr, and J. H. Hurley. 2006. Structural and functional organization of the ESCRT-I trafficking complex. *Cell* 125:113-126.
 43. Le Roy, C., and J. L. Wrana. 2005. Clathrin- and non-clathrin-mediated endocytic regulation of cell signalling. *Nat. Rev. Mol. Cell Biol.* 6:112-126.
 44. Li, L., and S. N. Cohen. 1996. Tsg101: a novel tumor susceptibility gene isolated by controlled homozygous functional knockout of allelic loci in mammalian cells. *Cell* 85:319-329.
 45. Liu, Y., L. A. Kimpler, T. V. Nalmsmith, J. M. Lauer, and P. I. Hanson. 2005. Interaction of the mammalian endosomal sorting complex required for transport (ESCRT) III protein hSnf7-1 with itself, membranes, and the AAA+ ATPase SKD1. *J. Biol. Chem.* 280:12799-12809.
 46. Martin-Serrano, J., A. Yaravoy, D. Perez-Caballero, and P. D. Bieniasz. 2003. Divergent retroviral late-budding domains recruit vacuolar protein sorting factors by using alternative adaptor proteins. *Proc. Natl. Acad. Sci. USA* 100:12414-12419.
 47. Martin-Serrano, J., T. Zang, and P. D. Bieniasz. 2001. HIV-1 and Ebola virus encode small peptide motifs that recruit Tsg101 to sites of particle assembly to facilitate egress. *Nat. Med.* 7:1313-1319.
 48. Martin-Serrano, J., T. Zang, and P. D. Bieniasz. 2003. Role of ESCRT-I in retroviral budding. *J. Virol.* 77:4794-4804.
 49. Meyer, H. H., Y. Wang, and G. Warren. 2002. Direct binding of ubiquitin conjugates by the mammalian p97 adaptor complexes, p47 and Ufd1-Npl4. *EMBO J.* 21:5645-5652.
 50. Moberg, K. H., S. Schelble, S. K. Burdick, and I. K. Hariharan. 2005. Mutations in *erupted*, the *Drosophila* ortholog of mammalian tumor susceptibility gene 101, elicit non-cell-autonomous overgrowth. *Dev. Cell.* 9:699-710.
 51. Morita, E., and W. I. Sundquist. 2004. Retrovirus budding. *Annu. Rev. Cell Dev. Biol.* 20:395-425.
 52. Myers, E. L., and J. F. Allen. 2002. Tsg101, an inactive homologue of ubiquitin ligase e2, interacts specifically with human immunodeficiency virus type 2 Gag polyprotein and results in increased levels of ubiquitinated Gag. *J. Virol.* 76:11226-11235.
 53. Myszka, D. G. 1999. Improving biosensor analysis. *J. Mol. Recognit.* 12:279-284.
 54. Naldini, L., U. Blomer, F. H. Gage, D. Trono, and I. M. Verma. 1996. Efficient transfer, integration, and sustained long-term expression of the transgene in adult rat brains injected with a lentiviral vector. *Proc. Natl. Acad. Sci. USA* 93:11382-11388.
 55. Nemeth, E., M. S. Tuttle, J. Powelson, M. B. Vaughn, A. Donovan, D. M. Ward, T. Ganz, and J. Kaplan. 2004. Hepcidin regulates cellular iron efflux by binding to ferroportin and inducing its internalization. *Science* 306:2090-2093.
 56. Nikko, E., A. M. Martini, and B. Andre. 2003. Permease recycling and ubiquitination status reveal a particular role for Bro1 in the multivesicular body pathway. *J. Biol. Chem.* 278:50732-50743.
 57. Ory, D. S., B. A. Neugeboren, and R. C. Mulligan. 1996. A stable human-derived packaging cell line for production of high titer retrovirus/vesicular stomatitis virus G pseudotypes. *Proc. Natl. Acad. Sci. USA* 93:11400-11406.
 58. Patnaik, A., V. Chau, and J. W. Wills. 2000. Ubiquitin is part of the retrovirus budding machinery. *Proc. Natl. Acad. Sci. USA* 97:13069-13074.
 59. Raymond, C. K., I. Howald-Stevenson, C. A. Vater, and T. H. Stevens. 1992. Morphological classification of the yeast vacuolar protein sorting mutants: evidence for a prevacuolar compartment in class E *vps* mutants. *Mol. Biol. Cell* 3:1389-1402.

60. Scheuring, S., R. A. Rohricht, B. Schoning-Burkhardt, A. Beyer, S. Muller, H. F. Abts, and K. Kohrer. 2001. Mammalian cells express two VPS4 proteins both of which are involved in intracellular protein trafficking. *J. Mol. Biol.* 312:469–480.
61. Schmidt, A. E., T. Miller, S. L. Schmidt, R. Shiekhattar, and A. Shilatifard. 1999. Cloning and characterization of the EAP30 subunit of the ELL complex that confers derepression of transcription by RNA polymerase II. *J. Biol. Chem.* 274:21981–21985.
62. Segura-Morales, C., C. Pescha, C. Chatellard-Causse, R. Sadoul, E. Bertrand, and E. Basyuk. 2005. Tsg101 and Alix interact with murine leukemia virus Gag and cooperate with Nedd4 ubiquitin ligases during budding. *J. Biol. Chem.* 280:27004–27012.
63. Sevrioukov, E. A., N. Moghrabi, M. Kuhn, and H. Kramer. 2005. A mutation in dVps28 reveals a link between a subunit of the endosomal sorting complex required for transport-I complex and the actin cytoskeleton in *Drosophila*. *Mol. Biol. Cell* 16:2301–2312.
64. Shehu-Khalaga, M., S. Ablan, D. G. Demirov, C. Chen, R. C. Montelaro, and E. O. Freed. 2004. Late domain-dependent inhibition of equine infectious anemia virus budding. *J. Virol.* 78:724–732.
65. Shilatifard, A. 1998. Identification and purification of the Holo-ELL complex. Evidence for the presence of ELL-associated proteins that suppress the transcriptional inhibitory activity of ELL. *J. Biol. Chem.* 273:11212–11217.
66. Shim, J. H., C. Xiao, M. S. Hayden, K. Y. Lee, E. S. Trombetta, M. Pypaert, A. Nara, T. Yoshimori, B. Wilin, H. Erdjument-Bromage, P. Tempst, B. L. Hogan, I. Mellman, and S. Ghosh. 2006. CHMP5 is essential for late endosome function and down-regulation of receptor signaling during mouse embryogenesis. *J. Cell Biol.* 172:1045–1056.
67. Slagsvold, T., R. Aasland, S. Hirano, K. G. Bache, C. Raiborg, D. Trambalolo, S. Wakatsuki, and H. Stenmark. 2005. Eap45 in mammalian ESCRT-II binds ubiquitin via a phosphoinositide-interacting GLUE domain. *J. Biol. Chem.* 280:19600–19606.
68. Stauffer, D. R., T. L. Howard, T. Nyun, and S. M. Hollenberg. 2001. CHMP1 is a novel nuclear matrix protein affecting chromatin structure and cell-cycle progression. *J. Cell Sci.* 114:2383–2393.
69. Strack, B., A. Callistri, S. Craig, E. Popova, and H. G. Gottlinger. 2003. AIP1/ALIX is a binding partner for HIV-1 p6 and EIAV p9 functioning in virus budding. *Cell* 114:689–699.
70. Stuchell, M. D., J. E. Garrus, B. Muller, K. M. Stray, S. Ghaffarian, R. McKinnon, H. G. Krausslich, S. G. Morham, and W. I. Sundquist. 2004. The human endosomal sorting complex required for transport (ESCRT-I) and its role in HIV-1 budding. *J. Biol. Chem.* 279:36059–36071.
71. Tanaka, N., K. Kaneko, H. Asao, H. Kasai, Y. Endo, T. Fujita, T. Takeshita, and K. Sugamura. 1999. Possible involvement of a novel STAM-associated molecule "AMSH" in intracellular signal transduction mediated by cytokines. *J. Biol. Chem.* 274:19129–19135.
72. Tanzl, G. O., A. J. Pfeifer, and P. Bates. 2003. Equine infectious anemia virus utilizes host vesicular protein sorting machinery during particle release. *J. Virol.* 77:8440–8447.
73. Teo, H., D. J. Gill, J. Sun, O. Perisic, D. B. Veprintsev, Y. Vallis, S. D. Emr, and R. L. Williams. 2006. ESCRT-I Core and ESCRT-II GLUE domain structures reveal role for GLUE in linking to ESCRT-I and membranes. *Cell* 125:99–111.
74. Teo, H., O. Perisic, B. Gonzalez, and R. L. Williams. 2004. ESCRT-II, an endosome-associated complex required for protein sorting: crystal structure and interactions with ESCRT-III and membranes. *Dev. Cell* 7:559–569.
75. Theos, A. C., S. T. Truschel, D. Tenza, I. Hurbain, D. C. Harper, J. F. Berson, P. C. Thomas, G. Raposo, and M. S. Marks. 2006. A luminal domain-dependent pathway for sorting to intraluminal vesicles of multivesicular endosomes involved in organelle morphogenesis. *Dev. Cell* 10:343–354.
76. Thompson, B. J., J. Mathieu, H. H. Sung, E. Loeser, P. Rorth, and S. M. Cohen. 2005. Tumor suppressor properties of the ESCRT-II complex component Vps25 in *Drosophila*. *Dev. Cell* 9:711–720.
77. Vaccari, T., and D. Bilder. 2005. The *Drosophila* tumor suppressor Vps25 prevents nonautonomous overproliferation by regulating notch trafficking. *Dev. Cell* 9:687–698.
78. van Weert, A. W., K. W. Dunn, H. J. Gueze, F. R. Maxfield, and W. Stoorvogel. 1995. Transport from late endosomes to lysosomes, but not sorting of integral membrane proteins in endosomes, depends on the vacuolar proton pump. *J. Cell Biol.* 130:821–834.
79. VerPlank, L., F. Bouamr, T. J. LaGrassa, B. Agresta, A. Kikonyogo, J. Lels, and C. A. Carter. 2001. Tsg101, a homologue of ubiquitin-conjugating (E2) enzymes, binds the L domain in HIV type 1 Pr55Gag. *Proc. Natl. Acad. Sci. USA* 98:7724–7729.
80. Vincent, O., L. Rainbow, J. Tilburn, H. N. Arst, Jr., and M. A. Penalva. 2003. YPX17 is a protein interaction motif recognized by *Aspergillus* PaA and its human homologue, AIP1/Alix. *Mol. Cell Biol.* 23:1647–1655.
81. Vogt, V. M. 2000. Ubiquitin in retrovirus assembly: actor or bystander? *Proc. Natl. Acad. Sci. USA* 97:12945–12947.
82. von Schwedler, U. K., T. L. Stemmler, V. Y. Kilshko, S. Li, K. H. Albertine, D. R. Davis, and W. I. Sundquist. 1998. Proteolytic refolding of the HIV-1 capsid protein amino-terminus facilitates viral core assembly. *EMBO J.* 17:1555–1568.
83. von Schwedler, U. K., M. Stuchell, B. Muller, D. M. Ward, H. Y. Chung, E. Morita, H. E. Wang, T. Davis, G. P. He, D. M. Cimbara, A. Scott, H. G. Krausslich, J. Kaplan, S. G. Morham, and W. I. Sundquist. 2003. The protein network of HIV budding. *Cell* 114:701–713.
84. Wang, C., L. Deng, M. Hong, G. R. Akkaraju, J. Inoue, and Z. J. Chen. 2001. TAK1 is a ubiquitin-dependent kinase of MKK and IKK. *Nature* 412:346–351.
85. Ward, D. M., M. B. Vaughn, S. L. Shiflett, P. L. White, A. L. Pollock, J. Hill, R. Schneggenberger, W. I. Sundquist, and J. Kaplan. 2005. The role of LIP5 and CHMP5 in multivesicular body formation and HIV-1 budding in mammalian cells. *J. Biol. Chem.* 280:10548–10555.
86. Xu, Z., L. Llang, H. Wang, T. Li, and M. Zhao. 2003. HCRP1, a novel gene that is downregulated in hepatocellular carcinoma, encodes a growth-inhibitory protein. *Biochem. Biophys. Res. Commun.* 311:1057–1066.
87. Yang, M., I. Coppens, S. Wormsley, P. Baetova, H. C. Hoppe, and K. A. Jolner. 2004. The *Plasmodium falciparum* Vps4 homolog mediates multivesicular body formation. *J. Cell Sci.* 117:3831–3838.
88. Yorikawa, C., H. Shibata, S. Waguri, K. Hata, M. Horii, K. Katoh, T. Kobayashi, Y. Uchiyama, and M. Maki. 2005. Human CHMP6, a myristoylated ESCRT-III protein, interacts directly with an ESCRT-II component EAP20 and regulates endosomal cargo sorting. *Biochem. J.* 387:17–26.
89. Yoshimori, T., F. Yamagata, A. Yamamoto, N. Mizushima, Y. Kabeyn, A. Nara, I. Miwako, M. Ohashi, M. Ohsumi, and Y. Ohsumi. 2000. The mouse SKD1, a homologue of yeast Vps4p, is required for normal endosomal trafficking and morphology in mammalian cells. *Mol. Biol. Cell* 11:747–763.

CHAPTER 4

STRUCTURAL BASIS FOR UBIQUITIN RECOGNITION BY THE HUMAN ESCRT-II EAP45 GLUE DOMAIN

Structural basis for ubiquitin recognition by the human ESCRT-II EAP45 GLUE domain

Steven L Alam¹, Charles Langelier¹, Frank G Whitby¹, Sajjan Koirala¹, Howard Robinson², Christopher P Hill¹ & Wesley I Sundquist¹

The ESCRT-I and ESCRT-II complexes help sort ubiquitinated proteins into vesicles that accumulate within multivesicular bodies (MVBs). Crystallographic and biochemical analyses reveal that the GLUE domain of the human ESCRT-II EAP45 (also called VPS36) subunit is a split pleckstrin-homology domain that binds ubiquitin along one edge of the β -sandwich. The structure suggests how human ESCRT-II can couple recognition of ubiquitinated cargoes and endosomal phospholipids during MVB protein sorting.

Late endosomal compartments called multivesicular bodies serve as primary sorting sites for cell-surface receptors and other membrane proteins that are ultimately downregulated through lysosomal degradation. Ubiquitinated cargoes are sorted into MVB vesicles through the sequential action of three multiprotein complexes called ESCRT-I, ESCRT-II and ESCRT-III¹. Both human and yeast ESCRT-I complexes bind ubiquitin (Ub) through ubiquitin E2 variant domains of the

TSG101 (yeast Vps23p) subunit^{2,3}. In contrast, the human and yeast ESCRT-II complexes must recognize ubiquitin differently, because yeast ESCRT-II binds Ub through the second of two Npl4 zinc finger (NZF) modules embedded within the 'GRAM-like Ub binding in EAP45' (GLUE) domain of the Vps36p subunit⁴, whereas the mammalian homolog, EAP45 (or VPS36), binds Ub directly through its GLUE domain⁵.

To learn how human ESCRT-II recognizes ubiquitinated protein cargoes, we determined crystal structures of the EAP45 GLUE-Ub complex (Fig. 1, Supplementary Methods and Supplementary Table 1 online). Like its yeast counterpart⁶, EAP45 GLUE adopts a pleckstrin-homology (PH) domain fold, with a seven-stranded β -sandwich capped by a C-terminal α -helix (Fig. 1a). The EAP45 and Vps36p GLUE domains are both 'split' by insertions within the S6-S7 loop. Split PH domains have been characterized previously⁷⁻⁹, but these are the first examples in which the insertion occurs at this position. The 16-residue insertion of EAP45 GLUE forms an exposed loop that buttresses the base of the bound Ub molecule and then extends into solution, whereas the larger insertion within Vps36p (~150 residues) contains two NZF modules that bind ESCRT-I and Ub^{4,6}, respectively. The structures of the human EAP45 and yeast Vps36p GLUE domains are otherwise very similar (r.m.s. deviation of 0.77 Å over secondary structure regions), despite sharing just 14% sequence identity (see Supplementary Figs. 1 and 2 online).

In the complex, the S5 edge of the second sheet of the EAP45 GLUE β -sandwich binds the exposed Ub β -sheet. The Ub interface is centered about Val70 and spans an extended hydrophobic patch

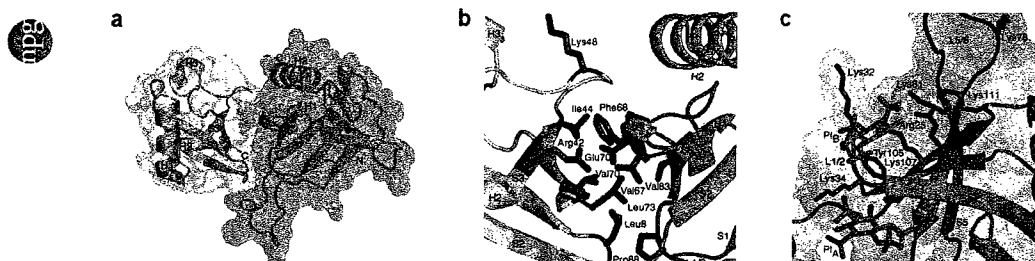


Figure 1 Structure of the EAP45 GLUE-Ub complex. (a) Ribbon and space-filling model of the complex, with the EAP45 GLUE molecule shown in cyan. (b) Expanded view of the Ub Ile44-EAP45 binding interface (orientation is similar to a). (c) Expanded view showing the approximate locations of the canonical (PI_A , orange) and noncanonical (PI_B , magenta) PI-binding sites. To identify the different PI-binding sites, the EAP45 GLUE structure was overlaid onto the PH domain complexes DAPP1/PHISH-I(1,3,4,5) P_4 (PDB 1FA0, secondary structure r.m.s. deviation = 2.8 Å, canonical PI-binding site)¹⁴ and β -spectrin-I(1,4,5) P_3 (PDB 1BTN, secondary structure r.m.s. deviation = 3.4 Å, noncanonical PI-binding site)¹⁵. The DAPP1 and β -spectrin backbones were then removed for clarity. Basic side chains in the binding site are shown explicitly, and the translucent space-filling model is color coded according to electrostatic potential (dark blue to red, +5 to -5 $k_B T e_c^{-1}$).

¹Department of Biochemistry, University of Utah, Salt Lake City, Utah 84112-5650, USA. ²Biology Department, 463 Brookhaven National Laboratory, Upton, New York 11973-5000, USA. Correspondence should be addressed to C.P.H. (chris@biochem.utah.edu) or W.I.S. (wes@biochem.utah.edu).

Received 26 July; accepted 2 October; published online 22 October 2006; doi:10.1038/nsmb1160

BRIEF COMMUNICATIONS

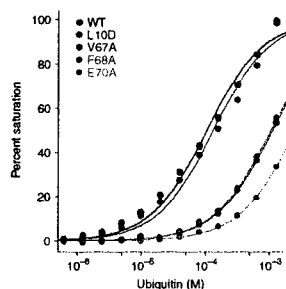


Figure 2 Biosensor binding analyses of the EAP45 GLUE-Ub interaction. Isotherms show Ub binding to wild-type and mutant EAP45 GLUE proteins (see inset for color coding). Measured K_d values (μM) were as follows: wild-type protein = 105 μM ; L10D = 133; V67A > 1,000; F68A > 1,000; E70A > 1,000. Error bars from triplicate measurements were smaller than the data points.

including Ile44, Leu73 and Leu8, whereas the EAP45 GLUE binding interface is centered about Phe68 and is comprised of residues from S5, S6, H2 and the S6-S7 loop (Fig. 1b). The interface core is hydrophobic on both sides, with peripheral hydrophilic side chain interactions, including Ub Arg42-EAP45 Glu70 (salt bridge) and possibly Ub Lys48-EAP45 Thr127 (hydrogen bond). Several key interacting residues are not conserved in yeast Vps36p, consistent with the idea that yeast ESCRT-II instead binds Ub through an NZF domain (Supplementary Figs. 1 and 2).

In the two crystal forms examined, each EAP45 GLUE domain makes similar contacts with two different ubiquitin molecules, one through the primary binding site described above and a second through an interface centered about EAP45 residue Leu10. Several Ub-binding domains (UBDs) have recently been shown to bind two Ub molecules^{10,11}, and we therefore tested the relevance of both crystallographic EAP45 GLUE interfaces for Ub binding in solution. Ub bound the immobilized wild-type EAP45 GLUE domain with a dissociation constant of $\sim 100 \mu\text{M}$, which matches the binding energies of many other UBD-Ub interactions (see Fig. 2 and Supplementary Table 2 online for full details)¹². Mutation of any of the three key residues in the primary EAP45 GLUE binding interface (V67A, F68A or E70A) reduced the Ub-binding affinity more than ten-fold (Fig. 2). Similarly, a single point mutation in the primary Ub-binding surface (I44A) also reduced EAP45 GLUE binding affinity up to 20-fold (Supplementary Table 2). In contrast, a mutation in the center of the second EAP45 GLUE-Ub crystallographic interface (L10D) did not reduce the Ub-binding affinity appreciably. These data all support the idea that the primary interface seen in the EAP45 GLUE-Ub crystal structure forms in solution, whereas the second interface does not.

Like many other PH domains, the GLUE domains from EAP45 and Vps36p also bind inositol phosphates/phosphatidylinositides (abbreviated PI)^{5,6}, and the yeast protein binds preferentially to liposomes containing PI(3)P (ref. 6), which is the predominant endosomal PI¹³. PH domains can bind PI ligands at two distinct sites: a canonical site located between the S1-S2 and S3-S4 loops (PI_A in Fig. 1c) and a noncanonical site located on the other side of the S1-S2 loop, in a pocket between the S1-S2 and S5-S6 loops (PI_B in Fig. 1c). An overlay of the EAP45 GLUE structure onto PH-PI

complexes from DAPP1 (canonical PI site) and β -spectrin (noncanonical PI site) illustrates that the noncanonical site in EAP45 GLUE forms an extended groove surrounded by basic residues, whereas the canonical site is actually slightly acidic. The EAP45 GLUE structure therefore indicates that PIs probably bind in the noncanonical site (PI_B), in good agreement with a recent mutational analysis of the Vps36p GLUE domain⁶. *In vitro*, the mammalian EAP45 GLUE domain preferentially binds phosphorylated 3-phosphoinositides such as PI(3,4,5)P₃ (ref. 5), and this apparent difference between the human and yeast proteins may reflect the presence of three additional basic residues in the human EAP45 PIP-binding site (Arg25, Lys34 and Lys107; see Fig. 1c and Supplementary Figs. 1 and 2).

In summary, we find that EAP45 GLUE adopts a split PH domain fold that couples the recognition of ubiquitinated cargoes and endosomal membranes. PIs appear to bind in the noncanonical site at the apex of the β -sandwich, whereas ubiquitin binds along the opposite edge of the second sheet. It appears possible that EAP45 GLUE could bind Ub and PIs cooperatively, as the two binding sites are physically linked through the intervening S5-S6 β -hairpin. We speculate that in the absence of ligand binding, the extended insertion that splits the EAP45 GLUE domain between strands S6 and S7 could act as a hinge that allows the S5-S6 hairpin to sample both closed (ligand binding) and open (nonbinding) conformations. Although speculative, such an allosteric binding model is consistent with suggestions that PH domain splitting may support regulated phospholipid binding in other biological systems^{7,8}.

Accession codes. Protein Data Bank: Coordinates and structure factors have been deposited with accession code 2HTH. Research Collaboratory for Structural Bioinformatics: 038741.

Note: Supplementary information is available on the Nature Structural & Molecular Biology website.

ACKNOWLEDGMENTS

Biosensor analyses, protein sequencing and mass spectrometry were performed at University of Utah core facilities, and we also thank I. Jafri for technical assistance. This work was supported by US National Institutes of Health grants to C.P.H. (GM66521) and W.L.S. (AI51174). The National Synchrotron Light Source is funded by the US National Center for Research Resources, by the US Department of Energy, Office of Basic Energy Sciences and by the US National Institutes of Health.

COMPETING INTERESTS STATEMENT

The authors declare that they have no competing financial interests.

Published online at <http://www.nature.com/nsmb/>

Reprints and permissions information is available online at <http://npg.nature.com/reprintsandpermissions/>

- Hurley, J.H. & Emr, S.D. *Annu. Rev. Biophys. Biomol. Struct.* **35**, 277–298 (2006).
- Sundquist, W.I. *et al. Mol. Cell* **13**, 783–789 (2004).
- Teo, H., Veprincev, D.B. & Williams, R.L. *J. Biol. Chem.* **279**, 28689–28696 (2004).
- Alam, S.L. *et al. EMBO J.* **23**, 1411–1421 (2004).
- Stagsvold, T. *et al. J. Biol. Chem.* **280**, 19600–19606 (2005).
- Teo, H. *et al. Cell* **125**, 99–111 (2006).
- Lemmon, M.A. *Cell* **120**, 574–576 (2005).
- Yan, J. *et al. EMBO J.* **24**, 3985–3995 (2005).
- Wen, W., Yan, J. & Zhang, M. *J. Biol. Chem.* **281**, 12060–12068 (2006).
- Trempe, J.F. *et al. EMBO J.* **24**, 3178–3189 (2005).
- Hirano, S. *et al. Nat. Struct. Mol. Biol.* **13**, 272–277 (2006).
- Hicke, L., Schubert, H.L. & Hill, C.P. *Nat. Rev. Mol. Cell Biol.* **6**, 610–621 (2005).
- Birkeland, H.C. & Stenmark, H. *Curr. Top. Microbiol. Immunol.* **282**, 89–115 (2004).
- Ferguson, K.M. *et al. Mol. Cell* **6**, 373–384 (2000).
- Hyvonen, M. *et al. EMBO J.* **14**, 4676–4685 (1995).

CHAPTER 5

THE MOLECULAR MECHANISM OF HEPCIDIN-MEDIATED FERROPORTIN DOWN-REGULATION

The Molecular Mechanism of Hepcidin-mediated Ferroportin Down-Regulation

Ivana De Domenico,* Diane McVey Ward,* Charles Langelier,[†]
Michael B. Vaughn,* Elizabeta Nemeth,[‡] Wesley I. Sundquist,[†] Tomas Ganz,[‡]
Giovanni Musci,[§] and Jerry Kaplan*

Departments of *Pathology and [†]Biochemistry, School of Medicine, University of Utah, Salt Lake City, UT 84132; [‡]Department of Medicine, David Geffen School of Medicine, University of California, Los Angeles, Los Angeles, CA 90095; and [§]Dipartimento di Scienze e Tecnologie Agro-alimentari, Ambientali e Microbiologiche, Università del Molise, Campobasso, Italy 86100

Submitted January 26, 2007; Revised April 10, 2007; Accepted April 19, 2007
Monitoring Editor: Sandra Schmid

Ferroportin (Fpn) is the only known iron exporter in vertebrates. Hepcidin, a peptide secreted by the liver in response to iron or inflammation, binds to Fpn, inducing its internalization and degradation. We show that after binding of hepcidin, Fpn is tyrosine phosphorylated at the plasma membrane. Mutants of human Fpn that do not get internalized or that are internalized slowly show either absent or impaired phosphorylation. We identify adjacent tyrosines as the phosphorylation sites and show that mutation of both tyrosines prevents hepcidin-mediated Fpn internalization. Once internalized, Fpn is dephosphorylated and subsequently ubiquitinated. An inability to ubiquitinate Fpn does not prevent hepcidin-induced internalization, but it inhibits the degradation of Fpn. Ubiquitinated Fpn is trafficked through the multivesicular body pathway en route to degradation in the late endosome/lysosome. Depletion of proteins involved in multivesicular body trafficking (Endosome Sorting Complex Required for Transport proteins), by small-interfering RNA, reduces the trafficking of Fpn-green fluorescent to the lysosome.

INTRODUCTION

Iron homeostasis in vertebrates is dominated by the lack of an excretory route for excess iron. Plasma iron level is regulated by the rate of iron entry through the duodenal mucosa, which affects net iron absorption, and by the rate of iron release from macrophages recycling iron from aged or damaged erythrocytes (Hentze *et al.*, 2004; Camaschella, 2005; Donovan *et al.*, 2006). Export of iron from duodenal enterocytes and macrophages into plasma is regulated by the plasma membrane transporter ferroportin (Fpn) (Abboud and Haile, 2000; Donovan *et al.*, 2000; McKie *et al.*, 2000). Fpn is the receptor for hepcidin, a peptide of 25 amino acids synthesized by the liver in response to inflammation and increased iron stores (Ganz and Nemeth, 2006). Binding of hepcidin to Fpn results in the internalization and degradation of Fpn, leading to a decrease in iron export (Nemeth *et al.*, 2004). Decreased plasma iron leads to a reduction in hepcidin synthesis, resulting in increased plasma membrane Fpn and increased iron delivery into plasma.

Inadequate hepcidin production can explain many of the genetic forms of iron overload disease, whereas high levels of hepcidin produced by prolonged inflammatory stimuli

can account for hypoferrremia and anemia of chronic disease (Weiss and Goodnough, 2005; Pietrangelo, 2006). There is one form of genetic iron overload disease, however, that is not caused by abnormal hepcidin production. This disease, referred to as ferroportin disease or hereditary hemochromatosis type 4, results from mutations in the Fpn gene (Pietrangelo, 2004). Characterization of mutant alleles of Fpn showed that some Fpn mutant proteins are not appropriately targeted to the cell surface, whereas other mutant proteins are appropriately targeted to the plasma membrane, but they have impaired internalization in response to hepcidin (De Domenico *et al.*, 2005; Drakesmith *et al.*, 2005; Liu *et al.*, 2005; Goncalves *et al.*, 2006). To understand the molecular basis of the defect in hepcidin-resistant Fpn mutants, we examined the mechanism of hepcidin-induced internalization and degradation. We show that in response to hepcidin, Fpn is phosphorylated and that phosphorylation is required for internalization. Once internalized, Fpn is ubiquitinated and trafficked through the multivesicular body (MVB) for degradation in the lysosome.

MATERIALS AND METHODS

Cells and Media

Mouse Fpn was expressed in a cytomegalovirus (CMV)-containing vector (pEGFP-N1, Clontech, Mountain View, CA, or pCMV-Tag4 (FLAG), Stratagene, La Jolla, CA) as described previously (De Domenico *et al.*, 2005). Human embryonic kidney (HEK293T) cells were maintained in DMEM with 10% fetal bovine serum and transfected with pFpn-enhanced green fluorescent protein (EGFP)-N1, pFpn(mutations)-EGFP-N1, pCMV-Fpn-FLAG, pDynamin-EGFP, or pDynamink44A-EGFP by using Nucleofector technology (Amaxa, Gaithersburg, MD), according to the manufacturer's directions. FM3A and ts85 cells were maintained in RPMI 1640 medium with 5% fetal bovine serum and transfected using Nucleofector technology. HEK293T Fpn,

This article was published online ahead of print in *MBC in Press* (<http://www.molbiolcell.org/cgi/doi/10.1091/mbc.E07-01-0060>) on May 2, 2007.

Address correspondence to: Jerry Kaplan (jerry.kaplan@path.utah.edu).

Abbreviations used: ESCRT, endosome sorting complex required for transport; Fpn, ferroportin; GFP, green fluorescent protein; MVB, multivesicular body.

I. De Domenico *et al.*

a stable cell line in which Fpn-green fluorescent protein (GFP) expression is regulated by the ecdysone promoter, has been described previously (Nemeth *et al.*, 2004; De Domenico *et al.*, 2005).

Generation of Fpn Constructs

All Fpn mutations were generated in pFpn-EGFP-N1 by using the QuikChange site-directed mutagenesis kit (Stratagene), amplified in *Escherichia coli*, and sequence-verified before transfecting into mammalian cells.

Small Interfering RNA (siRNA) Transfection

siRNA oligonucleotide or siRNA pools matching selected regions of TSC101, LIP5, and CHMP5 were as described previously (Garrus *et al.*, 2001; Ward *et al.*, 2005). siRNA oligonucleotides for CHMP6 and EAP20 were as described in Langelier *et al.* (2006). siRNA oligonucleotide pools matching selected regions of *epsin* were obtained from Dharmacon RNA Technologies (Lafayette, CO). HEK293T Fpn-GFP cells were transfected with siRNA oligonucleotides at a final concentration of 50–100 nM by using OligofectAMINE reagent (Invitrogen, Carlsbad, CA). Twenty-four to 48 h after transfection, the cells were trypsinized and plated onto 60-mm plates with or without coverslips. Twenty-four hours after plating, the cells were induced to express Fpn-GFP, incubated in the presence or absence of 1 μ g/ml hepcidin, and then processed for fluorescence microscopy or Western analysis.

Other Procedures

Biotinylation of the plasma membrane of HEK293T cells was performed using sulfo-succinimidyl-2-(biotinamido)ethyl-1,3-dithiopyrinate (sulfo-NHS-SS-biotin) (Pierce Chemical, Rockford, IL) according to the manufacturer's instructions. Immunoprecipitation of Fpn-GFP or Fpn-FLAG was performed as described previously (De Domenico *et al.*, 2005) using either protein A/G resin (Santa Cruz Biotechnology, Santa Cruz, CA) and rabbit anti-GFP (ab65561; Abcam, Cambridge, MA), anti-FLAG M2 affinity gel (Sigma-Aldrich, St. Louis, MO), or immobilized streptavidin affinity gel (Pierce Chemical). Immunoprecipitation of phosphotyrosine was performed using mouse anti-phosphotyrosine antibody (1:500) (Calbiochem, San Diego, CA) and protein A/G resin (Santa Cruz Biotechnology). Samples were analyzed by SDS-polyacrylamide gel electrophoresis under nonreducing conditions. Samples were heated at 37°C for 10 min before being applied to the SDS-PAGE. Western analysis was performed using either mouse anti-FLAG antibody (1:10,000; Sigma-Aldrich); rabbit anti-GFP (1:10,000; ab6556; Abcam); goat anti-human actin (1:1000; Santa Cruz Biotechnology); mouse anti-tubulin (1:1000; GeneTex, San Antonio, TX); mouse anti-phosphotyrosine clone 16F4 (1:500; Calbiochem); mouse anti-ubiquitin (1:1000; Covance, Berkeley, CA); mouse anti-TSC101 (1:1000; GeneTex); rabbit anti-LIP5 (1:500); rabbit anti-CHMP5 (1:500); rabbit anti-CHMP6 (1:1000); rabbit anti-EAP20 (1:1000); or rabbit anti-*epsin* (1:1000; Santa Cruz Biotechnology) followed by either peroxidase-conjugated goat anti-mouse immunoglobulin (IgG) (1:10,000; Jackson ImmunoResearch Laboratories, West Grove, PA), peroxidase-conjugated goat anti-rabbit IgG (1:10,000; Jackson ImmunoResearch Labs, West Grove, PA) or peroxidase-conjugated donkey anti-goat IgG (1:5000; Santa Cruz Biotechnology). All Westerns were normalized for the total protein concentration using the bicinchoninic acid assay (Pierce Chemical). Immunofluorescence and ferritin analysis were performed as described previously (De Domenico *et al.*, 2005). All experiments were performed a minimum of three times, and error bars represent the SD. Analysis of fluorescent images was performed as described previously (Langelier *et al.*, 2006). The calf intestinal phosphatase was obtained from New England Biolabs (Ipswich, MA), and it was used according to the manufacturer's instructions.

RESULTS

Fpn Is Ubiquitinated and Phosphorylated in Response to Hepcidin

Ubiquitination and phosphorylation are two protein modifications known to signal the internalization of plasma membrane proteins (Bonifacino and Traub, 2003). We examined whether hepcidin binding to Fpn induces either of these modifications. Hepcidin was added to cells, and Fpn-GFP was immunoprecipitated and examined for Fpn modifications by Western blot analysis using specific antibodies. As shown previously, Fpn-GFP is fully active for iron export and is hepcidin responsive (Nemeth *et al.*, 2004). A 15-min incubation of Fpn-GFP-expressing cells with hepcidin led to both ubiquitination and tyrosine phosphorylation of Fpn-GFP (Figure 1A). Both modifications were independent of the epitope tag on Fpn, and tyrosine phosphorylation was detected using four different monoclonal antibodies (data not shown). Both ubiquitination and phosphorylation changed the appar-

ent molecular mass of Fpn-GFP. Although the change in molecular mass of the ubiquitinated species was consistent with addition of multiple ubiquitins, a polyubiquitin "ladder" was not seen. The change in the molecular mass of the phosphorylated species was also unexpectedly large. The samples are run under nonreducing conditions because reduction and heat treatment result in an inability to detect Fpn. In the Western blot, the high-molecular-mass Fpn-GFP species are a small fraction of the total Fpn-GFP, suggesting that phosphorylation and ubiquitination are brief transient events.

Phosphorylation of Fpn Occurs at the Cell Surface

We next examined whether ubiquitination and phosphorylation were required for internalization. To determine whether these events occur at the cell surface, we used the membrane-impermeable biotinylation reagent sulfo-NHS-SS-biotin to distinguish between cell surface and internalized Fpn. Cells were treated with sulfo-NHS-SS-biotin at specific times after incubation with hepcidin to distinguish cell surface Fpn-GFP from internalized Fpn-GFP. Biotinylated proteins were purified using streptavidin beads, and the affinity-purified samples were examined for Fpn-GFP by Western blot analysis using antibodies against GFP. Treatment of cells with the sulfo-NHS-SS-biotin resulted in biotinylation of Fpn-GFP (Figure 1B, bottom). In the absence of ponasterone A (no Fpn-GFP expression), there was no detectable biotinylated Fpn-GFP. No Fpn-GFP was detected in the absence of sulfo-NHS-SS-biotin. The amount of biotinylated Fpn-GFP decreased upon addition of hepcidin. The disappearance of total cellular Fpn-GFP closely parallels the disappearance of cell surface Fpn-GFP, indicating that internalized Fpn-GFP is rapidly degraded. We note that Fpn-GFP often occurs as a doublet (De Domenico *et al.*, 2005). Biotinylated Fpn-GFP was examined for protein modifications. Cell surface Fpn-GFP was phosphorylated within 15 min of hepcidin addition (Figure 1C, lane 5, top) but not ubiquitinated (Figure 1C, lane 5, middle). In contrast, internalized Fpn-GFP, which was not biotinylated and did not bind to streptavidin beads ("flow-through"), was ubiquitinated (Figure 1C, lane 6, middle), but phosphorylation was no longer detected (Figure 1C, lane 6, top). These results suggest that phosphorylation is the primary event in response to hepcidin and that it occurs on the cell surface followed by ubiquitination, which occurs once Fpn-GFP has been internalized.

A dominant-negative mutant of dynamin 1, unable to hydrolyze GTP, inhibits both clathrin- and caveolin-mediated internalization (Damke *et al.*, 1994). We took advantage of this dynamin mutant to confirm that phosphorylation is a proximal effect of hepcidin binding to Fpn. Transfection of HEK293T cells with plasmids expressing wild-type dynamin-GFP and Fpn-FLAG did not prevent hepcidin-induced Fpn-FLAG internalization (Figure 2A). In contrast, transfection with a dominant-negative dynamin(K44A)-GFP inhibited hepcidin-induced internalization of Fpn-FLAG. Likewise, Western blot analysis showed that cells transfected with the dynamin(K44A)-GFP and treated with hepcidin had higher levels of Fpn-FLAG compared with hepcidin-treated cells expressing wild-type dynamin-GFP (Figure 2B). Immunoprecipitation of Fpn-FLAG followed by Western blot analysis showed that Fpn was phosphorylated at the plasma membrane; however, it was not ubiquitinated in cells expressing the dynamin mutant (Figure 2B). These results confirm that phosphorylation is an early event that occurs at the cell surface and that ubiquitination occurs after Fpn is internalized. We note that the migration pattern of ubiquitinated Fpn-FLAG does not increase as would be predicted. Ubiquitination of Fpn-FLAG is not detected in the

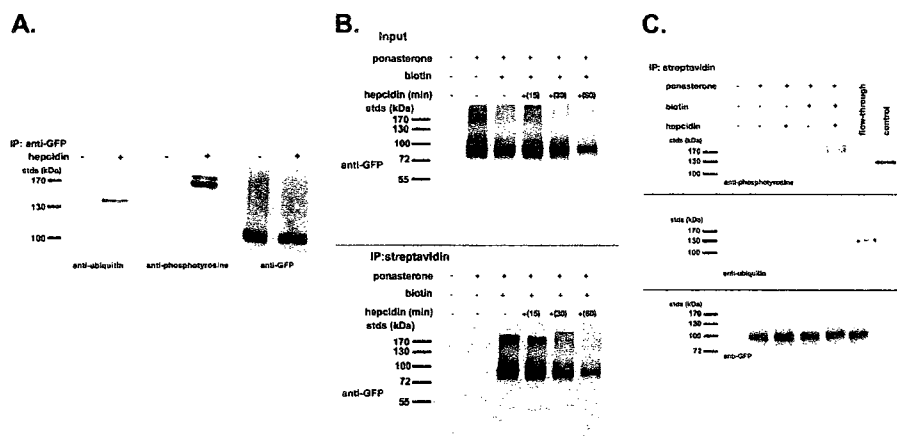


Figure 1. Fpn-GFP is ubiquitinated and phosphorylated. (A) HEK293T cells (stably transfected with an inducible Fpn-GFP) induced to express Fpn-GFP (+ponasterone) were incubated in the presence or absence of $1 \mu\text{g/ml}$ hepcidin for 15 min. Cells were placed at 0°C and solubilized in 1.0% Triton X-100, 150 mM NaCl, 10 mM EDTA, 10 mM Tris, pH 7.4, protease inhibitor mixture, 50 mM *N*-ethylmaleimide, and protein phosphatase inhibitor set. Samples were immunoprecipitated with rabbit anti-GFP antibodies as described in *Materials and Methods*. Immunoprecipitated samples were analyzed by Western blots probing for ubiquitin by using mouse anti-ubiquitin or for phosphotyrosine by using mouse anti-phosphotyrosine followed by a peroxidase-conjugated goat anti-mouse IgG as secondary antibody. Blots were also probed for Fpn-GFP by using rabbit anti-GFP followed by peroxidase-conjugated goat anti-rabbit IgG as secondary. (B) HEK293T cells were induced to express Fpn-GFP with ponasterone for 18 h. Cells were incubated in the presence or absence of $1 \mu\text{g/ml}$ hepcidin for the indicated times, placed at 0°C , and the cell surface was biotinylated using sulfo-NHS-SS-biotin. After biotinylation, cells were solubilized as described in A, and the biotinylated proteins were affinity purified using streptavidin affinity gel. The affinity-purified samples were analyzed by Western blot using a rabbit anti-GFP followed by peroxidase-conjugated goat anti-rabbit IgG. (C) HEK293T Fpn-GFP cells were induced to express Fpn-GFP as described in B. Cells were incubated in the presence or absence of $1 \mu\text{g/ml}$ hepcidin for 15 min, placed at 0°C , and the cell surface was biotinylated. Biotinylated samples were purified using streptavidin beads as described in B. Affinity-purified samples were analyzed by Western blot with mouse anti-phosphotyrosine, mouse anti-ubiquitin followed by a peroxidase-conjugated goat anti-mouse IgG as secondary, or Fpn-GFP by using rabbit anti-GFP followed by peroxidase-conjugated goat anti-rabbit IgG as secondary. "Control" in the top panel is a mixture of tyrosine-modified proteins purchased from Calbiochem as a control for the anti-phosphotyrosine antibody. Flow-through is the sample that did not bind the streptavidin affinity gel (nonbiotinylated Fpn-GFP) but that was subsequently immunopurified using rabbit anti-GFP and the immunopurified sample analyzed by Western blot to test for the presence of phosphotyrosine or ubiquitin modifications on Fpn-GFP.

absence of hepcidin, suggesting that this Fpn-FLAG modification is specific to hepcidin incubation. To determine whether Fpn is internalized through clathrin-coated pits, we silenced epsin, a protein required for clathrin-mediated endocytosis (Chen *et al.*, 1998). Cells expressing Fpn-GFP were transfected with nonspecific oligonucleotide pools or pools specific to epsin. Depletion of epsin, as shown by Western blot analysis (Figure 2C), inhibited hepcidin-mediated Fpn-GFP internalization and degradation (Figure 2D). These results indicate that hepcidin-mediated internalization of Fpn-GFP occurs through clathrin-coated pits.

Tyrosine phosphorylation of Fpn is a rapid response to hepcidin binding, occurring within 15 min of hepcidin addition (Figure 3A). Phosphorylation of Fpn-GFP was independent of the mode of Fpn expression (inducible vs. transient/CMV) or epitope. Critically, mutants of Fpn that are expressed at the cell surface at similar levels to wild type bind hepcidin, but they are not internalized [Fpn(N144H)-GFP] or are internalized at a slower rate than wild type [Fpn(Q182H)-GFP] (De Domenico *et al.*, 2005) showed either no phosphorylation or delayed phosphorylation, respectively, supporting the hypothesis that phosphorylation is the signal for internalization. There is a large difference in the

mobility of the protein detected by the anti-phosphotyrosine antibody and that of Fpn-GFP, raising the possibility that the phosphoprotein might not be Fpn. Alternatively, phosphorylation might affect Fpn conformation, because the samples of Fpn applied to SDS-PAGE are not boiled nor do they contain reducing agents; boiling or reducing agents results in an inability to detect Fpn. To examine this issue, we immunoprecipitated extracts with anti-phosphotyrosine antibody and then probed the immunoprecipitate for Fpn-GFP. After hepcidin addition, the anti-phosphotyrosine antibody precipitated a high-molecular-mass Fpn-GFP, as shown by Western blotting (Figure 3B). The immunoprecipitate was treated with calf intestinal phosphatase, which resulted in the detection of Fpn-GFP at a lower molecular mass, similar to cells not incubated with hepcidin. Based on these results, we conclude that Fpn-GFP is phosphorylated after hepcidin treatment.

Although the topology of Fpn has not been conclusively resolved, a working model was proposed by Haile and colleagues (Liu *et al.*, 2005). This model suggests that there are four tyrosine residues that face the cytosolic surface. We mutated each of these residues (227, 302, 303, and 537) individually to phenylalanine. The mutated proteins local-

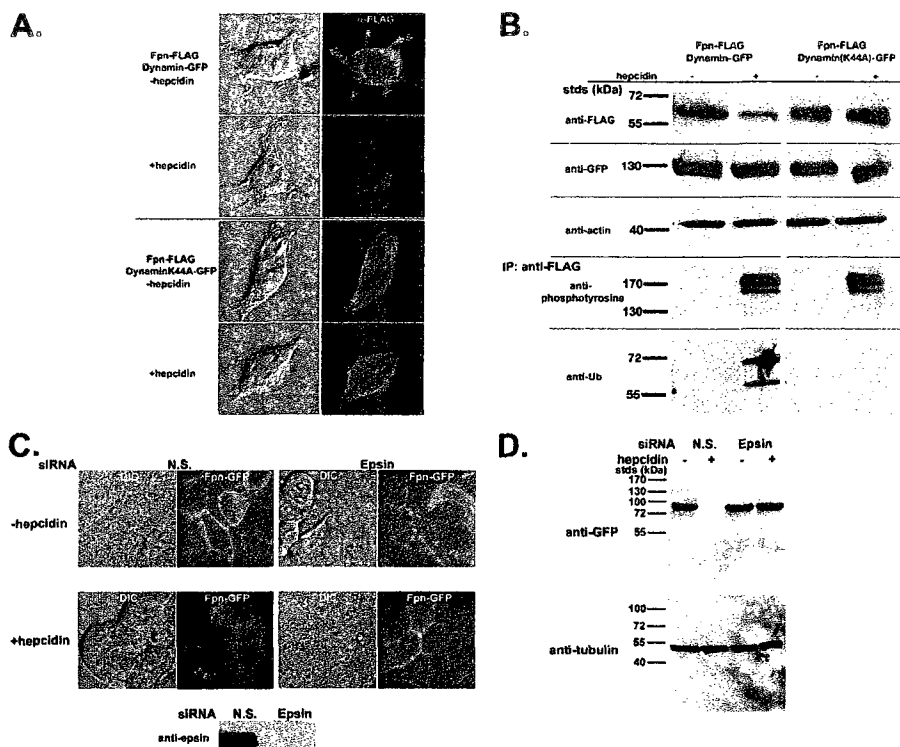
I. De Domenico *et al.*

Figure 2. Fpn is phosphorylated at the plasma membrane. (A) HEK293T cells were transiently transfected with Fpn-FLAG and either Dynamin-GFP or DynaminK44A-GFP. Cells were incubated in the presence or absence of 1 μ g/ml hepcidin for 60 min and processed for immunofluorescence using mouse anti-FLAG followed by Alexa 594-conjugated goat anti-mouse IgG (1:750) as secondary antibody. (B) HEK293T cells were transiently transfected as described in A. Cells were incubated in the presence or absence of 1 μ g/ml hepcidin as in A, extracts obtained as described in Figure 1 and Western blotted for Fpn-FLAG, Dynamin-GFP, and actin (loading control). Extracts were immunoprecipitated using anti-FLAG resin (M2), and the immunoprecipitates were examined for the presence of tyrosine phosphorylated Fpn-FLAG or ubiquitinated Fpn-FLAG by using mouse anti-phosphotyrosine or mouse anti-ubiquitin antibodies followed by peroxidase-conjugated goat anti-mouse IgG. (C and D) HEK293T Fpn-GFP cells were transfected with nonspecific (NS) or epsin-specific siRNA oligonucleotide pools. After 48 h of incubation, cells were induced to express Fpn-GFP and then 18 h later 1 μ g/ml hepcidin was added for 1 h. The efficiency of epsin depletion was assessed by Western blot analysis using antibodies to epsin. The presence of Fpn-GFP was assessed by epifluorescence (C) and Western blot analysis (D).

ized to the plasma membrane, and they were internalized similarly to wild-type Fpn in response to hepcidin (data not shown). This result suggests that either the topological model is wrong and other tyrosines are cytosolic or that multiple tyrosines can be phosphorylated. We then mutated multiple tyrosines. We mutated two adjacent tyrosines contained within a putative cytosolic peptide located between transmembrane regions VI and VII. The mutant protein Fpn(Y302-303F)-GFP, expressed in HEK293T cells, was targeted appropriately to the plasma membrane, but it was not internalized in response to hepcidin, even after 24 h (Figure 3C). To determine whether the mutant protein was phosphorylated, Fpn-GFP or Fpn(Y302-303F)-GFP expressed us-

ing the CMV promoter was immunoprecipitated from cells after a brief (15-min) exposure to hepcidin. This brief exposure to hepcidin is not long enough to see significant loss of Fpn-GFP. Western blot analysis of the immunoprecipitate confirmed the absence of the high-molecular-weight phosphorylated species (Figure 3D). Sequence analysis of Fpn does not suggest that it is a kinase. A number of potassium and chloride channels are tyrosine phosphorylated by a nonreceptor tyrosine kinase, usually belonging to the src kinase family (Davis *et al.*, 2001). Cells expressing Fpn-GFP were incubated with PP2, a src kinase inhibitor. The inhibitor did not affect the expression of Fpn-GFP, but it prevented hepcidin-mediated tyrosine phosphorylation, inter-

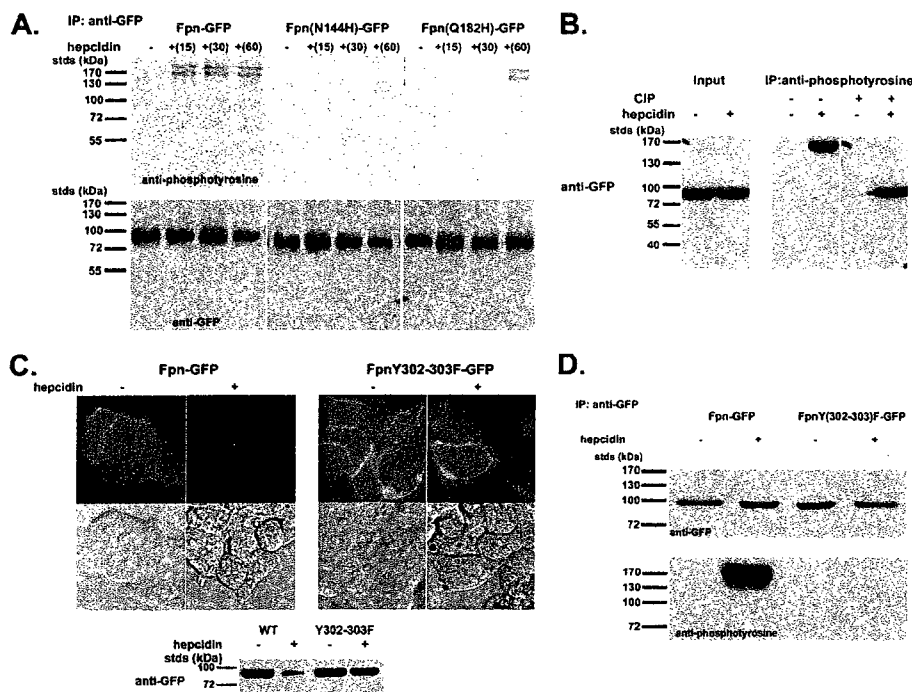


Figure 3. Phosphorylation, location, and function of human Fpn mutations. (A) HEK293T cells were transiently transfected with Fpn-GFP, Fpn(N144H)-GFP, or Fpn(Q182H)-GFP expressed under a CMV promoter. Cells were incubated in the presence or absence of 1 μ g/ml hepcidin for indicated times, solubilized, and immunoprecipitated with rabbit anti-GFP antibodies. Immunoprecipitated samples were analyzed on nonreducing 10% SDS-PAGE, and Western blots were probed for either phosphotyrosine by using mouse anti-phosphotyrosine followed by a peroxidase-conjugated goat anti-mouse IgG as secondary or Fpn-GFP by using rabbit anti-GFP followed by peroxidase-conjugated goat anti-rabbit IgG as secondary. (B) HEK293T cells expressing wild-type Fpn-GFP were incubated with and without 1 μ g/ml hepcidin for 15 min. Cell extracts were immunoprecipitated with anti-phosphotyrosine antibodies, and the immunoprecipitate was incubated in the presence or absence of calf intestinal phosphatase (CIP) for 60 min at 37°C. The samples were analyzed by SDS-PAGE and Western blot probing for Fpn-GFP. (C) HEK293T cells transfected with Fpn-GFP or Fpn(Y302-303F)-GFP were incubated in the presence of 1 μ g/ml hepcidin for up to 24 h. Fpn-GFP localization was examined by fluorescence microscopy after 4 h of hepcidin incubation, and Fpn-GFP levels were measured by Western blot analysis after 24 h of hepcidin incubation. (D) HEK293T cells transfected with Fpn-GFP or Fpn(Y302-303F)-GFP were incubated with hepcidin for 15 min. The cells were solubilized, and Fpn-GFP was immunoprecipitated and analyzed by Western blots as described in A.

nalization, and degradation of Fpn-GFP (Figure 4A). These data indicate that phosphorylation of Fpn is required for its internalization. Fpn(Y302-303F)-GFP is a functional iron exporter, because expression in iron-loaded cells resulted in decreased levels of the iron storage protein ferritin similar to wild-type Fpn-GFP (Figure 4B). Addition of hepcidin does not, however, prevent iron export as shown by the low level of ferritin in Fpn(Y302-303F)-GFP-expressing cells. This result confirms the conclusion based on human Fpn mutants that hepcidin regulates Fpn iron export activity by facilitating Fpn removal.

Ubiquitination of Fpn Is Required for Trafficking and Degradation

Once internalized, Fpn is targeted to the lysosome where it is degraded (Nemeth *et al.*, 2004). Most membrane proteins

degraded in the lysosome are trafficked through the MVB pathway en route to lysosomes, and entry into the MVB typically requires ubiquitination of target proteins (Hurley and Emr, 2006). To determine whether ubiquitination is a requirement for internalized Fpn to enter the MVB, we took advantage of the cell line ts85 that has a temperature-sensitive E1-ubiquitin ligase. This cell line cannot add ubiquitin to target proteins at the restrictive temperature of 39°C (Ikehata *et al.*, 1997). Both wild-type (FM3A) and mutant cells (ts85) were transformed with a plasmid containing a CMV-regulated Fpn-GFP. Fpn-GFP was found on the cell surface at the permissive (Figure 5A) and restrictive temperatures (data not shown). Addition of hepcidin to either wild-type or ts85 cells led to the internalization of Fpn-GFP at both permissive and restrictive temperatures. Fpn was degraded in both cell types at the permissive temperature;

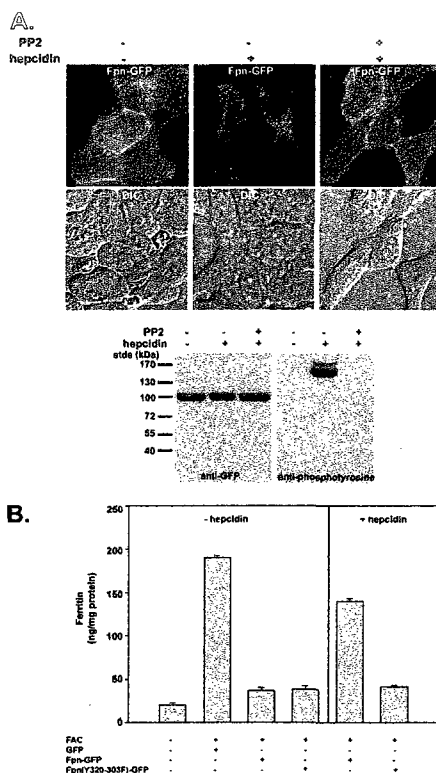
I. De Domenico *et al.*

Figure 4. Effect of src kinase inhibitor PP2 on hepcidin-induced phosphorylation and internalization of Fpn-GFP. (A) HEK293T Fpn-GFP-expressing cells were incubated with 100 μ M PP2 for 15 min. Hepcidin was added for an additional 20 min, and Fpn-GFP localization was examined by fluorescence microscopy, and tyrosine phosphorylation was assayed as on immunoprecipitated Fpn-GFP as described in Figure 3. (B) HEK293T cells, transfected with either pEGF vector, Fpn-GFP, or Fpn(Y302-303F)-GFP, were incubated with or without ferric ammonium citrate (FAC) (10 μ M Fe) for 16 h, and the amount of cell-associated ferritin was determined. Iron-loaded cells expressing Fpn-GFP or Fpn(Y302-303F)-GFP were incubated in the presence of 1 μ g/ml hepcidin for 24 h, and the amount of cell-associated ferritin was determined.

however, at the restrictive temperature Fpn-GFP was degraded in wild-type cells, but it was not degraded in ts85 cells. In ts85 cells, at the restrictive temperature, Fpn-GFP accumulated in intracellular vesicles with some present on the plasma membrane.

Haile's model of Fpn topology (Liu *et al.*, 2005) suggests that there are 11 lysine residues on the cytosolic surface of Fpn that may be sites for ubiquitin addition. We focused our attention on the lysines present in the large cytoplasmic loop that is between two putative transmembrane (TM) domains

(TM-VI and -VII), because this loop also contains tyrosines 302 and 303. Mutation of lysine residues 253, 258, or 269 to alanine had no effect on the plasma membrane localization of Fpn-GFP or on the ability of the mutated Fpn to be internalized and degraded in response to hepcidin (data not shown). Mutation of lysine residue 253 resulted in a protein that targeted to the cell surface and could be internalized by hepcidin (Figure 5B). The mutant protein Fpn(K253A)-GFP was degraded at a much slower rate than wild-type protein and was found in intracellular vesicles. Fpn(K253A)-GFP was phosphorylated in response to hepcidin, but it was no longer ubiquitinated, suggesting that residue 253 is a site for ubiquitination (Figure 5C). These results show that ubiquitination is not required for internalization but that it is required for degradation. There was a difference in the appearance of internalized Fpn-GFP in ts85 cells and in Fpn(K253A)-GFP in HEK293T cells. We feel that this difference can be ascribed to the difference in morphology between the nonadherent ts85 cells and the adherent HEK293T cells.

Fpn Traffics through the MVB En Route to the Lysosome

Trafficking of plasma membrane proteins to the lysosome is dependent on sorting through the MVB (Raiborg *et al.*, 2003; Hurley and Emr, 2006). Many proteins involved in sorting through the MVB have been identified, and most are associated with three complexes that are sequentially recruited to the endosomal membrane during MVB formation, endosome sorting complex required for transport (ESCRT) I-III (Babst *et al.*, 2002a,b; Katzmann *et al.*, 2002). We used RNA interference oligonucleotide pools specific to different proteins in the MVB pathway to determine whether degradation of Fpn requires trafficking through the MVB. TSG101 (Vps23p) is a component of the ESCRT-I complex, which is required for recognition of ubiquitinated cargos destined for the MVB (Garrus *et al.*, 2001; Katzmann *et al.*, 2001). Depletion of TSG101 in mammalian cells results in the accumulation of epidermal growth factor-epidermal growth factor receptor (EGFR) in endocytic compartments (Bishop *et al.*, 2002), and deletion of the yeast homologue results in the missorting of the vacuolar peptidase carboxypeptidase S (CPS) and the formation of a vesicle termed the "class E compartment" (Babst *et al.*, 2000). EAP20 (Vps25p) is a component of ESCRT-II, and ESCRT-II has been shown to bridge ESCRT-I and ESCRT-III (Babst *et al.*, 2002b; Teo *et al.*, 2004, 2006; Yorikawa *et al.*, 2005; Langelier *et al.*, 2006). The absence of ESCRT-II components in yeast results in the accumulation of CPS and a class E or enlarged MVB compartment (Babst *et al.*, 2002b). CHMP6 (Vps20p) binds EAP20 and is part of the ESCRT-III complex (Teo *et al.*, 2004; Langelier *et al.*, 2006). The absence of Vps20p also results in the missorting and accumulation of CPS in a class E compartment (Babst *et al.*, 2002a). CHMP5 (Vps60p) is thought to be a part of the ESCRT-III complex, and it has been shown to be involved in trafficking EGFR through the MVB/lysosomal pathway (Ward *et al.*, 2005). Finally, LIP5 (Vta1p) is thought to act after ESCRT-III, binding and activating the MVB ATPase Vps4 (Scott *et al.*, 2005; Azmi *et al.*, 2006; Lottridge *et al.*, 2006). LIP5 is involved in trafficking EGFR through the MVB/lysosomal pathway (Fujita *et al.*, 2004). siRNA transfection by using oligonucleotide pools directed against specific ESCRT proteins did not affect the cell surface localization of Fpn-GFP nor hepcidin-mediated internalization (Figure 6A). Depletion of ESCRT-I, ESCRT-II, and ESCRT-III proteins or ESCRT III accessory proteins (CHMP5 or LIP5), however, did lead to a delay in the degradation of Fpn-GFP, as assessed by

Hepcidin-mediated Ferroportin Internalization

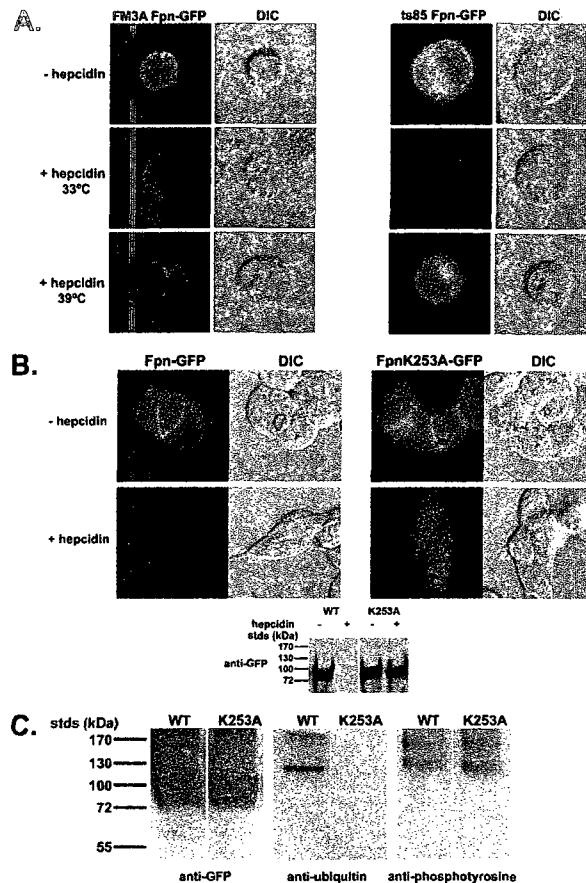


Figure 5. Ubiquitination is required for Fpn-GFP trafficking to the lysosome. (A) Wild-type (FM3A) or mutant cells (ts85) were transfected with Fpn-GFP. Cells were then incubated at the permissive (33°C) or restrictive (39°C) temperature in the presence or absence of 1 μ g/ml hepcidin for 60 min. Cells were examined by epifluorescence microscopy for the localization of Fpn-GFP. (B) HEK293T cells were transiently transfected with Fpn-GFP or Fpn(K253A)-GFP and grown for 12 h. Cells were incubated in the presence or absence of 1 μ g/ml hepcidin for 60 min at 37°C, and then they were examined for the localization of Fpn-GFP, and protein levels were assessed by Western blot. (C) Cells expressing wild-type or Fpn(K253A)-GFP were incubated in the presence of 1 μ g/ml hepcidin for 15 min. The cells were solubilized, and Fpn-GFP was immunoprecipitated as in Figure 1. Immunoprecipitates were analyzed by SDS-PAGE and Western blot for the presence of Fpn-GFP by using rabbit anti-GFP followed by peroxidase-conjugated goat anti-rabbit IgG or for ubiquitinated or tyrosine-phosphorylated Fpn-GFP by using mouse anti-ubiquitin or mouse anti-phosphotyrosine antibodies followed by peroxidase-conjugated goat anti-mouse IgG.

Western blot analysis (Figure 6B) with Fpn-GFP accumulation in endocytic vesicles (Figure 6A). The relative amounts of Fpn-GFP after hepcidin addition was quantified (Figure 6C). Protein depletion by specific siRNA oligonucleotide pools was assessed by Western analysis using protein-specific antibodies (Figure 6D). These data demonstrate that upon internalization, Fpn-GFP is trafficked through the MVB in route to the lysosomes for degradation and that efficient degradation requires all three ESCRT complexes as well as late-acting accessory factors.

DISCUSSION

The relationship between hepcidin and Fpn provides insight into mammalian iron homeostasis and its dysregulation.

Hepcidin-mediated internalization of Fpn results in reduced cellular iron export and provides an explanation for the regulation of iron absorption and for malregulation of iron absorption leading to both iron deficiency and excessive iron accumulation (Ganz and Nemeth, 2006). In this study, we examined the initial events after the binding of hepcidin to Fpn. Our results show that hepcidin induces Fpn phosphorylation, which is critical for internalization (Figure 7A). The data that support this conclusion are as follows: 1) Fpn tyrosine phosphorylation occurs at the cell surface; 2) Fpn tyrosine phosphorylation is not blocked by inhibitors of endocytosis; 3) Fpn tyrosine phosphorylation is defective in human Fpn mutants N144H and Q182H that are not internalized or that are internalized slowly; 4) mutation of Fpn Y302 and Y303 prevents phosphorylation, and thus Fpn endo-

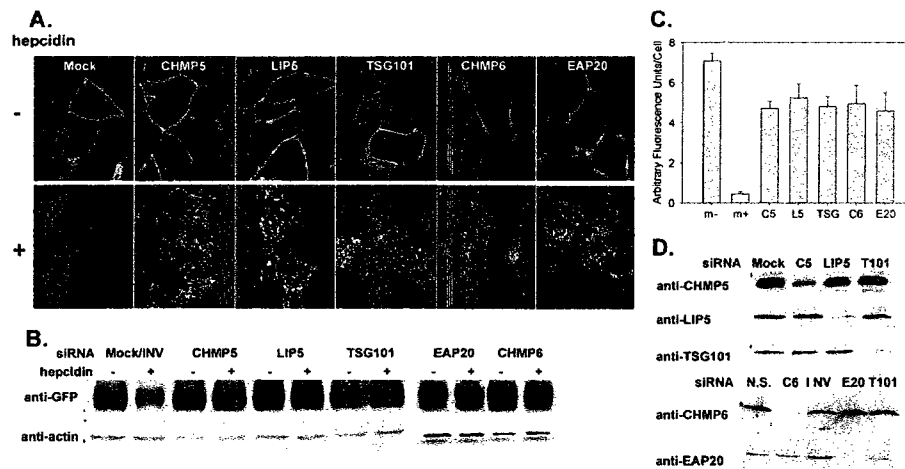
I. De Domenico *et al.*

Figure 6. Depletion of MVB proteins affects the trafficking and degradation of Fpn-GFP. (A) HEK293T Fpn-GFP cells were transfected with siRNA oligonucleotide pools specific for TSG101 (ESCRT I), EAP20 (ESCRT II), CHMP6 (ESCRT III), CHMP5 (ESCRT III), LIP5, nonspecific (N.S.), or inverted TSG101 (INV) by using OligofectAMINE. Forty-eight hours later, cells were induced to express Fpn-GFP, and after 18 h, the cells were incubated in the presence or absence of hepcidin. Cells were examined by confocal microscopy, and the localization of Fpn-GFP was determined. (B) Cells treated as described in A were solubilized as in Figure 1, analyzed on SDS-PAGE under nonreducing conditions, and Western blotted for either Fpn-GFP or actin. (C) Images from A were analyzed using National Institutes of Health ImageJ, and the amount of relative fluorescence per cell was determined. The data are expressed as arbitrary fluorescence units per cell, and error bars represent the analysis of greater than five fields per sample. (D) To assess silencing, samples from A were applied to SDS-PAGE under reducing conditions and analyzed by Western blot by using mouse or rabbit antibodies against TSG101 (T101), EAP20 (E20), CHMP6 (C6), CHMP5 (C5), or LIP5 followed by peroxidase-conjugated goat anti-mouse/rabbit IgG.

cytosol; and 5) inhibitors of src kinases prevent Fpn-GFP phosphorylation and also prevent Fpn-GFP internalization.

These results show that phosphorylation of either Fpn Y302 or Fpn Y303 is an early event after hepcidin binding and that it is required for internalization. Phosphorylation of Fpn can occur on either of these adjacent tyrosines, because mutation of either tyrosine alone has little effect on internalization. This result suggests that only one of the two tyrosines needs to be phosphorylated for Fpn internalization. We note that phosphorylation of Fpn leads to a decreased mobility on SDS-PAGE that is discrepant with the additional mass of either one or two phosphates. We feel confident that it is Fpn that is phosphorylated and hypothesize that the nonboiled protein retains some conformation that is affected by phosphorylation. We cannot, however, rule out the possibility that the migration on SDS-PAGE is due to a protein that binds to the phosphorylated residues. The Y302 and Y303 residues are adjacent to a potential transmembrane segment (Figure 7B), and it is possible that phosphorylation results in a significant structural alteration in the protein-lipid interaction. Furthermore, sequence analysis (ExPASy-prosite database) suggests that the amino acids surrounding the two tyrosines 302-303 may be a src homology 2 domain, indicating that the phosphorylated protein could interact with a variety of adaptor proteins to effect internalization. There is a precedent for tyrosine phosphorylation of membrane transporters/channels leading to either internalization or modification of channel function (for review, see Davis *et al.*, 2001). Our data suggest that Fpn, like other ion

transporters such as potassium and chloride channels, is tyrosine phosphorylated by a src kinase. It remains to be determined what conformational features in Fpn are altered upon binding of hepcidin and how these features recruit a nonreceptor tyrosine kinase. Similarly, the nature of the structural changes resulting from N144H and Q182H, which are predicted to be on a cytoplasmic loop but not the loop containing the phosphorylation site are also unknown. Fpn is a dimer, and these mutations might affect the conformation of the multimeric protein (De Domenico *et al.*, 2007; Zohn *et al.*, 2007).

Our data show that ubiquitination of Fpn occurs subsequently to internalization (Figure 7A). Inhibition of ubiquitination, through the use of cells with a temperature-sensitive E1 ligase or through site-directed mutagenesis of lysine residue K253, leads to the accumulation of Fpn-GFP in intracellular vesicles as well as at the plasma membrane. The presence of Fpn-GFP at the plasma membrane may reflect a decrease in the internalization of Fpn-GFP, or it may represent the recycling of Fpn-GFP when it is not ubiquitinated. The recycling of membrane proteins back to the plasma membrane, if not ubiquitinated, has been demonstrated for the EGFR (Grovdal *et al.*, 2004), and it may indicate specific sorting of membrane proteins that have been internalized but not ubiquitinated. It is of interest that the ubiquitination site is on the same large cytosolic loop as the phosphorylation sites (Figure 7B), suggesting that a ubiquitin ligase may respond to alterations in Fpn structure or binding partners induced by phosphorylation.

Hepcidin-mediated Ferroportin Internalization

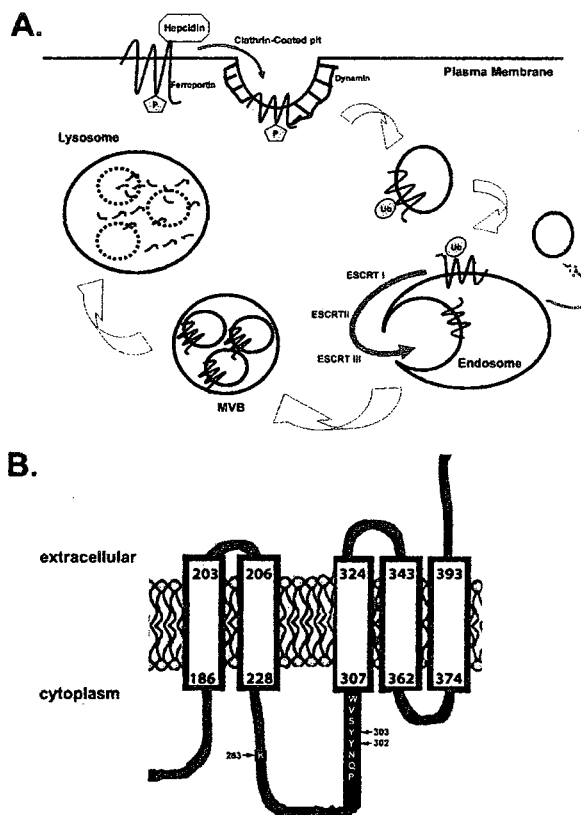


Figure 7. Model for Fpn internalization and degradation. (A) Hepcidin binds Fpn at the plasma membrane where Fpn is tyrosine phosphorylated. Once Fpn is internalized, the phosphates are removed, and Fpn is ubiquitinated, which targets it to the MVB for degradation in the lysosomes. (B) Topology of Fpn showing the potential transmembrane domain containing the phosphorylation (Y302 and Y303) and ubiquitination (K253) sites.

Targeting of most membrane proteins to the lysosome is accomplished by their entry into the MVB. Data suggest, however, that not all ESCRT subunits are required for trafficking through the mammalian MVB. Depletion of HRS by siRNA prevents the agonist induced lysosomal degradation of δ opioid receptors, whereas depletion of TSG101/ESCRT-I does not prevent δ opioid receptor lysosomal degradation (Hislop *et al.*, 2004). Similarly, TSG101/ESCRT-I depletion inhibits MHC class I degradation, whereas EAP20/ESCRT-II is not required for major histocompatibility complex (MHC)-I receptor down-regulation (Bowers *et al.*, 2006), although this complex is required for efficient degradation of internalized epidermal growth factor-receptors (Langelier *et al.*, 2006). Our data demonstrate that trafficking of Fpn-GFP to the lysosome goes through the MVB pathway and requires participation of all of the ESCRT complexes. Depletion of members of ESCRT I, ESCRT II, or ESCRT III complexes leads to the accumulation of Fpn-GFP in intracellular vesicles and reduced degradation. We note that the block

on degradation is not absolute, as Fpn-GFP levels do decrease with time. Whether the lack of a complete block is due to incomplete silencing or to redundancy in ESCRT proteins is unresolved. Nevertheless, our studies demonstrate a role for the MVB pathway in hepcidin-mediated degradation of Fpn.

Many mutations in Fpn cause iron overload disease, which has two distinct presentations (Pietrangelo, 2006). One form of the disease results from Fpn mutants that are unable to reach the plasma membrane (De Domenico *et al.*, 2005; Schimanski *et al.*, 2005). Cells expressing these Fpn mutations are compromised in their ability to export iron and show excessive iron accumulation. A second form of the disease results from Fpn mutants that are targeted to the plasma membrane but do not bind hepcidin and are not internalized (De Domenico *et al.*, 2005; Drakesmith *et al.*, 2005). These results confirm that hepcidin regulates Fpn-mediated iron export by regulating the concentration of Fpn at the plasma membrane and not by affecting the transport activity of Fpn.

I. De Domenico *et al.*

ACKNOWLEDGMENTS

We express our appreciation to Dr. Martin Rechsteiner (University of Utah) for the cell lines FM3A and ts85, to Dr. Matt Mulvey (University of Utah) for dynamin constructs, and to the Kaplan laboratory for critically reading this manuscript. Images for confocal microscopy were obtained at the University of Utah Imaging Core under the direction of Dr. Chris Rodesch. This work was supported by National Institutes of Health grants DK-070947 and HL-26922 (to J.K.) and AI-051174 (to W.I.S.).

REFERENCES

- Abboud, S., and Haile, D. J. (2000). A novel mammalian iron-regulated protein involved in intracellular iron metabolism. *J. Biol. Chem.* 275, 19906–19912.
- Azmi, I., Davies, B., Dimaano, C., Payne, J., Eckert, D., Babst, M., and Katzmann, D. J. (2006). Recycling of ESCRTs by the AAA-ATPase Vps4 is regulated by a conserved VSL region in Vta1. *J. Cell Biol.* 172, 705–717.
- Babst, M., Katzmann, D. J., Estepa-Sabal, E. J., Meerloo, T., and Emr, S. D. (2002a). Escrt-III, an endosome-associated heterooligomeric protein complex required for mvb sorting. *Dev. Cell* 3, 271–282.
- Babst, M., Katzmann, D. J., Snyder, W. B., Wendland, B., and Emr, S. D. (2002b). Endosome-associated complex, ESCRT-II, recruits transport machinery for protein sorting at the multivesicular body. *Dev. Cell* 3, 283–289.
- Babst, M., Odorizzi, C., Estepa, E. J., and Emr, S. D. (2000). Mammalian tumor susceptibility gene 101 (TSG101) and the yeast homologue, Vps23p, both function in late endosomal trafficking. *Traffic* 1, 248–258.
- Bishop, N., Horman, A., and Woodman, P. (2002). Mammalian class E Vps proteins recognize ubiquitin and act in the removal of endosomal protein-ubiquitin conjugates. *J. Cell Biol.* 157, 91–101.
- Bonifacino, J. S., and Traub, L. M. (2003). Signals for sorting of transmembrane proteins to endosomes and lysosomes. *Annu. Rev. Biochem.* 72, 395–447.
- Bowers, K., Piper, S. C., Edeling, M. A., Gray, S. R., Owen, D. J., Lehner, P. J., and Luzzio, J. P. (2006). Degradation of endocytosed epidermal growth factor and virally ubiquitinated major histocompatibility complex class I is independent of mammalian ESCRTIII. *J. Biol. Chem.* 281, 5094–5105.
- Camaschella, C. (2005). Understanding iron homeostasis through genetic analysis of hemochromatosis and related disorders. *Blood* 106, 3710–3717.
- Chen, H., Fre, S., Slepnev, V. I., Capua, M. R., Takei, K., Butler, M. H., Di Fiore, P. P., and De Camilli, P. (1998). Epsin is an EH-domain-binding protein implicated in clathrin-mediated endocytosis. *Nature* 394, 793–797.
- Danke, H., Baba, T., Warmock, D. E., and Schmid, S. L. (1994). Induction of mutant dynamin specifically blocks endocytic coated vesicle formation. *J. Cell Biol.* 127, 915–934.
- Davis, M. J., Wu, X., Nurkiewicz, T. R., Kawasaki, J., Gui, P., Hill, M. A., and Wilson, E. (2001). Regulation of ion channels by protein tyrosine phosphorylation. *Am. J. Physiol.* 281, H1835–H1862.
- De Domenico, I., Ward, D. M., Musci, G., and Kaplan, J. (2007). Evidence for the multimeric structure of ferroportin. *Blood* 109, 2205–2209.
- De Domenico, I., Ward, D. M., Nemeth, E., Vaughn, M. B., Musci, G., Ganz, T., and Kaplan, J. (2005). The molecular basis of ferroportin-linked hemochromatosis. *Proc. Natl. Acad. Sci. USA* 102, 8955–8960.
- Donovan, A. *et al.* (2000). Positional cloning of zebrafish ferroportin1 identifies a conserved vertebrate iron exporter. *Nature* 403, 776–781.
- Donovan, A., Roy, C. N., and Andrews, N. C. (2006). The ins and outs of iron homeostasis. *Physiology* 21, 115–123.
- Drakesmith, H. *et al.* (2005). Resistance to hepcidin is conferred by hemochromatosis-associated mutations of ferroportin. *Blood* 106, 1092–1097.
- Fujita, H. *et al.* (2004). Mammalian class E Vps proteins, SBP1 and mVps2/CHMP2A, interact with and regulate the function of an AAA-ATPase SKD1/Vps4B. *J. Cell Sci.* 117, 2997–3009.
- Ganz, T., and Nemeth, E. (2006). Iron imports. IV. Hepcidin and regulation of body iron metabolism. *Am. J. Physiol.* 290, G199–G203.
- Garnus, J. E. *et al.* (2001). Tsg101 and the vacuolar protein sorting pathway are essential for HIV-1 budding. *Cell* 107, 55–65.
- Concalves, A. S., Muzau, F., Blaybel, R., Hetet, G., Driss, F., Delaby, C., Canonne-Hergaux, F., and Beaumont, C. (2006). Wild-type and mutant ferroportins do not form oligomers in transfected cells. *Biochem. J.* 396, 265–275.
- Grovdal, L. M., Stang, E., Sorkin, A., and Madhus, I. H. (2004). Direct interaction of Cbl with pTyr 1045 of the EGF receptor (EGFR) is required to sort the EGFR to lysosomes for degradation. *Exp. Cell Res.* 300, 388–395.
- Hentze, M. W., Muckenthaler, M. U., and Andrews, N. C. (2004). Balancing acts: molecular control of mammalian iron metabolism. *Cell* 117, 285–297.
- Hislop, J. N., Marley, A., and Von Zastrow, M. (2004). Role of mammalian vacuolar protein-sorting proteins in endocytic trafficking of a non-ubiquitinated G protein-coupled receptor to lysosomes. *J. Biol. Chem.* 279, 22522–22531.
- Hurley, J. H., and Emr, S. D. (2006). The ESCRT complexes: structure and mechanism of a membrane-trafficking network. *Annu. Rev. Biophys. Biomol. Struct.* 35, 277–298.
- Ikehata, H., Kaneda, S., Yamao, F., Seno, T., Ono, T., and Hanaoka, F. (1997). Incubation at the nonpermissive temperature induces deficiencies in UV resistance and mutagenesis in mouse mutant cells expressing a temperature-sensitive ubiquitin-activating enzyme (E1). *Mol. Cell Biol.* 17, 1484–1489.
- Katzmann, D. J., Babst, M., and Emr, S. D. (2001). Ubiquitin-dependent sorting into the multivesicular body pathway requires the function of a conserved endosomal protein sorting complex, ESCRT-I. *Cell* 106, 145–155.
- Katzmann, D. J., Odorizzi, G., and Emr, S. D. (2002). Receptor downregulation and multivesicular-body sorting. *Nat. Rev. Mol. Cell Biol.* 3, 893–905.
- Langelier, C., von Schwedler, U. K., Fisher, R. D., De Domenico, I., White, P. L., Hill, C. P., Kaplan, J., Ward, D., and Sundquist, W. I. (2006). Human ESCRT-II complex and its role in human immunodeficiency virus type 1 release. *J. Virol.* 80, 9465–9480.
- Liu, X. B., Yang, F., and Haile, D. J. (2005). Functional consequences of ferroportin 1 mutations. *Blood Cells Mol. Dis.* 35, 33–46.
- Lottridge, J. M., Flannery, A. R., Vincelli, J. L., and Stevens, T. H. (2006). Vta1p and Vps46p regulate the membrane association and ATPase activity of Vps4p at the yeast multivesicular body. *Proc. Natl. Acad. Sci. USA* 103, 6202–6207.
- McKie, A. T. *et al.* (2000). A novel duodenal iron-regulated transporter, IREG1, implicated in the basolateral transfer of iron to the circulation. *Mol. Cell* 5, 299–309.
- Nemeth, E., Tuttle, M. S., Powelson, J., Vaughn, M. B., Donovan, A., Ward, D. M., Ganz, T., and Kaplan, J. (2004). Hepcidin regulates cellular iron efflux by binding to ferroportin and inducing its internalization. *Science* 306, 2090–2093.
- Pietrangelo, A. (2004). The ferroportin disease. *Blood Cells Mol. Dis.* 32, 131–138.
- Pietrangelo, A. (2006). Hereditary hemochromatosis. *Biochim. Biophys. Acta* 1763, 700–710.
- Raiborg, C., Rusten, T. E., and Stenmark, H. (2003). Protein sorting into multivesicular endosomes. *Curr. Opin. Cell Biol.* 15, 446–455.
- Schimanski, L. M. *et al.* (2005). In vitro functional analysis of human ferroportin (FPN) and hemochromatosis-associated FPN mutations. *Blood* 105, 4096–4102.
- Scott, A., Gaspar, J., Stuchell-Brereton, M. D., Alam, S. L., Skalicky, J. J., and Sundquist, W. I. (2005). Structure and ESCRT-III protein interactions of the MIT domain of human VPS4A. *Proc. Natl. Acad. Sci. USA* 102, 13813–13818.
- Teo, H., Gill, D. J., Sun, J., Perisic, O., Veprintsev, D. B., Vallis, Y., Emr, S. D., and Williams, R. L. (2006). ESCRT-I core and ESCRT-II GLUE domain structures reveal role for GLUE in linking to ESCRT-I and membranes. *Cell* 125, 99–111.
- Teo, H., Perisic, O., Gonzalez, B., and Williams, R. L. (2004). ESCRT-II, an endosome-associated complex required for protein sorting: crystal structure and interactions with ESCRT-III and membranes. *Dev. Cell* 7, 559–569.
- Ward, D. M., Vaughn, M. B., Shufflett, S. L., White, P. L., Pollock, A. L., Hill, J., Schneggenberger, R., Sundquist, W. I., and Kaplan, J. (2005). The role of LIP5 and CHMP5 in multivesicular body formation and HIV-1 budding in mammalian cells. *J. Biol. Chem.* 280, 10548–10555.
- Weiss, C., and Goodnough, L. T. (2005). Anemia of chronic disease. *N. Engl. J. Med.* 352, 1011–1023.
- Yorikawa, C., Shibata, H., Waguri, S., Hatta, K., Horii, M., Katoh, K., Kobayashi, T., Uchiyama, Y., and Maki, M. (2005). Human CHMP6, a myristoylated ESCRT-III protein, interacts directly with an ESCRT-II component EAP20 and regulates endosomal cargo sorting. *Biochem. J.* 387, 17–26.
- Zohn, I. E., De Domenico, I., Pollock, A., Ward, D. M., Goodman, J. F., Liang, X., Sanchez, A. J., Niswander, L., and Kaplan, J. (2007). The flitration mutation in mouse ferroportin acts as a dominant negative to cause ferroportin disease. *Blood* (*in press*).

CHAPTER 6

STRUCTURAL BASIS FOR ESCRT-III PROTEIN AUTOINHIBITION

Structural basis for ESCRT-III protein autoinhibition

Monika Bajorek^{1,2}, Heidi L Schubert^{1,2}, John McCullough^{1,2}, Charles Langelier¹, Debra M Eckert¹, William-May B Stubblefield¹, Nathan T Uter¹, David G Myszka¹, Christopher P Hill¹ & Wesley I Sundquist¹

Endosomal sorting complexes required for transport-III (ESCRT-III) subunits cycle between two states: soluble monomers and higher-order assemblies that bind and remodel membranes during endosomal vesicle formation, midbody abscission and enveloped virus budding. Here we show that the N-terminal core domains of increased sodium tolerance-1 (IST1) and charged multivesicular body protein-3 (CHMP3) form equivalent four-helix bundles, revealing that IST1 is a previously unrecognized ESCRT-III family member. IST1 and its ESCRT-III binding partner, CHMP1B, both form higher-order helical structures *in vitro*, and IST1-CHMP1 interactions are required for abscission. The IST1 and CHMP3 structures also reveal that equivalent downstream $\alpha 5$ helices can fold back against the core domains. Mutations within the CHMP3 core- $\alpha 5$ interface stimulate the protein's *in vitro* assembly and HIV-inhibition activities, indicating that dissociation of the autoinhibitory $\alpha 5$ helix from the core activates ESCRT-III proteins for assembly at membranes.

The endosomal sorting complexes required for transport (ESCRT) pathway functions in a series of important membrane-remodeling processes, including multivesicular body vesicle formation at endosomal membranes, enveloped virus budding from the plasma membrane and midbody abscission during cytokinesis (reviewed in refs. 1–4). In performing these functions, ESCRT components cycle between two different states: an inactive state, in which they are dispersed throughout the cytoplasm, and an active state, in which they are recruited to specific membranes by upstream adaptor proteins that induce tight membrane binding and component assembly. ESCRT recruitment and assembly ultimately lead to membrane fission, producing endosomal vesicles, budded viruses or daughter cells. The ESCRT pathway is therefore apparently a mobile machine that can be recruited to different membranes to help mediate membrane remodeling and fission.

Most of the approximately 30 proteins of the human ESCRT pathway function as components of one of five different complexes (termed the ESCRT-0–III and VPS4 complexes). These complexes are recruited sequentially to sites of action, with each successive complex recruiting and activating downstream complexes for membrane association and assembly^{1–4}. Recent studies have revealed that subunits of the late-acting ESCRT-III complex can form rings, helical filaments and tubes *in vitro* and *in vivo*. Thus, ESCRT-III complexes may form 'collars' within the cytoplasm-filled necks of membrane vesicles and tubules that can constrict the neck and promote membrane fission^{5–10}. Variants of this general model suggest that one specific subset of ESCRT-III proteins, those of the CHMP4/Snf7p (Snf7p is a yeast CHMP4 homolog) family, may create an encircling ring or spiral, and the other ESCRT-III proteins serve primarily to nucleate and cap the CHMP4 filament^{8–10}. ESCRT-III proteins also recruit VPS4 ATPases

and induce them to assemble into active complexes. Enzyme recruitment and activation are further promoted by the accessory factors IST1^{11–14} and LIP5 (Vtalp in yeast)^{1–4}, both of which can bind ESCRT-III and VPS4 proteins. Once assembled, VPS4 uses the energy of ATP hydrolysis to release the assembled ESCRT-III machinery back into the cytoplasm, thereby allowing multiple rounds of membrane deformation and fission¹⁰.

The 11 known human ESCRT-III-like proteins can be divided into seven different families, six of which (CHMP1–6) correspond to the six ESCRT-III-like proteins of *Saccharomyces cerevisiae*. Most ESCRT-III proteins can form both homo- and hetero-oligomers and can pair preferentially at membrane sites of action (for example, CHMP4–CHMP6 and CHMP2–CHMP3)^{6,15}. ESCRT-III proteins vary considerably in primary sequence, but all share common N-terminal core domains of ~150 residues. The core domain of one ESCRT-III protein, CHMP3_{8–183}, has been crystallized and shown to form a four-helix bundle¹⁶. The longer first two helices form an extended hairpin, and the shorter two helices pack at the open end of the hairpin. Sequences located beyond the helical core have autoinhibitory activities, and there is now considerable biochemical and genetic evidence that these downstream sequences prevent premature membrane binding and assembly^{6,16–21}. Downstream sequence elements also bind various late-acting ESCRT factors, including ALIX²² and a series of microtubule-interacting and transport (MIT) domain-containing proteins and enzymes such as ubiquitin hydrolases (for example, AMSH and UBPY)^{23,24}, proteases (calpain 7)^{25,26}, ATPases (Spastin and VPS4 proteins)^{21,27–30} and ATPase activators (LIP5 (Vtalp))^{31–33}. Different ESCRT-III subunits have distinct binding partner specificities, helping to explain the need for so many different ESCRT-III proteins.

¹Department of Biochemistry, University of Utah, Salt Lake City, Utah, USA. ²These authors contributed equally to this work. Correspondence should be addressed to C.P.H. (chris@biochem.utah.edu) or W.I.S. (wes@biochem.utah.edu).

Received 4 January; accepted 19 May; published online 14 June 2009; doi:10.1038/nsmb.1621

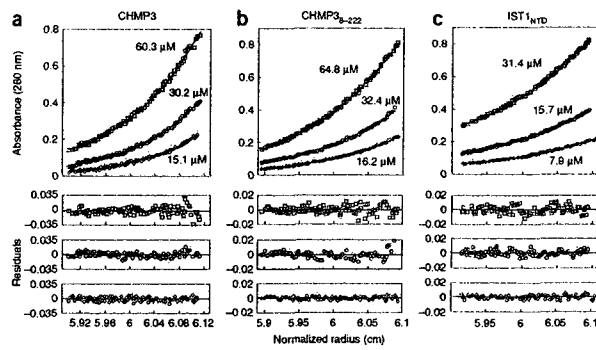


Figure 1 CHMP3, CHMP3₈₋₂₂₂ and IST1_{NTD} are monomers in solution. (a–c) Equilibrium sedimentation distributions of recombinant CHMP3 (a), CHMP3₈₋₂₂₂ (b) and IST1_{NTD} (c) (above), and residual differences (below), with data points shown in open symbols and the single species models shown as solid lines. Rotor speeds were 20,000 r.p.m. and the initial subunit protein concentrations are shown. Data sets were also collected at 24,000 r.p.m. (not shown) and all of the data were globally fit to single species models in which the molecular weights were allowed to float during the refinement. Estimated molecular weights were: CHMP3, 25,840 Da (molecular weight of the monomer ($MW_{monomer}$) = 25,267 Da, M_{obs}/M_{calc} = 1.02); CHMP3₈₋₂₂₂, 24,390 Da ($MW_{monomer}$ = 24,663 Da, M_{obs}/M_{calc} = 0.99); IST1_{NTD}, 20,520 Da ($MW_{monomer}$ = 21,791 Da, M_{obs}/M_{calc} = 0.94).

© 2009 Nature America, Inc. All rights reserved.

IST1 is a recently identified, late-acting ESCRT pathway factor that binds LIP5, VPS4 and CHMP1 (Did2p in yeast)^{11–14}. The precise function(s) of IST1 are not well understood and, indeed, IST1 can exert both positive^{11–14} and negative¹² effects on ESCRT pathway functions. Yeast Ist1p has synthetic interactions with the Vta1p-Vps60p (LIP5–CHMP5) complex in endosomal protein-sorting reactions, implying that Ist1p functions in the formation of multivesicular bodies (MVB), albeit in a non-essential role^{12,13}. Human IST1 localizes to midbodies, and its depletion inhibits abscission but not HIV budding^{11,14}. IST1 proteins therefore seem to have important roles in cytokinesis, auxiliary roles in endosomal protein sorting and no essential role in HIV budding. Biochemical and secondary-structure analyses indicate that IST1 is composed of a helical N-terminal domain (residues 1–189, here termed IST1_{NTD}, but also called the ‘ELYC’ domain after a conserved tetrapeptide sequence¹²), C-terminal MIT-interacting motifs (MIM) (residues 321–366) that can bind cooperatively to the MIT domains of VPS4 (refs. 11,14) and a central linker region that is predicted to lack persistent secondary structure (residues ~190–320)^{11,14}.

Extensive structural and biochemical analyses have revealed many of the relevant molecular interactions that allow different ESCRT components to associate with one another, with phosphatidylinositol-3-phosphate (PI(3)P)-containing membranes and with ubiquitylated protein cargoes^{1–4}. In contrast, the mechanisms that regulate ESCRT pathway assembly and disassembly are much less well understood. Here we have determined crystal structures of the human IST1 and CHMP3 proteins. Furthermore, we have performed complementary biochemical analyses that characterize the functional importance of the IST1–CHMP1 binding interaction in cytokinesis, and we suggest how ESCRT-III proteins can switch between their inactive, soluble states and their active, membrane-bound assemblies.

RESULTS

Characterization of recombinant CHMP3 and IST1 proteins

We developed methods for expressing and purifying recombinant human IST1 and CHMP3 proteins for structural and biochemical studies. Full-length CHMP3 and an N-terminally truncated construct (CHMP3₈₋₂₂₂) were both monomeric in solution, as analyzed by equilibrium sedimentation (Fig. 1a,b), in good agreement with a previous report¹⁶. Full-length IST1 was also monomeric under high-ionic-strength conditions (>300 mM NaCl)¹¹, but aggregated at lower ionic strength. The purified N-terminal domain of IST1

(IST1_{NTD}) behaved similarly to the full-length protein in that it was also monomeric under high-ionic-strength conditions (Fig. 1c) and insoluble in lower-ionic-strength solutions. This construct was particularly amenable for structural and biochemical studies, presumably because it lacked the proline-rich linker region present in the full-length protein.

Crystal structures of IST1_{NTD}

We crystallized IST1_{NTD} under high-ionic-strength conditions and determined the structure in space groups $P2_1$ (1.8-Å resolution) and $P4_32_12$ (2.6-Å resolution) (Table 1 and Supplementary Fig. 1). The structures were similar, and the higher-resolution $P2_1$ structure is described here. IST1_{NTD} is composed of eight helices that pack to create a flat, elongated structure, with overall dimensions of $21 \times 30 \times 60$ Å (Fig. 2a). The two longest helices, $\alpha 1$ and $\alpha 2$, form a helical hairpin that packs against the smaller $\alpha 3$ and $\alpha 4$ helices to create an asymmetric four-helix bundle (termed the ‘core’). Beyond the core, the segment between helices $\alpha 4$ and $\alpha 5$ forms a flap that tracks along the length of the molecule, packing against the $\alpha 2$ – $\alpha 3$ edge. The flap contains two short helices, designated αA and αB to maintain a consistent numbering scheme for conserved ESCRT-III helices. Helix $\alpha 5$ packs perpendicularly across helices $\alpha 1$ and $\alpha 2$ near the closed end of the hairpin and is termed the ‘autoinhibitory helix’. A final turn takes the polypeptide across the hairpin loop and into $\alpha 6$, which projects away from the core. This helix was seen in only the $P2_1$ crystal form, where it is stabilized by lattice contacts. As discussed below, the IST1_{NTD} structure seems to represent a closed, autoinhibited ESCRT-III conformation in which the flap and autoinhibitory helix fold against the core to prevent higher-order interactions.

IST1_{NTD} bears an unexpected resemblance to the published CHMP3₈₋₁₈₃ structure¹⁶ (Fig. 2a–c), and the four helices of the IST1_{NTD} core superimpose with the first four helices of CHMP3 with an r.m.s. deviation of 2.4 Å (128 C α positions). Muziol *et al.* noted that the $\alpha 1$ edge of CHMP3 is distinctly cationic and proposed that this surface binds membranes¹⁶. The equivalent IST1 surface is also basic, although the $\alpha 3$ – $\alpha 4$ face is even more so (Fig. 2d–f).

In addition to their similar core structures, the autoinhibitory $\alpha 5$ helices of CHMP3₈₋₁₈₃ and IST1_{NTD} sit in equivalent positions (Fig. 2a–c, $\alpha 5$, orange). Thus, all of the ordered helices in the CHMP3₈₋₁₈₃ structure have analogs in IST1_{NTD}. However, the assigned connectivity of the autoinhibitory helices differ between the two structures because this helix is connected in *cis* to the IST1_{NTD}

ARTICLES

Table 1 IST1_{NTD} and CHMP3 crystallographic statistics

	IST1 _{NTD} : Native 1	IST1 _{NTD} : Peak 1	IST1 _{NTD} : Inflection 1	IST1 _{NTD} : Remote 1	IST1 _{NTD} : Native 2	CHMP3 ₈₋₂₂₂	CHMP3 ₁₋₁₅₀
Data collection							
Space group	<i>P4₃2₁2</i>	<i>P4₃2₁2</i>	<i>P4₃2₁2</i>	<i>P4₃2₁2</i>	<i>P2₁</i>	<i>P2₁</i>	<i>P6₁</i>
Cell dimensions							
a, b, c (Å)	57.2, 57.2, 157.2	57.6, 57.6, 157.1	57.6, 57.6, 157.2	57.7, 57.7, 157.3	29.3, 92.4, 33.25	36.5, 131.5, 48.5	111.5, 111.5, 30.6
α, β, γ (°)	90.0, 90.0, 90.0	90.0, 90.0, 90.0	90.0, 90.0, 90.0	90.0, 90.0, 90.0	90.0, 97.0, 90.0	90.0, 108.1, 90.0	90.0, 90.0, 120.0
Resolution (Å) ^a	40–2.6 (2.7–2.6)	40–3.4 (3.5–3.4)	40–3.4 (3.5–3.4)	40–3.4 (3.5–3.4)	50–1.80 (1.86–1.80)	50–4.0 (4.14–4.0)	25–3.7 (3.83–3.7)
R _{sym}	6.8 (34)	7.5 (16)	5.9 (15)	6.5 (14)	5.8 (15)	0.16 (15)	0.063 (55)
I/σI	13.5 (1.7)	23.9 (5.0)	24.3 (4.4)	24.4 (3.8)	19.2 (4.6)	9.3 (2.9)	18.4 (2.2)
Completeness (%)	97.7 (88.3)	88.5 (56.5)	87.7 (55.4)	83.4 (42.8)	97.2 (79.1)	78.7 (43.9)	99.2 (96.8)
Redundancy	3.8 (2.8)	6.7 (5.8)	3.9 (3.6)	3.9 (4.0)	3.1 (1.8)	4.0 (2.8)	3.2 (3.1)
Refinement							
Resolution (Å)	40–2.6				50–1.80	38–4.0	24–3.7
No. reflections	7,968				15,213	2,936	2,449
R _{work} / R _{free} (%)	25.9 / 29.8				19.5 / 24.7	37	41
No. atoms							
Protein	1,438				1,558	2,274	973
Water	35				163	0	0
B-factors (Å ²)							
Protein	87.2				26.0	n/a ^b	n/a ^b
Water	69.0				39.4	n/a ^b	n/a ^b
r.m.s. deviations							
Bond lengths (Å)	0.0007				0.011	n/a ^b	n/a ^b
Bond angles (°)	1.2				1.3	n/a ^b	n/a ^b

^aValues in parentheses are for the highest-resolution shell. ^bB-factors and individual atomic parameters were not refined and are unchanged from the molecular replacement model.

core via the flap segment, whereas it was assigned to an adjacent molecule in the CHMP3₈₋₁₈₃ lattice¹⁶. Muziol *et al.* noted, however, that the CHMP3₈₋₁₈₃ connectivity could not be defined unambiguously owing to a lack of visible electron density for the flap region¹⁶. We therefore speculate that the CHMP3₈₋₁₈₃ connectivity may actually match that of IST1_{NTD} and that the CHMP3₈₋₁₈₃ structure may also represent a closed conformation.

Crystal structures of CHMP3

The CHMP3₈₋₁₈₃ construct lacked the final 39 CHMP3 residues, which may have favored an open conformation¹⁶. We therefore attempted to remove this ambiguity by crystallizing both the full-length monomeric CHMP3₁₋₂₂₂ protein and a slightly truncated CHMP3₈₋₂₂₂ protein. Both proteins crystallized isomorphously in space group *P2₁*, but CHMP3₈₋₂₂₂ diffracted to slightly higher resolution (4.0 Å), and this structure is therefore reported (Fig. 2c and Table 1). We determined the CHMP3₈₋₂₂₂ structure by molecular

replacement, using the core of CHMP3₈₋₁₈₃ as a search model, and then subjected the structure to rigid body refinement. Discernible features beyond the search model were limited, but the structure solution is supported by the molecular replacement statistics (see Online Methods) and by unbiased electron density maps (Supplementary Fig. 2). In addition to the four core helices, density for the autoinhibitory helix was evident in unbiased electron density maps, particularly for one of the two independent molecules in the asymmetric unit (Supplementary Fig. 2c,d). Although the connectivity between α4 and α5 was not defined by experimental electron density,

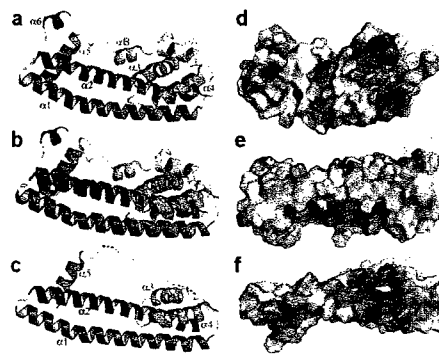


Figure 2 Structures of IST1_{NTD} and CHMP3. (a) Ribbon diagram and helix-labeling scheme for IST1_{NTD}. (b) Overlay of the ordered regions of IST1_{NTD} and CHMP3₈₋₁₈₃. (c) Ribbon diagram of CHMP3₈₋₂₂₂. (d) Space-filling model of IST1_{NTD}, color coded to show the surface charge distribution (blue, basic; red, acidic; ±7 kV)³⁵ (created using PyMOL (<http://pymol.sourceforge.net>)). The molecule is shown in the same orientation as in a. (e) Same as d with the view toward α1. Figure generated from d by rotation about the horizontal so that the bottom edge of d faces the viewer. (f) Space-filling model of CHMP3₈₋₂₂₂ shown in an equivalent orientation to the view of IST1_{NTD} shown in e, emphasizing the basicity of the α1 surface of CHMP3 (ref. 16).



ARTICLES

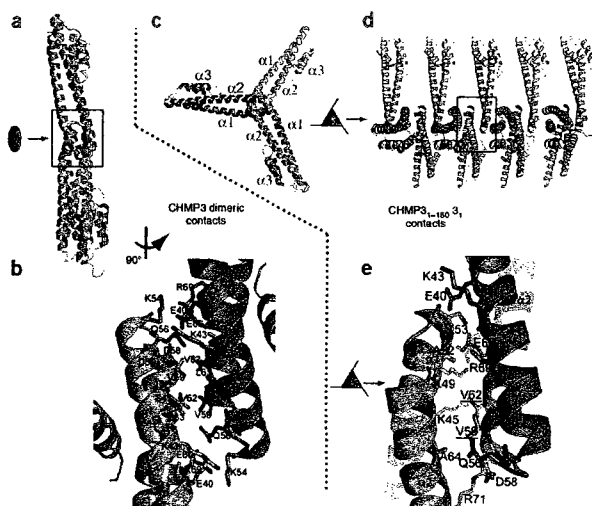


Figure 3 CHMP3 crystal packing interactions. (a) Overlay of the cores of the tip-to-tip dimers in the crystal lattices of CHMP3₈₋₁₈₃ (orange)¹⁶ and CHMP3₈₋₂₂₂ (blue and green). The upper subunits were aligned, and the lower subunits diverge owing to small differences in their tip-to-tip interfaces. (b) Detailed expansion of the boxed region of CHMP3₈₋₂₂₂ shown in a. Most side chain conformations are shown as defined in the CHMP3₈₋₁₈₃ search model, with some minor adjustments to avoid clashes. Precise description of these side chain conformations is not possible at current resolutions. (c) Subunit packing down the 3₁ screw axis of the CHMP3₁₋₁₅₀ crystal lattice, with a single CHMP3₁₋₁₅₀ molecule highlighted in blue. (d) Same assembly as in c but viewed perpendicularly to the 3₁ screw axis. (e) Detailed expansion of the boxed area shown in d. As in b, most side chain conformations are shown as defined in the CHMP3₈₋₁₈₃ search model, with some minor adjustments to avoid clashes.

Crystal packing interactions

We analyzed lattice contacts in the different IST1 and CHMP3 crystal structures to determine whether they were strong candidates for authentic interactions used in ESCRT-III protein assembly (see **Supplementary Figure 3** for a complete catalog of the different lattice interactions). Overall, there are no compelling reasons to believe that any of the various crystal contacts represent authentic assembly interfaces. Moreover, both of our CHMP3 structures lacked the 'side-to-side' dimer interface seen in the CHMP3₈₋₁₈₃ structure¹⁶ and postulated as a possible ESCRT-III assembly interface^{6,7}.

Two of the new CHMP3 interfaces merit comment because they are mediated by a conserved, exposed hydrophobic surface on the closed 'tip' of the $\alpha 1$ - $\alpha 2$ hairpin. In the CHMP3₈₋₂₂₂ structure, two adjacent molecules associate through a small (359 Å²) two-fold symmetric 'tip-to-tip' dimer interface (Fig. 3a,b). A similar tip-to-tip interface was also present in the CHMP3₈₋₁₈₃ lattice¹⁶, and this is the only interface that has been seen in more than one crystal form.

$\alpha 5$ seems to sit in the same position in both the CHMP3₈₋₁₈₃ and the CHMP3₈₋₂₂₂ structures, despite different crystal packing interactions in the two lattices. We have connected $\alpha 4$ and $\alpha 5$ in *cis* rather than in *trans* to create a structure with the same topology as IST1_{NTD}, and this assignment is consistent with biochemical analyses described below.

Finally, we reasoned that a construct corresponding to the CHMP3 core alone could not adopt an autoinhibited conformation and might therefore reveal authentic protein-protein interactions used for ESCRT-III assembly. We crystallized the CHMP3 core construct (CHMP3₁₋₁₅₀) in space group P6₁ and solved the structure by molecular replacement (3.7-Å resolution; **Table 1** and **Supplementary Fig. 2b**). As expected, the CHMP3₁₋₁₅₀ core was similar to the cores of the other CHMP3 and IST1_{NTD} structures, although, as described below, the lattice interactions were unique.

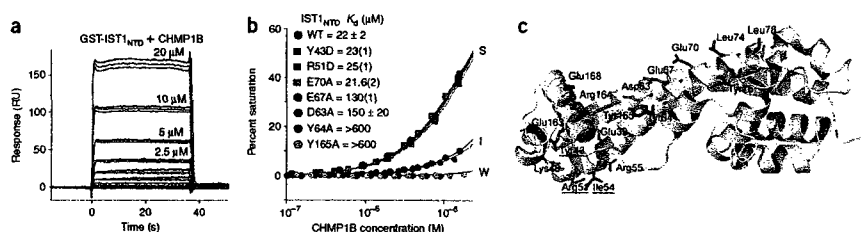


Figure 4 Mutational analyses of IST1-CHMP1B interactions. (a) Sensorgrams showing different concentrations of purified CHMP1B binding to immobilized GST-IST1_{NTD}. Triplicate measurements in response units (RU) are shown for each CHMP1B concentration. (b) Representative biosensor binding isotherms showing CHMP1B binding to wild-type (WT) and mutant GST-IST1_{NTD} proteins with strong (S), intermediate (I) and weak (W) binding affinities. IST1_{NTD} mutations and estimated dissociation constants are given in the inset. Errors represent either s.d. from multiple independent measurements ($n \geq 3$) or s.d. derived from single isotherms measured in triplicate (values in parentheses report the s.d. in the final digit of the measurement). (c) Ribbon diagram showing the location of all IST1_{NTD} mutations tested for CHMP1B binding. Mutated residues are shown explicitly, and the binding affinities of the mutant proteins are color coded as follows: blue, strong (S) binding (binding affinities within 1.5-fold of wild-type IST1_{NTD}); green, intermediate (I) binding (binding affinity reduced 1.5-fold to 8-fold); magenta, weak (W) binding (binding affinity reduced ≥ 8 -fold).

ARTICLES

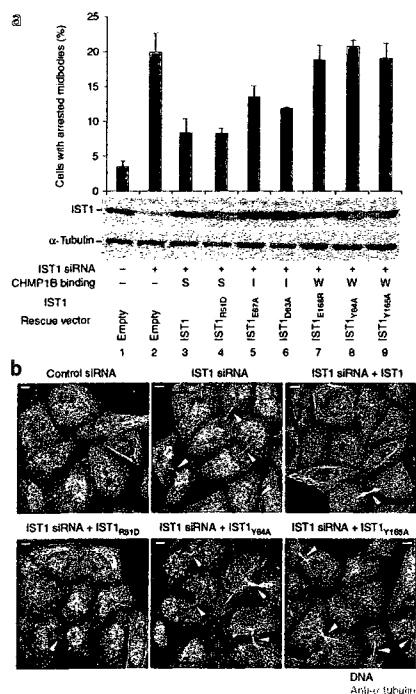


Figure 5 Requirement for IST1-CHMP1 interactions during abscission. (a) Above, quantified abscission defects as reflected in the percentages of HeLa M cells with visible midbodies following siRNA treatment to deplete endogenous IST1 (lanes 2–9) and rescue with an empty vector control (lane 2, negative control) or with vectors expressing wild-type IST1 (lane 3, positive control) or the designated IST1 mutants (lanes 4–9). Untreated cells are shown in lane 1. Error bars show s.d. from three independent repetitions of the experiment. Middle, western blot (anti-IST1) showing levels of soluble endogenous IST1 (lanes 1 and 2) or exogenously expressed IST1 proteins (lanes 3–9). Below, a western blot (anti- α -tubulin) showing expression levels of endogenous α -tubulin (loading control). CHMP1B binding phenotypes of the different IST1 proteins are shown below: strong (S), intermediate (I) or weak (W). (b) Immunofluorescence images showing the midbody phenotypes of cells from a designated subset of the experiments from a. Microtubules (anti- α -tubulin, gray) and nuclei (SYTOX Green) were stained for reference, and yellow arrowheads highlight midbodies. Scale bars, 10 μ m.

CHMP1B bound wild-type IST1_{NTD} with an estimated dissociation constant of $22 \pm 2 \mu$ M (Fig. 4a,b). CHMP1B binding was unaltered by most mutations tested, including mutations within the closed tip of the α 1- α 2 hairpin (for example, E39A, Y43D, K48D, R51D, I54D and R55D) and in the IST1_{NTD} surface that corresponded to the side-to-side dimer interface seen in the crystal structure of CHMP3₁₋₁₈₃ and included the signature 73-ELYCEL-78 motif (for example, E70A, L74R, Y75A and L78R). However, one mutation along helix 2 (E67A) reduced CHMP1B binding in the immunoprecipitation and pull-down experiments and lowered the CHMP1B binding affinity six-fold in the biosensor binding assay, suggesting that this residue contributed to the CHMP1B binding site. We therefore tested mutations in adjacent surface-exposed residues to identify the CHMP1B binding site more precisely. Three IST1 mutants bound CHMP1B weakly (reductions in affinity of more than eight-fold; IST1_{Y64D}, IST1_{Y165A} and IST1_{E168R}), three bound CHMP1B with intermediate affinities (two- to eight-fold reductions; IST1_{D63A}, IST1_{E67A} and IST1_{R164D}) and one still bound strongly to CHMP1B (IST1_{E163R}; data not shown).

Given the proximity of the apparent CHMP1B binding site to the IST1 autoinhibitory helix α 5, we also tested the effects of a series of IST1 mutations predicted to destabilize the α 5-core interface (V56D, I60D, L166D and I169D). All of these IST1 mutations blocked CHMP1B binding entirely (data not shown), indicating that CHMP1B binds the closed conformation of IST1_{NTD} seen in the crystal structures. As summarized in Figure 4c, mutations that inhibited CHMP1B binding clustered within or near a groove created by packing of autoinhibitory helix α 5 against core helix α 2. The groove features a pair of exposed tyrosine residues (Tyr64 and Tyr165) that probably contribute to CHMP1B binding.

The IST1-CHMP1B interactions function in cytokinesis

To determine whether CHMP1B binding was necessary for IST1 cytokinesis function(s), we tested whether IST1 mutations that impaired CHMP1B binding also inhibited abscission. Depletion of endogenous IST1 increased the percentage of HeLa cells with visible midbodies from $4 \pm 1\%$ to $20 \pm 3\%$ (Fig. 5a, compare lanes 1 and 2, and Fig. 5b, compare image above left with image above middle), and this midbody arrest defect was largely (but not entirely) rescued by re-expression of a wild-type, small interfering RNA (siRNA)-resistant IST1 construct ($8 \pm 2\%$; Fig. 5a, lane 3, and Fig. 5b, above right)¹¹. Midbody arrest was also corrected by an IST1 protein with a mutation in the tip of the α 1- α 2 hairpin that retained strong (S) CHMP1B binding (IST1_{R51D}; $8 \pm 1\%$; Fig. 5a, lane 4,

A different type of tip-to-tip interaction is present in the CHMP3₁₋₁₅₀ lattice. In this case, the interaction lacks two-fold rotational symmetry and instead follows a crystallographic 3₁ screw axis that creates an infinite CHMP3₁₋₁₅₀ filament with interfaces on both sides of the tip (Fig. 3c-e). The yeast homolog of CHMP3 (Vps24p) can assemble into three-stranded filaments *in vitro*⁷, although the relationship between the Vps24p filaments and the crystallographic CHMP3 filaments remains to be determined. In summary, the crystal packing interactions in our IST1 and CHMP3 structures do not obviously correspond to authentic biological interfaces, but do reinforce the idea that the exposed hydrophobic surface located at the tip of the helix 1-helix 2 loop is a preferred site for protein-protein interactions^{6,7,16}.

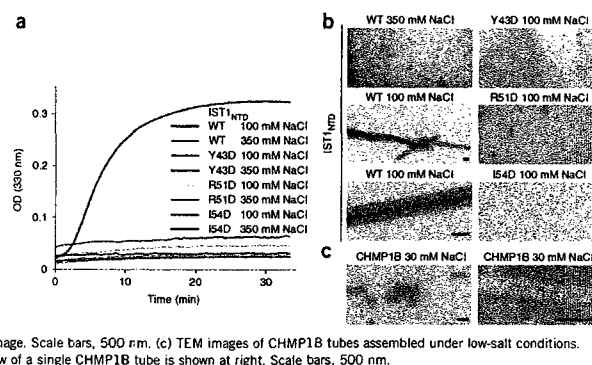
IST1_{NTD} binds CHMP1 proteins

Many ESCRT-III proteins bind one another, and previous studies have shown that the N-terminal domain of IST1 binds preferentially to the C-terminal region of the CHMP1 subset of ESCRT-III proteins¹¹⁻¹⁴. To map the IST1 binding surface more precisely, we created an ensemble of IST1 proteins with point mutations at conserved, surface-exposed residues and tested them for CHMP1A and CHMP1B interactions using: (i) immunoprecipitation reactions in 293T cells (not shown), (ii) glutathione S-transferase (GST) pull-down experiments with recombinant proteins (not shown) and (iii) biosensor binding experiments in which pure recombinant CHMP1B bound immobilized GST-IST1_{NTD} (Fig. 4).



ARTICLES

Figure 6 IST1_{NTD} and CHMP1B tube assembly. (a) Assembly of wild-type (WT) IST1_{NTD} or three different IST1_{NTD} mutants with the designated amino acid substitutions at the tip of the $\alpha 1$ - $\alpha 2$ hairpin (mutated residues are underlined in Figure 4c). IST1_{NTD} proteins were diluted from concentrated protein stocks in high-salt buffers to final concentrations of 62 μ M. Salt concentrations in the assembly buffers are provided in the inset key and protein assembly was followed by light scattering at 330 nm. (b) TEM images of a subset of the wild-type and mutant IST1_{NTD} assembly reactions from a. Note that IST1_{NTD} assembled only under low-salt conditions (compare upper and middle left images) and that IST1_{NTD} proteins with different point mutations at the tip of the $\alpha 1$ - $\alpha 2$ hairpin did not assemble in either high-salt (not shown) or low-salt conditions (right). An expanded view of a single IST1_{NTD} tube is shown in the lower left image. Scale bars, 500 nm. (c) TEM images of CHMP1B tubes assembled under low-salt conditions. A field of tubes is shown at left and an expanded view of a single CHMP1B tube is shown at right. Scale bars, 500 nm.

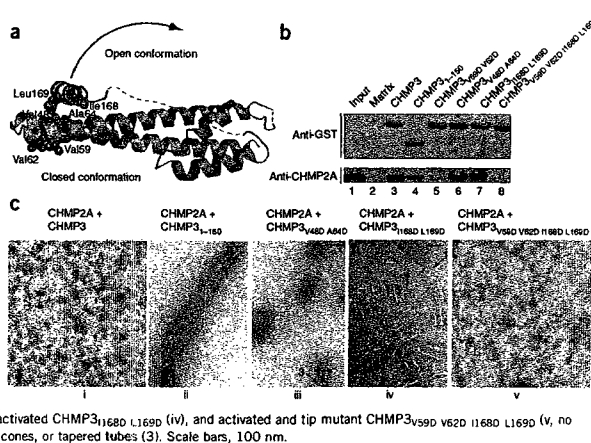


and Fig. 5b, below left). In contrast, three weakly binding IST1 mutants failed to rescue midbody arrest (18–21%; Fig. 5a, lanes 7–9, and Fig. 5b, images below middle and below right). Point mutations within the $\alpha 5$ -core interface that blocked CHMP1B binding also blocked rescue of the midbody arrest defect. However, these mutant proteins partitioned almost exclusively into the insoluble, membrane-bound cellular fractions, and their failure to support abscission may therefore reflect either aberrant CHMP1 binding or IST1 protein mislocalization (Supplementary Fig. 4 and Supplementary Discussion). Finally, two IST1 mutants with intermediate (I) CHMP1B binding affinities rescued midbody arrest to an intermediate extent (12–13%; Fig. 5a, lanes 5 and 6). Hence, there was an excellent correlation between the ability of different IST1 constructs to bind CHMP1B *in vitro* and to function in abscission, indicating that CHMP1 binding is required for IST1 abscission function(s).

IST1_{NTD} and CHMP1B form homopolymeric helices *in vitro*
 CHMP3 can co-polymerize with truncated CHMP2A proteins to form helical tubes 50 nm in diameter *in vitro*⁶. As noted above, both IST1 and IST1_{NTD} became insoluble under low-ionic-strength conditions, and we therefore tested whether these proteins assembled into regular structures. We initially surveyed assembly conditions using light scattering to follow complex formation. Monomeric IST1_{NTD} spontaneously polymerized into high-molecular-weight complexes that strongly scattered light at 330 nm when the protein was diluted from a high-salt buffer (350 mM NaCl) into a low-salt buffer (100 mM NaCl) (Fig. 6a). In contrast, IST1_{NTD} did not scatter light when diluted into an otherwise equivalent high-salt buffer (350 mM NaCl).

EM analyses revealed that the light-scattering IST1_{NTD} assemblies were large tubular structures with diameters of ~ 700 nm (Fig. 6b, lower left images). The tubes seemed to be open along one edge and may therefore be curled sheets rather than fully closed

Figure 7 CHMP3 activation *in vitro*. (a) Ribbon diagram showing the locations of mutated CHMP3 residues at the tip of the $\alpha 1$ - $\alpha 2$ hairpin (purple) and activating mutations on either side of the interface between the core $\alpha 2$ helix (cyan) and the autoinhibitory $\alpha 5$ helix (magenta). The red arrow suggests how the closed CHMP3 conformation might convert into an open conformation by dissociation of the autoinhibitory $\alpha 5$ helix from the core. (b) GST pull-down analyses of the binary CHMP3-CHMP2A interaction. Pure recombinant CHMP2A (below, anti-CHMP2A) was tested for binding to a glutathione-Sepharose matrix (lane 2, negative control) or to immobilized wild-type (lane 3) or mutant GST-CHMP3 proteins (lanes 4–8). Both proteins were detected by western blotting, and input CHMP2A (0.3%) is shown in lane 1 for reference. (c) EM analyses of helical CHMP3-CHMP2A assembly. Different panels show assemblies formed by 1:1 mixtures of CHMP2A with: full length, wild-type CHMP3 (i, negative control, no assembly), CHMP3₁₋₁₅₀ core domain (ii, positive control), activated CHMP3_{V48D A64D} (iii), activated CHMP3_{I168D L169D} (iv), and activated and tip mutant CHMP3_{V59D V62D I168D L169D} (v, no assemblies). Arrows highlight rings (1), tubes (2) and cones, or tapered tubes (3). Scale bars, 100 nm.



ARTICLES

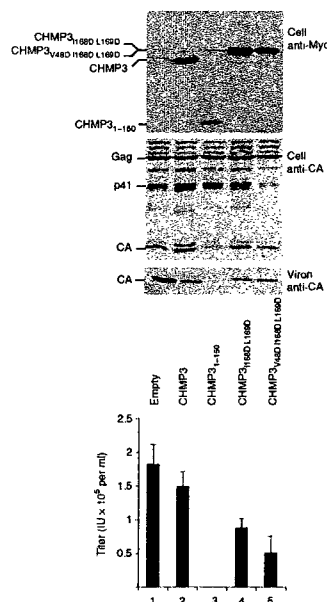


Figure 8 CHMP3 activation *in vivo*. HIV-1 vector expression and release upon co-expression with an empty vector (negative control, lane 1), or with vectors expressing wild-type CHMP3 (negative control, lane 2), a CHMP3₁₋₁₅₀ protein lacking the entire autoinhibitory region (positive control, lane 3), proteins with activating mutations in the $\alpha 5$ -core interface: CHMP3_{1168D 1169D} (lane 4) and CHMP3_{V48D 1168D 1169D} (lane 5). The two uppermost western blots show cellular expression levels of CHMP3-Myc proteins (panel 1, anti-Myc) and of the viral Gag protein and its p41 and CA-processing products (panel 2, anti-CA). The western blot below shows levels of released, virion-associated CA proteins. The graph shows the infectious titers of HIV-1 vectors released under the different conditions (infectious units (IU) per ml; error bars show s.d. in multiple titer measurements, $n \geq 4$).

were not detectable (35 μ M CHMP2A, ~ 7 μ M GST-CHMP3). CHMP2A protein bound GST-CHMP3 (Fig. 7b, lane 3) but did not bind a matrix control (lane 2). CHMP2A also bound the truncated GST-CHMP3₁₋₁₅₀ protein (lane 4), indicating that CHMP2A interacted with the CHMP3 core and that the binary interaction was not strongly affected by removal of the terminal CHMP3 autoinhibitory sequences. In contrast, a double point mutation (V59D V62D) that disrupted the exposed hydrophobic surface on one side of the tip of the CHMP3 $\alpha 1$ - $\alpha 2$ hairpin eliminated CHMP2A binding (lane 5). These data suggest that CHMP2A and CHMP3 interact through a tip-to-tip interaction and demonstrate that the binary CHMP2A-CHMP3 and IST1-CHMP1B pairs interact via different binding surfaces, and therefore form structurally distinct complexes.

Autoinhibitory helix inhibits CHMP3 polymerization

Comparative analyses of the IST1_{NTD}, CHMP3₈₋₁₈₃ and CHMP3₈₋₂₂₂ structures suggested a model for ESCRT-III autoinhibition in which the $\alpha 5$ helix and flap elements fold back against the protein core to prevent higher-order assembly. We tested this idea by introducing destabilizing mutations within the $\alpha 5$ -core interface of the full-length CHMP3 protein and testing their effects on CHMP2A co-assembly. Although the full-length CHMP2A and CHMP3 proteins bind one another, these two proteins do not readily form higher-order helical assemblies⁶ (Fig. 7c,i). In contrast, a CHMP3₁₋₁₅₀ protein that lacked the flap and autoinhibitory helix readily co-polymerized with CHMP2A to form long, regular helical tubes (Fig. 7c,ii, positive control). As CHMP2A forms binary complexes with both CHMP3 and CHMP3₁₋₁₅₀, these experiments imply that CHMP3 residues 151-222 inhibit additional interaction(s) required for higher-order assembly.

To examine the mechanism of CHMP3 autoinhibition, we mixed full-length CHMP2A with full-length CHMP3 proteins that contained mutations on either side of the core- $\alpha 5$ interface (CHMP3_{V48D A64D} and CHMP3_{1168D 1169D}, Fig. 7a). Both sets of mutations activated CHMP3 for assembly, as reflected in the formation of numerous rings, tubes and cones (Fig. 7c,iii,iv). The tubes were similar in diameter to those formed in the CHMP2A-CHMP3₁₋₁₅₀ control reaction (~ 50 nm) but were typically shorter, possibly because the point mutations activated CHMP3 proteins less fully than removal of the entire autoinhibitory region.

We also tested whether the binary CHMP2A-CHMP3 interface detected at low protein concentrations was required for higher-order assembly. As expected, mutations on either side of the CHMP3 autoinhibitory interface did not substantially affect CHMP2A binding to GST-CHMP3 (CHMP3_{V48D A64D} and CHMP3_{1168D 1169D}; Fig. 7b, lanes 6 and 7). However, a CHMP3 protein carrying mutations in both the tip and autoinhibitory interfaces (CHMP3_{V59D V62D 1168D 1169D}) could neither bind CHMP2A in the GST pull-down assay (Fig. 7b, lane 8) nor assemble into helical tubes (Fig. 7c,v). These experiments

helices. Lattice lines were evident in some assemblies, and the clearest lattice spacing was ~ 440 Å, which presumably represents a supermolecular spacing because the maximal length of a single IST1_{NTD} molecule is only ~ 60 Å. As noted above, CHMP3 interactions can be mediated by various different kinds of tip-to-tip interactions^{6,7} (Fig. 3). A series of three point mutations in the analogous IST1 surface (Y43D, R51D and I54D) also inhibited IST1_{NTD} polymerization (Fig. 6a,b, right) (see Supplementary Fig. 5 for ESCRT-III protein alignments). IST1_{NTD} assembly therefore probably also requires some type of tip-to-tip interaction.

We also attempted to test whether IST1_{NTD} and CHMP1B could co-polymerize in a manner similar to the CHMP2A₉₋₁₆₁-CHMP3 pair⁶. However, controls for these experiments revealed that pure recombinant CHMP1B alone polymerized into helical tubes when diluted into low-salt buffers, even in the absence of IST1_{NTD} (Fig. 6c). CHMP1B tubes were of intermediate size (~ 230 nm in diameter), seemed to be fully closed and had visible lattice spacing of ~ 420 Å, similar to the lattice spacing in the IST1_{NTD} tubes. Thus, both IST1_{NTD} and CHMP1B, as for CHMP2A-CHMP3 (ref. 6), form tubular structures *in vitro*, and the ability to assemble into helical tubes therefore seems to be a property common to many ESCRT-III core domains. However, the IST1 and CHMP1B tubes were homopolymeric, and they were substantially larger than those formed by CHMP2A-CHMP3 heteropolymers⁶.

CHMP3 $\alpha 1$ - $\alpha 2$ hairpin tip binds CHMP2A

As with the IST1-CHMP1 pair, CHMP2A and CHMP3 bind one another preferentially. To investigate this interaction further, we used GST pull-down assays to test for binary interactions between CHMP2A and GST-CHMP3 (Fig. 7a,b). We performed these experiments at low protein concentrations where higher-order assemblies



imply that tip-to-tip interactions contribute to CHMP2-CHMP3 co-assembly, in good agreement with a previous study⁶.

Mutations in the autoinhibitory helix activate CHMP3 *in vivo*

Although co-expression of full-length CHMP3 has only minimal effects on HIV-1 budding, truncated CHMP3 constructs lacking the C-terminal autoinhibitory elements potentially inhibit virus budding, presumably because the activated protein sequesters itself and other ESCRT-III proteins on cellular membranes²⁰. Inhibition of HIV release therefore provides a sensitive assay for CHMP3 activation *in vivo*. We used this system to examine whether mutations in the $\alpha 5$ -core interface also activate CHMP3 *in vivo*. Overexpression of full-length CHMP3 together with an HIV-1 vector system in 293T cells had little effect on the release of viral particles, as measured by the levels of virion-associated CA proteins released (Fig. 8, image 3, compare lanes 1 and 2) or by viral titers (Fig. 8, image 4, compare lanes 1 and 2). In contrast, HIV release and infectivity were potently inhibited by co-expression of a CHMP3 protein that lacked the autoinhibitory region entirely (CHMP3₁₋₁₅₀, positive control, compare lanes 2 and 3, showing a >250-fold infectivity reduction). In the actual experiment, two different CHMP3 proteins with point mutations within the $\alpha 5$ -core interface (CHMP3_{1168D 1169D} and CHMP3_{1168D 1169D 1169D}) reduced HIV vector release and infectivity by 1.7-fold and 3-fold, respectively (compare lanes 4 and 5 to lane 2). Western blots confirmed that the full-length CHMP3 proteins and viral Gag proteins and proteolytic processing products were expressed at similar levels (images 1 and 2, respectively). Thus, point mutations in the $\alpha 5$ -core interface enhanced the ability of CHMP3 proteins to inhibit HIV-1 budding *in vivo*, although this enhancement was much weaker than that seen upon deletion of the entire autoinhibitory region. We presume that the weaker effects seen for the point mutants reflects either incomplete activation and/or their ability to interact with VPS4, which will reduce their propensity to become 'trapped' on membranes, as compared to CHMP3₁₋₁₅₀ (which lacks a terminal VPS4 binding site).

DISCUSSION

Our studies have unexpectedly revealed that the N-terminal domain of IST1 contains an asymmetric four-helix bundle that closely resembles the core of the ESCRT-III protein CHMP3 (Fig. 2). As is true for other ESCRT-III proteins, IST1 (i) localizes to midbodies and functions in cytokinesis^{11,14} and MVB vesicle sorting^{12,13}, (ii) binds preferentially to another subset of ESCRT-III proteins (the CHMP1 proteins)¹¹⁻¹⁴, (iii) contains MIM elements near its C terminus that can bind VPS4 and LIPS MIT domains^{11,14} and (iv) can self-assemble into tubular structures *in vitro* (Fig. 6). Thus, despite its larger size and primary sequence divergence, IST1 is an ESCRT-III protein family member.

Despite these similarities, there are also important differences between IST1 and CHMP3, particularly in the binary interactions that they make with their CHMP1 and CHMP2 binding partners. Our mutational analyses mapped the CHMP1 binding site to a groove formed by the autoinhibitory $\alpha 5$ helix and the core $\alpha 2$ helix of IST1_{NTD} (Fig. 4). CHMP1B binding was also inhibited by mutations expected to favor the (hypothetical) open IST1_{NTD} conformation, implying that CHMP1 binds the closed conformation seen in our IST1_{NTD} crystal structures (Fig. 2). IST1 mutations that blocked CHMP1B binding also prevented IST1 from functioning in abscission, implying that these two proteins must act together during this final stage of cytokinesis (Fig. 5). In contrast, binary interactions between CHMP2 and CHMP3 were not inhibited by mutations that displaced or even removed the $\alpha 5$ helix entirely (Fig. 7). This interaction was

sensitive to mutations at the tip of the $\alpha 1$ - $\alpha 2$ hairpin, however, suggesting that, unlike IST1 and CHMP1B, CHMP2 and CHMP3 probably interact through some sort of a tip-to-tip interaction (Fig. 7).

In vitro assemblies formed by ESCRT-III proteins include filaments, rings, cones, curled sheets and tubes^{6,7} (Figs. 6b,c and 7c). At present, we do not know which (if any) of these different *in vitro* assemblies mimic different ESCRT-III assemblies formed *in vivo*. As noted previously⁵⁻⁷, however, filaments, rings and/or tubes could correspond to 'collars' within the necks of budding particles, and tapered tubes or spiraling cones could provide a mechanism for closing the neck during budding⁶ (Fig. 7c, structure type 3). Although the precise molecular interactions that mediate higher-order ESCRT-III assembly remain to be determined, both IST1_{NTD} and CHMP2-CHMP3 assemblies are inhibited by point mutations within the conserved, exposed hydrophobic surface located at the tip of the $\alpha 1$ - $\alpha 2$ hairpin (Figs. 6b and 7c), suggesting that some type of tip-mediated interface forms within both assemblies. Two distinct types of homopolymeric ESCRT-III tip-to-tip interactions have now been seen crystallographically¹⁶ (Fig. 3), and a third type was inferred from cryo-EM studies of helical yeast Vps24 (CHMP3) assemblies⁷. Thus, the conserved hydrophobic surface at the tip of ESCRT-III proteins is a preferred interaction site, although it is not yet clear which, if any, of the tip-to-tip interactions characterized to date represent biologically relevant interactions. We also note that, although the IST1_{RS1D} tip mutation inhibits IST1 assembly (Fig. 6a,b) it does not block the ability of IST1 to function in cytokinesis (Fig. 5), implying that there are different requirements for IST1 assembly *in vitro* and abscission function *in vivo*. Finally, in addition to tip contacts, at least one more protein-protein interface is required to create two-dimensional surfaces in helices or sheets. These secondary interaction(s) are disfavored by C-terminal autoinhibitory interactions (ref. 6 and this work) and may correspond to one of the several different kinds of higher-order packing interactions that have been proposed on the basis of cryo-EM analyses of helical ESCRT-III protein assemblies^{6,7}.

Our IST1_{NTD} structure revealed that the downstream flap and autoinhibitory helix can fold back against the ESCRT-III core, and this topology was unambiguously established by high-quality electron density throughout the flap region (Fig. 2 and Supplementary Fig. 1). Analogous models can be built for the CHMP3₈₋₁₈₃ and CHMP3₈₋₂₂₂ structures, although in those cases the connectivity has not been established unambiguously. Nevertheless, we suggest that all of these structures probably correspond to the closed, autoinhibited ESCRT-III conformation, for several reasons: (i) both IST1_{NTD} and CHMP3₈₋₂₂₂ are monomers in solution under the conditions used for crystallization (although IST1_{NTD} polymerizes under low-salt conditions) (Fig. 1); (ii) IST1 is redistributed into the insoluble membrane-bound, assembled fractions of cellular extracts by mutations that disrupt core packing of the autoinhibitory elements (Supplementary Fig. 4); (iii) CHMP3 and CHMP2A can be activated for co-assembly by deletions that remove the autoinhibitory helices from CHMP2A⁶ or CHMP3, or by point mutations that destabilize packing of the CHMP3 autoinhibitory helix against the core (Fig. 7); (iv) mutations that remove the autoinhibitory helix or destabilize its core packing interactions render CHMP3 a dominant inhibitor of HIV-1 budding^{17,20} (Fig. 8). Nevertheless, there is also good evidence that additional contacts beyond those visualized in our IST1_{NTD} or CHMP3 structures help to stabilize the closed CHMP3 conformation even further, because point mutations in the autoinhibitory helix-core interface do not activate CHMP3 to the same extent as does deletion of the entire autoinhibitory region (Figs. 7c and 8), and because short



ARTICLES

C-terminal deletions downstream of the autoinhibitory $\alpha 5$ helix can also enhance ESCRT-III membrane binding and inhibition of HIV-1 budding, albeit to a lesser extent than deletions that include $\alpha 5$ (refs. 17,20). These observations indicate that the terminal ESCRT-III helix 6 (and possibly also flap sequences) make energetically important contacts that favor the closed ESCRT-III conformation.

In summary, many ESCRT-III proteins can adopt two distinct conformational states^{6,16-21}, and our studies provide a molecular model for the closed, monomeric state adopted by ESCRT-III proteins when they are distributed throughout the cytoplasm (or loosely associated with nonspecific membranes)³⁴. Primary sequence and secondary-structure analyses indicate that all ESCRT-III proteins have analogous $\alpha 5$ helices in equivalent positions, and the mechanism of autoinhibition described here is probably quite general (Supplementary Fig. 5a). Surrounding elements can vary substantially in sequence, length and secondary structure, however, and they probably mediate various protein-protein interactions³⁵. Notably, these different protein-protein interactions can be enhanced, inhibited or unchanged by mutations that favor the open states of various ESCRT-III proteins (for example, refs. 21,22,28,33). Thus, changes in protein-protein and protein-membrane interactions that accompany ESCRT-III activation and assembly are likely to reflect the conformational changes described here, coupled with avidity effects created by the assembly of oligomeric ESCRT-III protein arrays.

METHODS

Methods and any associated references are available in the online version of the paper at <http://www.nature.com/nsmb/>.

Accession Codes. Protein Data Bank: Coordinates and structure factor amplitudes have been deposited for the two IST1_{NTD} crystal forms (3FRR and 3FRS), CHMP₈₋₂₂₂ (3FRT) and CHMP₃₋₁₅₀ (3FRV).

Note: Supplementary information is available on the Nature Structural & Molecular Biology website.

ACKNOWLEDGMENTS

Portions of this research were carried out at the Stanford Synchrotron Radiation Light Source (SSRL), a national user facility operated by Stanford University on behalf of the US Department of Energy, Office of Basic Energy Sciences. The SSRL Structural Molecular Biology Program is supported by the Department of Energy, Office of Biological and Environmental Research and by the US National Institutes of Health (NIH), National Center for Research Resources, Biomedical Technology Program, and the National Institute of General Medical Sciences. We thank M. Babst for helpful discussions. This work was supported by NIH grants A051174 (W.I.S.) and GM082545 (W.I.S. and C.P.H.).

Published online at <http://www.nature.com/nsmb/>

Reprints and permissions information is available online at <http://npg.nature.com/reprintsandpermissions/>

- Hurley, J.H. ESCRT complexes and the biogenesis of multivesicular bodies. *Curr. Opin. Cell Biol.* **20**, 4–11 (2008).
- Williams, R.L. & Urbe, S. The emerging shape of the ESCRT machinery. *Nat. Rev. Mol. Cell Biol.* **8**, 355–368 (2007).
- Saksena, S., Sun, J., Chu, T. & Emr, S.D. ESCRTing proteins in the endocytic pathway. *Trends Biochem. Sci.* **32**, 561–573 (2007).
- Piper, R.C. & Katzmann, D.J. Biogenesis and function of multivesicular bodies. *Annu. Rev. Cell Dev. Biol.* **23**, 519–547 (2007).
- Hanson, P.I., Roth, R., Lin, Y. & Heuser, J.E. Plasma membrane deformation by circular arrays of ESCRT-III protein filaments. *J. Cell Biol.* **180**, 389–402 (2008).

- Lata, S. *et al.* Helical structures of ESCRT-III are disassembled by VPS4. *Science* **321**, 1354–1357 (2008).
- Ghazi-Tabatabaee, S. *et al.* Structure and disassembly of filaments formed by the ESCRT-III subunit Vps24. *Structure* **16**, 1345–1356 (2008).
- Teis, D., Saksena, S. & Emr, S.D. Ordered assembly of the ESCRT-III complex on endosomes is required to sequester cargo during MVB formation. *Dev. Cell* **15**, 578–589 (2008).
- Saksena, S., Wahlman, J., Teis, D., Johnson, A.E. & Emr, S.D. Functional reconstitution of ESCRT-III assembly and disassembly. *Cell* **136**, 97–109 (2009).
- Wollert, T., Wunder, C., Lippincott-Schwartz, J. & Hurley, J.H. Membrane scission by the ESCRT-III complex. *Nature* **458**, 172–177 (2009).
- Bajorek, M. *et al.* Biochemical analyses of human IST1 and its function in cytokinesis. *Mol. Biol. Cell* **20**, 1360–1373 (2009).
- Dimaano, C., Jones, C.B., Hanono, A., Curtiss, M. & Babst, M. Ist1 regulates vps4 localization and assembly. *Mol. Biol. Cell* **19**, 465–474 (2008).
- Rue, S.M., Mattei, S., Saksena, S. & Emr, S.D. Novel Ist1–Dtd2 complex functions at a late step in multivesicular body sorting. *Mol. Biol. Cell* **19**, 475–484 (2008).
- Agromayor, M. *et al.* Essential role of hIST1 in cytokinesis. *Mol. Biol. Cell* **20**, 1374–1387 (2009).
- Babst, M., Katzmann, D., Estepa-Sabal, E., Meerloo, T. & Emr, S. ESCRT-III. An endosome-associated heterooligomeric protein complex required for mvb sorting. *Dev. Cell* **3**, 271–282 (2002).
- Muziol, T. *et al.* Structural basis for budding by the ESCRT-III factor CHMP3. *Dev. Cell* **10**, 821–830 (2006).
- Shim, S., Kimpler, L.A. & Hanson, P.I. Structure/function analysis of four core ESCRT-III proteins reveals common regulatory role for extreme C-terminal domain. *Traffic* **8**, 1068–1079 (2007).
- Lata, S. *et al.* Structural basis for autoinhibition of ESCRT-III CHMP3. *J. Mol. Biol.* **378**, 818–827 (2008).
- Lin, Y., Kimpler, L.A., Naismith, T.V., Lauer, J.M. & Hanson, P.I. Interaction of the mammalian endosomal sorting complex required for transport (ESCRT) III protein hSnf7-1 with itself, membranes, and the AAA+ ATPase SKD1. *J. Biol. Chem.* **280**, 12799–12809 (2005).
- Zamborini, A. *et al.* Release of autoinhibition converts ESCRT-III components into potent inhibitors of HIV-1 budding. *Proc. Natl. Acad. Sci. USA* **103**, 19140–19145 (2006).
- Kieffer, C. *et al.* Two distinct modes of ESCRT-III recognition are required for VPS4 functions in lysosomal protein targeting and HIV-1 budding. *Dev. Cell* **15**, 62–73 (2008).
- McCullough, J., Fisher, R.D., Whitby, F.G., Sundquist, W.I. & Hill, C.P. ALIX-CHMP4 interactions in the human ESCRT pathway. *Proc. Natl. Acad. Sci. USA* **105**, 7687–7691 (2008).
- Tsang, H.T. *et al.* A systematic analysis of human CHMP protein interactions: Additional MIT domain-containing proteins bind to multiple components of the human ESCRT III complex. *Genomics* **88**, 333–346 (2006).
- Row, P.E. *et al.* The MIT domain of UBPY constitutes a CHMP binding and endosomal localization signal required for efficient epidermal growth factor receptor degradation. *J. Biol. Chem.* **282**, 30929–30937 (2007).
- Rodriguez-Galan, O., Galindo, A., Hervas-Aguilar, A., Arst, H.N. & Penava, M.A. Physiological involvement in pH signalling of Vps24-mediated recruitment of Aspergillus PalB cysteine protease to ESCRT-III. *J. Biol. Chem.* **284**, 4404–4412 (2008).
- Yorikawa, C. *et al.* Human catpain 7/PalBH associates with a subset of ESCRT-III-related proteins in its N-terminal region and partly localizes to endocytic membrane compartments. *J. Biochem.* **143**, 731–745 (2008).
- Yang, D. *et al.* Structural basis for midbody targeting of spastin by the ESCRT-III protein CHMP1B. *Nat. Struct. Mol. Biol.* **15**, 1278–1286 (2008).
- Stuchell-Breton, M.D. *et al.* ESCRT-III recognition by VPS4 ATPases. *Nature* **449**, 740–744 (2007).
- Obita, T. *et al.* Structural basis for selective recognition of ESCRT-III by the AAA ATPase Vps4. *Nature* **449**, 735–739 (2007).
- Samson, R.Y., Obita, T., Freund, S.M., Williams, R.L. & Bell, S.D. A role for the ESCRT system in cell division in archaea. *Science* **322**, 1710–1713 (2008).
- Azmi, I.F. *et al.* ESCRT-III family members stimulate Vps4 ATPase activity directly or via Vta1. *Dev. Cell* **14**, 50–61 (2008).
- Xiao, J. *et al.* Structural basis of Vta1 function in the multivesicular body sorting pathway. *Dev. Cell* **14**, 37–49 (2008).
- Shim, S., Merrill, S.A. & Hanson, P.I. Novel interactions of ESCRT-III with LIP5 and VPS4 and their implications for ESCRT-III disassembly. *Mol. Biol. Cell* **19**, 2661–2672 (2008).
- Welsch, S. *et al.* Ultrastructural analysis of ESCRT proteins suggests a role for endosome-associated tubular-vesicular membranes in ESCRT function. *Traffic* **7**, 1551–1566 (2006).
- Baker, N.A., Sept, D., Joseph, S., Holst, M.J. & McCammon, J.A. Electrostatics of nanosystems: application to microtubules and the ribosome. *Proc. Natl. Acad. Sci. USA* **98**, 10037–10041 (2001).



ONLINE METHODS

Expression vectors and antibodies. Vectors and antibodies are summarized in Supplementary Tables 1 and 2.

Protein expression and purification. We expressed IST1 and CHMP proteins in *Escherichia coli* with N-terminal GST-affinity tags. Protein expression, purification and tag removal are described in the Supplementary Methods.

Equilibrium sedimentation analyses. We centrifuged purified CHMP3, CHMP3₈₋₂₂₂ and IST1_{NTD} in 10 mM Tris-HCl pH 8.0, 100 mM NaCl (CHMP3 proteins) or 50 mM Tris-HCl pH 7.0, 350 mM NaCl and 1 mM DTT (IST1_{NTD}) at 4 °C in an Optima XL-A centrifuge (Beckman). Initial protein concentrations are given in Figure 1a–c. Data were collected after equilibrium was reached at two speeds (20,000 r.p.m. and 24,000 r.p.m.) in a Beckman An-60 Ti rotor, and the molecular masses were determined from the resulting six data sets for each protein by globally fitting to single ideal species models using the nonlinear least-squares algorithms in the Heteroanalysis software²⁶. Protein partial specific volumes and solvent densities were calculated with the program SEDNTERP (version 1.09)³⁷.

Protein crystallization and data collection. We crystallized IST1_{NTD}, CHMP3₈₋₂₂₂ and CHMP3₁₋₁₅₀ by vapor diffusion at 13 °C. IST1_{NTD} crystals grew from a 12 mg ml⁻¹ solution in gel filtration buffer. Crystal form I (diamond-shaped morphology, P4₃2₁2, 1 molecule per asymmetric unit) grew in 1–3 d by simple dehydration of a 2- μ l drop. Crystals were cryoprotected by passage through silica oil, suspended in a nylon loop and plunged into liquid nitrogen. Crystal form II (rods and plates, P2₁, 1 molecule per asymmetric unit) grew from a 1:1 (v/v) mixture of protein and well solution (180 mM KCl, 50 mM HEPES pH 7.6, 35% pentaerythritol propoxylate and 7% (v/v) ethylene glycol). Crystals were cryo-cooled directly without solution modification. Native data for both crystal forms were collected on a Rigaku Micromax 007HF rotating anode generator equipped with VeniMax-HR optics.

CHMP3₈₋₂₂₂ crystals (flat plates, P2₁, 2 molecules per asymmetric unit) grew from a 1:2 (v/v) mixture of protein (30 mg ml⁻¹ in gel filtration buffer) and well solution (10–22% PEG 6000 and 0.1M Na-HEPES pH 7.0–8.0). Data were collected at SSRL beamline 11-I. CHMP3₁₋₁₅₀ crystals (hexagonal rods, P6₁) grew from a 1:1 (v/v) mixture of protein (22 mg ml⁻¹ in gel filtration buffer) and well solution (16% (v/v) PEG 3350, 0.1 M Na HEPES pH 7.0–8.0, 200 mM proline). Data were collected on a rotating anode generator. Despite extensive effort, we were unable to collect better data at the synchrotron. Data were indexed and scaled with the program HKL2000 (ref. 38) (Table 1).

Structure determinations. We collected three-wavelength MAD data from selenomethionine-substituted IST1_{NTD} at SSRL beamline 9–1 to 3.4 Å. Three of the six potential selenium sites were identified using SOLVE³⁹, and the resulting 4.0-Å phases were solvent flattened and extended to 2.6-Å resolution using the native data and the program DM⁴⁰. The four core helices (α 1– α 4) were built using O⁴¹, and this partial model was used for molecular replacement determination of the higher-resolution form II crystal structure using PHASER⁴². The models were completed with COOT⁴³, refined with REFMAC5 (ref. 44) and analyzed using programs within the CCP4 suite⁴⁵. The similar IST1_{NTD} structures in the two crystal forms overlapped with an r.m.s. deviation of 1.25 Å on C α atoms 12–170.

We determined both CHMP3 structures by molecular replacement using the published CHMP3₈₋₁₈₃ structure (PDB 2GD5)¹⁶ as the search model. The correctness of the solutions is supported by PHASER⁴² Z-scores of 9.1 (CHMP3₈₋₂₂₂) and 8.6 (CHMP3₁₋₁₅₀) and by the appearance of electron density when portions of the search model were omitted from the molecular replacement calculation (Supplementary Fig. 2). Both structures are hampered by low resolution and a correspondingly low number of unique reflections. R_{free} sets of 5% contain too few reflections (~120) to be statistically useful. An optimal strategy was therefore determined by considering R_{free} values from multiple refinement runs, each starting from the same molecular replacement solution and with a different small number (~200) of reflections in the test set. This indicated that the best results were obtained using rigid-body refinement in PHENIX⁴⁶ with each helix treated as a rigid unit. This approach was

therefore applied to the starting molecular replacement solution but using all of the reflections in the calculation (no test set).

Biosensor binding assays. We used BIACORE2000 and BIACORE3000 instruments (GE Healthcare) to measure the binding of pure recombinant CHMP1B to immobilized GST-IST1_{NTD} proteins captured from *E. coli* extracts²⁸, as described in Supplementary Methods.

ISTI depletion and rescue experiments. We transfected HeLa-M cells with IST1 expression vectors (1 μ g per well, using Lipofectamine 2000, Invitrogen) and siRNA (20nM, Lipofectamin RNAi MAX, Invitrogen) following the time course: $t = 0$, seed cells in DMEM and 10% (v/v) FCS (six-well plates, 4×10^5 cells per well); $t = 24$ h, add IST1 expression vector; $t = 32$ h, change media and add IST1 vector; $t = 44$ h, trypsinize and reseed cells on 18-mm glass cover slips for immunofluorescence analyses (3×10^4 cells per cover slip) and in six-well plates for western blotting (3×10^5 cells per well); $t = 56$ h, change media and add siRNA; $t = 68$ h, change media and add siRNA; $t = 94$ h, fix or harvest cells and analyze.

Direct visualization of cytokinesis defects. We fixed transfected HeLa-M cells with 4% (v/v) paraformaldehyde and stained with SYTOX Green (Invitrogen) and with mouse anti- α -tubulin and a secondary Alexa 594-conjugated goat anti-mouse antibody. We scored midbody arrest manually for ≥ 3 blinded sets of 200 cells by direct visualization using fluorescence microscopy.

ESCRT-III assembly reactions. Assembly conditions for CHMP2A and CHMP3, IST1_{NTD}, and CHMP1B proteins are provided in the Supplementary Methods.

Transmission electron microscopy. We analyzed assembly reactions using TEM with negative staining. Carbon-coated grids were placed on aliquots of each assembly reaction (7 μ l, 90 s), washed with 3–4 drops of 0.1 M KCl, stained with 3–4 drops of 4% (v/v) uranyl acetate, air dried and imaged (Hitachi 7100 TEM).

GST pull-down assays. We tested the binding of pure recombinant CHMP2A proteins to various GST-CHMP3 proteins as described in the Supplementary Methods.

HIV-1 vector release and infectivity. We co-transfected 293T cells with vectors expressing CHMP3-Myc and HIV-1 and harvested supernatants and cells after 24 h. Western blotting was used to analyze cellular proteins and virions pelleted through 20% sucrose cushion and HeLa-M cell transduction to measure vector titers. Full details are provided in Supplementary Methods.

36. Cole, J.L. Analysis of heterogeneous interactions. *Methods Enzymol.* **384**, 212–232 (2004).

37. Laue, T., Shah, B., Ridgeway, T. & Pelletier, S. Computer-aided interpretation of analytical sedimentation data for proteins. in *Ultracentrifugation in Biochemistry and Polymer Science* (eds. Rowe, A. & Horton, J.) 90–125 (Royal Society of Chemistry, Cambridge, UK, 1992).

38. Otwinowski, Z. Oscillation data reduction program. in *Data Collection and Processing* (eds. Sawyer, L., Isaacs, N. & Bailey, S.J.) 56–62 (SERC Daresbury Laboratory, Warrington, UK, 1993).

39. Terwilliger, T.C. & Berendzen, J. Automated structure solution for MIR and MAD. *Acta Crystallogr. D Biol. Crystallogr.* **55**, 849–861 (1999).

40. Cowtan, K.D. & Zhang, K.Y. Density modification for macromolecular phase improvement. *Prog. Biophys. Mol. Biol.* **72**, 245–270 (1999).

41. Jones, T.A., Zou, J.Y., Cowan, S.W. & Kjeldgaard, M. Improved methods for binding protein models in electron density maps and the location of errors in these models. *Acta Crystallogr. A* **47**, 110–119 (1991).

42. McCoy, A.J., Grosse-Kunstleve, R.W., Storoni, L.C. & Read, R.J. Likelihood-enhanced fast translation functions. *Acta Crystallogr. D Biol. Crystallogr.* **61**, 458–464 (2005).

43. Emsley, P. & Cowtan, K. Coot: model-building tools for molecular graphics. *Acta Crystallogr. D Biol. Crystallogr.* **60**, 2126–2132 (2004).

44. Murshudov, G.N., Vagin, A.A. & Dodson, E.J. Refinement of macromolecular structures by the maximum-likelihood method. *Acta Crystallogr. D Biol. Crystallogr.* **53**, 240–255 (1997).

45. Collaborative Computational Project, Number 4. The CCP4 suite: programs for protein crystallography. *Acta Crystallogr. D* **50**, 760–763 (November 4, 1994).

46. Zwart, P.H. *et al.* Automated structure solution with the PHENIX suite. *Methods Mol. Biol.* **426**, 419–435 (2008).



CHAPTER 7

CONCLUSIONS AND FUTURE DIRECTIONS

The global HIV/AIDS pandemic represents one of the most significant afflictions to confront humanity during the past century. Moreover, although very significant progress has been made in developing effective combination chemotherapies that inhibit viral replication and dramatically extend life expectancies, drug resistance is a very significant (and growing) problem (3, 18) and little progress has been made in developing an effective preventative vaccine against HIV (5). Thus, there remains a need to understand and investigate the molecular mechanisms of retroviral pathogenesis, both to identify potential new targets for therapeutic intervention and to understand how and why immune responses to the virus succeed and fail. Toward this end, the work described in this dissertation focused on examining early events in retroviral replication and on the mechanisms by which these events can be inhibited by the restriction factor TRIM5 α .

TRIM5 α Restriction

Intrinsic immune systems help vertebrates defend against viral infections by producing interferon-inducible proteins that can target and disrupt many different stages of viral replication (1, 15, 25). The restriction factor, TRIM5 α , is

one such central mediator of intrinsic antiretroviral immunity in primates. TRIM5 α was identified in 2004 and has been intensively studied in the ensuing past five years (2, 9, 10, 16, 17, 22, 23). Nevertheless, several key mechanistic aspects of TRIM5 α restriction are still not well understood, and these gaps in our understanding provided the motivation for much of my dissertation research.

A general model for TRIM5 α restriction that encompasses available data (including results from this dissertation) is that: 1) dimeric TRIM5 α proteins initially recognize incoming viral capsids, 2) capsid recognition leads to higher-order TRIM5 α assembly, thereby creating more stable complexes through avidity effects, 3) capsid binding and assembly induce TRIM5 α auto-ubiquitylation, which creates signals that recruit proteasomes, and 4) proteasomal extraction and degradation of bound TRIM5 α proteins may destabilize the capsid and induce premature capsid dissociation, thereby inhibiting accumulation of reverse transcripts (2, 9, 10, 16, 17, 22, 23).

I have employed biochemical approaches to examine the mechanism of TRIM5 α restriction. Chapter 2 describes the development of methods for expressing and purifying recombinant TRIM5 α proteins, and their biochemical characterization. Previous attempts to purify full-length TRIM5 α proteins had been hampered by low expression levels and by their tendency to form insoluble complexes in both mammalian and *E.coli* cells. I overcame these problems by using an insect cell/baculovirus system to express TRIM5-21R, a chimeric TRIM5 protein composed primarily of the rhesus TRIM5 α protein, but with the RING domain of human TRIM21 protein replacing rhesus TRIM5 α RING domain. This

substitution increased the cellular half-life of the protein (leading to higher protein expression levels), and also increased protein solubility (making the protein easier to purify) (4, 8, 9). Importantly, TRIM5-21R retained good restriction activity against HIV-1 and other retroviruses that are normally restricted by the wild type rhesus TRIM5 α protein (4, 9). TRIM5-21R (and related) proteins were purified using a three-stage chromatography scheme, which led to the isolation of milligram quantities of highly pure recombinant protein suitable for biochemical and structural analyses.

The oligomeric states of recombinant and native TRIM5-21R and rhesus TRIM5 α proteins were characterized using a combination of gel filtration chromatography, analytical ultracentrifugation, and chemical crosslinking. These studies led to the discovery that TRIM5 proteins are dimers (8, 9), not trimers as had been initially reported (14). Our recombinant TRIM5-21R proteins also exhibited several additional functional attributes, including ubiquitin E3 ligase activity and retroviral capsid recognition. TRIM5-21R bound directly and specifically both to purified EIAV cores and to synthetic CA-NC capsid assemblies, as analyzed by sedimentation-based *in vitro* binding assays and by electron microscopy. However, interactions between TRIM5-21R proteins and isolated CA subunits were not observed in several different types of binding assays, implying that tight TRIM5-21R binding requires an intact hexameric capsid lattice. High affinity binding appears to involve recognition of the conserved lattice spacing found in all mature retroviral capsids, together with templated higher order TRIM5 α assembly. These properties explain how

individual TRIM5 α isoforms can interact with a variety of different retroviral capsids, in spite of the fact that their CA subunits often differ considerably in primary sequence. Experimental evidence in support of this capsid recognition mode comes from the recent discovery that the B-Box-2 domain mediates TRIM5 α higher order assembly (10) and from 2D electron crystallography-based structural studies, discussed below (Ganser-Pornillos et al., unpublished).

The development of TRIM5 α expression and purification methods was undertaken in part to facilitate structural studies of TRIM5 α proteins and their complexes with retroviral capsid assemblies. Electron crystallographic analyses of 2D crystals formed from TRIM5-21R/CA complexes are now underway in a collaborative effort led by Barbie Ganser-Pornillos (University of Virginia, Yeager laboratory), Vish Chandrasekaran (Sundquist laboratory), and Owen Pornillos (University of Virginia). Our initial findings indicate that TRIM5 α proteins can assemble into hexameric superlattices upon capsid templates. Intriguingly, the unit cell spacing of the hexameric TRIM5-21R lattice (assembled from hexameric subunits of TRIM5 α dimers) is four times larger than that of the hexameric CA lattice. These results imply that there is a size and symmetry match between the TRIM5-21R and CA lattices that may help to nucleate assembly of a TRIM5 α cage that entraps cytoplasmic retroviral core particles. TRIM5 α binding and assembly then lead to a series of events that likely include TRIM5 α autoubiquitylation, proteasomal degradation, disruption of capsid integrity and inhibition of reverse transcription.

While the electron crystallographic reconstructions of 2D crystals of TRIM5-21R are exciting, resolution is currently limited by the low intrinsic order of the crystals. Higher resolution structural studies of TRIM5 α : capsid complexes will also be important for understanding the details of capsid recognition and for explaining how substitution of a single charged amino acid at SPRY domain residue 332 can confer HIV-1 restriction ability upon the human TRIM5 α isoform (20, 24, 26). Conceivably, this understanding could facilitate the design of small molecules capable of stabilizing the human TRIM5 α : capsid-binding interface, perhaps by mimicking a residue 332 substitution. We note that TRIM5 α expression and *in vitro* capsid binding systems like those described in Chapter 2 could prove useful for screening the efficacy of such compounds.

Early Events in Lentiviral Replication and the Development of Cell-Free Uncoating and Restriction Assays

The early events of uncoating, reverse transcription, and preintegration complex formation are critical for viral replication and are targets of restriction, but are not yet understood in mechanistic detail. To help remedy this deficiency, a cell free assay to study these processes is in development, but not described in detail here because the data have not yet been published. In brief, this assay involves incubation of purified EIAV core particles with soluble cell extracts, dNTPs and an ATP regeneration system, followed by analysis of reverse transcription and capsid dissociation. This cell free retroviral replication assay will provide a potentially valuable tool for second-generation studies aimed at

dissecting the processes of reverse transcription, capsid uncoating and retroviral restriction in greater detail. For example, the system could provide an assay for identifying and characterizing new cellular factors that influence retroviral replication and restriction as they are purified by fractionation of cell extracts. Candidate factors purified in this fashion could then be verified functionally using IP and siRNA depletion experiments performed *in vitro* and *in vivo*.

We also envision that the assay can form the basis for reconstitution of additional stages of the retroviral life cycle *in vitro*. For example, it is possible that this assay could be adapted to reconstitute the activity of APOBEC3G, a cytidine deaminase that also functions as a potent retroviral restriction factor. In this case, restricting APOBEC3G proteins would need to be expressed in the cells used to produce the EIAV core particles because APOBEC3G is incorporated into virions as they assemble, but then exerts its effects when the genome is reverse transcribed in the new host cell (11-13, 19, 21). It will also be of interest to determine whether or not full length reverse transcripts produced *in vitro* form integration-competent PICs. Gaining the ability to study these processes *in vitro* would also be a significant step forward because we currently lack a comprehensive understanding of PIC composition, activity and nuclear targeting/import.

Finally, it would be of interest to modify this cell free system to examine the early lifecycle events of other retroviruses, particularly HIV-1. Such studies would, of course, have more direct relevance to human pathology, and would also allow us to take advantage of the large body of information and reagents

available for HIV-1, including well characterized CA mutants, known HIV-specific host replication factors like cyclophilin-A, and specific inhibitors of early stages of the HIV life cycle including reverse transcription and integration (6, 7). In principle, an HIV assay could also be used to screen for new pharmaceutical inhibitors capable of targeting additional steps in the HIV-1 lifecycle, including uncoating, reverse transcription or PIC formation. In short, the development of a new system for studying lentiviral replication and restriction in a cell free system has opened up new research opportunities whose ultimate impact will depend, in large part, on just how expandable and general this system proves to be.

References

1. **Bieniasz, P. D.** 2004. Intrinsic immunity: a front-line defense against viral attack. *Nat Immunol* **5**:1109-15.
2. **Campbell, E. M., O. Perez, J. L. Anderson, and T. J. Hope.** 2008. Visualization of a proteasome-independent intermediate during restriction of HIV-1 by rhesus TRIM5alpha. *J Cell Biol* **180**:549-61.
3. **Clavel, F., and A. J. Hance.** 2004. HIV drug resistance. *N Engl J Med* **350**:1023-35.
4. **Diaz-Griffero, F., X. Li, H. Javanbakht, B. Song, S. Welikala, M. Stremlau, and J. Sodroski.** 2006. Rapid turnover and polyubiquitylation of the retroviral restriction factor TRIM5. *Virology* **349**:300-15.
5. **Fauci, A. S.** 2008. 25 years of HIV. *Nature* **453**:289-90.
6. **Hazuda, D., M. Iwamoto, and L. Wenning.** 2009. Emerging pharmacology: inhibitors of human immunodeficiency virus integration. *Annu Rev Pharmacol Toxicol* **49**:377-94.
7. **Jochmans, D.** 2008. Novel HIV-1 reverse transcriptase inhibitors. *Virus Res* **134**:171-85.
8. **Kar, A. K., F. Diaz-Griffero, Y. Li, X. Li, and J. Sodroski.** 2008. Biochemical and biophysical characterization of a chimeric TRIM21-TRIM5alpha protein. *J Virol* **82**:11669-81.
9. **Langelier, C. R., V. Sandrin, D. M. Eckert, D. E. Christensen, V. Chandrasekaran, S. L. Alam, C. Aiken, J. C. Olsen, A. K. Kar, J. G. Sodroski, and W. I. Sundquist.** 2008. Biochemical characterization of a recombinant TRIM5alpha protein that restricts human immunodeficiency virus type 1 replication. *J Virol* **82**:11682-94.
10. **Li, X., and J. Sodroski.** 2008. The TRIM5alpha B-box 2 domain promotes cooperative binding to the retroviral capsid by mediating higher-order self-association. *J Virol* **82**:11495-502.
11. **Mangeat, B., P. Turelli, G. Caron, M. Friedli, L. Perrin, and D. Trono.** 2003. Broad antiretroviral defence by human APOBEC3G through lethal editing of nascent reverse transcripts. *Nature* **424**:99-103.
12. **Mariani, R., D. Chen, B. Schrofelbauer, F. Navarro, R. Konig, B. Bollman, C. Munk, H. Nymark-McMahon, and N. R. Landau.** 2003.

- Species-specific exclusion of APOBEC3G from HIV-1 virions by Vif. *Cell* **114**:21-31.
13. **Marin, M., K. M. Rose, S. L. Kozak, and D. Kabat.** 2003. HIV-1 Vif protein binds the editing enzyme APOBEC3G and induces its degradation. *Nat Med* **9**:1398-403.
 14. **Mische, C. C., H. Javanbakht, B. Song, F. Diaz-Griffero, M. Stremlau, B. Strack, Z. Si, and J. Sodroski.** 2005. Retroviral restriction factor TRIM5alpha is a trimer. *J Virol* **79**:14446-50.
 15. **Nisole, S., J. P. Stoye, and A. Saib.** 2005. TRIM family proteins: retroviral restriction and antiviral defence. *Nat Rev Microbiol* **3**:799-808.
 16. **Perron, M. J., M. Stremlau, M. Lee, H. Javanbakht, B. Song, and J. Sodroski.** 2007. The human TRIM5alpha restriction factor mediates accelerated uncoating of the N-tropic murine leukemia virus capsid. *J Virol* **81**:2138-48.
 17. **Rold, C. J., and C. Aiken.** 2008. Proteasomal degradation of TRIM5alpha during retrovirus restriction. *PLoS Pathog* **4**:e1000074.
 18. **Sendagire, H., P. J. Easterbrook, I. Nankya, E. Arts, D. Thomas, and S. J. Reynolds.** 2009. The challenge of HIV-1 antiretroviral resistance in Africa in the era of HAART. *AIDS Rev* **11**:59-70.
 19. **Sheehy, A. M., N. C. Gaddis, and M. H. Malim.** 2003. The antiretroviral enzyme APOBEC3G is degraded by the proteasome in response to HIV-1 Vif. *Nat Med* **9**:1404-7.
 20. **Song, B., B. Gold, C. O'Huigin, H. Javanbakht, X. Li, M. Stremlau, C. Winkler, M. Dean, and J. Sodroski.** 2005. The B30.2 (SPRY) domain of the retroviral restriction factor TRIM5alpha exhibits lineage-specific length and sequence variation in primates. *J Virol* **79**:6111-21.
 21. **Stopak, K., C. de Noronha, W. Yonemoto, and W. C. Greene.** 2003. HIV-1 Vif blocks the antiviral activity of APOBEC3G by impairing both its translation and intracellular stability. *Mol Cell* **12**:591-601.
 22. **Stremlau, M., C. M. Owens, M. J. Perron, M. Kiessling, P. Autissier, and J. Sodroski.** 2004. The cytoplasmic body component TRIM5alpha restricts HIV-1 infection in Old World monkeys. *Nature* **427**:848-53.
 23. **Stremlau, M., M. Perron, M. Lee, Y. Li, B. Song, H. Javanbakht, F. Diaz-Griffero, D. J. Anderson, W. I. Sundquist, and J. Sodroski.** 2006.

Specific recognition and accelerated uncoating of retroviral capsids by the TRIM5alpha restriction factor. *Proc Natl Acad Sci U S A* **103**:5514-9.

24. **Stremlau, M., M. Perron, S. Welikala, and J. Sodroski.** 2005. Species-specific variation in the B30.2(SPRY) domain of TRIM5alpha determines the potency of human immunodeficiency virus restriction. *J Virol* **79**:3139-45.
25. **Wolf, D., and S. P. Goff.** 2008. Host restriction factors blocking retroviral replication. *Annu Rev Genet* **42**:143-63.
26. **Yap, M. W., S. Nisole, and J. P. Stoye.** 2005. A single amino acid change in the SPRY domain of human Trim5alpha leads to HIV-1 restriction. *Curr Biol* **15**:73-8.